New States of Matter in Strongly Frustrated Quantum Magnets

im Fachbereich Physik der Freien Universität Berlin eingereichte Dissertation zur Erlangung des Grades eines Doktors der Naturwissenschaften

von

Max Hering

Dahlem Center for Complex Quantum Systems

Berlin, November 2018

First referee: Prof. Dr. Johannes Reuther
Second referee: Prof. Dr. Piet Wibertus Brouwer
Date of defence: 17 December 2018

I dedicate this thesis to life, Mister Richards.

"Information is not knowledge.
Knowledge is not wisdom.
Wisdom is not truth.
Truth is not beauty.
Beauty is not love.
Love is not music.
Music is the best."

Frank Zappa

Affidavit

Herewith, I affirm that I wrote this thesis independently. I used the named references and nothing but the named references.

Berlin, 22 November 2018 Max Hering

Contents

1. Introduction

Quantum physics is one of the most fascinating research topics that mankind ever initiated. We not only know that its implications define a large part of nature, *e.g.*, how matter, chemistry, and biology emerge from elementary particles, but we also utilise it every day in (classical) computers for instance which rely on thousands of field effect transistors. Despite that, we only have very little intuition for the variety of quantum phenomena such as superposition and quantum entanglement since they are not directly observable in everyday life. It seems as if there is still an entire universe filled with open questions and sometimes the answer to just one of them can yield an incredible improvement for society. For example, the discovery of superconductivity by Heike Kamerlingh Onnes in 1911 [43] provides us with the capability to save lives worldwide everyday using magnetic resonance imaging. The applicability of a superconducting state lies in the fact that it is a macroscopic quantum state which is robust in a sense and can therefore be used to construct actual devices.

The key to the quantum world is that classical variables such as position and momentum can fluctuate on small scales and can hence not be determined with arbitrary precision. This effect is suppressed in our classical experience by too large thermal fluctuations on one hand which render the quantum fluctuations irrelevant and by permanent measurement on the other hand which naturally occurs if multiple interactions are present. In order to find novel quantum phenomena with possible applications, many physicists thus investigate systems at low temperatures, typically solid states. If most of their atomic constituents are then somehow confined into a crystalline structure, an effective model of only a few interacting quantum particles may accurately describe the system and one might have a chance of finding the desired macroscopic quantum states.

One natural candidate for such quantum systems are Mott insulators [17, 131]. At low temperatures, their nuclei and most of their electrons are bound in some atomic lattice which acts as an effective potential for the remaining unbound valence electrons. Mott insulators have exactly one valence electron per lattice site and are hence no band insulators. Instead, the electronic orbitals between adjacent lattice sites have little overlap and the valence electrons are unlikely to tunnel from one atom to a different one. The effective model which reliably characterises the properties of Mott insulators is the Hubbard model [77–82]. It incorporates a hopping t of the valence electrons between different atoms and a Coulomb repulsion U that energetically penalises two electrons at the same site. This model shows a transition from a conducting phase for small U to an insulating Mott phase if $U \gg t$. In the latter scenario, the valence electrons are very unlikely to tunnel through their potential barriers from the beginning and the large repulsion term then drastically suppresses electronic transport. At half filling which is accurate for Mott insulators, the Hubbard model for the localised valence electrons in the large-U limit effectively turns via direct exchanges and superexchanges into the Heisenberg model which is described by the Hamiltonian

$$\hat{H} = \sum_{(i,j)} J_{ij} \hat{\boldsymbol{S}}_i \cdot \hat{\boldsymbol{S}}_j \,. \tag{1.1}$$

Here, the brackets (i, j) denote that the sum runs over pairs of lattice sites and the coupling constant is given by $J_{ij} = \frac{4t_{ij}^2}{U}$.

Even though the Heisenberg model only deals with a small percentage of the underlying system's intrinsic degrees of freedom, finding a solution for it is, especially in the quantum spin-$\frac{1}{2}$ limit, a notoriously difficult task because there are merely interaction terms present. For a lattice of N spins, the required diagonalisation of a $2^N \times 2^N$ matrix is feasible for the best computers currently available only up to $N \approx 40$ depending on the concrete symmetries. Since macroscopic systems contain a number of atoms that is to the order of $N \approx 10^{23}$, these computational limitations seem quite unfortunate. Nevertheless, already in 1973 Philip Warren Anderson proposed the so-called resonating valence bond (RVB) state as a possible ground state for the antiferromagnetic ($J_{ij} > 0$) spin-$\frac{1}{2}$ Heisenberg model on the triangular lattice [6]. Anderson realised that there might be a dense manifold of states which cover a frustrated lattice with spin singlets on short-ranged bonds in different ways. Instead of selecting one of these energetically very similar states, the system could then fluctuate between different singlet covers in the presence of thermal or quantum fluctuations. This behaviour inspired the name of the RVB state. Meanwhile, it is believed that RVB states are closely related to the formation of cooper pairs in high-T_c superconductors. The prime examples for such materials like the copper oxide La_2CuO_4 are doped Mott insulators and it has been proposed that the superconductivity at high temperatures is strongly connected to a RVB state in the parent Heisenberg model [7].

In the same context, it was realised that a resonating cover of the lattice with spin singlets does neither break any symmetry of the underlying Heisenberg Hamiltonian, nor does it exhibit magnetic long-range order. Hence, the RVB state matches two of the three possible definitions of a *quantum spin liquid* (QSL). The third potential definition demands the existence of fractionalised excitations in the considered spin model [126]. Since spin singlets are $S = 0$ states, the fundamental excitations in the RVB picture are spin triplets which carry the spin quantum number $S = 1$. Due to the degenerate and fluctuating nature of the RVB state though, these spin-1 excitations can fractionalise in some cases into a pair of deconfined spin-$\frac{1}{2}$ excitations called *spinons* [51, 65–67]. If those spinons are spatially separated, they leave a trace of rearranged spin singlets behind. By mapping a RVB ground state of a two-dimensional spin system onto a torus, one can show that the process of creating two spinons, propagating them around the torus' circumference, and recombining them afterwards into a $S = 0$ singlet will transform the RVB ground state into yet another RVB ground state. The initial and the final state can then not be discriminated in terms of local observables because all spin expectation values vanish. The only distinction between the states before and after spinon creation, propagation, and recombination is the arrangement of spin singlets along the path that the spinons took around the torus. This singlet structure is a non-local observable. As a result, one calls initial and final state *topologically degenerate* [181, 183, 184, 187] which is a necessary condition for the existence of fractional excitations such as spinons [136].

In addition to being excellent models for understanding the principles behind high-T_c superconductivity, quantum spin liquids might also be utilised in the aspiring field of quantum computation. In 2006, Alexei Kitaev proposed a spin-$\frac{1}{2}$ model with Ising-like interactions coupling the three spin components $\hat{S}_x$, $\hat{S}_y$, and $\hat{S}_z$ separately along the three different nearest-neighbour bonds of a honeycomb lattice. Due to its somewhat artificial construction, this model is exactly solvable and features a spin liquid ground state with non-Abelian quasiparticles called *anyons* as excitations [101]. Though it is challenging to realise this model in a laboratory and one already knows that the spin liquid phase is quite unstable with respect to perturbations in the Hamiltonian, Kitaev's idea for making use of these anyons as decoherence-protected quantum memory has attracted a large interest in spin liquids also for feasible applications in quantum information technology.

One of the fundamental ingredients in order to observe a QSL as the true ground state of a Heisenberg model is the frustration of spins, *i.e.*, there are different terms in the Hamiltonian which cannot be minimised simultaneously. This can, for instance, occur if there are finite antiferromagnetic Heisenberg interactions on different types of bonds or if the lattice consists of corner-sharing triangles. Furthermore, quantum fluctuations which are largest if $S = \frac{1}{2}$ are a necessity as well since they can prevent the emergence of magnetic long-range order. Due to the complexity of the consequential models, there are still very few techniques available for their unbiased analysis. As explained above, exact diagonalisation suffers from finite size effects which prohibits a true investigation of the thermodynamic limit. The same statement holds for the density-matrix renormalisation group (DMRG) method in two dimensions because it has to map the system onto a torus with finite circumference.

For example, the J_1-J_2 Heisenberg model on the square lattice is highly debated to this day. Here, J_1 (J_2) denotes the Heisenberg coupling on the nearest-neighbour (second-neighbour) bonds. In the classical limit, this model exhibits a phase transition from an antiferromagnetic Néel state into a collinearly ordered state at a coupling ratio of $J_2/J_1 = 0.5$ [144]. However, for the quantum spin-$\frac{1}{2}$ model, the situation is not that clear. From early quantum Monte Carlo studies, it is known that the magnetisation of the Néel or the collinear state in the respective non-frustrated limit ($J_1 = 0$ or $J_2 = 0$) is diminished by roughly 40% from the saturation value due to quantum fluctuations [142]. In addition, these fluctuations lift the collinear state's classical continuous degeneracy into a two-fold degeneracy [31] by means of a process which is often referred to as *order by disorder* [74]. There is a more or less general agreement between various studies that the Néel-ordered phase persists up to a coupling ratio of $J_2/J_1 \lesssim 0.4$ and that the collinear phase appears at around $J_2/J_1 \gtrsim 0.6$ in the quantum model [42, 48, 61, 64, 91, 96, 161, 167, 172, 180]. The concrete values of the phase boundaries depend slightly on the specific method or the implemented cluster sizes. Also, it is known from spin-wave theory for almost precisely thirty years now that the intermediate coupling regime houses a paramagnetic phase around $J_2/J_1 \approx 0.5$ [32, 46] which immediately triggered a debate about whether that phase was rather characterised by a valence bond crystal (VBS) [41, 141] or a QSL [32]. Since then,

this topic has been addressed in numerous works including exact diagonalisation [21, 25, 48, 114, 161], field theories [141, 171], coupled cluster methods [16, 42], series expansions [59, 167, 169, 172], quantum Monte Carlo approaches [25, 26], and DMRG [61, 64, 96, 180], but there is hitherto no consensus amongst them. The system might realise a VBS, a QSL, or in fact both [61, 180] and there are different predictions for the type of QSL as well. It could be gapped, gapless, or even topological.

A new method which was shown to being capable of describing the thermodynamic limit of a spin system is the functional renormalisation group (FRG). Since its first application by Johannes Reuther to the spin-$\frac{1}{2}$ square lattice Heisenberg model in 2010 [147], it was used to accurately map out magnetic phase diagrams for various types of spin couplings in two and three dimensions. As confirmed by FRG, the J_1-J_2 square lattice model around $J_2/J_1 = 0.5$ and the nearest-neighbour kagome lattice model are promising candidates for finding a QSL due to their lack of magnetic long-range order. However, this method can only cope with diagonal spin interactions so far and it provides the system's spin susceptibility as a result. This spin-spin correlator is related to the experimentally measurable spin structure factor and thereby to the spinon dispersion, and it gives information about whether a certain system tends to order magnetically or not. Nevertheless, until now the FRG does neither provide any knowledge about the precise nature of a model's excitations, nor can it deal with off-diagonal spin interactions. This is why, in this thesis, we not only show the path how to extend this powerful method to more realistic models by implementing it including the Dzyaloshinsky-Moriya interaction, but we also develop a method that can characterise the effective low-energy spinon theories for quantum spin models from the results of a FRG analysis.

During the entire thesis, we represent the spin-$\frac{1}{2}$ operators in a pseudo-fermion representation developed in 1965 by Alexei Alexeyevich Abrikosov in order to describe the resistivity of a metal with paramagnetic impurities and the Kondo effect [1, 2]. If $\hat{f}^{(\dagger)}_{i,\uparrow}$ annihilates (creates) a spin-up fermion at lattice site i and $\hat{f}^{(\dagger)}_{i,\downarrow}$ does precisely the same with a spin-down fermion, a spin operator at site i can be expressed as

$$\hat{S}^{\mu}_{i} = \frac{1}{2} \sum_{\alpha,\beta} \hat{f}^{\dagger}_{i,\alpha} \sigma^{\mu}_{\alpha\beta} \hat{f}_{i,\beta} \,, \tag{1.2}$$

where $\mu \in \{x, y, z\}$, and $\sigma^x, \sigma^y, \sigma^z$ are the three standard Pauli matrices. This representation enables us to utilise standard Feynman diagrammatic techniques (invented by Richard Phillips Feynman [53–55]) which is very convenient for large quantum-many-body systems. Unfortunately, every coin has two sides and the decomposition into pseudo fermions yields a Heisenberg Hamiltonian that is purely quartic in the fermionic operators, *i.e.*,

$$\hat{H} = \sum_{\langle i,j \rangle} \sum_{\mu} \sum_{\alpha,\beta,\gamma,\delta} \frac{J_{ij}}{4} \hat{f}^{\dagger}_{i,\alpha} \sigma^{\mu}_{\alpha\beta} \hat{f}_{i,\beta} \hat{f}^{\dagger}_{j,\gamma} \sigma^{\mu}_{\gamma\delta} \hat{f}_{j,\delta} \,. \tag{1.3}$$

As we shall notice soon, such a Hamiltonian is very hard to investigate due to its lack of quadratic terms and the fact that the Hilbert space of a system containing N spin-$\frac{1}{2}$

particles is enlarged by a factor of 2^N is also not beneficial. Because we are going to extend the existing method in a rather elaborate fashion, we want to dedicate the first part of this work to the mathematical framework on which the PFFRG is built.

This thesis is structured as follows. In the next chapter, we properly introduce all entities that are necessary for the further investigation of quantum spin models. After a brief summary of the results needed from statistical physics, we show how experimental observables are related to Green's functions and how to efficiently calculate them using the so-called functional integral formalism. The FRG method is then developed in Chap. 3 where we derive flow equations for bosonic or fermionic one- and two-particle vertex functions in phases with particle-number conservation. This technique is applied to two different spin models afterwards. We study the spin-$\frac{1}{2}$ kagome model with nearest-neighbour Heisenberg and Dzyaloshinsky-Moriya, and second-nearest-neighbour Heisenberg interactions in Chap. 4. Here, we extend the existing PFFRG to spin systems with off-diagonal spin interactions for the first time. The investigated model is motivated by the recently synthesised mineral *herbertsmithite* which shows no magnetic order down to lowest temperatures and therefore seems to be an ideal candidate for finding a QSL in reality [68, 69]. Chap. 5 focuses on another probable QSL material which is the spin-1 A-site spinel $NiRh_2O_4$ [30]. For this nickel compound, we utilise the arbitrary-S generalisation of the PFFRG developed by Maria Laura Baez in 2017 [9]. The flow equations for the relevant XXZ model directly follow from those in the chapter before and only need to be implemented for the diamond lattice that A-site spinels form. For both models considered in Chaps. 4 and 5, we map out phase diagrams of their magnetic ordering tendencies depending on the involved coupling strengths. This is achieved by examining the spin-spin susceptibility which can be computed from the PFFRG vertex functions. In Chap. 6, we change perspective and ask ourselves how to gain even more insight on quantum spin models from the method employed so far. For that purpose, we use a classification scheme for QSLs invented by Xiao-Gang Wen which is called the projective symmetry group (PSG) and which determines all possible effective free spinon models that are consistent with a certain spin Hamiltonian [182]. The different conceivable spinon hopping and pairing ansätze that follow from this classification are then probed by investigating the systems propensity to develop them with a newly designed self-consistent Fock-like mean-field method including FRG vertex functions.

Before turning to spin models though, we introduce the Green's and vertex functions which are later frequently used and derive relations for them in a bosonic and a fermionic language, respectively. Readers who are familiar with Green's functions and the functional integral formalism may skip Chap. 2. Also the third chapter is redundant for readers who know the FRG procedure by heart. Therefore, the well-experienced audience is referred to Chap. 4 as a good point to continue reading this thesis and to perhaps consult the definitions in Chaps. 2 and 3 once in a while if necessary. A reader who does not yet have this kind of background in theoretical physics and perhaps even wants to use and extend the described methods is sincerely invited to peruse the entire work from cover to cover.

Especially in the next sections, we try to provide a brief but complete overview of the motivations and techniques behind all following analyses.

2. Theoretical concepts

2.1. Reminders on quantum-many-body theory

Since we want to derive general formalisms for spin systems, it will be of great benefit for readers who try to reproduce or extend our calculations to know the precise nature of all utilised symbols and approaches. We will therefore start in this chapter with some general reminders on quantum physics.

2.1.1. Thermodynamic ensembles, partition function, and grand-canonical potential

There are three very important thermodynamic ensembles used in quantum physics, *i.e.*, the micro-canonical, the canonical, and the grand-canonical ensemble. The former describes an isolated system which can neither exchange energy nor particles with its surrounding. If a system is at energy E and there are $n(E)$ possible states at this energy, the probability to find the system in a particular state of energy E' in the micro-canonical ensemble is

$$p_{\mathrm{mc}}(E') = \begin{cases} 0 & \text{if } E' \neq E\,, \\ 1/n(E') & \text{if } E' = E\,. \end{cases} \tag{2.1}$$

In the canonical ensemble, the system is allowed to exchange energy with a heat bath that is kept at a constant temperature T. Now, if considered by itself, the system does not have a fixed but only an average energy which is controlled by T. The probability to find it at energy E is now

$$p_{\mathrm{c}}(E) = e^{-\frac{E}{k_{\mathrm{B}}T}}\,, \tag{2.2}$$

where k_{B} is the Boltzmann constant.

If we also want to allow the system to exchange particles with its environment, we have to utilise the grand-canonical ensemble in which, in addition to the heat bath from before, the average particle number of the system is controlled by the chemical potential μ of a particle reservoir connected to it. In this ensemble, the probability to find the system at energy E and particle number N is

$$p_{\mathrm{gc}}(E,N) = e^{-\frac{E-\mu N}{k_{\mathrm{B}}T}}\,. \tag{2.3}$$

Usually, we are interested in properties for the thermodynamic limit. This is obtained by simultaneously sending the system's volume V and particle number N to infinity while keeping the particle density $\rho = N/V$ constant. In this limit, the particular choice of the thermodynamic ensemble does not make a difference for most systems and it will often be convenient to use the grand-canonical ensemble. However, in a Bose Einstein condensate for instance, the particle number in the grand-canonical ensemble diverges and one needs to employ the canonical ensemble instead. For our convenience, we will use the grand-canonical ensemble from now on if we do not note otherwise. The expectation value of a

quantum many-body operator $\hat{O}$ is then given by

$$\left\langle \hat{O} \right\rangle = \frac{\sum\limits_{\alpha} \langle \gamma_\alpha | e^{-\beta\left(\hat{H}-\mu\hat{N}\right)} \hat{O} | \gamma_\alpha \rangle}{\sum\limits_{\alpha} \langle \gamma_\alpha | e^{-\beta\left(\hat{H}-\mu\hat{N}\right)} | \gamma_\alpha \rangle} \,, \tag{2.4}$$

where $\beta = (k_\mathrm{B}T)^{-1}$ and $\{|\gamma_\alpha\rangle\}$ is an orthonormal basis of the fermionic (bosonic) Fock space $\mathcal{F}$ ($\mathcal{B}$) [confer Sec. 2.2.1].

Since the above sums only run over diagonal elements of our operators, we use the shorthand notation of the trace of an operator $\mathrm{tr}\left(\hat{O}\right) = \sum_\alpha \langle \gamma_\alpha | \hat{O} | \gamma_\alpha \rangle$ together with the density matrix $\hat{\rho}$ and the partition function $\mathcal{Z}$ to derive the well-known result

$$\left\langle \hat{O} \right\rangle = \frac{1}{\mathcal{Z}} \mathrm{tr}\left(\hat{\rho}\,\hat{O}\right), \tag{2.5}$$

$$\hat{\rho} = e^{-\beta\left(\hat{H}-\mu\hat{N}\right)}, \tag{2.6}$$

$$\mathcal{Z} = \mathrm{tr}\left(\hat{\rho}\right) . \tag{2.7}$$

In order to calculate the expectation value of the operator $\hat{O}$, we therefore need to compute the partition function $\mathcal{Z}$. This entity also defines the thermodynamic grand-canonical potential $\Omega(\mu, V, T)$ via the relation

$$\mathcal{Z} = e^{-\beta\Omega} \quad \Longleftrightarrow \quad \Omega = -\frac{1}{\beta} \ln\left(\mathcal{Z}\right) . \tag{2.8}$$

Hence, if we know the precise form of the partition function $\mathcal{Z}$, we also know the grand-canonical potential which in turn directly yields the thermodynamic quantities pressure P, entropy S, particle number N, and the internal energy U via

$$P = -\frac{\partial\Omega}{\partial V} \,, \tag{2.9a}$$

$$S = -\frac{\partial\Omega}{\partial T} \,, \tag{2.9b}$$

$$N = -\frac{\partial\Omega}{\partial \mu} \,, \tag{2.9c}$$

$$U = TS - PV + \mu N \,. \tag{2.9d}$$

Of course, using an appropriate Lengendre transform, Ω will yield any desired thermodynamic potential and we will derive a formalism to efficiently compute $\mathcal{Z}$ and Ω for a quantum many-body systems in the next section.

2.1.2. Green's functions

Theoretical physics aims at describing systems based on their most fundamental constituents and interactions. However, if a theory wants to relate to questions from realistic experiments, it needs to make predictions about actually measurable quantities. In an experiment, one usually measures the response of a system due to an external excitation and

the theoretical description of such a process is based on the respective response function or Green's function.

Let us consider a system that is prepared in an eigenstate $|\gamma_\alpha(t_i)\rangle$ of the Hamiltonian $\hat{H}$ at time t_i. It then evolves in the Schrödinger picture under a new Hamiltonian

$$\hat{H}_X(t) = \hat{H} + X(t)\hat{O}_1\,, \tag{2.10}$$

where an external field $X(t)$ couples to the system via an operator $\hat{O}_1$ which has to be hermitian. The time-evolution operator $\hat{U}(t,t_i)$ for which $|\gamma_\alpha(t)\rangle = \hat{U}(t,t_i)|\gamma_\alpha(t_i)\rangle$ then needs to satisfy

$$i\hbar\frac{\partial}{\partial t}\hat{U}(t,t_i) = \hat{H}_X(t)\hat{U}(t,t_i)\,, \tag{2.11a}$$

$$\hat{U}(t_i,t_i) = \mathbb{1}\,. \tag{2.11b}$$

This directly implies

$$\hat{U}(t,t_i) = T_t\left[e^{-\frac{i}{\hbar}\int_{t_i}^{t}\mathrm{d}t'\,\hat{H}_X(t')}\right]\,, \tag{2.12}$$

where the time-ordering operator T_t is defined via

$$T_t\left[\hat{O}_1(t_1)\hat{O}_2(t_2)\dots\hat{O}_n(t_n)\right] = \zeta^P\hat{O}_{P(1)}\left(t_{P(1)}\right)\hat{O}_{P(2)}\left(t_{P(2)}\right)\dots\hat{O}_{P(n)}\left(t_{P(n)}\right)\,, \tag{2.13a}$$

$$\zeta = \begin{cases} +1 \text{ for bosons}\,, \\ -1 \text{ for fermions}\,. \end{cases} \tag{2.13b}$$

Here, P denotes a permutation arranging the operators such that $t_{P(1)} \geq t_{P(2)} \geq \dots \geq t_{P(n)}$ and ensuring that creation operators are on the left side of annihilation operators at identical times. ζ^P will from now on denote the sign of the permutation, *i.e.*, $\zeta^P = 1$ ($\zeta^P = \zeta$) if an even (odd) number of permutations was performed. The time-ordered exponential can be interpreted in two analogous ways, *i.e.*, its Taylor series

$$T_t\left[e^{-\int_{t_i}^{t_f}\mathrm{d}t\,\hat{A}(t)}\right] = \sum_{n=0}^{\infty}\frac{-1^n}{n!}\int_{t_i}^{t_f}\mathrm{d}t_1\,\mathrm{d}t_2\,\dots\mathrm{d}t_n\,T_t\left[\hat{A}(t_1)\hat{A}(t_1)\dots\hat{A}(t_n)\right] \tag{2.14}$$

or the $m\to\infty$ limit of an m-step time discretisation

$$T_t\left[e^{-\int_{t_i}^{t_f}\mathrm{d}t\,\hat{A}(t)}\right] = \lim_{m\to\infty} e^{-\Delta\hat{A}(t_m)}e^{-\Delta\hat{A}(t_{m-1})}\dots e^{-\Delta\hat{A}(t_1)}e^{-\Delta\hat{A}(t_0)}\,, \tag{2.15a}$$

$$\Delta = \frac{t_f - t_i}{m}\,, \tag{2.15b}$$

$$t_n = t_i + n\Delta\,. \tag{2.15c}$$

The response of a state $|\gamma_\alpha(t)\rangle$ that is caused by an infinitesimal perturbation due to the external field $U(t_1)$ acting at $t_1 \in (t_i, t)$ is hence given by a functional derivative

$$\begin{aligned}\delta|\gamma_\alpha(t)\rangle &= \int_{t_i}^{t} \mathrm{d}t_1\, \delta U(t_1)\, \frac{\delta \hat{U}(t,t_i)}{\delta U(t_1)}\bigg|_{U=0} |\gamma_\alpha(t_i)\rangle \\ &= -\frac{i}{\hbar}\int_{t_i}^{t} \mathrm{d}t_1\, \delta U(t_1) e^{-\frac{i}{\hbar}\hat{H}t}\hat{O}_1^{(H)}(t_1)|\gamma_\alpha^{(H)}\rangle\,. \end{aligned} \tag{2.16}$$

Here, we considered the discrete version of the time-ordered exponential in order to derive that

$$\frac{\delta \hat{U}(t,t_i)}{\delta U(t_1)} = T_t\left[e^{-i\int_{t_1}^{t}\mathrm{d}t'\,\hat{H}_X(t')}\right]\left(-\frac{i}{\hbar}\hat{O}_1\right) T_t\left[e^{-i\int_{t_i}^{t_1}\mathrm{d}t'\,\hat{H}_X(t')}\right], \tag{2.17}$$

and, for short-hand notation, used the Heisenberg picture [denoted with superscript (H)]

$$\hat{O}^{(H)}(t) = e^{\frac{i}{\hbar}\hat{H}t}\hat{O}e^{-\frac{i}{\hbar}\hat{H}t}\,, \tag{2.18a}$$

$$|\gamma^{(H)}\rangle = e^{\frac{i}{\hbar}\hat{H}t}|\gamma(t)\rangle\,. \tag{2.18b}$$

We now want to determine that part of the expectation value of another operator $\hat{O}_2$ at time t_2 in state $|\gamma_\alpha(t_2)\rangle$ that is induced due to external field $X(t)$ and find

$$\begin{aligned}\delta\left\langle\gamma_\alpha(t_2)|\hat{O}_2|\gamma_\alpha(t_2)\right\rangle =& \left(\delta\langle\gamma_\alpha(t_2)|\right)\hat{O}_2|\gamma_\alpha(t_2)\rangle + \langle\gamma_\alpha(t_2)|\hat{O}_2\left(\delta|\gamma_\alpha(t_2)\rangle\right) \\ =& \frac{i}{\hbar}\left(\langle\gamma_\alpha^{(H)}|\int_{t_i}^{t_2}\mathrm{d}t_1\,\delta U(t_1)\hat{O}_1^{\dagger(H)}(t_1)e^{\frac{i}{\hbar}\hat{H}t_2}\right)\hat{O}_2|\gamma_\alpha(t_2)\rangle \\ & - \frac{i}{\hbar}\langle\gamma_\alpha(t_2)|\hat{O}_2\left(\int_{t_i}^{t_2}\mathrm{d}t_1\,\delta U(t_1)e^{-\frac{i}{\hbar}\hat{H}t_2}\hat{O}_1^{(H)}(t_1)|\gamma_\alpha^{(H)}\rangle\right) \\ =& \frac{i}{\hbar}\left(\langle\gamma_\alpha^{(H)}|\int_{t_i}^{t_2}\mathrm{d}t_1\,\delta U(t_1)\hat{O}_1^{\dagger(H)}(t_1)e^{\frac{i}{\hbar}\hat{H}t_2}\right)\hat{O}_2e^{-\frac{i}{\hbar}\hat{H}t_2}|\gamma_\alpha^{(H)}\rangle \\ & - \frac{i}{\hbar}\left(\langle\gamma_\alpha^{(H)}|e^{\frac{i}{\hbar}\hat{H}t_2}\right)\hat{O}_2\left(\int_{t_i}^{t_2}\mathrm{d}t_1\,\delta U(t_1)e^{-\frac{i}{\hbar}\hat{H}t_2}\hat{O}_1^{(H)}(t_1)|\gamma_\alpha^{(H)}\rangle\right) \\ =& -\frac{i}{\hbar}\int_{t_i}^{t_2}\mathrm{d}t_1\,\delta U(t_1)\langle\gamma_\alpha^{(H)}|\left[\hat{O}_2^{(H)}(t_2),\hat{O}_1^{(H)}(t_1)\right]_-|\gamma_\alpha^{(H)}\rangle\,, \end{aligned} \tag{2.19}$$

where we utilised the hermiticity of $\hat{O}_1$ in the last line and the brackets $\left[\hat{A},\hat{B}\right]_- = \hat{A}\hat{B}-\hat{B}\hat{A}$ denote a commutator. This equation can now be weighted with the appropriate prefactor of $\frac{1}{\mathcal{Z}}$ and then summed over α. Also, sending the initial time t_i to minus infinity and

including the upper bound of the integral into a Heaviside function, we can extend the integral to $\int_{-\infty}^{\infty} \mathrm{d}t_1$ yielding

$$\frac{\delta \left\langle \hat{O}_2(t_2) \right\rangle}{\delta U(t_1)} = -\frac{i}{\hbar}\theta(t_2 - t_1) \left\langle \left[\hat{O}_2^{(H)}(t_2), \hat{O}_1^{(H)}(t_1) \right]_- \right\rangle . \tag{2.20}$$

Hence, the desired response function is characterised by expectation values of time-ordered products of operators like $-i\theta(t_2 - t_1) \left\langle \hat{O}_2^{(H)}(t_2)\hat{O}_1^{(H)}(t_1) \right\rangle$. This is precisely the definition of a retarded Green's function. From the previously derived result one can relate dissipation in the investigated system describing with the fluctuations of the corresponding operators which are represented in form of the Green's functions here. This concept is also known as the fluctuation-dissipation theorem. The two examples to be named here are, on one hand, spins coupling to a magnetic field whose behaviour can be expressed in terms of the spin-spin correlation function (magnetic susceptibility) and, on the other hand, charged particles coupling to an electric field which is described by the current-current correlator (conductivity).

As it turns out, the precise evaluation of a retarded Green's function is rather unfeasible. A common way of circumventing this problem is to compute the imaginary-time ordered Green's function instead which is crucially easier to obtain. The remaining challenge lies then in an analytic continuation back to real times which, unfortunately, will not be performed during this thesis. For the majority of the following chapters, we investigate the imaginary-time ordered spin susceptibility

$$\chi_{ij}^{\mu\nu}(\tau) = \left\langle T_\tau \hat{S}_i^\mu(\tau)\hat{S}_j^\nu(0) \right\rangle , \qquad \text{with } \tau > 0 , \tag{2.21}$$

where T_τ acts on imaginary-time operators as T_t acts on real-time operators, see Eq. (2.13). Using the Abrikosov decomposition into fermionic operators (denoted by $\hat{f}^{(\dagger)}$ for the moment) from Eq. (1.2), the susceptibility is given by

$$\chi_{ij}^{\mu\nu}(\tau) = \sum_{\alpha,\beta,\gamma,\delta} \sigma_{\alpha\beta}^\mu \sigma_{\gamma\delta}^\nu \left\langle T_\tau \hat{f}_{i,\alpha}^\dagger(\tau)\hat{f}_{i,\beta}(\tau)\hat{f}_{j,\gamma}^\dagger(0)\hat{f}_{j,\delta}(0) \right\rangle . \tag{2.22}$$

Hence, we are looking for a systematic approach to determine imaginary-time ordered expectation values of fermionic and (in general) bosonic creation and annihilation operators.

So far, we can only deal with small perturbations in $\hat{H}$ (linear response). However, also for strong perturbations, the concept of Green's functions is often employed and can be very meaningful as we shall see later on. Let us provide the generic definition of a real-time ordered n-particle Green's function here, *i.e.*,

$$\begin{aligned} G^{(n)}(1,2,\ldots,n|1',2',\ldots,n') &= G^{(n)}(\alpha_1,\ldots,\alpha_n;t_1,\ldots,t_n|\alpha_{1'},\ldots,\alpha_{n'};t_{1'},\ldots,t_{n'}) \\ &= (-i)^n \left\langle T_t \left[a_{\alpha_1}(t_1)a_{\alpha_2}(t_2)\ldots a_{\alpha_n}(t_n)a_{\alpha_{n'}}^\dagger(t_{n'})\ldots a_{\alpha_{2'}}^\dagger(t_{2'})a_{\alpha_{1'}}^\dagger(t_{1'}) \right] \right\rangle , \end{aligned} \tag{2.23}$$

where the combined indices $1, 2, \ldots, n = \{\alpha_1, t_1\}, \{\alpha_2, t_2\}, \ldots, \{\alpha_n, t_n\}$ and $1', 2', \ldots, n' = \{\alpha_{1'}, t_{1'}\}, \{\alpha_{2'}, t_{2'}\}, \ldots, \{\alpha_{n'}, t_{n'}\}$ now label quantum numbers and real times. The operators $a_{\alpha_i}(t_i)$ and $a^\dagger_{\alpha_i}(t_i)$ denote fermionic *or* bosonic annihilation and creation operators of a particle in state α_i at time t_i in the Heisenberg picture. We omitted the superscript (H) and will always use the Heisenberg picture in the following [see Eqs. (2.18)] if operators depend on time and we do not note otherwise. Please note that the above definition does not include an additional factor of ζ^n which is commonly used in a different convention for the n-particle Green's function.

As already mentioned, instead of the above real-time function, we rather investigate the imaginary-time Green's function

$$\begin{aligned} G^{(n)}(1, 2, \ldots, n|1', 2', \ldots, n') &= G^{(n)}(\alpha_1, \ldots, \alpha_n; \tau_1, \ldots, \tau_n|\alpha_{1'}, \ldots, \alpha_{n'}; \tau_{1'}, \ldots, \tau_{n'}) \\ &= \left\langle T_\tau \left[a_{\alpha_1}(\tau_1) a_{\alpha_2}(\tau_2) \ldots a_{\alpha_n}(\tau_n) a^\dagger_{\alpha_{n'}}(\tau_{n'}) \ldots a^\dagger_{\alpha_{2'}}(\tau_{2'}) a^\dagger_{\alpha_{1'}}(\tau_{1'}) \right] \right\rangle . \end{aligned} \tag{2.24}$$

It is easier to compute since the imaginary time and energy are treated on equal footings, but one has to be aware of the fact that $a^\dagger_{\alpha_i}(\tau_i)$ is not the hermitian conjugate of $a_{\alpha_i}(\tau_i)$. With this definition, we can recast Eq. (2.22) in terms of the imaginary-time ordered Green's functions. The desired spin susceptibility can be obtained from

$$\chi^{\mu\nu}_{ij}(\tau) = \sum_{\alpha,\beta,\gamma,\delta} \sigma^\mu_{\alpha\beta} \sigma^\nu_{\gamma\delta} G^{(2)}\left(\{j, \delta\}, \{i, \beta\}; 0, \tau | \{j, \gamma\}, \{i, \alpha\}; 0, \tau\right) , \tag{2.25}$$

where the complete sets of quantum numbers are characterised by a lattice site and a spin index per fermionic operator.

2.1.3. Feynman path integrals

As we already know, the time-evolution operator plays an important role in the calculation of response functions. The Feynman path integral is simply defined as its matrix element of some particle governed by the Hamiltonian $H(\hat{p}, \hat{x})$[1] in an initial position at x_i at time t_i and a final position x_f at time t_f, *i.e.*,

$$U(x_f, t_f | x_i, t_i) = \langle x_f | e^{-\frac{i}{\hbar} H(\hat{p}, \hat{x})(t_f - t_i)} | x_i \rangle . \tag{2.26}$$

Due to the, in general, cumbersome evaluation of the occurring exponential, this entity can only be computed for infinitesimally small time differences at arbitrary precision. We therefore rewrite

$$\begin{aligned} U(x_f, t_f | x_i, t_i) &= \langle x_f | \left(e^{-\frac{i}{\hbar} H(\hat{p}, \hat{x})\epsilon} \right)^M | x_i \rangle \\ &= \int_{-\infty}^{\infty} \prod_{j=1}^{M-1} (\mathrm{d}x_j) \prod_{k=1}^{M} \left(\langle x_k | e^{-\frac{i}{\hbar} H(\hat{p}, \hat{x})\epsilon} | x_{k-1} \rangle \right) , \end{aligned} \tag{2.27}$$

[1] We consider the Hamiltonian to be a function of single-particle position and momentum operators for now.

where we renamed $x_i = x_0$ and $x_f = x_M$, discretised our real time according to

$$t_n = t_i + n\epsilon \qquad \epsilon = \frac{t_f - t_i}{M}, \tag{2.28}$$

and utilised the completeness relation of the position eigenstates $(M-1)$ times.

We now need to find a credible approximation for the infinitesimal evolution-operator matrix element $\langle x_n|e^{-\frac{i}{\hbar}H(\hat{p},\hat{x})\epsilon}|x_{n-1}\rangle$. The two criteria that this approximation needs to fulfill are that, in the limit $\epsilon \to 0$, the correct time evolution of the wave function as well as the proper action on position and momentum eigenstates $|x\rangle$ and $|p\rangle$ need to be guaranteed. Without giving a detailed proof (the interested reader is, for instance, encouraged to go through the according paragraphs in reference [135]), this can be achieved using normal-ordered operators. The normal order of some function of operators $O(\hat{p},\hat{x})$ is denoted as $:O(\hat{p},\hat{x}):$ and simply sorts all momentum operators on the left-hand side of all position operators. For instance, any Hamiltonian consisting of a kinetic term and a potential that is only a function of the position operator is automatically normal ordered

$$H_U(\hat{p},\hat{x}) = \frac{\hat{p}^2}{2m} + U(\hat{x}) =: H_U(\hat{p},\hat{x}): \ . \tag{2.29}$$

Using the normal order for the exponential of the desired matrix element yields

$$\begin{aligned}
\langle x_n|:e^{-\frac{i}{\hbar}H(\hat{p},\hat{x})\epsilon}:|x_{n-1}\rangle &= \int_{-\infty}^{\infty} \mathrm{d}p_n \ \langle x_n|p_n\rangle \langle p_n|:e^{-\frac{i}{\hbar}H(\hat{p},\hat{x})\epsilon}:|x_{n-1}\rangle \\
&= \int_{-\infty}^{\infty} \frac{\mathrm{d}p_n}{2\pi\hbar}\, e^{\frac{i}{\hbar}p_n x_n} \langle p_n|e^{-\frac{i}{\hbar}H(p_n,x_{n-1})\epsilon}|x_{n-1}\rangle \\
&= \int_{-\infty}^{\infty} \frac{\mathrm{d}p_n}{2\pi\hbar}\, e^{\frac{i}{\hbar}p_n(x_n-x_{n-1})} e^{-\frac{i}{\hbar}H(p_n,x_{n-1})\epsilon} \, .
\end{aligned} \tag{2.30}$$

The key benefit of using the normal ordered approximation of our exponential is that it yields convergent momentum integrals in real time as well as in imaginary time due to an overall factor of $e^{-\frac{i\epsilon}{\hbar}\frac{p^2}{2m}}$ or $e^{-\frac{\epsilon}{\hbar}\frac{p^2}{2m}}$ from the kinetic part of the Hamiltonian which guarantees convergence for physical systems. We evaluate the infinitesimal evolution operator using the identity

$$\int_{-\infty}^{\infty} \mathrm{d}p\, e^{ap-bp^2} = \frac{\sqrt{\pi}}{\sqrt{b}} e^{\frac{a^2}{4b}} \, . \tag{2.31}$$

This yields that

$$\begin{aligned}\langle x_n|:e^{-\frac{i}{\hbar}H_U(\hat{p},\hat{x})\epsilon}:|x_{n-1}\rangle &= \int_{-\infty}^{\infty}\frac{\mathrm{d}p_n}{2\pi\hbar}\,e^{\frac{i}{\hbar}p_n(x_n-x_{n-1})-\frac{i}{\hbar}\left(\frac{p_n^2}{2m}+U(x_{n-1})\right)\epsilon}\\ &= \frac{\sqrt{\pi}}{2\pi\hbar}\sqrt{\frac{2\hbar m}{i\epsilon}}e^{\frac{im}{2\hbar\epsilon}(x_n-x_{n-1})^2-\frac{i}{\hbar}U(x_{n-1})\epsilon}\\ &= \frac{\sqrt{m}}{\sqrt{2\pi\hbar i\epsilon}}e^{\frac{i}{\hbar}\left(\frac{m}{2\epsilon}(x_n-x_{n-1})^2-U(x_{n-1})\epsilon\right)}\,. \end{aligned}\tag{2.32}$$

It is important to note that Eq. (2.31) mathematically only holds if $\mathrm{Re}[b]>0$ which is technically not the case in the current real-time formalism. Nevertheless, we are able to use the resulting expressions as a formal result. The reason behind this is that the momentum integrals are limited in actual physical systems due to, for instance, relativistic effects. A similar argument would also hold for real-space integrals due to the limitation of space. In the end, such an integration cutoff has the same effect as a finite positive $\mathrm{Re}[b]$ and we will not need to revisit this issue because of the prospective imaginary-time formalism.

Inserting Eq. (2.32) into Eq. (2.27) and taking the limit $\epsilon\to 0$ or $M\to\infty$, correspondingly, we find for the Feynman path integral

$$U(x_f,t_f|x_i,t_i)=\lim_{M\to\infty}\int_{-\infty}^{\infty}\prod_{j=1}^{M-1}(\mathrm{d}x_j)\,\left(\frac{m}{2\pi\hbar i\epsilon}\right)^{\frac{M}{2}}e^{\frac{i\epsilon}{\hbar}\sum_{n=1}^{M}\left(\frac{m}{2}\left(\frac{x_n-x_{n-1}}{\epsilon}\right)^2-U(x_{n-1})\right)}\,.\tag{2.33}$$

This result is holds for a single particle in one dimension. The extension to three dimensions is trivial and produces

$$U(\boldsymbol{r}_f,t_f|\boldsymbol{r}_i,t_i)=\lim_{M\to\infty}\int_{-\infty}^{\infty}\prod_{j=1}^{M-1}(\mathrm{d}^3r_j)\,\left(\frac{m}{2\pi\hbar i\epsilon}\right)^{\frac{3M}{2}}e^{\frac{i\epsilon}{\hbar}\sum_{n=1}^{M}\left(\frac{m}{2}\left(\frac{\boldsymbol{r}_n-\boldsymbol{r}_{n-1}}{\epsilon}\right)^2-U(\boldsymbol{r}_{n-1})\right)}\,,\tag{2.34}$$

where we defined the volume element as $\mathrm{d}^3r_j=\mathrm{d}x_j\,\mathrm{d}y_j\,\mathrm{d}z_j$.

The set of points $\{x_0,x_1,\ldots,x_M\}$ marks a trajectory $x(t)$ with discrete time steps $x(t_n)=x_n$ which does neither need to be continuous nor differentiable, not even in the limit $\epsilon\to 0$. Nevertheless, we formally rewrite for this limit

$$\frac{x_n-x_{n-1}}{\epsilon}\longrightarrow\frac{\partial x}{\partial t}\,,\tag{2.35a}$$

$$\epsilon\sum_{n=1}^{M}\frac{m}{2}\left(\frac{x_n-x_{n-1}}{\epsilon}\right)\longrightarrow\int_{t_i}^{t_f}\mathrm{d}t\,\frac{m}{2}\left(\frac{\partial x}{\partial t}\right)^2\,,\tag{2.35b}$$

$$\epsilon\sum_{n=1}^{M}V(x_{n-1})\longrightarrow\int_{t_i}^{t_f}\mathrm{d}t\,V[x(t)]\,.\tag{2.35c}$$

It is crucial to remember that this is only a formal representation in which the rectangular brackets denote that V is now a functional depending on the possible trajectories $x(t)$. Any calculation now needs to be performed on the basis of discrete time steps, taking their number to infinity afterwards. Using this short-hand notation, we find for the Feynman path integral in one dimension

$$U(x_f, t_f | x_i, t_i) = \int_{x_i, t_i}^{x_f, t_f} \mathcal{D}\left[x(t)\right] \, e^{\frac{i}{\hbar} S[x(t)]} \,, \tag{2.36}$$

where the action is defined as the time integral of the Lagrangian $L\left[x(t)\right]$

$$S\left[x(t)\right] = \int_{t_i}^{t_f} \mathrm{d}t \, L\left[x(t)\right] = \int_{t_i}^{t_f} \mathrm{d}t \, \left(\frac{m}{2} \left(\frac{\partial x}{\partial t} \right)^2 - V[x(t)] \right) \tag{2.37}$$

and the functional integral needs to be understood as its discrete version that integrates over all possible trajectories starting at (x_i, t_i) and ceasing at (x_f, t_f)

$$\int_{x_i, t_i}^{x_f, t_f} \mathcal{D}\left[x(t)\right] = \lim_{M \to \infty} \int_{-\infty}^{\infty} \prod_{j=1}^{M-1} \left(\mathrm{d}x_j\right) \, \left(\frac{m}{2\pi\hbar i \epsilon} \right)^{\frac{M}{2}} \,. \tag{2.38}$$

The three-dimensional expression is completely analogue. Only the exponent $(M/2) \to (3M/2)$ changes and the integrations run over entire real spaces $\mathbb{R}^3$. For completeness, we also write down the corresponding equations

$$U(\boldsymbol{r}_f, t_f | \boldsymbol{r}_i, t_i) = \int_{\boldsymbol{r}_i, t_i}^{\boldsymbol{r}_f, t_f} \mathcal{D}\left[\boldsymbol{r}(t)\right] \, e^{\frac{i}{\hbar} S[\boldsymbol{r}(t)]} \,, \tag{2.39a}$$

$$S\left[\boldsymbol{r}(t)\right] = \int_{t_i}^{t_f} \mathrm{d}t \, \left(\frac{m}{2} \left(\frac{\partial \boldsymbol{r}}{\partial t} \right)^2 - V[\boldsymbol{r}(t)] \right) \,, \tag{2.39b}$$

$$\int_{\boldsymbol{r}_i, t_i}^{\boldsymbol{r}_f, t_f} \mathcal{D}\left[\boldsymbol{r}(t)\right] = \lim_{M \to \infty} \int_{-\infty}^{\infty} \prod_{j=1}^{M-1} \left(\mathrm{d}^3 r_j\right) \, \left(\frac{m}{2\pi\hbar i \epsilon} \right)^{\frac{3M}{2}} \,. \tag{2.39c}$$

In this form, the Feynman path integral representation of the time-evolution operator has a clear physical interpretation, *i.e.*, the sum running over all paths p starting from (x_i, t_i) ending at (x_f, t_f) of the corresponding $e^{\frac{i}{\hbar} S[p]}$ where $S[p]$ is the action acquired along the path p. This explicit notation called the Lagrangian form of the path integral, however, is only valid if the Hamiltonian is of the type $H_U(\hat{p}, \hat{x}) = \frac{\hat{p}^2}{2m} + U(\hat{x})$. For a general Hamiltonian $H(\hat{p}, \hat{x})$, we are not able to perform the momentum integration from

Eq. (2.30). In this case, we have to evaluate the Hamiltonian form of the path integral which is more general but also requires greater care handling the integrations. It reads

$$U(x_f,t_f|x_i,t_i) = \int\limits_{x_i,t_i}^{x_f,t_f} \mathcal{D}\left[x(t)\right]\,\mathcal{D}\left[p(t)\right]\,e^{\frac{i}{\hbar}\int\limits_{-\infty}^{\infty}\mathrm{d}t\left[p(t)\frac{\partial x(t)}{\partial t}-H[p(t),x(t)]\right]}, \tag{2.40a}$$

$$\int\limits_{x_i,t_i}^{x_f,t_f} \mathcal{D}\left[x(t)\right]\,\mathcal{D}\left[p(t)\right] = \lim_{M\to\infty}\int\limits_{-\infty}^{\infty}\prod_{j=1}^{M-1}(\mathrm{d}x_j)\prod_{k=1}^{M}\left(\frac{\mathrm{d}p_k}{2\pi\hbar}\right), \tag{2.40b}$$

where the real-space coordinates fulfill the same boundary conditions as before and the moment coordinates have none thereof. This, again, is only a formal expression and the $M\to\infty$ limit of the discretised-time version needs to be considered for a concrete evaluation.

In both forms, Lagrangian and Hamiltonian, the path integral representation of the evolution operator includes the two fundamental phenomena of quantum mechanics. Interference is already included due to the summation over all possible paths and the superposition principle directly follows from the mathematical identity

$$U(x_f,t_f|x_i,t_i) = \int \mathrm{d}x\, U(x_f,t_f|x,t)U(x,t|x_i,t_i) \tag{2.41}$$

at any time $t\in(t_i,t_f)$. One natural approximation of the path integral is the so-called stationary phase approximation. Here, the limit in which $\hbar$ is very small is considered and it turns out that only paths surrounding the classical trajectory will contribute to the transmission amplitude.

The great benefit of the path integral formalism is that it automatically generates time-ordered products. In the Hamiltonian form, for instance, it turns out that for any two operators $O_1(\hat{x},t_1)$ and $O_2(\hat{x},t_2)$ acting at times $t_1\geq t_2$, the expectation value

$$\begin{aligned}\langle x_f|T_t O_1(\hat{x},t_1)O_2(\hat{x},t_2)e^{-\frac{i}{\hbar}\int\limits_{t_i}^{t_f}\mathrm{d}t\,\hat{H}(t)}|x_i\rangle = &\int\limits_{x_i,t_i}^{x_f,t_f}\mathcal{D}\left[x(t)\right]\,\mathcal{D}\left[p(t)\right]\,O_1(x(t_1))O_2(x(t_2))\\ &\times e^{\frac{i}{\hbar}\int\limits_{-\infty}^{\infty}\mathrm{d}t\left[p(t)\frac{\partial x(t)}{\partial t}-H[p(t),x(t)]\right]}\end{aligned} \tag{2.42}$$

or equivalently, in the Lagrangian form

$$\langle x_f|T_t O_1(\hat{x},t_1)O_2(\hat{x},t_2)e^{-\frac{i}{\hbar}\int\limits_{t_i}^{t_f}\mathrm{d}t\,\hat{H}(t)}|x_i\rangle = \int\limits_{x_i,t_i}^{x_f,t_f}\mathcal{D}\left[x(t)\right]\,O_1(x(t_1))O_2(x(t_2))e^{\frac{i}{\hbar}\int\limits_{-\infty}^{\infty}\mathrm{d}t\,L[x(t)]}. \tag{2.43}$$

Note that, on the right-hand-side of both equations, there is no time-ordering operator anymore since the discretised time in the path integrals and the normal order of our Hamiltonian automatically guarantee the correct time order.

So far, we know how to compute time-ordered products of operators using Feynman's path integral for the evolution operator. As we saw in the previous section, for any kind of statistical analysis of a quantum mechanical system, we have to calculate its partition function. This will be possible in an imaginary-time version of the path integral.

2.1.4. Imaginary-time path integral

Let us at this point consider the single-particle partition function

$$\mathcal{Z} = \operatorname{tr} e^{-\beta \hat{H}} = \int \mathrm{d}x \, \langle x | e^{-\beta \hat{H}} | x \rangle \,, \tag{2.44}$$

which can trivially be rewritten using the imaginary-time evolution operator

$$\mathcal{Z} = \int_{(x;\tau_f)} \mathrm{d}x \, U(x;\tau_f|x;\tau_i) \,, \tag{2.45a}$$

$$U(x;\tau_f|x;\tau_i) = \langle x | e^{-\frac{1}{\hbar}\hat{H}(\tau_f - \tau_i)} | x \rangle = \int_{(x;\tau_i)} \mathcal{D}\left[x(\tau)\right] \, e^{-\frac{1}{\hbar}\int_0^{\beta\hbar} \mathrm{d}\tau \, H[x(\tau)]} \,, \tag{2.45b}$$

where we defined $\tau_f - \tau_i = \beta\hbar$. This, as indicated by the integration variables, is the imaginary-time equivalent of the Lagrangian path integral. The appearance of the Hamiltonian in this form is caused by the Wick rotation

$$t = -i\tau \,, \tag{2.46a}$$

$$\frac{\partial x}{\partial t} = i \frac{\partial x}{\partial \tau} \,, \tag{2.46b}$$

$$\frac{i}{\hbar} \int_{t_i}^{t_f} \mathrm{d}t \, \left(\frac{m}{2} \left(\frac{\partial x}{\partial t} \right)^2 - V(x(t)) \right) = -\frac{1}{\hbar} \int_{\tau_i}^{\tau_f} \mathrm{d}\tau \, \left(\frac{m}{2} \left(\frac{\partial x}{\partial \tau} \right)^2 + V(x(\tau)) \right) . \tag{2.46c}$$

The integration measure appearing is also mathematically rigorous in imaginary time [135] and follows from identical considerations as for real times. This enables us to find a surprisingly compact way of writing down the partition function

$$\mathcal{Z} = \int \mathrm{d}x \int_{x(0)=x}^{x(\beta\hbar)=x} \mathcal{D}[x(\tau)] \, e^{-\frac{1}{\hbar}\int_0^{\beta\hbar} \mathrm{d}\tau \, H[x(\tau)]} \,. \tag{2.47}$$

Finally, we should also denote the partition function of an N-particle system at this point. Using a many-body Hamiltonian of the type

$$\hat{H} = \sum_{j=1}^{N} \frac{p_j^2}{2m} + \frac{1}{2} \sum_{j \neq k}^{N} V(\hat{x}_j - \hat{x}_k) \,, \tag{2.48}$$

we find that

$$\begin{aligned}\mathcal{Z}_N &= \frac{1}{N!}\sum_P \zeta^P \int \prod_{j=1}^{N} (\mathrm{d}x_j)\ \langle x_{P(1)}, x_{P(2)}, \ldots, x_{P(N)}|e^{-\beta\hat{H}}|x_1, x_2, \ldots, x_N\rangle \\ &= \frac{1}{N!}\sum_P \zeta^P \int\limits_{\substack{x_1(\hbar\beta)\,=\,x_{P(1)}(0)\\ \vdots \\ x_N(\hbar\beta)\,=\,x_{P(N)}(0)}} \prod_{k=1}^{N} \left(\mathcal{D}\left[x_k(\tau)\right]\right)\ e^{-\frac{1}{\hbar}\int_0^{\beta\hbar}\mathrm{d}\tau\left[\sum_{j=1}^{N}\frac{1}{2m}\left(\frac{\partial x_j(\tau)}{\partial\tau}\right)^2+\frac{1}{2}\sum_{j\neq k}^{N}V(x_j(\tau)-x_k(\tau))\right]}\end{aligned} \tag{2.49}$$

where $\{|x_1, x_2, \ldots, x_N\rangle\}$ is an orthonormal basis of the N-particle Hilbert space and the prefactor $\sum_P \zeta^P$ guarantees their correct symmetrisation for bosons ($\zeta = 1$) or anti symmetrisation for fermions ($\zeta = -1$).

This concludes our preliminaries and we continue in the next section with developing an efficient technique of calculating Green's functions based on the functional integral formalism. There are different ways that could be chosen this point. The functional integral, however, is closely related to the functional renormalisation group upon which we will build our theory later on.

2.2. Functional integral

Up to now, we calculated a quantum many-body system's partition function in the Feynman path integral representation of the imaginary-time evolution operator using real-space and momentum eigenstates. However, often it is desired to write the Hamiltonian of a many-body problem in terms of creation and annihilation operators as we shall see later on for our spin systems. In this case, it is convenient to rewrite the theory in the basis of coherent states. The path integral then turns into what is called a functional integral. In order to provide the largest amount of clarity for the following chapters of this thesis, we start this section by presenting the general properties of this special representation.

2.2.1. Coherent states

The coherent states are a non-orthonormal basis of the fermionic or bosonic Fock space. They are eigenstates of all single-particle annihilation operators which, in contrast to eigenstates of creation operators, is a meaningful concept because any state in Fock space has a contribution with a minimal but not necessarily with a maximal occupation number. Since a creation operator always increases the minimal occupation number by one, it cannot have eigenstates. For the annihilation operators, this is not the case.

Let us consider a general vector in Fock space denoted by

$$|\gamma\rangle = \sum_{n=0}^{\infty}\sum_{\alpha_1,\ldots,\alpha_n} \gamma_{\alpha_1\ldots\alpha_n}|\alpha_1\ldots\alpha_n\rangle\,, \tag{2.50}$$

where $\{|\alpha_1 \dots \alpha_n\rangle\}$ is an orthonormal set of eigenstates of the anti symmetrised (symmetrised) n-particle Hilbert space $\mathcal{F}_n = \mathcal{A}\mathcal{H}_n$ ($\mathcal{B}_n = \mathcal{S}\mathcal{H}_n$). Here, $\mathcal{A}$ ($\mathcal{S}$) projects onto the fully anti symmetric (symmetric) subspace of $\mathcal{H}_n$, and

$$\mathcal{H}_n = \begin{cases} |0\rangle, & \text{for } n = 0\,, \\ \mathcal{H}, & \text{for } n = 1\,, \\ \bigotimes_{k=1}^{n} \mathcal{H}, & \text{for } n \geq 2\,, \end{cases} \tag{2.51}$$

where $\mathcal{H}$ is the single-particle Hilbert space. The fermionic (bosonic) Fock space $\mathcal{F}$ ($\mathcal{B}$) is defined as the direct sum of all anti-symmetrised (symmetrised) n-particle Hilbert space

$$\mathcal{F} = \bigoplus_{n=0}^{\infty} \mathcal{F}_n\,, \tag{2.52a}$$

$$\mathcal{B} = \bigoplus_{n=0}^{\infty} \mathcal{B}_n\,. \tag{2.52b}$$

Now, we require for the state $|\gamma\rangle$ to be an eigenstate of the annihilation operator a_{α_j}

$$a_{\alpha_j}|\gamma\rangle = \gamma_{\alpha_j}|\gamma\rangle \tag{2.53}$$

which automatically implies that due to the commutation relation of the bosonic and the anti-commutation relation of the fermionic operators

$$\left[\gamma_{\alpha_j}, \gamma_{\alpha_k}\right]_{-\zeta} = \gamma_{\alpha_j}\gamma_{\alpha_k} - \zeta\gamma_{\alpha_k}\gamma_{\alpha_j} = 0\,, \tag{2.54}$$

i.e., the coefficients γ_{α_j} are complex numbers for a bosonic theory and Graßmann numbers for a fermionic theory. Even though, up to keeping track of ζ, the final results of this section do not differ for both cases, it is still useful to separate them in the beginning.

Bosonic coherent states

The bosonic coherent state from above can be written down in an easy fashion

$$|\gamma\rangle = e^{\sum_{\alpha_j} \gamma_{\alpha_j} a^\dagger_{\alpha_j}}|0\rangle\,, \qquad \Longrightarrow \qquad a_{\alpha_j}|\gamma\rangle = \gamma_{\alpha_j}|\gamma\rangle\,, \qquad a^\dagger_{\alpha_j}|\gamma\rangle = \frac{\partial}{\partial\gamma_{\alpha_j}}|\gamma\rangle\,, \tag{2.55a}$$

$$\langle\gamma| = \langle 0|e^{\sum_{\alpha_j} \gamma^*_{\alpha_j} a_{\alpha_j}}\,, \qquad \Longrightarrow \qquad \langle\gamma|a^\dagger_{\alpha_j} = \langle\gamma|\gamma^*_{\alpha_j}\,, \qquad \langle\gamma|a_{\alpha_j} = \frac{\partial}{\partial\gamma^*_{\alpha_j}}\langle\gamma|\,. \tag{2.55b}$$

where all the γ_{α_j} denote complex numbers. From these expressions, it is easy to derive that the overlap between two coherent states is $\langle\gamma|\gamma'\rangle = e^{\sum_{\alpha_j} \gamma^*_{\alpha_j}\gamma'_{\alpha_j}}$ which means that they are not orthonormal. Despite this, they form an over-complete basis of the Fock space which is denoted in the closure relation

$$\int \prod_{\alpha_j} \frac{\mathrm{d}\gamma^*_{\alpha_j}\mathrm{d}\gamma_{\alpha_j}}{2\pi i}\, e^{-\sum_{\alpha_j} \gamma^*_{\alpha_j}\gamma_{\alpha_j}} |\gamma\rangle\langle\gamma| = \mathbb{1}\,, \tag{2.56}$$

where $\mathbb{1}$ denotes the unit operator in Fock space and the integral measure extends over all values for the real and imaginary part of the complex γ_{α_j}

$$\frac{\mathrm{d}\gamma^*_{\alpha_j}\mathrm{d}\gamma_{\alpha_j}}{2\pi i} = \frac{\mathrm{dRe}(\gamma_{\alpha_j})\,\mathrm{dIm}(\gamma_{\alpha_j})}{\pi}\,. \tag{2.57}$$

Let us now consider our system to be in some state $|\phi\rangle$. The coefficient to find it in the coherent state $|\gamma\rangle$ upon measurement is then given by $\langle\gamma|\phi\rangle = \phi(\gamma^*)$ which is by definition of the bra $\langle\gamma|$ from Eq. (2.55b) a function of the complex conjugated parameters γ^*. It is then clear from the previous considerations that

$$\langle\gamma|a_{\alpha_j}|\phi\rangle = \frac{\partial}{\partial\gamma^*_{\alpha_j}}\phi(\gamma^*)\,, \tag{2.58a}$$

$$\langle\gamma|a^\dagger_{\alpha_j}|\phi\rangle = \gamma^*_{\alpha_j}\phi(\gamma^*)\,. \tag{2.58b}$$

Therefore, we formally rewrite $a_{\alpha_j} = \frac{\partial}{\partial\gamma^*_{\alpha_j}}$ and $a^\dagger_{\alpha_j} = \gamma^*_{\alpha_j}$ with the corresponding commutation relations

$$\left[\frac{\partial}{\partial\gamma_{\alpha_j}}, \frac{\partial}{\partial\gamma_{\alpha_k}}\right]_- = \left[\frac{\partial}{\partial\gamma^*_{\alpha_j}}, \frac{\partial}{\partial\gamma^*_{\alpha_k}}\right]_- = 0 \tag{2.59a}$$

$$\left[\gamma_{\alpha_j}, \gamma_{\alpha_k}\right]_- = \left[\gamma^*_{\alpha_j}, \gamma^*_{\alpha_k}\right]_- = 0\,, \tag{2.59b}$$

$$\left[\frac{\partial}{\partial\gamma_{\alpha_j}}, \gamma_{\alpha_k}\right]_- = \left[\frac{\partial}{\partial\gamma^*_{\alpha_j}}, \gamma^*_{\alpha_k}\right]_- = \delta_{\alpha_j,\alpha_k}\,. \tag{2.59c}$$

Finally, we provide a formula for calculating the trace of an operator in the basis of bosonic coherent states, *i.e.*,

$$\mathrm{tr}\left(\hat{A}\right) = \int\prod_{\alpha_j}\frac{\mathrm{d}\gamma^*_{\alpha_j}\mathrm{d}\gamma_{\alpha_j}}{2\pi i}\,e^{-\sum_{\alpha_j}\gamma^*_{\alpha_j}\gamma_{\alpha_j}}\,\langle\gamma|\hat{A}|\gamma\rangle\,. \tag{2.60}$$

Coherent states have a true physical correspondence in the bosonic scenario. They naturally occur when we take the classical limit of a field theory, so if the commutators of the field operators $\hat{\chi}^\dagger(x) = \sum_{\alpha_j}\langle\alpha_j|x\rangle\,a^\dagger_{\alpha_j}$ and $\hat{\chi}(x) = \sum_{\alpha_j}\langle x|\alpha_j\rangle\,a_{\alpha_j}$ are sent to zero. Then, the definition of a classical field $\gamma_\mathrm{c}(x)$ is identical to considering the coherent state $|\gamma_\mathrm{c}\rangle = e^{\int\mathrm{d}x\,\gamma_\mathrm{c}(x)\hat{\chi}^\dagger(x)}|0\rangle$.

Fermionic coherent states

Let us now repeat the thoughts from the previous section for fermions. For this, we need to define a Graßmann algebra using the set of its generators denoted by $\{\gamma_{\alpha_j}\}$, for $j = 1, 2, \ldots, n$ and n not being further specified at the moment. The generators fulfill the anti-commutation relation

$$\left[\gamma_{\alpha_j}, \gamma_{\alpha_k}\right]_+ = \gamma_{\alpha_j}\gamma_{\alpha_k} + \gamma_{\alpha_k}\gamma_{\alpha_j} = 0\,. \tag{2.61}$$

This automatically implies that $\gamma_{\alpha_j}^2 \equiv 0$ and all Graßmann numbers of this algebra are now defined as the possible linear combinations from the set of all distinct products of the generators $\{1, \gamma_{\alpha_1}, \gamma_{\alpha_1}\gamma_{\alpha_2}, \ldots, \gamma_{\alpha_1}\gamma_{\alpha_2}\ldots\gamma_{\alpha_n}\}$ with complex coefficients.

If we have an algebra at hand with an even number of generators, *e.g.*, $n = 2p$, $p \in \mathbb{N}$, we can associate p of them as the complex conjugate of the remaining p and one has to note that the complex conjugation acts on any product of Graßmann generators as

$$(\gamma_{\alpha_1}\gamma_{\alpha_2}\ldots\gamma_{\alpha_n})^* = \gamma_{\alpha_n}^*\ldots\gamma_{\alpha_2}^*\gamma_{\alpha_1}^*\,, \tag{2.62}$$

whereas $\left(c\gamma_{\alpha_j}\right)^* = c^*\gamma_{\alpha_j}^*$, $c \in \mathbb{C}$. Since now any conjugate pair γ_{α_j} and $\gamma_{\alpha_j}^*$ fulfills Eq. (2.61), it directly follows that $\frac{\partial}{\partial\gamma_{\alpha_j}}\left(\gamma_{\alpha_j}^*\gamma_{\alpha_j}\right) = -\gamma_{\alpha_j}^*$. Hence, also the partial derivatives anti commute

$$\left[\frac{\partial}{\partial\gamma_{\alpha_j}}, \frac{\partial}{\partial\gamma_{\alpha_j}^*}\right]_+ = 0\,. \tag{2.63}$$

Because there is no analogue of Riemann's integral for Graßmann generators, we have to define a meaningful Graßmann integral. This is provided by

$$\int \mathrm{d}\gamma_{\alpha_j}\, 1 = \int \mathrm{d}\gamma_{\alpha_j}^*\, 1 \quad = 0\,, \tag{2.64a}$$

$$\int \mathrm{d}\gamma_{\alpha_j}\, \gamma_{\alpha_j} = \int \mathrm{d}\gamma_{\alpha_j}^*\, \gamma_{\alpha_j}^* = 1\,, \tag{2.64b}$$

which implies that the Graßmann integration is identical to the Graßmann differentiation. Also, one should note that the differentials appearing in the integrals are no Graßmann numbers, and that, according to $\left(\gamma_{\alpha_x}^{(*)}\right)^2 = 0$, any function A depending only on a particular γ_{α_x} or any function B depending on both, γ_{α_x} and $\gamma_{\alpha_x}^*$ for a fixed x, can be written as

$$A(\gamma_{\alpha_x}) = A_0 + A_1\gamma_{\alpha_x}\,, \tag{2.65a}$$

$$B(\gamma_{\alpha_x}, \gamma_{\alpha_x}^*) = B_{00} + B_{01}\gamma_{\alpha_x} + B_{10}\gamma_{\alpha_x}^* + B_{11}\gamma_{\alpha_x}^*\gamma_{\alpha_x}\,. \tag{2.65b}$$

In order to construct fermionic coherent states, we now need to define a generalised Fock space containing any linear combination of states from the fermionic Fock space with coefficients from a Graßmann algebra generated by $\{\gamma_{\alpha_1}^*, \gamma_{\alpha_1}, \gamma_{\alpha_2}^*, \gamma_{\alpha_2}, \ldots, \gamma_{\alpha_n}^*, \gamma_{\alpha_n}\}$, so one generator each for all creation and annihilation operators $a_{\alpha_j}^\dagger$ and a_{α_j} from the fermion system. We require that the Graßmann generators and the fermionic operators anti commute amongst each other

$$\left[\gamma_{\alpha_j}^{(*)}, a_{\alpha_k}^{(\dagger)}\right]_+ = 0\,, \tag{2.66}$$

and that the hermitian conjugation therefore acts on their products according to

$$\left(\gamma_{\alpha_j}a_{\alpha_k}\right)^\dagger = a_{\alpha_k}^\dagger\gamma_{\alpha_j}^*\,. \tag{2.67}$$

Then we are able to give an expression for the fermionic coherent states

$$|\gamma\rangle = e^{-\sum\limits_{\alpha_j} \gamma_{\alpha_j} a^\dagger_{\alpha_j}} |0\rangle = \prod_{\alpha_j} \left(1 - \gamma_{\alpha_j} a^\dagger_{\alpha_j}\right) |0\rangle \,, \tag{2.68}$$

where the second identity holds because of $\left(\gamma_{\alpha_j} a^\dagger_{\alpha_j}\right)^2 = 0$. The adjoint equation is

$$\langle\gamma| = \langle 0| e^{-\sum\limits_{\alpha_j} a_{\alpha_j} \gamma^*_{\alpha_j}} \tag{2.69}$$

and the Graßmann derivatives can be expressed via

$$a^\dagger_{\alpha_j} |\gamma\rangle = -\frac{\partial}{\partial \gamma_{\alpha_j}} |\gamma\rangle \,, \tag{2.70a}$$

$$\langle\gamma| a_{\alpha_j} = \frac{\partial}{\partial \gamma^*_{\alpha_j}} \langle\gamma| \,. \tag{2.70b}$$

This, again, encourages us to formally recast the operators according to their action in the coherent state basis for fermions

$$a_{\alpha_j} = \frac{\partial}{\partial \gamma^*_{\alpha_j}} \,, \qquad a^\dagger_{\alpha_j} = \gamma^*_{\alpha_j} \,, \tag{2.71}$$

with the corresponding anti-commutation relations

$$\left[\frac{\partial}{\partial \gamma_{\alpha_j}}, \frac{\partial}{\partial \gamma_{\alpha_k}}\right]_+ = \left[\frac{\partial}{\partial \gamma^*_{\alpha_j}}, \frac{\partial}{\partial \gamma^*_{\alpha_k}}\right]_+ = 0 \tag{2.72a}$$

$$\left[\gamma_{\alpha_j}, \gamma_{\alpha_k}\right]_+ = \left[\gamma^*_{\alpha_j}, \gamma^*_{\alpha_k}\right]_+ = 0 \,, \tag{2.72b}$$

$$\left[\frac{\partial}{\partial \gamma_{\alpha_j}}, \gamma_{\alpha_k}\right]_+ = \left[\frac{\partial}{\partial \gamma^*_{\alpha_j}}, \gamma^*_{\alpha_k}\right]_+ = \delta_{\alpha_j, \alpha_k} \,. \tag{2.72c}$$

One of the great benefits when coherent states are used is that formally very identical equations arise for fermions and bosons. For instance, the overlap of two coherent states again is

$$\langle\gamma|\gamma'\rangle = e^{\sum\limits_{\alpha_j} \gamma^*_{\alpha_j} \gamma'_{\alpha_j}} \,. \tag{2.73}$$

Due to the coherent state's over completeness in the fermionic (*not the generalised!*) Fock space

$$\int \prod_{\alpha_j} \mathrm{d}\gamma^*_{\alpha_j} \mathrm{d}\gamma_{\alpha_j} \, e^{-\sum\limits_{\alpha_j} \gamma^*_{\alpha_j} \gamma_{\alpha_j}} |\gamma\rangle\langle\gamma| = \mathbb{1} \,, \tag{2.74}$$

we are able to expand every physical fermionic state in terms of the coherent states as well. The trace in the fermionic Fock space can be evaluated as

$$\mathrm{tr}\left(\hat{A}\right) = \int \prod_{\alpha_j} \mathrm{d}\gamma^*_{\alpha_j} \mathrm{d}\gamma_{\alpha_j} \, e^{-\sum\limits_{\alpha_j} \gamma^*_{\alpha_j} \gamma_{\alpha_j}} \, \langle -\gamma | \hat{A} | \gamma \rangle \,. \tag{2.75}$$

Despite the fact that every physical fermionic state can be expressed in terms of the coherent states, unlike in the bosonic case, there are no physical fermionic coherent states since they are not part of the physical Fock space. Since we already saw that coherent states emerge by taking the classical limit, this can be well understood by considering that there are indeed no classical fermions.

Due to the similar expressions for fermions and bosons, we are now able to write down the path integral from Sec. 2.1.3 in the basis of coherent states. This expression is then known as the functional integral.

2.2.2. Coherent state path integral

Let us consider our system to be in the initial coherent state $|\gamma_i\rangle$ with components $\gamma_{\alpha_j,i}$ and we are again interested in its transition amplitude with some final state $\langle\gamma_f|$ with components $\gamma^*_{\alpha_j,f}$ after evolving in time under some Hamiltonian $H\left(a^\dagger_{\alpha_j}, a_{\alpha_j}\right)$ which has normal form, *i.e.*, all creation operators occur on the left side of all annihilation operators in the second quantisation language. The coherent states can now be fermionic or bosonic, and the coefficients are Graßmann or complex numbers, respectively. We utilise the same time discretisation as before and denote

$$\gamma_{\alpha_j,0} = \gamma_{\alpha_j,i}\,, \qquad \gamma^*_{\alpha_j,M} = \gamma^*_{\alpha_j,f}\,, \tag{2.76}$$

$$\epsilon = \frac{t_f - t_i}{M}\,. \tag{2.77}$$

The matrix element of the evolution operator is then given by

$$\begin{aligned} U(\gamma^*_{\alpha_j,f}, t_f|\gamma_{\alpha_j,i}, t_i) &= \langle\gamma_f|e^{-\frac{i}{\hbar}H\left(a^\dagger_{\alpha_j},a_{\alpha_j}\right)(t_f-t_i)}|\gamma_i\rangle \\ &= \lim_{M\to\infty}\int\prod_{k=1}^{M-1}\prod_{\alpha_j}\frac{\mathrm{d}\gamma_{\alpha_j,k}\,\mathrm{d}\gamma^*_{\alpha_j,k}}{\mathcal{N}}\,e^{-\sum\limits_{k=1}^{M-1}\sum\limits_{\alpha_j}\gamma^*_{\alpha_j,k}\gamma_{\alpha_j,k}} \\ &\quad\times e^{-\sum\limits_{k=1}^{M-1}\left(\sum\limits_{\alpha_j}\gamma^*_{\alpha_j,k}\gamma_{\alpha_j,k-1}-\frac{i}{\hbar}H(\gamma^*_{\alpha_j,k},\gamma_{\alpha_j,k-1})\right)}\,, \end{aligned} \tag{2.78}$$

where we now defined

$$\mathcal{N} = \begin{cases} 2\pi i\,, \text{ for bosons} \\ 1\,, \text{ for fermions}\,, \end{cases} \tag{2.79}$$

in order to arrive at the same formula for both types of fundamental quantum particles. Continuing in the usual fashion of introducing the trajectory $\gamma_{\alpha_j}(t)$ which is described by the time-discretised set $\{\gamma_{\alpha_j,0}, \gamma_{\alpha_j,1}, \ldots, \gamma_{\alpha_j,M}\}$, we are again able to formally rewrite for the limit $M \to \infty$

$$\gamma^*_{\alpha_j,k}\frac{\gamma_{\alpha_j,k} - \gamma_{\alpha_j,k-1}}{\epsilon} \Longrightarrow \gamma^*_{\alpha_j}(t)\frac{\partial\gamma_{\alpha_j}(t)}{\partial t}\,, \tag{2.80a}$$

$$H\left(\gamma^*_{\alpha_j,k}, \gamma_{\alpha_j,k-1}\right) \Longrightarrow H\left[\gamma^*_{\alpha_j}(t), \gamma_{\alpha_j}(t)\right]\,. \tag{2.80b}$$

Once more, the rectangular brackets denote the functional dependence on $\gamma^*_{\alpha_j}(t)$ and $\gamma_{\alpha_j}(t)$. Introducing the Schrödinger-Lagrange operator $L = i\hbar\frac{\partial}{\partial t} - H$, we reformulate the above result as

$$U(\gamma^*_{\alpha_j,f}, t_f|\gamma_{\alpha_j,i}, t_i) = \int\limits_{\gamma_{\alpha_j}(t_i)=\gamma_{\alpha_j,i}}^{\gamma^*_{\alpha_j}(t_f)=\gamma^*_{\alpha_j,f}} \mathcal{D}[\gamma^*_{\alpha_j}(t)\gamma_{\alpha_j}(t)]\, e^{\sum\limits_{\alpha_j}\left(\gamma^*_{\alpha_j}(t_f)\gamma_{\alpha_j}(t_f)\right)+\frac{i}{\hbar}\int\limits_{t_i}^{t_f}\mathrm{d}t\, L\left[\gamma^*_{\alpha_j}(t),\gamma_{\alpha_j}(t)\right]} \tag{2.81a}$$

$$L\left[\gamma^*_{\alpha_j}(t),\gamma_{\alpha_j}(t)\right] = \sum_{\alpha_j}\left(i\hbar\gamma^*_{\alpha_j}(t)\frac{\partial\gamma_{\alpha_j}(t)}{\partial t}\right) - H\left[\gamma^*_{\alpha_j}(t),\gamma_{\alpha_j}(t)\right], \tag{2.81b}$$

$$\int\mathcal{D}[\gamma^*_{\alpha_j}(t)\gamma_{\alpha_j}(t)] = \lim_{M\to\infty}\int\prod_{k=1}^{M-1}\prod_{\alpha_j}\frac{\mathrm{d}\gamma_{\alpha_j,k}\,\mathrm{d}\gamma^*_{\alpha_j,k}}{\mathcal{N}}, \tag{2.81c}$$

where the boundaries are now defined by the values of $\gamma^*_{\alpha_j,f}$ and $\gamma_{\alpha_j,i}$. All remaining variables are integrated over including $\gamma_{\alpha_j,f}$ and $\gamma^*_{\alpha_j,i}$. The left-over term in the exponent, *i.e.*, $\sum\limits_{\alpha_j}\left(\gamma^*_{\alpha_j}(t_f)\gamma_{\alpha_j}(t_f)\right)$, is caused by the definition of the time derivatives. One could also derive an alternative form with a dependence on $\sum\limits_{\alpha_j}\left(\gamma^*_{\alpha_j}(t_i)\gamma_{\alpha_j}(t_i)\right)$. If this causes any issues during a specific calculation, an average of both expressions should be considered.

As we briefly mentioned in Sec. 2.1.3, the Feynman path integral provides the classical limit if $\hbar \to 0$. Due to its dependence via an overall prefactor $\hbar^{-1}$ in the exponent as well as in the Schrödinger Lagrange operator, the $\hbar \to 0$ limit of the functional integral, however, is not the classical one.

2.2.3. Functional integral form of partition function

Let us now compute a quantum many-body system's partition function for the grand-canonical ensemble in the coherent-state functional-integral formalism. For both, fermions and bosons, it can formally be written as

$$\mathcal{Z} = \mathrm{tr}\left(e^{-\beta(\hat{H}-\mu\hat{N})}\right) = \int\prod_{\alpha_j}\mathrm{d}\gamma^*_{\alpha_j}\mathrm{d}\gamma_{\alpha_j}\, e^{-\sum\limits_{\alpha_j}\gamma^*_{\alpha_j}\gamma_{\alpha_j}}\,\langle\zeta\gamma|e^{-\beta(\hat{H}-\mu\hat{N})}|\gamma\rangle\ . \tag{2.82}$$

Inserting the evolution operator's matrix element from Eqs. (2.81) and using the trajectory notation of the imaginary-time discretisation, we find that

$$\mathcal{Z} = \int\limits_{\gamma_{\alpha_j}(\beta)=\zeta\gamma_{\alpha_j}(0)}\mathcal{D}[\gamma^*_{\alpha_j}(\tau)\gamma_{\alpha_j}(\tau)]\, e^{-\int\limits_0^\beta\mathrm{d}\tau\left\{\sum\limits_{\alpha_j}\left(\gamma^*_{\alpha_j}(\tau)\left(\frac{\partial}{\partial\tau}-\mu\right)\gamma_{\alpha_j}(\tau)\right)+H\left[\gamma^*_{\alpha_j}(\tau),\gamma_{\alpha_j}(\tau)\right]\right\}}, \tag{2.83}$$

where we rescaled $\tau \to \frac{\tau}{\hbar}$, and the trace imposes periodic boundary conditions on the complex variables for bosons and anti-periodic boundary conditions on the Graßmann

variables for fermions [135]. Of course, an analytic evaluation of this functional integral is usually not possible. One, for instance, has to expand it in a small parameter which is typically the interaction between particles. Nevertheless, the imaginary-time-ordered Green's functions can be represented in a convenient form using the functional integral language. If we remind ourselves of the fact that we replaced the creation and annihilation operators by the coherent state variables, we can simply write down that

$$\begin{aligned} &G\big(1,2,\ldots,n|1',2',\ldots,n'\big) \\ &\quad= \mathcal{Z}^{-1} \int\limits_{\gamma_{\alpha_j}(\beta)=\zeta\gamma_{\alpha_j}(0)} \mathcal{D}[\gamma^*_{\alpha_j}(\tau)\gamma_{\alpha_j}(\tau)] \left[e^{-\int\limits_0^\beta \mathrm{d}\tau \left\{ \sum\limits_{\alpha_j} \left[\gamma^*_{\alpha_j}(\tau)\left(\frac{\partial}{\partial\tau}-\mu\right)\gamma_{\alpha_j}(\tau)\right] + H\left[\gamma^*_{\alpha_j}(\tau),\gamma_{\alpha_j}(\tau)\right]\right\}} \right. \\ &\qquad\qquad \left. \times\, \gamma_{\alpha_1}(\tau_1)\gamma_{\alpha_2}(\tau_2)\ldots\gamma_{\alpha_n}(\tau_n)\gamma^*_{\alpha_{n'}}(\tau_{n'})\ldots\gamma^*_{\alpha_{2'}}(\tau_{2'})\gamma^*_{\alpha_{1'}}(\tau_{1'}) \right]. \end{aligned} \tag{2.84}$$

Before explaining how to proceed for a general Hamiltonian, we show how to compute the partition function and the imaginary-time-ordered Green's function in this representation for the simplest possible example, *i.e.*, a non-interacting Hamiltonian.

2.2.4. Partition function and Green's function for non-interacting Hamiltonian

Let us consider a non-interacting Hamiltonian which, in general, is diagonal in some basis

$$\hat{H}_0 = \sum_{\alpha_j} \varepsilon_{\alpha_j} a^\dagger_{\alpha_j} a_{\alpha_j} \,. \tag{2.85}$$

Plugging this Hamiltonian as a functional of the coherent state variables into Eq. (2.83) for the partition function yields

$$\mathcal{Z}_0 = \int\limits_{\gamma_{\alpha_j}(\beta)=\zeta\gamma_{\alpha_j}(0)} \mathcal{D}[\gamma^*_{\alpha_j}(\tau)\gamma_{\alpha_j}(\tau)]\, e^{-\int\limits_0^\beta \mathrm{d}\tau \left\{ \sum\limits_{\alpha_j} \left[\gamma^*_{\alpha_j}(\tau)\left(\frac{\partial}{\partial\tau}+\varepsilon_{\alpha_j}-\mu\right)\gamma_{\alpha_j}(\tau)\right]\right\}}. \tag{2.86}$$

This can now be computed using the time-discretised version of our variables. For the detailed calculation, we refer the reader to Ref. [135] and simply provide its result here. One finds

$$\mathcal{Z}_0 = \prod_{\alpha_j} \left(1-\zeta e^{-\beta(\varepsilon_{\alpha_j}-\mu)}\right)^{-\zeta} . \tag{2.87}$$

In a similar fashion, we can now also determine the non-interacting single-particle Green's function in imaginary time. Using the short-hand notation

$$n_{\alpha_j} = \left(e^{\beta(\varepsilon_{\alpha_j}-\mu)} - \zeta\right)^{-1} \tag{2.88}$$

for the Fermi ($\zeta = -1$) and Bose ($\zeta = 1$) distribution, it is straightforward to derive that

$$\begin{aligned} G_0^{(1)}\left(1|1'\right) &= \langle T_\tau a_{\alpha_1}(\tau_1) a^\dagger_{\alpha_{1'}}(\tau_{1'})\rangle \\ &= \delta_{\alpha_1,\alpha_{1'}} g_{\alpha_{1'}}(\tau_1 - \tau_{1'}) \end{aligned} \tag{2.89a}$$

$$g_{\alpha_{1'}}(\tau_1 - \tau_{1'}) = e^{-(\varepsilon_{\alpha_{1'}}-\mu)(\tau_1-\tau_{1'})}\left[\theta(\tau_1 - \tau_{1'} - \eta)(1 + \zeta n_{\alpha_{1'}}) + \theta(\tau_{1'} - \tau_1 + \eta)\zeta n_{\alpha_{1'}}\right], \tag{2.89b}$$

where the infinitesimal $\eta > 0$ ensures the correct behaviour at equal times. Again, please note that an additional factor of ζ can occur if a different convention for the single-particle Green's function is used (confer Sec. 2.1.2). With the non-interacting partition and Green's functions from above, we are able to perturbatively include the interacting part of the Hamiltonian into the theory.

2.3. Perturbation theory

While treating non-interacting quantum systems might be helpful to understand the underlying theory's fundamental mathematical properties, the physically interesting, though mathematically challenging phenomena arise due to interactions. We can write a general Hamiltonian $\hat{H}$ into a sum of its non-interacting part $\hat{H}_0$ and an interacting part $\hat{V}$ which can contain any number of n-particle interactions, but has to be normal ordered for our purposes.

$$\hat{H} = \hat{H}_0 + \hat{V} = \sum_{\alpha_j}\left(\varepsilon_{\alpha_j} a^\dagger_{\alpha_j} a_{\alpha_j}\right) + V\left(a^\dagger_{\alpha_j}, a_{\alpha_j}\right) \tag{2.90}$$

The concept behind perturbation theory is to at least pretend that the interacting part is small compared to $\hat{H}_0$. Therefore, one might first solve the non-interacting part separately and then investigate the small corrections to this solution arising from interactions. If interactions in the corresponding physical system are indeed (coincidentally) small, that might already suffice. If not, one might still be lucky in finding an infinite, but converging series that accounts for all relevant effects of $\hat{V}$.

Later, it will turn out that in quantum spin models we are not that fortunate. However, this common technique of perturbation theory can familiarise us with some essential ingredients for the subsequent functional renormalisation group method.

In the functional integral language, we can rewrite the partition function as

$$\begin{aligned} \mathcal{Z} &= \int\limits_{\gamma_{\alpha_j}(\beta)=\zeta\gamma_{\alpha_j}(0)} \mathcal{D}[\gamma^*_{\alpha_j}(\tau)\gamma_{\alpha_j}(\tau)]\, e^{-\int_0^\beta \mathrm{d}\tau \left\{\sum_{\alpha_j}\left[\gamma^*_{\alpha_j}(\tau)\left(\frac{\partial}{\partial\tau}+\varepsilon_{\alpha_j}-\mu\right)\gamma_{\alpha_j}(\tau)\right]+V\left[\gamma^*_{\alpha_j}(\tau),\gamma_{\alpha_j}(\tau)\right]\right\}}, \\ &= \mathcal{Z}_0\left\langle e^{-\int_0^\beta \mathrm{d}\tau\, V\left[\gamma^*_{\alpha_j}(\tau),\gamma_{\alpha_j}(\tau)\right]}\right\rangle_0, \end{aligned} \tag{2.91}$$

where the non-interacting partition function was already calculated in Eq. (2.87) and the non-interacting expectation value $\langle \dots \rangle_0$ of any functional of the coherent state variables $F\left[\gamma^*_{\alpha_j}(\tau), \gamma_{\alpha_j}(\tau)\right]$ is given by

$$\left\langle F\left[\gamma^*_{\alpha_j}(\tau), \gamma_{\alpha_j}(\tau)\right]\right\rangle_0 = \mathcal{Z}_0^{-1} \int\limits_{\gamma_{\alpha_j}(\beta)=\zeta\gamma_{\alpha_j}(0)} \mathcal{D}[\gamma^*_{\alpha_j}(\tau)\gamma_{\alpha_j}(\tau)]\, e^{-\int\limits_0^\beta \mathrm{d}\tau \sum\limits_{\alpha_j}\left[\gamma^*_{\alpha_j}(\tau)\left(\frac{\partial}{\partial\tau}+\varepsilon_{\alpha_j}-\mu\right)\gamma_{\alpha_j}(\tau)\right]} \times F\left[\gamma^*_{\alpha_j}(\tau), \gamma_{\alpha_j}(\tau)\right] \tag{2.92}$$

Note again that, in the functional integral language, the correct time order of the coherent state variables is automatically guaranteed.

We now want to expand the exponent from Eq. (2.91) in thermal averages with respect to $\hat{H}_0$

$$\frac{\mathcal{Z}}{\mathcal{Z}_0} = \sum_{n=0}^{\infty} \frac{(-1)^n}{n!} \int \mathrm{d}\tau_1 \dots \mathrm{d}\tau_n \left\langle V\left[\gamma^*_{\alpha_j}(\tau), \gamma_{\alpha_j}(\tau)\right] \dots V\left[\gamma^*_{\alpha_j}(\tau), \gamma_{\alpha_j}(\tau)\right]\right\rangle_0 . \tag{2.93}$$

For that purpose, we need to employ Wick's theorem.

2.3.1. Wick's theorem

Wick's theorem corresponds to the following integral identity for polynomial times Gaussian functions of complex or Graßmann numbers

$$\frac{\int \mathcal{D}[\gamma^*_k\gamma_l]\, \gamma_1 \dots \gamma_n \gamma^*_{n'} \dots \gamma^*_{1'} e^{-\sum\limits_{k,l}\gamma^*_k M_{kl}\gamma_l}}{\int \mathcal{D}[\gamma^*_k\gamma_l]\, e^{-\sum\limits_{k,l}\gamma^*_k M_{kl}\gamma_l}} = \sum_P \zeta^P M^{-1}_{P(n)n} \dots M^{-1}_{P(1)1}\,, \tag{2.94}$$

where M is an invertible matrix and k, l denote now both time label and quantum number. Therefore, the sum $\sum\limits_k = \sum_{\alpha_k} \int_0^\beta \mathrm{d}\tau_k$ needs to be interpreted as a sum over the quantum number α_k and an integral over τ_k, and $\mathcal{D}[\gamma^*_k\gamma_l] = \mathcal{D}[\gamma^*_{\alpha_k}(\tau_k)\gamma_{\alpha_l}(\tau_l)]$ is the measure corresponding to our variables. This identity is proven in the same way as the single-particle Green's function from Eq. (2.89) was calculated an we, again, refer the reader to Ref. [135] for more details. We will, however, encounter this technique later in Sec. 2.4.1. One needs to utilise the $(2n)$-*th* partial derivative of a generating functional with respect to its included so-called source terms.

If we replace the matrix M_{kl} from Eq. (2.94) with the operator $\left(\partial_\tau + \hat{H}_0 - \mu\right)$ in the basis of the coherent state variables, an element of M^{-1} can be identified with a non-

interacting single-particle Green's function.

$$G_0^{(1)}(1|1') = \frac{\int \mathcal{D}[\gamma^*_{\alpha_j}(\tau)\gamma_{\alpha_j}(\tau)]\,\gamma_{\alpha_1}(\tau_1)\gamma^*_{\alpha_{1'}}(\tau_{1'}) e^{-\int_0^\beta \mathrm{d}\tau \sum_{\alpha_j} \gamma^*_{\alpha_j}(\tau)\left(\partial_\tau + \varepsilon_{\alpha_j} - \mu\right)\gamma_{\alpha_j}(\tau)}}{\int \mathcal{D}[\gamma^*_{\alpha_j}(\tau)\gamma_{\alpha_j}(\tau)]\, e^{-\int_0^\beta \mathrm{d}\tau \sum_{\alpha_j} \gamma^*_{\alpha_j}(\tau)\left(\partial_\tau + \varepsilon_{\alpha_j} - \mu\right)\gamma_{\alpha_j}(\tau)}}$$

$$= \left(\partial_\tau + \varepsilon_{\alpha_j} - \mu\right)^{-1}\Big|_{(\alpha_1;\tau_1|\alpha_{1'};\tau_{1'})} \tag{2.95a}$$

$$= \delta_{\alpha_1,\alpha_{1'}} g_{\alpha_{1'}}(\tau_1 - \tau_{1'}) \tag{2.95b}$$

The precise form of $g_{\alpha_1}(\tau_1 - \tau_{1'})$ is given in Eq. (2.89b). In this particular setup, Wick's theorem corresponds to the statement that an n-particle non-interacting Green's function is comprised of all possible permutations of products of n single-particle Green's functions

$$G_0^{(n)}(1,\ldots,n|1',\ldots,n') = \sum_P \zeta^P \prod_{k=1}^n G_0^{(1)}(P(k)|k') \tag{2.96a}$$

$$= \sum_P \zeta^P \prod_{k=1}^n \delta_{\alpha_{P(k)},\alpha_{k'}} g_{\alpha_{k'}}(\tau_{P(k)} - \tau_{k'})\,. \tag{2.96b}$$

Sometimes, one refers to the right-hand side of this equation as the sum over all complete sets of contractions, where a contraction corresponds to taking the expectation value of a product of two operators or the corresponding coherent state variable.

Any product of two creation operators $\langle a^\dagger_{\alpha_j} a^\dagger_{\alpha_k}\rangle_0$ or annihilation operators $\langle a_{\alpha_j} a_{\alpha_k}\rangle_0$ as well as the expectation values of their corresponding coherent state variables $\langle \gamma^*_{\alpha_j}\gamma^*_{\alpha_k}\rangle_0$ and $\langle \gamma_{\alpha_j}\gamma_{\alpha_k}\rangle_0$ vanish in phases with conserved particle numbers. This implies that the number of possible contractions in such a phase reduces to only those where a creation operator is combined with an annihilation operator or every $\gamma^*_{\alpha_j}$ is contracted with a γ_{α_k}. Furthermore, this also suggests that any Green's function including n annihilation operators and $m \neq n$ creation operators has to vanish as well.

Even though Eqs (2.96) suffice for our purposes, one important remark is that Wick's theorem also holds for a basis in which $\hat{H}_0$ is not diagonal. Finally, using Wick's theorem, we are now able to resolve the power series of $\frac{\mathcal{Z}}{\mathcal{Z}_0}$ in terms of all possible ways to connect products of interactions V with single-particle Green's functions.

2.3.2. Labeled Feynman diagrams

Since we are now ready to explore the effects of interactions using the functional integral form of the many-particle partition function, we want to develop a technique to keep track of all possible contractions of Green's functions in connection to the interaction potentials. For simplicity, let us consider a general type of an instantaneous two-body interaction

$$V\left[\gamma^*_{\alpha_j}(\tau), \gamma_{\alpha_j}(\tau)\right] = \frac{1}{2} \sum_{\alpha_1,\beta_1,\alpha_{1'},\beta_{1'}} \langle \alpha_1\beta_1|\hat{V}|\alpha_{1'}\beta_{1'}\rangle\, \gamma^*_{\alpha_1}(\tau)\gamma^*_{\beta_1}(\tau)\gamma_{\beta_{1'}}(\tau)\gamma_{\alpha_{1'}}(\tau)\,, \tag{2.97}$$

$G_0^{(1)}(\alpha_1;\tau_1|\alpha_{1'};\tau_{1'}) =$ 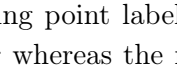

$\frac{1}{2}\langle\alpha_1\beta_1|\hat{V}|\alpha_{1'}\beta_{1'}\rangle =$ 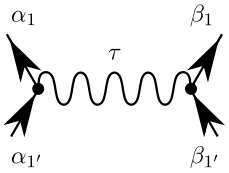

Figure 2.1.: Definitions of the two constituents for the labeled Feynman diagrams: The directed and dashed line represents a bare single-particle Green's function $G_0^{(1)}(1|1')$. The dashed index at its starting point labels the coherent state variable for the fermionic or bosonic creation operator whereas the non-dashed index at its end is associated with an annihilation operator. The undirected wiggly line stands for an interaction vertex where now the ingoing legs with dashed indices represent annihilation processes and the outgoing legs with non-dashed indices denote creation processes. Note that the bare interaction vertex carries only one imaginary-time argument being valid for all four connected operators.

where $\langle\alpha_1\beta_1|\hat{V}|\alpha_{1'}\beta_{1'}\rangle$ denotes a matrix element of the interaction potential in the considered basis. Using this simple type of interaction, we are immediately able to write down the term proportional to the nth power of $\hat{V}$ in our expansion for $\frac{\mathcal{Z}}{\mathcal{Z}_0}$, *i.e.*,

$$\left(\frac{\mathcal{Z}}{\mathcal{Z}_0}\right)_{(n)} = \frac{(-1)^n}{n!\,2^n}\prod_{k=1}^{n}\left(\sum_{\alpha_k,\beta_k,\alpha_{k'},\beta_{k'}}\langle\alpha_k\beta_k|\hat{V}|\alpha_{k'}\beta_{k'}\rangle\int_0^\beta \mathrm{d}\tau_k\right) \times\left\langle\gamma^*_{\alpha_1}(\tau_1)\gamma^*_{\beta_1}(\tau_1)\gamma_{\beta_{1'}}(\tau_1)\gamma_{\alpha_{1'}}(\tau_1)\ldots\gamma^*_{\alpha_n}(\tau_n)\gamma^*_{\beta_n}(\tau_n)\gamma_{\beta_{n'}}(\tau_n)\gamma_{\alpha_{n'}}(\tau_n)\right\rangle_0 , \quad (2.98)$$

where the time ordering is again automatically provided by the thermal average in the functional integral formalism.

Now, we need to perform any contraction of all γ^* with all the γ. Every bare Green's function $G_0^{(1)}(1|1') = \delta_{\alpha_1,\alpha_{1'}}g_{\alpha_{1'}}(\tau_1-\tau_{1'})$, also called bare propagator, is for that reason represented by a solid, directed line starting from $\gamma^*_{\alpha_{1'}}(\tau_{1'})$ and terminating at $\gamma_{\alpha_1}(\tau_1)$. Any interaction potential, often referred to as a vertex function, is denoted by a dashed and undirected line with two ingoing legs that correspond to $\gamma_{\alpha_{j'}}(\tau_j)$ and $\gamma_{\beta_{j'}}(\tau_j)$ and two outgoing legs representing $\gamma^*_{\alpha_j}(\tau_j)$ and $\gamma^*_{\beta_j}(\tau_j)$. The constriction that all legs of the vertex must have identical time arguments can also be incorporated into a concrete time dependence proportional to a δ distributions of the vertex function itself.

The definitions of the two types of constituents for the labeled Feynman diagrams are shown in Fig. 2.1 and the two distinct diagrams contributing to first order in $\hat{V}$ to the expansion of $\frac{\mathcal{Z}}{\mathcal{Z}_0}$ can be seen in Fig. 2.2. Those diagrams are the direct diagram and the

$$-\frac{1}{2}\zeta \int_0^\beta \mathrm{d}\tau \sum_{\alpha_1\beta_1} g_{\alpha_1}(0) g_{\beta_1}(0) \langle \beta_1\alpha_1|\hat{V}|\alpha_1\beta_1\rangle =$$

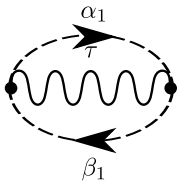

$$-\frac{1}{2}\zeta^2 \int_0^\beta \mathrm{d}\tau \sum_{\alpha_1\beta_1} g_{\alpha_1}(0) g_{\beta_1}(0) \langle \alpha_1\beta_1|\hat{V}|\alpha_1\beta_1\rangle =$$

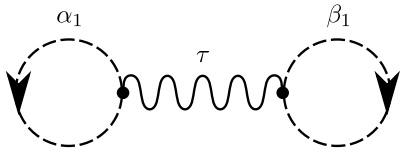

Figure 2.2.: The two distinct diagrams for the expansion of $\frac{\mathcal{Z}}{\mathcal{Z}_0}$ to first order in $\hat{V}$: To first order in the interaction, there are only two possible ways of contracting coherent state variables, *i.e.*, the upper exchange diagram D^1_{exchange} which connects both sides of the vertex function with each other via propagators, and the lower direct diagram D^1_{direct} which contracts them separately. Where D^1_{direct} features two closed loops yielding a prefactor of $\zeta^2 = 1$, D^1_{exchange} consists only of one loop and one has to keep track of the arising ζ.

exchange diagram

$$\left(\frac{\mathcal{Z}}{\mathcal{Z}_0}\right)_{(1)} = D^1_{\text{direct}} + D^1_{\text{exchange}}\,, \tag{2.99a}$$

$$D^1_{\text{direct}} = -\frac{1}{2}\zeta^2 \int_0^\beta \mathrm{d}\tau \sum_{\alpha_1,\beta_1} g_{\alpha_1}(0) g_{\beta_1}(0) \langle \alpha_1\beta_1|\hat{V}|\alpha_1\beta_1\rangle\,, \tag{2.99b}$$

$$D^1_{\text{exchange}} = -\frac{1}{2}\zeta \int_0^\beta \mathrm{d}\tau \sum_{\alpha_1,\beta_1} g_{\alpha_1}(0) g_{\beta_1}(0) \langle \beta_1\alpha_1|\hat{V}|\alpha_1\beta_1\rangle\,. \tag{2.99c}$$

Due to the fact that the formation of a single closed loop of propagators involves precisely one permutation of coherent state variables in Eq. (2.98), any diagram which includes n closed loops acquires a prefactor of ζ^n. We also have to integrate over one imaginary-time variable and sum over four quantum number indices for each interaction vertex. The bare propagator though is chosen diagonal in the quantum numbers rendering $2n$ summations in an nth-order diagram trivial. This is why, in the above equation, only 2 summations appear in the first-order diagrams. Plugging in the previously derived result for the non-interacting Green's function, we find for our partition-function expansion up to first order in $\hat{V}$

$$\frac{\mathcal{Z}}{\mathcal{Z}_0} \simeq 1 - \frac{\beta}{2} \sum_{\alpha_1,\beta_1} n_{\alpha_1} n_{\beta_1} \left[\langle \alpha_1\beta_1|\hat{V}|\alpha_1\beta_1\rangle + \zeta \langle \beta_1\alpha_1|\hat{V}|\alpha_1\beta_1\rangle\right], \tag{2.100}$$

where n_{α_1} is the Fermi or Bose distribution from Eq. (2.88).

This summarises the Feynman rules for labeling and computing diagrams. Continuing like this, we would encounter a vastly increasing number of diagrams for higher orders in

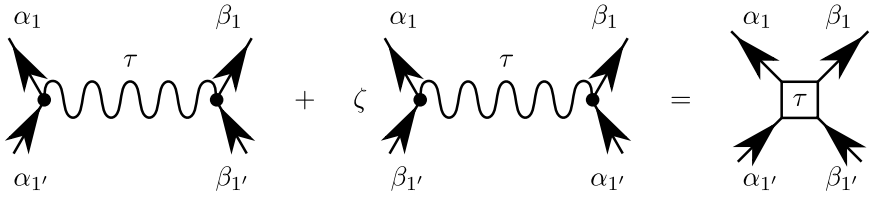

Figure 2.3.: Hugenholtz diagrams for two-body interaction: The Hugenholtz diagram is the sum of two vertex functions, namely, the direct and the exchange vertex. With its definition given in Eq. (2.103), it is invariant under the exchange of the two incoming or outgoing legs which might be convenient during calculations.

the interaction, namely $(2n)!$ diagrams for the nth order in $\hat{V}$. Hence, there is still some work to be done.

2.3.3. Unlabeled Feynman diagrams

So far, we are still concerned with calculating the ratio $\frac{\mathcal{Z}}{\mathcal{Z}_0}$. As mentioned before, for that we need to contract $2n$ coherent state variables representing creation operators with $2n$ variables associated with annihilation operators yielding $(2n)!$ diagrams to compute. However, since

$$\langle \alpha_1 \beta_1 | \hat{V} | \alpha_{1'} \beta_{1'} \rangle = \langle \beta_1 \alpha_1 | \hat{V} | \beta_{1'} \alpha_{1'} \rangle \tag{2.101}$$

for both fermions and bosons, there are 2^n diagrams contributing the same value due to two-particle exchange. Also, any permutation of imaginary-time variables over which we integrate yields identical results leading to another factor of $n!$ diagrams equaling each other. Those two different transformations which leave a labeled Feynman diagram invariant, mathematically speaking, amount to the exchange of two internal integration variables or summation indices. Sometimes, they yield an identical diagram and sometimes a distinct one and the task of this section is to determine the correct number of distinct diagrams with the same value.

All transformations together build a group $\mathcal{G}$ with $2^n n!$ elements and we are looking for that particular subgroup $\mathcal{G}_D$ which map a labeled Feynman diagram D onto itself. We denote the number of elements of $\mathcal{G}_D$ with S_D and refer to it as the symmetry factor of the diagram D. If now a distinct diagram D' is generated from D through an element of $\mathcal{G}$, all elements of $\mathcal{G}_D$ also leave D' invariant. This implies that there must be exactly $\frac{2^n n!}{S_D}$ groups of S_D diagrams diagrams yielding the same result. Hence, there actually are also $\frac{2^n n!}{S_D}$ distinct diagrams to nth order in the interaction with equal contributions. In the end, it therefore suffices to calculate one of the distinct diagrams and multiply its result with the factor of $\frac{2^n n!}{S_D}$.

Unlabeled Feynman diagrams $\tilde{D}$ are now obtained by omitting all quantum numbers and time labels of the labeled diagrams. Accordingly, only the diagram's topology and the directions of the bare propagators matter. The contribution of all distinct labeled diagrams

now equals the value of all distinct unlabeled diagrams times $\frac{2^n n!}{S_D}$. Therefore, we need to calculate one distinct unlabeled Feynman diagram each an determine its symmetry factor. For instance, to first order in $\hat{V}$, the symmetry factor is $S_D = 2$. To second order and depending on the diagram $\tilde{D}$, it can be $S_D = \in \{4, 2, 1\}$. In general, determining S_D of all unlabeled Feynman diagram can be quite challenging. However, since we know that we must arrive at a total number of diagrams $(2n)! = \sum_{\tilde{D}} \frac{2^n n!}{S_D}$, we find that

$$\sum_{\tilde{D}} \frac{1}{S_D} = (2n-1)!! = (2n-1)(2n-3)(2n-5)\ldots 5 \cdot 3 \cdot 1\,. \tag{2.102}$$

This provides an easy check whether the determined symmetry factors can be correct or not.

We would like to spend one last comment on the so-called Hugenholtz diagrams. They are the sum of the direct and the exchange interaction

$$\begin{aligned} & V\left[\gamma^*_{\alpha_j}(\tau), \gamma_{\alpha_j}(\tau)\right] \\ &= \frac{1}{2} \sum_{\alpha_1,\beta_1,\alpha_{1'},\beta_{1'}} \langle \alpha_1\beta_1|\hat{V}|\alpha_{1'}\beta_{1'}\rangle\, \gamma^*_{\alpha_1}(\tau)\gamma^*_{\beta_1}(\tau)\gamma_{\beta_{1'}}(\tau)\gamma_{\alpha_{1'}}(\tau) \\ &= \frac{1}{4} \sum_{\alpha_1,\beta_1,\alpha_{1'},\beta_{1'}} \left[\langle \alpha_1\beta_1|\hat{V}|\alpha_{1'}\beta_{1'}\rangle + \zeta\, \langle \alpha_1\beta_1|\hat{V}|\beta_{1'}\alpha_{1'}\rangle\right] \gamma^*_{\alpha_1}(\tau)\gamma^*_{\beta_1}(\tau)\gamma_{\beta_{1'}}(\tau)\gamma_{\alpha_{1'}}(\tau)\,. \end{aligned} \tag{2.103}$$

If we regroup the interactions like this and treat the two terms in brackets in the second line as one vertex function (confer Fig. 2.3), this vertex function is invariant under the exchange of two incoming and outgoing legs separately.

In principle, this theory can be extended to more general types of interactions like single-body or m-body interactions. During this thesis though, we do not encounter such phenomena and continue without providing details on them.

2.3.4. Frequency and momentum space representations

One of the most powerful tools to analytically treat interacting systems is the Fourier transform (FT). Mathematically speaking, it amounts to a basis transform in completely periodic or anti-periodic functions, *i.e.*, sine and cosine, and it is always helpful if the investigated system has some intrinsic translation invariance.

Let us briefly consider a one-dimensional system of length L with a translation invariance along the sole spatial x axis and periodic boundary conditions. This implies that any function depending on two coordinates can in fact only depend on their difference

$$f(x_1, x_2) = f(x_1 - x_2, 0)\,, \tag{2.104a}$$

$$f(x_1, x_2) = f(x_1 + L, x_2) = f(x_1, x_2 + L) = f(x_1 + L, x_2 + L)\,. \tag{2.104b}$$

As we saw already for the Feynman diagrams, including interactions requires the summation or integration over internal indices which can, for instance, be of a spatial type

$$f(x_1, x_2) = \int_0^L \mathrm{d}x\, g(x_1, x) h(x, x_2)\,, \tag{2.105}$$

where the functions f, g, and k could be Green's functions for example. We can properly[2] define a Fourier transform with respect to the two (coherent state) variables x_1 and x_2 according to

$$\tilde{f}(k_1, k_2) = \int_0^L \mathrm{d}x_1\, \mathrm{d}x_2\, e^{i(k_1 x_1 - k_2 x_2)} f(x_1, x_2), \tag{2.106a}$$

$$f(x_1, x_2) = \frac{1}{L^2} \sum_{k_1, k_2 = -\infty}^{\infty} e^{-i(k_1 x_1 - k_2 x_2)} \tilde{f}(k_1, k_2)\,. \tag{2.106b}$$

Due to the periodic boundary conditions[3] from Eq. (2.104b), the values of k_1 and k_2 in the second line now become discretised via the condition that $k_1 = \frac{2n_1\pi}{L}$ and $k_2 = \frac{2n_2\pi}{L}$ where $n_1, n_2 \in \mathbb{Z}$. This implies a summation rather than an integration over k. The normalisation constant L^{-1} per k summation is obtained by computing the Fourier transform of 1

$$\begin{aligned} \int_0^L \mathrm{d}x_1\, e^{i(k_1 x_1)} \cdot 1 &= \begin{cases} L\,, & \text{if } k_1 = 0 \\ 0\,, & \text{else} \end{cases} \\ &= L\, \delta_{k_1, 0}\,, \end{aligned} \tag{2.107a}$$

$$\implies \qquad \frac{1}{L} \sum_{k_1 = -\infty}^{\infty} L\, \delta_{k_1, 0} = 1\,. \tag{2.107b}$$

For periodic functions, this basis transformation is an expansion in $\cos(k)$, whereas, for anti-periodic functions, the expansion is in $\sin(k)$. One often refers to the spatial representation $f(x)$ as the function in real space and the k-space representation $f(k)$ as the function in momentum space.

The translation invariance [cf. Eq. (2.104a)] can now be used to simplify convolution

[2] The different signs in the exponent for the two different spatial variables ensure that the coherent state variables of a Green's function are still the correct adjoints of each other after the Fourier transform.

[3] Anti-periodic boundary conditions would simply imply that $k_i = \frac{(2n_i+1)\pi}{L}$.

integrals. Since we can write for the functions f, g, and h that

$$\begin{aligned}\tilde{f}(k_1,k_2) &= \int_0^L \mathrm{d}x_1\,\mathrm{d}x_2\, e^{i(k_1x_1-k_2x_2)} f(x_1-x_2,0)\\ &= \int_0^L \mathrm{d}x_1\,\mathrm{d}x_2\, e^{i(k_1(x_1-x_2)-(k_2-k_1)x_2)} f(x_1-x_2,0)\\ &= L\,\delta_{k_1,k_2}\int_0^L \mathrm{d}x\, e^{ik_1x} f(x,0)\\ &= L\,\delta_{k_1,k_2}\tilde{f}(k_1)\,,\end{aligned} \tag{2.108}$$

we find for Eq. (2.105)

$$\begin{aligned}L\,\delta_{k_1,k_2}\tilde{f}(k_1) &= \int_0^L \mathrm{d}x_1\,\mathrm{d}x_2\, e^{i(k_1x_1-k_2x_2)} \int_0^L \mathrm{d}x\, g(x_1,x)h(x,x_2)\\ &= \int_0^L \mathrm{d}x_1\,\mathrm{d}x_2\,\mathrm{d}x\, L^{-4} \sum_{k_3,k_4,k_5,k_6=-\infty}^{\infty} e^{i((k_1-k_3)x_1+(k_6-k_2)x_2+(k_4-k_5)x)}\tilde{g}(k_3,k_4)\tilde{h}(k_5,k_6)\\ &= L \sum_{k_3,k_4,k_5,k_6=-\infty}^{\infty} \delta_{k_1,k_3}\delta_{k_4,k_5}\delta_{k_6,k_2}\delta_{k_3,k_4}\delta_{k_5,k_6}\,\tilde{g}(k_3)\tilde{h}(k_5)\\ &= L\delta_{k_1,k_2}\, g(k_1)h(k_1)\,.\end{aligned} \tag{2.109}$$

Hence, convolutions of translation invariant entities Fourier transform as

$$f(x_1,x_2) = \int_0^L \mathrm{d}x\, g(x_1,x)h(x,x_2) \qquad \overset{\mathrm{FT}}{\longleftrightarrow} \qquad \tilde{f}(k_1) = \tilde{g}(k_1)\tilde{h}(k_1) \tag{2.110}$$

which can save a tremendous amount of computational time. It should be obvious that the functions $f(x)$ and $\tilde{f}(k)$ do not have identical dependences on x and k. However, we do not want to litter this script with tilde symbols, but rather clearly separate both pictures such that the correct functions can always be identified in the following.

In practice, if our system is translation invariant, we need to perform a FT with respect to its spatial coordinates. Each vertex and each propagator then conserves momentum, meaning that, if the momenta $\boldsymbol{k}_1, \boldsymbol{k}_2, \ldots, \boldsymbol{k}_n$ go into a diagrammatic constituent with the outgoing momenta $\boldsymbol{k}_{1'}, \boldsymbol{k}_{2'}, \ldots, \boldsymbol{k}_{n'}$, we find that

$$\sum_{i=1}^{n} \boldsymbol{k}_i = \sum_{i'=1'}^{n'} \boldsymbol{k}_{i'}\,. \tag{2.111}$$

There is a very important observation to make here. Let us consider taking the continuum limit where the system's volume $V = L_x L_y L_z \to \infty$ and the discrete points in momentum space become dense. Therefore, we have to rewrite

$$\sum_{k_x,k_y,k_z=-\infty}^{\infty} = \sum_{\boldsymbol{k}} \qquad \xrightarrow{V\to\infty} \qquad \frac{V}{(2\pi)^3}\int_{-\pi}^{\pi} \mathrm{d}k_x\,\mathrm{d}k_y\,\mathrm{d}k_z = \frac{V}{(2\pi)^3}\int \mathrm{d}\boldsymbol{k}\,. \tag{2.112}$$

Any two-particle interaction's matrix element in momentum space has to be calculated using two somehow normalised states which have to be $\propto V^{-1}$ each. Therefore, the matrix element becomes $\propto V^{-2}$ but due the translation invariance there is an additional factor of V yielding an overall matrix element of the interaction being $\propto V^{-1}$ [confer Eq. (2.108)]. Thus, any diagram to nth order in the two-particle interaction is $\propto V^{-n}$ which brings the concept of diagrammatic connectedness in our focus. A Feynman diagram is called connected if and only if a continuous sequence of propagators connects all vertices contributing to the diagram. Of course, every Feynman diagram can be viewed as the product of some number of connected diagrams. Every diagram to nth order in $\hat{V}$ involves $2n$ propagators providing us with $2n$ momentum variables to be integrated over. If a diagram is connected, the momentum conservation at each vertex provides us with $n-1$ constraints on the momentum integrations. Therefore, we have $n+1$ independent momenta to integrate over yielding another factor of V^{n+1}. Combined with the factor of V^{-n} from the interaction's matrix elements, we find that every connected diagram is $\propto V$. So if an nth-order diagram is composed of m connected parts, it contributes with a factor V^m. Hence, only the fully connected diagrams with $m = 1$ contribute extensively to $\frac{\mathcal{Z}}{\mathcal{Z}_0}$.

Besides a translation invariance in real space, our system is also invariant under shifts of the imaginary time. Because of their mathematical properties, it is highly recommendable to perform an additional Fourier transform of the utilised Green's functions with respect to τ into what is called the Matsubara space. The bare propagator transforms according to

$$G_0^{(1)}(\alpha_1;\omega_1|\alpha_{1'};\omega_{1'}) = \int_0^\beta \mathrm{d}\tau_1 \int_0^\beta \mathrm{d}\tau_{1'}\, e^{i(\omega_1\tau_1-\omega_{1'}\tau_{1'})} G_0^{(1)}(\alpha_1;\tau_1|\alpha_{1'};\tau_{1'})\,, \tag{2.113a}$$

$$G_0^{(1)}(\alpha_1;\tau_1|\alpha_{1'};\tau_{1'}) = \frac{1}{\beta}\sum_{1=-\infty}^{\infty}\frac{1}{\beta}\sum_{1'=-\infty}^{\infty} e^{-i(\omega_1\tau_1-\omega_{1'}\tau_{1'})} G_0^{(1)}(\alpha_1,\omega_1|\alpha_{1'},\omega_{1'})\,, \tag{2.113b}$$

and takes the form

$$G_0^{(1)}(1|1') = \beta G_0^{(1)}(1)\delta_{\alpha_1,\alpha_{1'}}\delta(\omega_1-\omega_{1'}) = \frac{1}{(\varepsilon_{\alpha_1}-\mu)-i\omega_1}\beta\delta_{\alpha_1,\alpha_{1'}}\delta(\omega_1-\omega_{1'})\,, \tag{2.114}$$

where $1 = \{\alpha_1,\omega_1\}$ and $1' = \{\alpha_{1'},\omega_{1'}\}$ again are combined labels for quantum numbers and now Matsubara frequencies. In imaginary time, every bosonic (fermionic) Green's function is (anti)symmetric and (anti)periodic with period $\hbar\beta$. Therefore, they are only

computed in the interval $-\hbar\beta < \tau \leq \hbar\beta$ and the Matsubara frequencies are discretised with $n \in \mathbb{Z}$ according to

$$\omega_n = \begin{cases} \frac{2n\pi T}{\hbar}\,, & \text{for bosons}\,, \\ \frac{(2n+1)\pi T}{\hbar}, & \text{for fermions}\,. \end{cases} \tag{2.115}$$

One significant remark on the Green's functions in Matsubara space is that, in order to obey imaginary-time ordering, we have to replace

$$G_0^{(1)}(1) \to e^{i\omega_1\eta} G_0^{(1)}(1)\,, \qquad \eta > 0\,, \tag{2.116}$$

if the propagator starts and ends at the same vertex.

Similar to the aforementioned momentum conservation, if the system is time-translation invariant, we find that the vertices and Green's functions do now conserve frequency, *e.g.*,

$$\sum_{i=1}^{n} \omega_i = \sum_{i'=1'}^{n'} \omega_{i'}\,. \tag{2.117}$$

Now, the $2n$ propagators contribute β^{-2n} to any nth order diagram, but every interaction vertex comes with an extra factor of β yielding a net result $\propto \beta^{-n}$ for every diagram involving n interaction lines. If applied to the right system, the transformations into momentum and Matsubara space are highly beneficial when it comes to the computational effort. Also, the connectedness of our diagrams tells us whether they are extensive quantities or not. We shall turn to that during the next section.

2.3.5. Linked cluster theorem

We now know that the interaction corrections to the partition function $\mathcal{Z}$ contain all powers of the system's volume V. However, in our introduction to thermodynamics, we saw that it is related to the grand potential which is an extensive quantity

$$\Omega = -\frac{1}{\beta}\ln(\mathcal{Z}) = -PV\,, \tag{2.118}$$

confer Eqs. (2.8) and (2.9a). This shows that $\ln(\mathcal{Z})$ must be $\propto V$ and is therefore extensive as well.

The linked cluster theorem now states that $\ln\left(\frac{\mathcal{Z}}{\mathcal{Z}_0}\right)$ is precisely comprised as the sum over all fully connected diagrams. It is usually proven using the replica trick which takes m identical copies of our system and computes

$$\left(\frac{\mathcal{Z}}{\mathcal{Z}_0}\right)^m = e^{m\ln\left(\frac{\mathcal{Z}}{\mathcal{Z}_0}\right)} = 1 + m\ln\left(\frac{\mathcal{Z}}{\mathcal{Z}_0}\right) + \sum_{k=2}^{\infty}\left[m\ln\left(\frac{\mathcal{Z}}{\mathcal{Z}_0}\right)\right]^k\,. \tag{2.119}$$

Evaluating the path integral on the left-hand side, one quickly finds that each connected diagram is then $\propto m$ and every disconnected diagram being a product of p connected ones

are hence $\propto m^p$. This shows that indeed

$$\Omega - \Omega_0 = -\frac{1}{\beta} \sum \text{ all connected diagrams}\,, \tag{2.120a}$$

$$\Omega_0 = \frac{\zeta}{\beta} \sum_{\alpha_j} \ln\left(1 - \zeta e^{-\beta\left(\varepsilon_{\alpha_j} - \mu\right)}\right)\,, \tag{2.120b}$$

where the grand potential of the non-interacting system Ω_0 was calculated from Eq. (2.87).

2.4. Observables and Green's functions

Let us consider any n-body operator $\hat{O}$ of which we desire its expectation value with respect to some Hamiltonian $\hat{H}$. For that purpose, we start by replacing

$$\hat{H} \longrightarrow \hat{H}(\lambda) = \hat{H} + \lambda \hat{O}\,. \tag{2.121}$$

The operator's expectation value is now computed from the respective grand potential $\Omega(\lambda)$ as

$$\begin{aligned} \langle \hat{O} \rangle &= \frac{\partial}{\partial \lambda} \Omega(\lambda) \Big|_{\lambda=0} \\ &= \frac{\partial}{\partial \lambda} \left(-\frac{1}{\beta} \ln \mathcal{Z}(\lambda) \right) \Big|_{\lambda=0} \\ &= -\frac{1}{\beta \mathcal{Z}} \left(\frac{\partial \mathcal{Z}(\lambda)}{\partial \lambda} \right) \Big|_{\lambda=0}\,. \end{aligned} \tag{2.122}$$

Alternatively, we could again employ the replica trick which would show us that only the fully connected diagrams contribute to the expectation value $\langle \hat{O} \rangle$ (see Ref. [135] for more details).

For a two-particle operator, this implies that the diagrammatic symmetry factors S_D are reduced to values of 1 or 2. There are no more possible time permutations within closed loops and only if on the sub diagrams on the two sides of the operator are identical, we can make a deformation of the diagram onto itself by exchanging all time labels and all extremities of the vertex functions yielding $S_D = 2$. In general, the symmetry factor is maximally $n!$ for an n-body operator. If one calculates Green's functions, the symmetry factor is even further reduced to $S_D = 1$ for all diagrams since now all external legs are already determined by the Green's function and therefore, in turn, are fixing the internal labels. Now, we only need to evaluate each distinct diagram's prefactor.

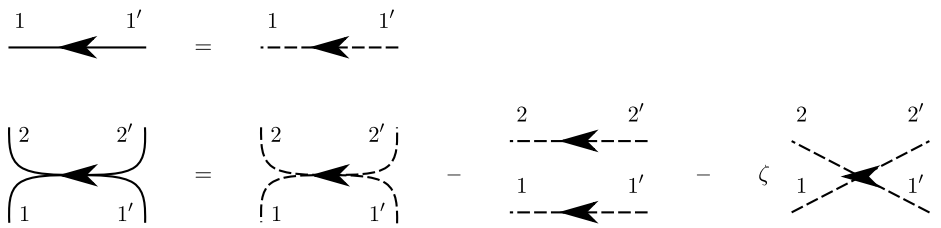

Figure 2.4.: Relation between connected (solid) and disconnected (dashed) Green's functions up to two-particle propagators: For the single-particle propagators, the connected Green's function equals the disconnected one [see Eq. (2.127a)]. The two-particle connected Green's function involves both, the single-body and the two-body disconnected propagators [confer Eq. (2.127b)]. To avoid confusion between two-particle Green's function and two crossed single-particle propagators, we use bent and straight lines respectively as in the first and the last diagram of the second equation.

2.4.1. Generating functionals for Green's functions

In complete analogy to the trick using the grand potential for calculating the expectation value of an operator, we define the generating functional for the Green's functions as

$$\mathcal{G}\left[\xi^*_{\alpha_j}(\tau),\xi_{\alpha_j}(\tau)\right] = \mathcal{Z}^{-1} \int\limits_{\gamma_{\alpha_j}(\beta)=\zeta\gamma_{\alpha_j}(0)} \mathcal{D}[\gamma^*_{\alpha_j}(\tau)\gamma_{\alpha_j}(\tau)] \times e^{-\int_0^\beta \mathrm{d}\tau \left\{\sum_{\alpha_j}\left(\gamma^*_{\alpha_j}(\tau)\left(\frac{\partial}{\partial\tau}-\mu\right)\gamma_{\alpha_j}(\tau)+\xi^*_{\alpha_j}(\tau)\gamma_{\alpha_j}(\tau)+\gamma^*_{\alpha_j}(\tau)\xi_{\alpha_j}(\tau)\right)+H\left[\gamma^*_{\alpha_j}(\tau),\gamma_{\alpha_j}(\tau)\right]\right\}}, \tag{2.123}$$

where $H\left[\gamma^*_{\alpha_j}(\tau),\gamma_{\alpha_j}(\tau)\right]$ is not further specified at the moment, and the partition function $\mathcal{Z}$ is found in Eq. (2.91) such that $\mathcal{G}(0,0)=1$.

Using the expression for the expectation value in the functional integral representation [see Eq. (2.92)], but this time with respect to the full interacting Hamiltonian, we can rewrite this generating functional as

$$\mathcal{G}\left[\xi^*_{\alpha_j}(\tau),\xi_{\alpha_j}(\tau)\right] = \left\langle e^{-\int_0^\beta \mathrm{d}\tau \sum_{\alpha_j}\left(\xi^*_{\alpha_j}(\tau)\gamma_{\alpha_j}(\tau)+\gamma^*_{\alpha_j}(\tau)\xi_{\alpha_j}(\tau)\right)}\right\rangle. \tag{2.124}$$

The newly introduced ξ^* and ξ are the so-called source terms which have to be complex or Graßmann variables in accordance to the bosonic or fermionic coherent state variables γ^* and γ. With this definition, we are ready to calculate the n-particle Green's function as

$$G^{(n)}(1,\ldots,n|1',\ldots,n') = \zeta^n \left.\frac{\delta^{2n}\mathcal{G}\left[\xi^*_{\alpha_j}(\tau),\xi_{\alpha_j}(\tau)\right]}{\delta\xi^*_1\ldots\delta\xi^*_n\delta\xi_{n'}\ldots\delta\xi_{1'}}\right|_{\xi^*=\xi=0}, \tag{2.125}$$

where we made again use of the combined quantum-number and imaginary-time labels and $\delta/\delta\xi^{(*)}$ now denotes a functional derivative.

The Green's functions that are obtained like this consist of connected and disconnected parts. If we are only concerned about the connected diagrams, which, as explained before, is the case for the calculation of expectation values of operators, we have to utilise the generating functional for the connected n-particle Green's functions $G_c^{(n)}$. It is obtained by employing the replica trick one last time yielding

$$\mathcal{W}\left[\xi^*_{\alpha_j}(\tau), \xi_{\alpha_j}(\tau)\right] = \ln\left[\mathcal{G}\left[\xi^*_{\alpha_j}(\tau), \xi_{\alpha_j}(\tau)\right]\right], \tag{2.126a}$$

$$G^{(n)c}(1,\ldots,n|1',\ldots,n') = \zeta^n \frac{\delta^{2n}\mathcal{W}\left[\xi^*_{\alpha_j}(\tau), \xi_{\alpha_j}(\tau)\right]}{\delta\xi^*_1 \ldots \delta\xi^*_n \delta\xi_{n'} \ldots \delta\xi_{1'}}\bigg|_{\xi^*=\xi=0}. \tag{2.126b}$$

Evaluating this expression in the language of Eq. (2.124) is straightforward. In a phase with fixed particle number, *i.e.*, all expectation values with unequal numbers of creation and annihilation processes are zero, we find the following relations between connected and disconnected Green's functions (up to $n = 2$)

$$G^{(1)c}(1|1') = G^{(1)}(1|1'), \tag{2.127a}$$

$$G^{(2)c}(1,2|1',2') = G^{(2)}(1,2|1',2') - G^{(1)}(1|1')G^{(1)}(2|2') - \zeta G^{(1)}(1|2')G^{(1)}(2|1'). \tag{2.127b}$$

The diagrammatic representation of these equations is shown in Fig. 2.4.

2.4.2. Effective potential

Even though we proved that we can compute every physical property of interest using Green's functions, in practice, this might be mathematically challenging since the Green's functions can be hard to approximate, for instance, for our spin systems. A common tool in physics and mathematics to circumvent this issue is a Lengendre transform.

We start by realising that, once the sources $\xi^*_{\alpha_j}(\tau), \xi_{\alpha_j}(\tau) \neq 0$ are included, the operators $a^\dagger_{\alpha_j}(\tau)$ and $a_{\alpha_j}(\tau)$ develop non-zero expectation values which we denote with

$$\psi_{\alpha_j}(\tau) = \langle a_{\alpha_j}(\tau)\rangle_{\xi^*,\xi} = \langle \gamma_{\alpha_j}(\tau)\rangle_{\xi^*,\xi} = -\frac{\delta}{\delta\xi^*_{\alpha_j}(\tau)}\mathcal{W}\left[\xi^*_{\alpha_j}(\tau), \xi_{\alpha_j}(\tau)\right], \tag{2.128a}$$

$$\psi^*_{\alpha_j}(\tau) = \langle a^\dagger_{\alpha_j}(\tau)\rangle_{\xi^*,\xi} = \langle \gamma^*_{\alpha_j}(\tau)\rangle_{\xi^*,\xi} = -\zeta\frac{\delta}{\delta\xi_{\alpha_j}(\tau)}\mathcal{W}\left[\xi^*_{\alpha_j}(\tau), \xi_{\alpha_j}(\tau)\right]. \tag{2.128b}$$

A Legendre transform of the generating functional for the connected Green's functions $\mathcal{W}\left[\xi^*_{\alpha_j}(\tau), \xi_{\alpha_j}(\tau)\right]$ with respect to the new fields $\psi^*_{\alpha_j}(\tau)$ and $\psi_{\alpha_j}(\tau)$ then provides us with the so-called effective potential or effective action

$$\Gamma\left[\psi^*_{\alpha_j}(\tau), \psi_{\alpha_j}(\tau)\right] = -\mathcal{W}\left[\xi^*_{\alpha_j}(\tau), \xi_{\alpha_j}(\tau)\right] - \int_0^\beta \mathrm{d}\tau' \sum_{\alpha_k}\left(\psi^*_{\alpha_k}(\tau')\xi_{\alpha_k}(\tau') + \xi^*_{\alpha_k}(\tau')\psi_{\alpha_k}(\tau')\right). \tag{2.129}$$

Now, we can use the above definitions to reobtain the sources from $\mathcal{W}$ as

$$\xi_{\alpha_j}(\tau) = -\frac{\delta}{\delta\psi^*_{\alpha_j}(\tau)}\Gamma\left[\psi^*_{\alpha_j}(\tau), \psi_{\alpha_j}(\tau)\right], \tag{2.130a}$$

$$\xi^*_{\alpha_j}(\tau) = -\zeta\frac{\delta}{\delta\psi_{\alpha_j}(\tau)}\Gamma\left[\psi^*_{\alpha_j}(\tau), \psi_{\alpha_j}(\tau)\right]. \tag{2.130b}$$

This expresses the old sources and hence also $\mathcal{W}$ in terms of the new variables $\psi^*_{\alpha_j}(\tau)$ and $\psi_{\alpha_j}(\tau)$. Taking $2n$ partial derivatives with respect to the new variables of $\Gamma\left[\psi^*_{\alpha_j}(\tau), \psi_{\alpha_j}(\tau)\right]$ provides us with the n-particle vertex function

$$\Gamma^{(n)}(1,\ldots,n|1',\ldots,n') = \left.\frac{\delta^{2n}\Gamma\left[\psi^*_{\alpha_j}(\tau), \psi_{\alpha_j}(\tau)\right]}{\delta\psi^*_1\ldots\delta\psi^*_n\delta\psi_{n'}\ldots\delta\psi_{1'}}\right|_{\xi^*=\xi=0}, \tag{2.131}$$

where setting the sources $\xi^* = \xi = 0$ amounts to an evaluation with respect to stationary $\psi^{(*)}_{\alpha_j}(\tau)$, *i.e.*, $\delta_{\psi^{(*)}_{\alpha_j}(\tau)}\Gamma\left[\psi^*_{\alpha_j}(\tau), \psi_{\alpha_j}(\tau)\right] = 0$.

Vertex functions are one-particle irreducible. This means that all contributing diagrams cannot be cut in two parts by removing a single propagator. Connected Green's functions are built from vertex functions with a tree expansion, which means that those expansions do strictly not contain loops anymore. This simultaneously implies that all the contributing loops must be contained in the vertices. The great benefit of using them is caused by the fact that diagrammatic divergences usually arise in loops. Therefore, the vertex functions now contain all divergences and are extremely useful for building up a renormalisation theory which tries to sum up diagrams in a non-diverging way yielding (hopefully) correct physical results. This work is essential for us. If we are not capable of reformulating our quantum theory in terms of analytically somehow controllable entities, we are left clueless about its predictions. Using vertex functions and functional renormalisation group methods in the next chapter is one of only a few possibilities enabling us to investigate the desired spin models.

2.4.3. Self energy and Dyson equation

Let us study the single-particle vertex $\Gamma^{(1)}(1|1')$. Using the chain rule for functional derivatives, we find that

$$\int \mathrm{d}2 \begin{pmatrix} \frac{\delta^2\mathcal{W}}{\delta\xi^*_3\delta\xi_2} & \zeta\frac{\delta^2\mathcal{W}}{\delta\xi^*_3\delta\xi^*_2} \\ \zeta\frac{\delta^2\mathcal{W}}{\delta\xi_3\delta\xi_2} & \frac{\delta^2\mathcal{W}}{\delta\xi_3\delta\xi^*_2} \end{pmatrix} \begin{pmatrix} \frac{\delta^2\Gamma}{\delta\psi^*_2\delta\psi_1} & \frac{\delta^2\Gamma}{\delta\psi^*_2\delta\psi^*_1} \\ \frac{\delta^2\Gamma}{\delta\psi_2\delta\psi_1} & \frac{\delta^2\Gamma}{\delta\psi_2\delta\psi^*_1} \end{pmatrix} = \begin{pmatrix} \delta_{3,1} & 0 \\ 0 & \delta_{3,1} \end{pmatrix}, \tag{2.132}$$

where again combined indices $1 = \{\alpha_1;\tau_1\}$ and $1' = \{\alpha_{1'};\tau_{1'}\}$ are used, and therefore the delta function $\delta_{3,1} = \delta_{\alpha_3,\alpha_1}\delta(\tau_3-\tau_1)$ as well as the integral $\int \mathrm{d}2 = \int_0^\beta \mathrm{d}\tau_2 \sum_{\alpha_2}$. If we consider the above equation as a matrix multiplication in the space of all possible quantum

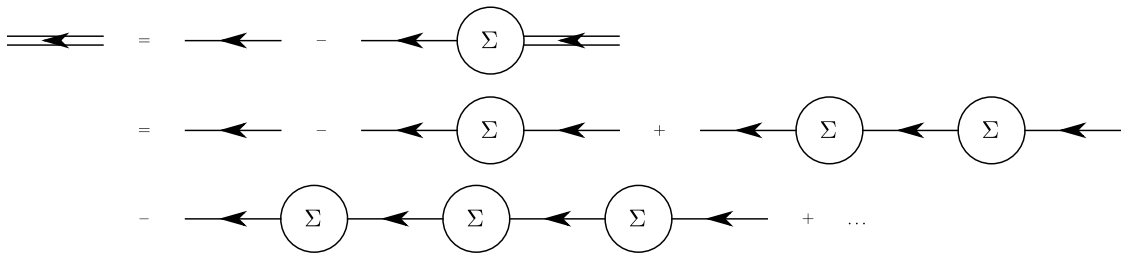

Figure 2.5.: Diagrammatic representation of Dyson's equation [Eq. (2.135b)]: While a single directed line stands for the bare connected single-particle propagator, a double directed line represents the full Green's function calculated with respect to the interacting Hamiltonian. The self energy $\Sigma(1|1')$, defined in Eq. (2.134), is denoted by a circle.

numbers and imaginary times, we straightforwardly write down the famous Dyson equation in its most abstract way

$$\begin{pmatrix} \frac{\delta^2\Gamma}{\delta\psi^*\delta\psi} & \frac{\delta^2\Gamma}{\delta\psi^*\delta\psi^*} \\ \frac{\delta^2\Gamma}{\delta\psi\delta\psi} & \frac{\delta^2\Gamma}{\delta\psi\delta\psi^*} \end{pmatrix} = \zeta \begin{pmatrix} \langle\gamma\gamma^*\rangle & \langle\gamma\gamma\rangle \\ \langle\gamma^*\gamma^*\rangle & \langle\gamma^*\gamma\rangle \end{pmatrix}^{-1} . \tag{2.133}$$

After setting the source fields $\xi^{(*)}$ to zero, this means that the matrix which is comprised of our vertex functions is the inverse of the matrix of connected[4] Green's functions.

If we are again in a phase with conserved particle number, the expectation values $\langle\gamma\gamma\rangle = \langle\gamma^*\gamma^*\rangle = 0$. Then, we define the self energy according to

$$\zeta\Sigma(1|1') = \Gamma^{(1)}(1|1') - \Gamma_0^{(1)}(1|1'), \tag{2.134}$$

where the bare vertex $\Gamma_0^{(1)}(1|1')$ is computed with respect to the non-interacting Hamiltonian $\hat{H}_0$. Using this definition yields the probably more familiar form of the Dyson equation

$$\left(G^{(1)c}\right)^{-1} = \left(G_0^{(1)c}\right)^{-1} + \Sigma\,, \tag{2.135a}$$

$$\Longrightarrow G^{(1)c} = G_0^{(1)c} - G_0^{(1)c}\Sigma G^{(1)c}\,, \tag{2.135b}$$

where the propagators and the self energy should be understood as being matrices in their former indices. A diagrammatic representation of this equation can be seen in Fig. 2.5.

In addition to connectedness and one-particle irreducibility, we need to define one further property for Feynman diagrams: A diagram is called amputated, if all external legs do not carry any propagators. This means that every external point is directly connected to a vertex function. From how we regrouped our expansion into connected Green's functions and vertices, it should be clear that $-\Sigma(1|1')$ therefore consists of the sum over all distinct

[4]For the single-body propagator, connected and disconnected Green's function are the same (confer Eq. (2.127a)).

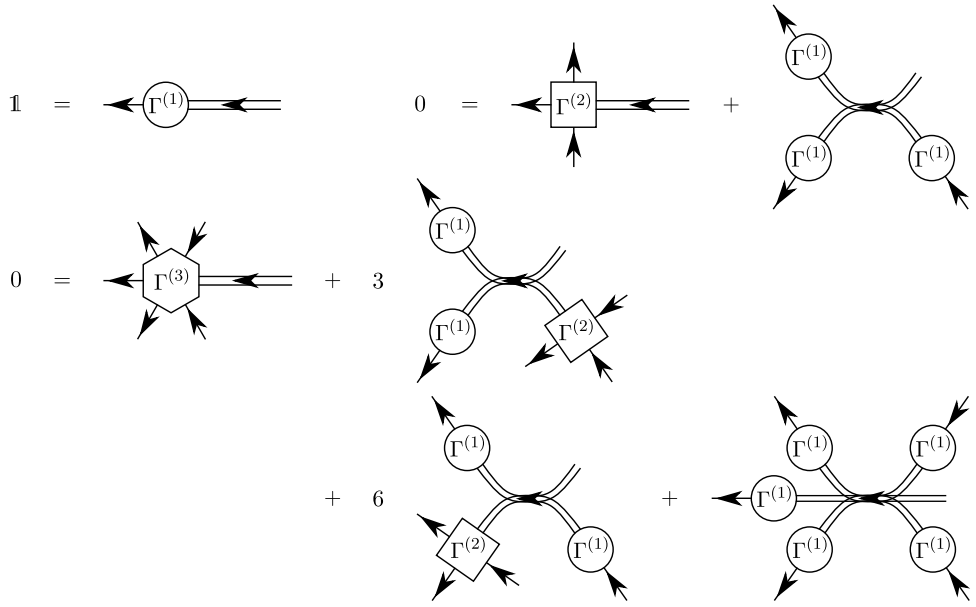

Figure 2.6.: Particle-number conserving diagrams for the derivation of the higher-order propagators [confer Eqs. (2.137) and (2.139)]: The diagrammatic expressions for the higher-order Dyson equations are given up to third order. Only vertices and propagators with equal numbers of incoming and outgoing legs are considered.

unlabeled Feynman diagrams connecting state 1 with $1'$, which are one-particle irreducible and amputated.

The reason why one calls Σ the self energy to begin with can be well understood by considering the fact that the inverse single-particle Green's function can be written as

$$\left(G^{(1)c}\right)^{-1}(1|1') = \left(\delta_{\alpha_1,\alpha_{1'}}(\frac{\partial}{\partial\tau_1} - \mu) + \langle\alpha_1|\hat{H}_0|\alpha_{1'}\rangle\right)\delta(\tau_1 - \tau_{1'}) + \Sigma(1|1')\,, \qquad (2.136)$$

which means that it plays the role of an effective single-particle potential due to virtual interaction processes with itself. To first order in the interaction, we immediately obtain the Hartree-Fock mean field equations which will become important in Chap. 6 when we turn to the projective symmetry group. We end this chapter though specifying the diagrammatic rules for arbitrary numbers of particles.

2.4.4. Higher-order vertices and propagators

We can continue the scheme that we previously employed for the self energy: We regroup the diagrams into n-particle vertices which contain all the amputated loop diagrams and obtain the connected n-particle propagators from tree expansions as in the Dyson equation. We constrict ourselves, however, to phases with conserved particle number, *e.g.*, only to vertices with equal number of incoming and outgoing legs.

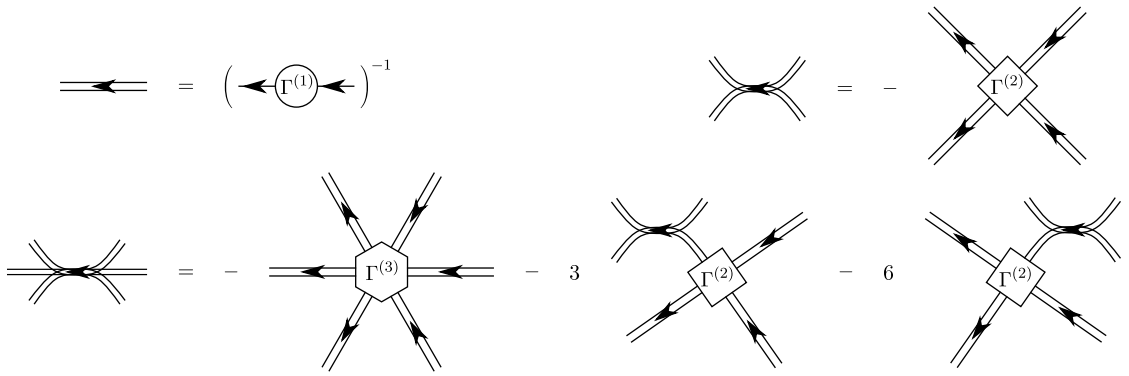

Figure 2.7.: Tree expansion for the n-particle Green's function up to $n = 3$: Each propagator consists of all possible combinations of vertices of order up to n connected by propagators of order up to $n - 1$. Again, we only consider diagrams which conserve particle number within each constituent.

By differentiation of the generating functionals $\mathcal{W}$ (Γ) with respect to the sources ξ^* and ξ (the fields ψ^* and ψ), we increase the number of incoming and outgoing legs of the generated connected Green's function (vertex function) by one. Utilising the chain rule for functional derivatives and Eqs. (2.130), we find that

$$\frac{\delta}{\delta\psi} = \frac{\delta\xi}{\delta\psi}\frac{\delta}{\delta\xi} + \frac{\delta\xi^*}{\delta\psi}\frac{\delta}{\delta\xi^*} = -\frac{\delta^2\Gamma}{\delta\psi\delta\psi^*}\frac{\delta}{\delta\xi} - \zeta\frac{\delta^2\Gamma}{\delta\psi\delta\psi}\frac{\delta}{\delta\xi^*}\,, \tag{2.137a}$$

$$\frac{\delta}{\delta\psi^*} = \frac{\delta\xi^*}{\delta\psi^*}\frac{\delta}{\delta\xi^*} + \frac{\delta\xi}{\delta\psi^*}\frac{\delta}{\delta\xi} = -\zeta\frac{\delta^2\Gamma}{\delta\psi^*\delta\psi}\frac{\delta}{\delta\xi^*} - \frac{\delta^2\Gamma}{\delta\psi^*\delta\psi^*}\frac{\delta}{\delta\xi}\,. \tag{2.137b}$$

Diagrammatically, this implies that if we take the $\psi^{(*)}$ derivative of the n-particle propagator, we have to increase the numbers of its incoming or outgoing legs by one and attach an appropriate two-particle vertex at each added leg. One has to be aware though that each derivative of the propagator now contributes two terms, one with a particle-number conserving vertex and an anomalous one [confer last terms in Eqs. (2.137)]. This is very practical and we utilised this trick already once when deriving the previous Dyson equation, which in quantum-label matrix language is simply

$$\frac{\delta\psi^*}{\delta\psi^*} = \mathbb{1} = \frac{\delta^2\Gamma}{\delta\psi^*\delta\psi}\frac{\delta^2\mathcal{W}}{\delta\xi^*\delta\xi} + \zeta\frac{\delta^2\Gamma}{\delta\psi^*\delta\psi^*}\frac{\delta^2\mathcal{W}}{\delta\xi\delta\xi}\,. \tag{2.138}$$

If we are interested in phases with particle number conservation only, the second term vanishes yielding $\mathbb{1} = \Gamma^{(1)}G^{(1)c}$. Applying ψ and ψ^* derivatives to all four terms from Eq. (2.138) then gives us the defining relations between two-particle Green's functions and vertices

$$\begin{aligned} 0 &= \frac{\delta^2}{\delta\psi^*\delta\psi}\left[\frac{\delta^2\Gamma}{\delta\psi^*\delta\psi}\frac{\delta^2\mathcal{W}}{\delta\xi^*\delta\xi} + \frac{\delta^2\Gamma}{\delta\psi^*\delta\psi^*}\frac{\delta^2\mathcal{W}}{\delta\xi\delta\xi}\right] \\ &= \frac{\delta^2}{\delta\psi^*\delta\psi}\left(\frac{\delta^2\Gamma}{\delta\psi^*\delta\psi}\right)\frac{\delta^2\mathcal{W}}{\delta\xi^*\delta\xi} + \frac{\delta^2\Gamma}{\delta\psi^*\delta\psi}\frac{\delta^2\Gamma}{\delta\psi^*\delta\psi}\frac{\delta^2\Gamma}{\delta\psi^*\delta\psi}\frac{\delta^2}{\delta\xi^*\delta\xi}\left(\frac{\delta^2\mathcal{W}}{\delta\xi^*\delta\xi}\right)\,. \end{aligned} \tag{2.139}$$

Here, we should still be aware of the structure of incoming and outgoing legs, but in principle this procedure can be used to relate all orders of vertices and Green's functions. We obtain the n-particle connected propagator by multiplying the corresponding equation with $2n-1$ inverse single-particle vertices which are, of course, the dressed and connected single-particle propagators $\left(\Gamma^{(1)}\right)^{-1} = G^{(1)c}$. Up to $n = 3$, the resulting diagrammatic expressions are summarised in Fig. 2.7 as well as the ones corresponding to the above equations in Fig. 2.6. Note that we only show the contributions from particle-number conserving vertices and propagators in both figures. For the correct derivation of higher-order equations, also the anomalous diagrams have to be considered up to a certain point. Fig. 2.7 shows that the two-particle vertex $\Gamma^{(2)}$ has to be the sum over all one-particle irreducible, amputated diagrams with two incoming and two outgoing legs, and plays the role of an effective two-particle interaction due to the virtual processes in the quantum many-body system. From it, we find $G^{(2)c}$ via a simple tree expansion using all $\Gamma^{(m)}$ with $m \leq 2$, where the self energy is contained in the full propagator. The same statement is true for all n-particle Green's functions and m-particle vertices with $m \leq n$.

Finally, we are able to determine the imaginary-time ordered Green's functions which are required for the computation of the spin susceptibility from Sec. 2.1.2. In the last section of this introduction, we present how to obtain it from the basic diagrammatic building blocks that were already defined.

2.4.5. Spin susceptibility from Green's and vertex functions

In Chaps. 4 and 5, we investigate the spin susceptibility $\chi_{ij}^{\mu\nu}(\tau)$ which is defined in Eq. (2.21). As shown in Eq. (2.25), this response function is related to the disconnected fermionic two-particle Green's functions and we now want to express it in terms of the two particle vertex and single-particle connected Green's functions since these are the objects of our further analysis. For this purpose, we first plug Eqs. (2.127) into Eq. (2.25) yielding

$$\begin{aligned}\chi_{ij}^{\mu\nu}(\tau) = \frac{1}{4}\sum_{\alpha,\beta,\gamma,\delta}\sigma_{\alpha\beta}^{\mu}\sigma_{\gamma\delta}^{\nu}\Big\{ & G^{(2)c}\left(\{j,\delta\},\{i,\beta\};0,\tau|\{j,\gamma\},\{i,\alpha\};0,\tau\right) \\ & + G^{(1)c}\left(\{j,\delta\};0|\{j,\gamma\};0\right)G^{(1)c}\left(\{i,\beta\};\tau|\{i,\alpha\};\tau\right) \\ & + \zeta G^{(1)c}\left(\{j,\delta\};0|\{i,\alpha\};\tau\right)G^{(1)c}\left(\{i,\beta\};\tau|\{j,\gamma\};0\right)\Big\}. \quad (2.140)\end{aligned}$$

The connected two-particle Green's function can be calculated from the two-particle vertex and the connected single-particle Green's function, confer Eq. (2.139). Using this result,

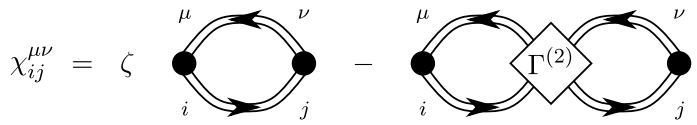

Figure 2.8.: Diagrammatic representation for the spin susceptibility: Black circles denote Pauli matrices $\frac{1}{2}\sigma^{\mu}$ and $\frac{1}{2}\sigma^{\nu}$, respectively. Closed loops contribute a factor of ζ and one needs to sum or integrate over all internal indices. For corresponding equations, confer Eqs. (2.146) and (2.142).

we find for the susceptibility that

$$\begin{aligned}\chi_{ij}^{\mu\nu}(\tau) = \frac{1}{4}\sum_{\alpha,\beta,\gamma,\delta}\sigma_{\alpha\beta}^{\mu}\sigma_{\gamma\delta}^{\nu}\Big\{ & G^{(1)c}\left(\{j,\delta\};0|\{j,\gamma\};0\right)G^{(1)c}\left(\{i,\beta\};\tau|\{i,\alpha\};\tau\right) \\ & + \zeta G^{(1)c}\left(\{j,\delta\};0|\{i,\alpha\};\tau\right)G^{(1)c}\left(\{i,\beta\};\tau|\{j,\gamma\};0\right)\Big\} \\ -\frac{1}{4}\sum_{\alpha,\beta,\gamma,\delta}\sigma_{\alpha\beta}^{\mu}\sigma_{\gamma\delta}^{\nu}\sum_{1',2',1,2}\Gamma^{(2)}(1',2'|1,2)G^{(1)c}\left(\{j,\delta\};0|1'\right)G^{(1)c}\left(\{i,\beta\};\tau|2'\right) \\ & \times G^{(1)c}\left(1|\{j,\gamma\};0\right)G^{(1)c}\left(2|\{i,\alpha\};\tau\right), \end{aligned} \tag{2.141}$$

where 1, 1′, 2, and 2′ are combined indices of lattice site, spin index, and imaginary time. The according sums have to be understood as a combination of the appropriate sums and a time integration. The Green's functions only depend on the imaginary time differences since we always perform our calculations in thermal equilibrium. Without spoiling too many upcoming results, we also note at this point that the propagators are entirely local and diagonal in spin space except for the mean-field analysis in Chap. 6 where we do not compute the susceptibility any longer. Hence, we can employ the diagonal structure of $G^{(1)c}$ yielding

$$\begin{aligned}\chi_{ij}^{\mu\nu}(\tau) = & \frac{\zeta}{4}\sum_{\alpha_1,\alpha_2}\sigma_{\alpha_1\alpha_2}^{\mu}\sigma_{\alpha_2\alpha_1}^{\nu}G_{\alpha_1}^{(1)}\left(-\tau\right)G_{\alpha_2}^{(1)}\left(\tau\right)\delta_{ij} - \frac{1}{4}\sum_{1',2',1,2}\sigma_{\alpha_1\alpha_{1'}}^{\mu}\sigma_{\alpha_2\alpha_{2'}}^{\nu}\Gamma^{(2)}(1',2'|1,2) \\ & \times G_{\alpha_{1'}}^{(1)}\left(\tau-\tau_{1'}\right)G_{\alpha_{2'}}^{(1)}\left(-\tau_{2'}\right)G_{\alpha_2}^{(1)}\left(\tau_2\right)G_{\alpha_1}^{(1)}\left(\tau_1-\tau\right). \end{aligned} \tag{2.142}$$

The first term in Eq. (2.141) vanishes due to its special spin structure. We also utilised that $G^{(1)} = G^{(1)c}$ is independent of its real space coordinates for the subsequently investigated systems of equivalent lattice sites. This enabled us to carry out the real-space sums yielding that $i_1 = i_{1'} = i$ and $i_2 = i_{2'} = j$ for the vertex function. Furthermore, the Green's functions now only depend on a single imaginary-time and a spin index and the sums over the combined indices represent spin sums and time integrations accordingly.

Since we are going to deal with Green's and vertex functions in Matsubara space in the following FRG analysis (confer Sec. 2.3.4), let us already calculate the Matsubara transformed spin susceptibility here. It is defined as

$$\chi_{ij}^{\mu\nu}(i\Omega) = \int_0^{\infty}\mathrm{d}\tau\, e^{i\Omega\tau}\left\langle T_\tau S_i^{\mu}(\tau)S_j^{\nu}(0)\right\rangle. \tag{2.143}$$

The Matsubara Green's function in thermal equilibrium are given by

$$G^{(1)}(\omega_n) = \int_0^\beta \mathrm{d}\tau\, e^{i\omega_n\tau} G^{(1)}(\tau)\,, \qquad G^{(1)}(\tau) = \frac{1}{\beta}\sum_{\omega_n} e^{-i\omega_n\tau} G^{(1)}(\omega_n)\,, \tag{2.144}$$

see Eqs. (2.113). In complete analogy, the transformed two-particle vertex should be computed via

$$\Gamma^{(2)}(\omega_{1'},\omega_{2'}|\omega_1,\omega_2) = \int_0^\infty \mathrm{d}\tau_{1'}\,\mathrm{d}\tau_{2'}\,\mathrm{d}\tau_1\,\mathrm{d}\tau_2\, e^{i(\omega_{1'}\tau_{1'}+\omega_{2'}\tau_{2'}-\omega_1\tau_1-\omega_2\tau_2)}\Gamma^{(2)}(\tau_{1'},\tau_{2'}|\tau_1,\tau_2)\,, \tag{2.145a}$$

$$\Gamma^{(2)}(\tau_{1'},\tau_{2'}|\tau_1,\tau_2) = \frac{1}{\beta^4}\sum_{\omega_{1'},\omega_{2'},\omega_1,\omega_2} e^{-i(\omega_{1'}\tau_{1'}+\omega_{2'}\tau_{2'}-\omega_1\tau_1-\omega_2\tau_2)}\Gamma^{(2)}(\omega_{1'},\omega_{2'}|\omega_1,\omega_2)\,. \tag{2.145b}$$

Plugging Eqs. (2.142), (2.144), and (2.145) into Eq. (2.143), one can ultimately relate the desired susceptibility to the diagrammatic constituents of the next chapters. It reads

$$\begin{aligned}\chi_{ij}^{\mu\nu}(i\Omega) = \frac{1}{4}\sum_{\alpha_{1'},\alpha_{2'},\alpha_1,\alpha_2} \sigma^\mu_{\alpha_1\alpha_{1'}}\sigma^\nu_{\alpha_2\alpha_{2'}} \Bigg\{ &\frac{\zeta}{\beta}\sum_{\omega_1} G^{(1)}_{\alpha_1}(\omega_1)\, G^{(1)}_{\alpha_2}(\omega_1+\Omega)\,\delta_{\alpha_{1'}\alpha_2}\delta_{\alpha_{2'}\alpha_1}\delta_{ij} \\ &- \frac{1}{\beta^2}\sum_{\omega_1,\omega_2}\Gamma^{(2)}(1',2'|1,2) G^{(1)}_{\alpha_{1'}}(\omega_1+\Omega)\, G^{(1)}_{\alpha_{2'}}(\omega_2)\, G^{(1)}_{\alpha_2}(\omega_2+\Omega)\, G^{(1)}_{\alpha_1}(\omega_1)\Bigg\}\,,\end{aligned} \tag{2.146}$$

where the combined indices are $1' = \{i, \alpha_{1'}, \omega_1+\Omega\}$, $2' = \{j, \alpha_{2'}, \omega_2\}$, $1 = \{i, \alpha_1, \omega_1\}$, and $2 = \{j, \alpha_2, \omega_2+\Omega\}$ for the two-particle vertex. A diagrammatic illustration for the spin susceptibility is shown in Fig. 2.8.

2.5. Summary

So far, we motivated that the so-called Green's functions or response functions provide answers to most of the physically relevant questions one can ask about a given quantum many-body system. Because Green's functions are in general not easy to obtain, we dedicated most of this chapter to show how all of their contributions that exist on a quantum level, *e.g.*, interference, superposition, virtual paths, *etc.*, are generically incorporated in the functional integral formalism. We now have a powerful scheme at our disposal which enables us to investigate arbitrary quantum systems and to gain insights on their properties. Depending on the precise nature of the considered model, one might already be able to make rather accurate predictions about experimental outcomes with the methods introduced until now. This is achieved by calculating self-energy and all necessary m-particle vertices up to a given order in the interacting part of the Hamiltonian. As it turns out

however, such a perturbation series always yields an uncontrolled approximation in the sense that one has *a priori* no knowledge about up to which order and up to which interaction strength the results are trustworthy, unless of course an exact solution is already known.

For quantum spin models, we derived how to relate the spin susceptibility to Green's functions which in turn can efficiently be computed from one-particle-irreducible vertices. In addition to its common difficulties, perturbation theory is unable to accurately describe the corresponding physics of such systems due to the absence of kinetic terms in the Hamiltonian, as briefly mentioned in the introduction. Fortunately though, the functional integral language remains valid for such models which is why we introduced it quite thoroughly. Within this formalism, we want to apply a method that goes beyond perturbation theory instead and thereby circumvents the mentioned issues. A prime candidate for this objective is the so-called functional renormalisation group analysis. It caught large attraction in the quantum spin physics community in recent years since it has shown to provide reliable results for Heisenberg models [11, 18, 87, 147, 168, 173] and anisotropic, but diagonal spin interactions [146, 168] regardless of their underlying lattices in two and three dimensions. Furthermore, unlike other currently available methods, *e.g.*, exact diagonalisation and density matrix renormalisation group [21, 25, 48, 61, 96, 114, 161, 180], this approach does not suffer from finite size effects. Later on, we will extend the existing method for diagonal spin interactions in order to investigate the effects of Dzyaloshinsky-Moriya interactions (Chap. 4) as well as different spin anisotropies (Chap. 5) and will eventually utilise the resulting vertex functions in order to self-consistently determine effective low-energy theories for the considered spin models (Chap. 6). Before doing so, we properly introduce the functional renormalisation group method in the following.

3. Functional renormalization group

As we know from the previous chapter, the standard procedure to obtain response functions like the spin susceptibility of a quantum many-body system is based on the computation of Feynman diagrams for the vertex functions. The Feynman diagrams consist of interaction vertices and Green's functions whose internal indices such as spin, time or frequency are summed up or integrated over, respectively. In a Heisenberg model however [see Eq. (1.1)], this yields non-converging results for our purposes. The reason behind this is that only spin-spin interactions are present in such a Hamiltonian which completely lacks any kind of terms being quadratic in the fermionic operators. This implies that all single-particle energies vanish yielding for the bare Matsubara Green's function

$$G_0^{(1)}(1|1') = \beta G_0^{(1)}(1)\delta_{\alpha_1,\alpha_{1'}}\delta(\omega_1 - \omega_{1'}) = \frac{-1}{i\omega_1}\beta\delta_{\alpha_1,\alpha_{1'}}\delta(\omega_1 - \omega_{1'}) \tag{3.1}$$

in the canonical ensemble (confer Eq. (2.114) and Sec. 2.1.1). In this fermionic model, our Green's function acquires an extra minus sign if compared to a different convention that is used frequently by other authors. Nevertheless, we retain the definition given in Sec. 2.1.2 because the resulting equations are often more compact. Since we try to identify quantum spin liquids that show no sign of magnetic order down to lowest temperatures, we are interested in the $T \to 0$ limit where Matsubara frequencies become dense. Hence, the appropriate integral over an internal Matsubara frequency of a given Feynman diagram can easily diverge around $\omega \approx 0$. For instance, the first term in Eq. (2.146) for the spin susceptibility contributes to zeroth order in the interaction via a product of two bare propagators [Eq. (3.1)]. In this case as well as for any other Feynman diagram that consists of a loop with two bare propagators, we are not able to perform the frequency integration in the $T \to 0$ limit.

Of course, the systems that we are investigating are typically Mott insulators at very low temperatures and do not tend to diverge in any observable way. The fact that perturbation theory breaks down in our case is related to the fact that we are only dealing with interactions which completely determine the relevant energy scale. Thus, there is no small parameter which one could meaningfully treat as a perturbation. Instead one would literally perturb the system around nothing.

The mathematical difficulties for quantum spin models arise at low frequencies as discussed above. Traditionally such challenges frequently occur in high-energy physics and, despite the difference in the responsible phenomena, one approach that was originally developed to study high-temperature phase transitions in particle physics [186] has proven itself to be a powerful tool for the investigation of low-energy spin systems as well. This is why we want to introduce this so-called functional renormalisation group (FRG) formalism in the current chapter which is based on a script by Volker Meden [117]. The FRG was mainly developed in Refs. [50, 72, 125, 155, 186] and has ever since been successfully applied to Luttinger liquids [4, 5, 124], the Anderson-Holstein model [105], correlated quantum dots [97, 98], and the Kondo dot model [39, 40, 159] for instance. In 2010, the method was then applied to the spin-$\frac{1}{2}$ square lattice Heisenberg model for the first time [147] which inspired a plethora of works on related systems.

3.1. Introducing an infrared cutoff

The functional renormalisation group uses four main ingredients in order to prevent the breakdown of an effective theory at low energies. They are:

1. replace the single-particle propagator[1]

$$G_0(\omega) = \frac{-1}{i\omega} \qquad \longrightarrow \qquad G_0^\Lambda(\omega) = \frac{-\theta(|\omega| - \Lambda)}{i\omega}\,, \tag{3.2}$$

2. redefine the generating functional for the vertex functions from Eq. (2.129) to be

$$\Gamma^\Lambda\left[\{\psi^*\},\{\psi\}\right] = -\mathcal{W}^\Lambda\left[\{\xi^*\},\{\xi\}\right] - (\psi^*,\xi) - (\xi^*,\psi) - \left(\psi^*, \left[G_0^\Lambda\right]^{-1}\psi\right)\,, \tag{3.3}$$

3. derive integro-differential equations for the vertex functions with respect to the infrared cutoff Λ,

4. choose proper initial values for the vertices for an infinite cutoff $\Lambda \to \infty$.

Note that we do not display the superscript (1) for the single-particle Green's function any longer since only this propagator is used from now on. Further, the short-hand notation with scalar and matrix products should be understood as

$$(\psi^*,\xi) = \sum_{\omega_j}\sum_{\alpha_j} \psi^*_{\alpha_j}(\omega_j)\xi_{\alpha_j}(\omega_j)\,, \tag{3.4a}$$

$$(\psi^*, A\psi) = \sum_{\omega_j,\omega_k}\sum_{\alpha_j,\alpha_k} \psi^*_{\alpha_j}(\omega_j)A_{\alpha_j\alpha_k}(\omega_j,\omega_k)\psi_{\alpha_k}(\omega_k)\,. \tag{3.4b}$$

Using these constituents, one has to solve the resulting initial value problem for $\Lambda \to 0$. If everything could be carried out correctly, one would obtain the correct vertex functions of the original system since $G^\Lambda \to G$ in this limit. As it turns out, however, this is an impossible task. The integro-differential equations couple all orders of vertices with each other, resulting in a stew of infinitely many coupled terms to keep track of. There is no known way for analysing such systems of equations exactly and all solutions that we present in the following chapters will thus be obtained in an appropriate approximation. Before discussing how to delicately carve a finite number of coupled equations off the infinite set (see in Sec. 4.2.1), we derive the so-called flow equations for the vertex functions in the remainder of this chapter.

3.2. Derivation of FRG flow equations

Next to the replacement of our bare single-particle Green's function with its regularised version from Eq. (3.2), we have to acknowledge how this change in the propagator translates

[1] We note at this point that the regularisation procedure can also be performed with functions other than the Heaviside function [125].

to the generating functionals for the connected Green's functions and the vertices. Let us start by realising that, using Eq. (2.123), Eq. (2.126a), and the short-hand notations from above, we can rewrite the generating functional for the connected Matsubara Green's functions $\mathcal{W}$ in the following way

$$\begin{aligned}\mathcal{W}^{\Lambda}\left[\{\xi^*\},\{\xi\}\right] &= \ln\left[\mathcal{G}^{\Lambda}\left[\{\xi^*\},\{\xi\}\right]\right] \\ &= \ln\left[\frac{1}{\mathcal{Z}_0^{\Lambda}}\int \mathcal{D}[\{\gamma^*\},\{\gamma\}]\, e^{-\left(\gamma^*,\left[G_0^{\Lambda}\right]^{-1}\gamma\right)-(\xi^*,\gamma)-(\gamma^*\xi)-V[\{\gamma^*\},\{\gamma\}]}\right], \end{aligned} \tag{3.5}$$

where we utilised that $\left(i\omega_j - \epsilon_{\alpha_j} + \mu\right) = -\left[G_0\right]^{-1}$ (confer Eq. (2.114)), but this time inserted the renormalised propagator G_0^{Λ}, and replaced $\mathcal{Z}$ by $\mathcal{Z}_0^{\Lambda}$ in the denominator. In this case, $G^{(0)c} = \mathcal{W}^{\Lambda=0}\left[\{\xi^*\},\{\xi\}\right]\big|_{\xi^*=\xi=0} = \ln\left[\frac{\mathcal{Z}}{\mathcal{Z}_0}\right]$ is no longer zero. However, for any higher-order vertices and Green's functions, this redefinition of the generating functional has no effect. Note that when rewriting the generating functionals in Matsubara space, the general structure of the equations is held up and the boundary conditions for the path integral are automatically fulfilled. We only have to consider the correct prefactors of β and the diagonal structure in frequencies for our diagrammatic constituents.

We stop denoting the arguments of our functionals from now on for brevity and proceed in the derivation of the *flow* equations by taking their scale derivatives with respect to Λ. For $\mathcal{W}$, we find

$$\dot{\mathcal{W}^{\Lambda}} = \frac{1}{\mathcal{G}^{\Lambda}}\int \mathcal{D}[\{\gamma^*\},\{\gamma\}]\,\frac{\mathrm{d}}{\mathrm{d}\Lambda}\left[\frac{1}{\mathcal{Z}_0^{\Lambda}}e^{-\left(\gamma^*,\left[G_0^{\Lambda}\right]^{-1}\gamma\right)}\right] e^{-(\xi^*,\gamma)-(\gamma^*\xi)-V[\{\gamma^*\},\{\gamma\}]}. \tag{3.6}$$

Denoting the full Λ derivative with a dot, we find for the left-over term from above

$$\begin{aligned}\frac{\mathrm{d}}{\mathrm{d}\Lambda}\left[\frac{1}{\mathcal{Z}_0^{\Lambda}}e^{-\left(\gamma^*,\left[G_0^{\Lambda}\right]^{-1}\gamma\right)}\right] =& \frac{-1}{\mathcal{Z}_0^{\Lambda}}\left(\gamma^*,\dot{\left[G_0^{\Lambda}\right]^{-1}}\gamma\right)e^{-\left(\gamma^*,\left[G_0^{\Lambda}\right]^{-1}\gamma\right)} + \left\{\left(\frac{1}{\mathcal{Z}_0^{\Lambda}}\right)^2 e^{-\left(\gamma^*,\left[G_0^{\Lambda}\right]^{-1}\gamma\right)}\right. \\ &\left.\times\int\mathcal{D}[\{\tilde{\gamma}^*\},\{\tilde{\gamma}\}]\left(\tilde{\gamma}^*,\dot{\left[G_0^{\Lambda}\right]^{-1}}\tilde{\gamma}\right)e^{-\left(\tilde{\gamma}^*,\left[G_0^{\Lambda}\right]^{-1}\tilde{\gamma}\right)}\right\} \\ =& \frac{1}{\mathcal{Z}_0^{\Lambda}}e^{-\left(\gamma^*,\left[G_0^{\Lambda}\right]^{-1}\gamma\right)}\left\{\zeta\,\mathrm{Tr}\left[\dot{\left[G_0^{\Lambda}\right]^{-1}}G_0^{\Lambda}\right] - \left(\gamma^*,\dot{\left[G_0^{\Lambda}\right]^{-1}}\gamma\right)\right\},\end{aligned} \tag{3.7}$$

where we employed integration by parts in the last line. Inserting this result into the original equation, making use of the definition of $\mathcal{G}^{\Lambda}$ including its sources and that $\dot{\mathcal{W}} = \frac{1}{\mathcal{G}}\dot{\mathcal{G}}$, one can show that

$$\dot{\mathcal{G}^{\Lambda}} = \zeta\,\mathrm{Tr}\left[\dot{\left[G_0^{\Lambda}\right]^{-1}}G_0^{\Lambda}\right]\mathcal{G}^{\Lambda} - \zeta\left(\delta_{\xi},\dot{\left[G_0^{\Lambda}\right]^{-1}}\delta_{\xi^*}\right)\mathcal{G}^{\Lambda}. \tag{3.8}$$

This is the differential equation for the generating functional of the disconnected Green's functions. If we want to derive such an equation for the connected Green's functions, we

have to use

$$\begin{aligned} e^{-\mathcal{W}^\Lambda}\left(\delta_\xi, \dot{[G_0^\Lambda]^{-1}}\delta_{\xi^*}\right)e^{\mathcal{W}^\Lambda} =& e^{-\mathcal{W}^\Lambda}\left\{\left(\delta_\xi, \dot{[G_0^\Lambda]^{-1}}\delta_{\xi^*}\mathcal{W}^\Lambda\right)e^{\mathcal{W}^\Lambda}\right\} \\ =& e^{-\mathcal{W}^\Lambda}\left(\delta_\xi\mathcal{W}^\Lambda, \dot{[G_0^\Lambda]^{-1}}\delta_{\xi^*}\mathcal{W}^\Lambda\right)e^{\mathcal{W}^\Lambda} \\ &+ e^{-\mathcal{W}^\Lambda}\left\{\left(\delta_\xi, \dot{[G_0^\Lambda]^{-1}}\delta_{\xi^*}\right)\mathcal{W}^\Lambda\right\}e^{\mathcal{W}^\Lambda} \\ =& \left(\delta_\xi\mathcal{W}^\Lambda, \dot{[G_0^\Lambda]^{-1}}\delta_{\xi^*}\mathcal{W}^\Lambda\right) + \left(\delta_\xi, \dot{[G_0^\Lambda]^{-1}}\delta_{\xi^*}\right)\mathcal{W}^\Lambda\,, \end{aligned} \tag{3.9}$$

where the derivatives only act within curly brackets in this notation. The term including second derivatives yet can be reformulated.

$$\left(\delta_\xi, \dot{[G_0^\Lambda]^{-1}}\delta_{\xi^*}\right)\mathcal{W}^\Lambda = \mathrm{Tr}\left[\left(\dot{[G_0^\Lambda]^{-1}}\right)^T\frac{\delta^2\mathcal{W}^\Lambda}{\delta\xi\delta\xi^*}\right] = \zeta\,\mathrm{Tr}\left[\frac{\delta^2\mathcal{W}^\Lambda}{\delta\xi^*\delta\xi}\dot{[G_0^\Lambda]^{-1}}\right] \tag{3.10}$$

Plugging these results into Eq. (3.6) and using the invariance of the trace under cyclic permutations, we finally arrive at the differential equation for the generating functional of connected Green's functions

$$\dot{\mathcal{W}}^\Lambda = \zeta\,\mathrm{Tr}\left[\dot{[G_0^\Lambda]^{-1}}G_0^\Lambda\right] - \zeta\left(\delta_\xi\mathcal{W}^\Lambda\,, \dot{[G_0^\Lambda]^{-1}}\delta_{\xi^*}\mathcal{W}^\Lambda\right) - \mathrm{Tr}\left[\dot{[G_0^\Lambda]^{-1}}\frac{\delta^2\mathcal{W}^\Lambda}{\delta\xi^*\delta\xi}\right]. \tag{3.11}$$

Our goal is to start the *flow* of the differential equations at $\Lambda \to \infty$. From thereon, we want to integrate out the high-energy degrees of freedom by successively lowering the cutoff. However, we do not develop the FRG with respect to Green's functions because it turns out that the method is ill-defined with the initial conditions that $G_0^{\Lambda\to\infty} = 0$ (see [117] for more details). Fortunately, this issue is circumvented by employing Eq. (3.3) because it turns out that the *flow* equations for the vertex functions ultimately are well defined. Before being able to calculate the Λ derivative of the generating functional Γ^Λ, we have to consider that since we are introducing new fundamental variables ψ and ψ^* the old variables ξ and ξ^* still being defined via Eqs. (2.130) now become cutoff dependent due to the additional term in Eq. (3.3). Also, the Dyson equation [Eq. (2.138)] changes for the same reason.

Computing ξ and ξ^* from the new generating functional Γ^Λ yields that

$$\xi^\Lambda_{\alpha_j}(\omega_j) = -\frac{\delta}{\delta\psi^*_{\alpha_j}(\omega_j)}\Gamma^\Lambda\left[\psi^*_{\alpha_j}(\omega_j), \psi_{\alpha_j}(\omega_j)\right] - \sum_{\omega_k}\sum_{\alpha_k}\left[G_0^\Lambda\right]^{-1}_{\alpha_j\alpha_k}(\omega_j,\omega_k)\psi_{\alpha_k}(\omega_k)\,, \tag{3.12a}$$

$$\xi^{\Lambda\,*}_{\alpha_j}(\omega_j) = -\zeta\frac{\delta}{\delta\psi_{\alpha_j}(\omega_j)}\Gamma^\Lambda\left[\psi^*_{\alpha_j}(\omega_j), \psi_{\alpha_j}(\omega_j)\right] - \sum_{\omega_k}\sum_{\alpha_k}\psi^*_{\alpha_k}(\omega_k)\left[G_0^\Lambda\right]^{-1}_{\alpha_k\alpha_j}(\omega_k,\omega_j)\,. \tag{3.12b}$$

For modifying the Dyson equation, we need to include those parts of $\delta\xi^{(*)\,\Lambda}/\delta\psi^{(*)}$ that occur due to the second terms in the equations above. A straightforward calculation shows

that our new relation between Γ and $\mathcal{W}$ reads in the former matrix language

$$\begin{pmatrix} \frac{\delta^2\Gamma}{\delta\psi^*\delta\psi} + \zeta\left[G_0^\Lambda\right]^{-1} & \frac{\delta^2\Gamma}{\delta\psi^*\delta\psi^*} \\ \frac{\delta^2\Gamma}{\delta\psi\delta\psi} & \frac{\delta^2\Gamma}{\delta\psi\delta\psi^*} + \left[\left[G_0^\Lambda\right]^{-1}\right]^T \end{pmatrix} \begin{pmatrix} \frac{\delta^2\mathcal{W}^\Lambda}{\delta\xi^*\delta\xi} & \zeta\frac{\delta^2\mathcal{W}^\Lambda}{\delta\xi^*\delta\xi^*} \\ \zeta\frac{\delta^2\mathcal{W}^\Lambda}{\delta\xi\delta\xi} & \frac{\delta^2\mathcal{W}^\Lambda}{\delta\xi\delta\xi^*} \end{pmatrix} = \begin{pmatrix} \mathbb{1} & 0 \\ 0 & \mathbb{1} \end{pmatrix}. \tag{3.13}$$

After setting the source fields to zero on both sides, this result can be compared to the Dyson equation $\left[G^\Lambda\right]^{-1} = \left[G_0^\Lambda\right]^{-1} + \Sigma^\Lambda$ (confer Eq. 2.135a) yielding that

$$\Sigma^\Lambda = \zeta\Gamma^{(1)\,\Lambda} \tag{3.14}$$

in a phase with particle-number conservation.

Using these considerations, we compute the scale derivative of Γ^Λ from Eq. (3.3) yielding

$$\begin{aligned} \dot{\Gamma^\Lambda}\left[\{\psi^*\},\{\psi\}\right] &= -\frac{\mathrm{d}}{\mathrm{d}\Lambda}\mathcal{W}^\Lambda\left[\left\{\xi^{\Lambda\,*}\right\},\left\{\xi^\Lambda\right\}\right] - \left(\psi^*,\dot{\xi^\Lambda}\right) - \left(\dot{\xi^\Lambda}{}^*,\psi\right) - \left(\psi^*,\dot{\left[G_0^\Lambda\right]^{-1}}\psi\right) \\ &= -\left(\dot{\xi^\Lambda}{}^*,\delta_{\xi^{\Lambda\,*}}\mathcal{W}^\Lambda\right) - \left(\dot{\xi^\Lambda},\delta_{\xi^\Lambda}\mathcal{W}^\Lambda\right) - \dot{\mathcal{W}}^\Lambda\left[\left\{\xi^{\Lambda\,*}\right\},\left\{\xi^\Lambda\right\}\right] \\ &\quad - \left(\psi^*,\dot{\xi^\Lambda}\right) - \left(\dot{\xi^\Lambda}{}^*,\psi\right) - \left(\psi^*,\dot{\left[G_0^\Lambda\right]^{-1}}\psi\right) \\ &= -\dot{\mathcal{W}}^\Lambda\left[\left\{\xi^{\Lambda\,*}\right\},\left\{\xi^\Lambda\right\}\right] - \zeta\left(\delta_{\xi^\Lambda}\mathcal{W}^\Lambda,\dot{\left[G_0^\Lambda\right]^{-1}}\delta_{\xi^{\Lambda\,*}}\mathcal{W}^\Lambda\right), \end{aligned} \tag{3.15}$$

where we employed the definitions of our fields $\psi^{(*)}$ from Eq. (2.128) in the last line. Inserting Eq. (3.11), we find that

$$\begin{aligned} \dot{\Gamma^\Lambda}\left[\{\psi^*\},\{\psi\}\right] &= -\zeta\,\mathrm{Tr}\left[\dot{\left[G_0^\Lambda\right]^{-1}}G_0^\Lambda\right] + \mathrm{Tr}\left[\dot{\left[G_0^\Lambda\right]^{-1}}\frac{\delta^2\mathcal{W}^\Lambda}{\delta\xi^*\delta\xi}\right] \\ &= -\zeta\,\mathrm{Tr}\left[\dot{\left[G_0^\Lambda\right]^{-1}}G_0^\Lambda\right] + \mathrm{Tr}\left[\dot{\left[G_0^\Lambda\right]^{-1}}\,X^\Lambda_{\psi^*,\psi}\big|_{1,1}\right], \end{aligned} \tag{3.16}$$

where $X^\Lambda_{\psi^*,\psi}\Big|_{1,1}$ is defined according to Eq. (3.13) as the top left element of the matrix

$$X^\Lambda_{\psi^*,\psi} = \begin{pmatrix} \frac{\delta^2\Gamma}{\delta\psi^*\delta\psi} + \zeta\left[G_0^\Lambda\right]^{-1} & \frac{\delta^2\Gamma}{\delta\psi^*\delta\psi^*} \\ \frac{\delta^2\Gamma}{\delta\psi\delta\psi} & \frac{\delta^2\Gamma}{\delta\psi\delta\psi^*} + \left[\left[G_0^\Lambda\right]^{-1}\right]^T \end{pmatrix}^{-1}. \tag{3.17}$$

Now, we want to expand $X^\Lambda_{\psi^*,\psi}\Big|_{1,1}$ in the full propagator G^Λ and therefore rewrite

$$\begin{aligned} \frac{\delta^2\Gamma^\Lambda}{\delta\psi^*\delta\psi} + \zeta\left[G_0^\Lambda\right]^{-1} &= \Gamma^{(1)\,\Lambda} + \Delta_{\psi^*,\psi} + \zeta\left[G_0^\Lambda\right]^{-1} \\ &= \zeta\Sigma^\Lambda + \Delta_{\psi^*,\psi} + \zeta\left[G_0^\Lambda\right]^{-1} \\ &= \zeta\left[G^\Lambda\right]^{-1} + \Delta_{\psi^*,\psi}, \end{aligned} \tag{3.18}$$

confer Eq. (3.14). Here, we defined

$$\begin{aligned}\Delta_{\psi^*,\psi} &= \frac{\delta^2\Gamma^\Lambda}{\delta\psi^*\delta\psi} - \Gamma^{(1)\,\Lambda} \\ &= \frac{\delta^2\Gamma^\Lambda}{\delta\psi^*\delta\psi} - \left.\frac{\delta^2\Gamma^\Lambda}{\delta\psi^*\delta\psi}\right|_{\xi^*=\xi=0} .\end{aligned} \tag{3.19}$$

Plugging Eqs. (3.18) and (3.19) into Eq. (3.17) provides us with the relation

$$\begin{aligned}X^\Lambda_{\psi^*,\psi} &= \left[\begin{pmatrix} \zeta\left[G^\Lambda\right]^{-1} & 0 \\ 0 & \left[\left[G^\Lambda\right]^{-1}\right]^T \end{pmatrix} + \begin{pmatrix} \Delta_{\psi^*,\psi} & \frac{\delta^2\Gamma}{\delta\psi^*\delta\psi^*} \\ \frac{\delta^2\Gamma}{\delta\psi\delta\psi} & \zeta\Delta^T_{\psi^*,\psi} \end{pmatrix}\right]^{-1} \\ &= \left[\begin{pmatrix} \mathbb{1} & 0 \\ 0 & \mathbb{1} \end{pmatrix} + \begin{pmatrix} \zeta G^\Lambda & 0 \\ 0 & \left[G^\Lambda\right]^T \end{pmatrix}\begin{pmatrix} \Delta_{\psi^*,\psi} & \frac{\delta^2\Gamma}{\delta\psi^*\delta\psi^*} \\ \frac{\delta^2\Gamma}{\delta\psi\delta\psi} & \zeta\Delta^T_{\psi^*,\psi} \end{pmatrix}\right]^{-1}\begin{pmatrix} \zeta G^\Lambda & 0 \\ 0 & \left[G^\Lambda\right]^T \end{pmatrix} .\end{aligned} \tag{3.20}$$

This enables us to give the desired expansion for the upper left element of this matrix, *i.e.*,

$$\begin{aligned}X^\Lambda_{\psi^*,\psi}\big|_{1,1} \simeq{}& \zeta G^\Lambda - G^\Lambda\Delta_{\psi^*,\psi}G^\Lambda + \zeta G^\Lambda\Delta_{\psi^*,\psi}G^\Lambda\Delta_{\psi^*,\psi}G^\Lambda \\ &+ G^\Lambda\frac{\delta^2\Gamma}{\delta\psi^*\delta\psi^*}\left[G^\Lambda\right]^T\frac{\delta^2\Gamma}{\delta\psi\delta\psi}G^\Lambda - \dots .\end{aligned} \tag{3.21}$$

According to the definition of the vertex functions from Eq. (2.131), we can expand their generating functional as follows

$$\Gamma^\Lambda\left[\{\psi^*\},\{\psi\}\right] = \sum_{k=0}^{\infty}\frac{\zeta^k}{(k!)^2}\sum_{1',\dots,k'}\sum_{1,\dots,k}\Gamma^{(k)\,\Lambda}(1',\dots,k'|1,\dots,k)\times\psi^*_{1'}\dots\psi^*_{k'}\psi_k\dots\psi_1 . \tag{3.22}$$

This expansion can now be plugged into both sides of Eq. (3.16) which, after a comparison of powers in the fields $\psi^{(*)}$, provides us with a hierarchy of coupled equations for the Λ-derivatives of our vertex functions on the left-hand and with products of vertices and Green's functions on the right-hand side. Here, one should note that $\Delta_{\psi^*,\psi}$ is at least quadratic in $\psi^{(*)}$.

For the zeroth-order term, we hence find that

$$\Gamma^{(\dot{0})\,\Lambda} = -\zeta\,\mathrm{Tr}\left[\left[\dot{G^\Lambda_0}\right]^{-1}G^\Lambda_0\right] + \zeta\,\mathrm{Tr}\left[G^\Lambda\left[\dot{G^\Lambda_0}\right]^{-1}\right] , \tag{3.23}$$

which couples $\Gamma^{(0)\,\Lambda}$ to $\Gamma^{(1)\,\Lambda}$ via G^Λ the Dyson equation. Therefore, we also need to determine the single-particle vertex for which we need to compute the part of $\Delta_{\psi^*,\psi}$ that is quadratic in the fields $\psi^{(*)}$. From Eq. (3.19), we see that only the second derivative of the generating functional but not the single-particle vertex contributes to this via the term

$\propto \Gamma^{(2)\,\Lambda}$ in the expansion of Eq. (3.22).

$$\begin{aligned}
&\frac{\delta^2}{\delta\psi^*_{k'}\delta\psi_k}\frac{\zeta^2}{(2!)^2}\sum_{1',2'}\sum_{1,2}\Gamma^{(2)\,\Lambda}(1',2'|1,2)\times\psi^*_{1'}\psi^*_{2'}\psi_2\psi_1 \\
&\quad=\frac{1}{(2!)^2}\sum_{1'}\sum_{1}\Big[\Gamma^{(2)\,\Lambda}(k',1'|1,k)\times\psi^*_{1'}\psi_1+\zeta\Gamma^{(2)\,\Lambda}(1',k'|1,k)\times\psi^*_{1'}\psi_1 \\
&\qquad\qquad+\Gamma^{(2)\,\Lambda}(1',k'|k,1)\times\psi^*_{1'}\psi_1+\zeta\Gamma^{(2)\,\Lambda}(k',1'|k,1)\times\psi^*_{1'}\psi_1\Big] \\
&\quad=\zeta\sum_{1'}\sum_{1}\Gamma^{(2)\,\Lambda}(1',k'|1,k)\times\psi^*_{1'}\psi_1
\end{aligned}\tag{3.24}$$

Using this result, we can compare the coefficients of the quadratic terms from left and right-hand side of Eq. (3.16) yielding that

$$\dot{\Gamma^{(1)\,\Lambda}}(1'|1)=-\operatorname{Tr}\left[S^\Lambda\Gamma^{(2)\,\Lambda}(1',l'|1,k)\right],\tag{3.25}$$

where now the matrix product and the trace act on the labels l' and k from the two-particle vertex. Here, we already introduced the single-scale propagator

$$S^\Lambda=G^\Lambda\big[\dot{G^\Lambda_0}\big]^{-1}G^\Lambda\,.\tag{3.26}$$

Eqs. (3.25) and (3.26) show that the single-particle vertex now couples to $\Gamma^{(2)\,\Lambda}$ and to itself due to the full propagator G^Λ.

For the two-particle vertex, we need to be aware of the fact that there are contributions due to the second and the third term in Eq. (3.21) which are proportional to $\Gamma^{(3)\,\Lambda}$ and $\Gamma^{(2)\,\Lambda}$, respectively. Thus, we still need to compute

$$\begin{aligned}
&\frac{\delta^2}{\delta\psi^*_{l'}\delta\psi_k}\frac{\zeta^3}{(3!)^2}\sum_{1',2',3'}\sum_{1,2,3}\Gamma^{(3)\,\Lambda}(1',2',3'|1,2,3)\times\psi^*_{1'}\psi^*_{2'}\psi^*_{3'}\psi_3\psi_2\psi_1 \\
&\quad=\frac{9}{(3!)^2}\sum_{1',2'}\sum_{1,2}\Gamma^{(3)\,\Lambda}(1',2',l'|1,2,k)\times\psi^*_{1'}\psi^*_{2'}\psi_2\psi_1\,.
\end{aligned}\tag{3.27}$$

An additional contribution due to the fourth term in Eq. (3.21) arises from the anomalous derivatives

$$\frac{\delta^2}{\delta\psi^*_{k'}\delta\psi^*_{l'}}\frac{\zeta^2}{(2!)^2}\sum_{1',2'}\sum_{1,2}\Gamma^{(2)\,\Lambda}(1',2'|1,2)\times\psi^*_{1'}\psi^*_{2'}\psi_2\psi_1=\frac{\zeta}{2}\sum_{1,2}\Gamma^{(2)\,\Lambda}(k',l'|1,2)\times\psi_2\psi_1\,,\tag{3.28}$$

$$\frac{\delta^2}{\delta\psi_k\delta\psi_l}\frac{\zeta^2}{(2!)^2}\sum_{1',2'}\sum_{1,2}\Gamma^{(2)\,\Lambda}(1',2'|1,2)\times\psi^*_{1'}\psi^*_{2'}\psi_2\psi_1=\frac{1}{2}\sum_{1',2'}\Gamma^{(2)\,\Lambda}(1',2'|k,l)\times\psi^*_{1'}\psi^*_{2'}\,.\tag{3.29}$$

Combining all considerations finally yields the flow equation for the two-particle vertex

$$\begin{aligned}\dot{\Gamma^{(2)\,\Lambda}}(1',2'|1,2) = &- \mathrm{Tr}\left[S^{\Lambda}\Gamma^{(3)\,\Lambda}(1',2',l'|1,2,k)\right] \\ &+ \zeta\,\mathrm{Tr}\left[S^{\Lambda}\Gamma^{(2)\,\Lambda}(l',k'|1,2)\left[G^{\Lambda}\right]^{T}\Gamma^{(2)\,\Lambda}(1',2'|k,l)\right] \\ &+ \zeta\,\mathrm{Tr}\left[S^{\Lambda}\Gamma^{(2)\,\Lambda}(1',l'|1,k)G^{\Lambda}\Gamma^{(2)\,\Lambda}(2',k'|2,l)\right] \\ &+ \zeta\,\mathrm{Tr}\left[S^{\Lambda}\Gamma^{(2)\,\Lambda}(2',l'|2,k)G^{\Lambda}\Gamma^{(2)\,\Lambda}(1',k'|1,l)\right] \\ &+ \mathrm{Tr}\left[S^{\Lambda}\Gamma^{(2)\,\Lambda}(1',l'|2,k)G^{\Lambda}\Gamma^{(2)\,\Lambda}(2',k'|1,l)\right] \\ &+ \mathrm{Tr}\left[S^{\Lambda}\Gamma^{(2)\,\Lambda}(2',l'|1,k)G^{\Lambda}\Gamma^{(2)\,\Lambda}(1',k'|2,l)\right] \end{aligned} \tag{3.30}$$

Again, we see that the two-particle vertex couples to all $\Gamma^{(m)\,\Lambda}$ with $m \leq 3$. This leads to an infinite hierarchy of coupled equations that we are not able to solve. Therefore we need to truncate the system at a certain point. Within this thesis, we do not compute the three-particle vertex directly and therefore stop at this point.

The last step now is to derive the initial conditions for $\Lambda \to \infty$ of our generating functional Γ^{Λ}. Considering that $G_0^{\Lambda} = 0$ in this case, one can realise that the sole remaining diagrammatic constituent of our vertex functions is the bare interaction from the Hamiltonian, *i.e.*,

$$\Gamma^{\Lambda\to\infty}\left[\{\psi^*\},\{\psi\}\right] = V\left[\{\psi^*\},\{\psi\}\right]. \tag{3.31}$$

Here, V is the interacting part of the Hamiltonian $H = H_0 + V$ which is not already incorporated in the non-interacting single-particle eigenenergies ϵ_{α_j} [see Eqs. (2.90) and (2.97)]. This important initial condition can also be derived in a mathematically rigorous fashion. We refer the interested reader again to Ref. [117] for more details. For our spin Hamiltonian in terms of Abrikosov fermions, this means that only the two-particle vertex has a non-vanishing initial value

$$\Gamma^{(n)\,\Lambda\to\infty}(1',2',\ldots,n'|1,2,\ldots,n) = \begin{cases} V(1',2'|1,2)\,, & \text{if } n=2\,, \\ 0\,, & \text{else}\,. \end{cases} \tag{3.32}$$

For this notation, we defined $V(1',2'|1,2)$ according to the Hugenholtz diagram from Eq. (2.103)

$$V(1',2'|1,2) = \left(\langle\alpha_{1'}\alpha_{2'}|V|\alpha_1\alpha_2\rangle + \zeta\,\langle\alpha_{1'}\alpha_{2'}|V|\alpha_2\alpha_1\rangle\right)\delta\left(\tau_{1'}-\tau_{2'}\right)\delta\left(\tau_{2'}-\tau_1\right)\delta\left(\tau_1-\tau_2\right), \tag{3.33}$$

such that the original interaction term in the coherent-state picture can be parameterised as

$$V\left[\{\psi^*\},\{\psi\}\right] = \frac{1}{4}\sum_{1',2'}\sum_{1,2} V(1',2'|1,2)\times\psi^*_{1'}\psi^*_{2'}\psi_2\psi_1\,. \tag{3.34}$$

This concludes the derivation of the flow equations for single and two-particle vertex functions of bosonic or fermionic quantum-many-body systems. We truncate the infinite

hierarchy of coupled integro-differential equations after $\Gamma^{(2)\,\Lambda}$ for two main reasons. Firstly, as one can extrapolate from the equations for $\Gamma^{(\dot{1})\,\Lambda}$ and $\Gamma^{(\dot{2})\,\Lambda}$ respectively, the mere complexity of all contributing terms that will occur for $\Gamma^{(\dot{3})\,\Lambda}$ is so vast that it, unfortunately, is beyond the scope of this thesis. Secondly, the increasing numerical effort would probably require a reduction of frequency-mesh points and real-space cluster sizes. Since the results that we obtain for the considered models crucially rely on a sufficient numerical resolution, this still seems unfeasible with the currently available computing resources. The three-particle vertex characterises interactions which involve three spins simultaneously. One physical reason why its contributions might actually be negligible for our considered systems is that there are no terms in the Hamiltonian containing products of three spin operators. For example, in models with a finite chiral spin interaction $\propto \boldsymbol{S}_i \cdot (\boldsymbol{S}_j \times \boldsymbol{S}_k)$ where $i \neq j \neq k$ are different lattice sites, a flow without $\Gamma^{(3)\,\Lambda}$ does not capture the effects of the chiral interaction and is thus also not justified.

Despite all this, certain corrections from the flow of $\Gamma^{(3)\,\Lambda}$ will have to be incorporated into the theory. In the following chapters, this will be achieved by employing the so-called Katanin truncation scheme [99, 156]. The scheme replaces the single-scale propagator by the full derivative of the dressed propagator

$$S^\Lambda \longrightarrow -\dot{G^\Lambda} = S^\Lambda + G^\Lambda \dot{\Sigma^\Lambda} G^\Lambda \tag{3.35}$$

in the flow equation for the two-particle vertex. Due to the Λ derivative of the self energy which is effectively given by Eq. (3.25), this substitution for S^Λ yields additional terms in Eq. (3.30). They appear due to the insertion of a two-particle vertex which is connected to Green's functions on two of its legs and contracted on the other two legs via a single-scale propagator. The resulting diagrams in the flow of $\Gamma^{(2)\,\Lambda}$ then involve products of three two-particle vertices. Such terms would otherwise only occur if contributions from the three-particle vertex were included explicitly. In this way, we consider those contributions from $\Gamma^{(3)\,\Lambda}$ that are needed for a complete feedback of Σ^Λ into $\Gamma^{(2)\,\Lambda}$ [147].

If applied to Heisenberg models, the FRG amounts to a mean-field analysis which treats the channels responsible for long-range order and spin fluctuations on equal footings and therefore was already proven to be exact in the large-S (spin length) and the large-N (symmetry group) limit [9, 19, 150]. Using the resulting vertices, we are able to compute the spin susceptibility as seen in Sec. 2.4.5. We continue in the next chapter with the first implementation of this method for spin systems with anisotropic and off-diagonal spin interactions, *i.e.*, the spin-$\frac{1}{2}$ kagome lattice model with Heisenberg and Dzyaloshinsky-Moriya interactions.

4. Functional-renormalization-group analysis of Dzyaloshinsky-Moriya and Heisenberg spin interactions on the kagome lattice

In this chapter, we apply the previously derived functional renormalization group method to our prime system of interest, *i.e.*, the highly frustrated, interacting spin-$\frac{1}{2}$ model on the kagome lattice. The main reason why this model caught huge attraction among physicists in the past years is that already on a nearest-neighbour Heisenberg interaction level it realises a paramagnetic phase with a possible spin-liquid state [83, 88, 95, 103, 109, 111, 118, 120, 140, 152, 173, 190]. Spin liquids are strongly correlated on short range but lack any kind of magnetic long-range order. They are proposed states for finding high-T_c superconductors [6–8] and decoherence-protected quantum memory [101]. The necessary spin frustrations can arise due to a strong competition between interactions (J_1-J_2 models), the lattice geometry (corner sharing triangles), and quantum fluctuations (spin-$\frac{1}{2}$).

So far, the FRG has been successfully applied to various spin systems with Heisenberg interactions [11, 18, 87, 147, 168, 173] and anisotropic, but diagonal spin interactions [146, 168]. A large benefit of this method is that, if applied sensibly, it treats the diagrammatic channels responsible for long-range correlations as well as quantum fluctuations on equal footings enabling it to reliably identify magnetically ordered as well as disordered phases on arbitrary lattice geometries in 2D and 3D. However, novel materials are often found to be influenced or even dominated by rather exotic and anisotropic spin interactions. For instance, rare-earth iridates like Na_2IrO_3 and Li_2IrO_3 as well as α-$RuCl_3$ show significant anisotropic and diagonal Kitaev interactions on the honeycomb lattice [28, 92, 138, 189] whereas the mineral *herbertsmithite* ($ZnCu_3(OH)_6Cl_2$) is influenced by a reasonably-sized Dzyaloshinsky-Moriya (DM) interaction on nearest-neighbour bonds of the underlying kagome lattice [149, 166, 192]. The reason for this is that these materials exhibit relatively large spin-orbit couplings (SOC) which can lead to Kitaev-like interactions if the magnetic ions are heavy (high atomic number Z) [58, 100, 137], or to DM interactions if the center of a bond is not an inversion center of the lattice [47, 129]. The effects of a sizable SOC can hence have quite drastic effects. The analytically solvable Kitaev honeycomb model, for instance, features a paramagnetic spin liquid phase with non-Abelian Majorana excitations [101]. In contrast, the DM interaction favours non-collinear magnetic order and possibly selects spiral order or skyrmions [132, 133].

While an extension of the spin FRG towards diagonal anisotropies like XXZ or Kitaev interactions is relatively straightforward [20, 146], implementing more general and off-diagonal terms like the DM interaction is mathematically and numerically much more involved. Therefore, we show, on one hand, that it is possible to go towards the most general spin interactions using FRG and, on the other hand, how finite DM terms affect the so far well studied Heisenberg model on the kagome lattice. Since unlike in the Kitaev model the DM interaction favours magnetic order of non-collinear types, studies have so far predicted that the paramagnetic phase is driven into a $\boldsymbol{q} = 0$ Néel state [27, 151, 162]. This state is conventionally ordered with a spin alignment that can be seen in Fig. 4.2(b). We want to investigate how the full J_1-J_2 kagome phase diagram is changed by a nearest-neighbour DM interaction and compare our findings to the previous studies and experimental data for *herbertsmithite* [68, 69] which is one of the most promising

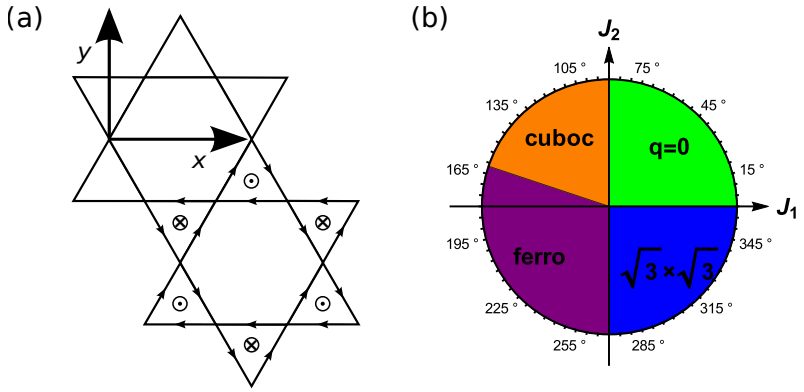

Figure 4.1.: (a) Kagome lattice and sign structure of DM interaction: The arrows on the bonds show the orientation of the DM term $\boldsymbol{D}_{ij} \cdot (\boldsymbol{S}_i \times \boldsymbol{S}_j)$ starting at site i and ending at site j. The DM vector $\boldsymbol{D}_{ij}$ is pointing out of (into) the x-y plane for up (down) triangles, respectively. (b) Classical phase diagram of the J_1-J_2 Heisenberg kagome model: There are four different magnetically ordered phases, *i.e.*, the $\boldsymbol{q} = 0$ Néel, the cuboc, the ferromagnetic, and the $\sqrt{3} \times \sqrt{3}$ Néel phase. All transitions between these phases coincide with the J_1 or J_2 axes, except for the one from the cuboc ordered into the ferromagnetic phase occurring at $J_2 = -J_1/3$ with $J_1 < 0$ [45].

candidates for finding a spin liquid at the moment [73, 119, 165, 177].

4.1. Phenomenological model

During the entire chapter, we investigate the J_1-J_2-D model on the kagome lattice. The Hamiltonian is

$$H = J_1 \sum_{\langle i,j \rangle} \boldsymbol{S}_i \cdot \boldsymbol{S}_j + J_2 \sum_{\langle\langle i,j \rangle\rangle} \boldsymbol{S}_i \cdot \boldsymbol{S}_j + \sum_{\langle i,j \rangle} \boldsymbol{D}_{ij} \cdot (\boldsymbol{S}_i \times \boldsymbol{S}_j) \ , \tag{4.1}$$

where $\langle i,j \rangle$ denotes that the sum is carried out over nearest-neighbour lattice sites and $\langle\langle i,j \rangle\rangle$ is the equivalent for second neighbours. Further, we omit the hat notation for operators from now on for a better readability. The Heisenberg terms in this model are due to the scalar product of spins invariant under global spin rotations (see App. E.2 for details) and exchanges of the two spins rendering them the most general bilinear and symmetric spin interactions. On the other hand, the DM term $\boldsymbol{D}_{ij} \cdot (\boldsymbol{S}_i \times \boldsymbol{S}_j)$ is the most general antisymmetric bilinear spin interaction. If the center of the bond linking the two involved spins is not an inversion center of the lattice, a non-magnetic ion can for instance be the cause for this type of interaction via an anisotropic superexchange [129]. Nevertheless, the combined Heisenberg and DM interactions are still not the most general bilinear spin interaction, *e.g.*, the quite important off-diagonal Γ term $\propto S_i^\mu S_j^\nu + S_i^\nu S_j^\mu$ is not accounted for in our model.

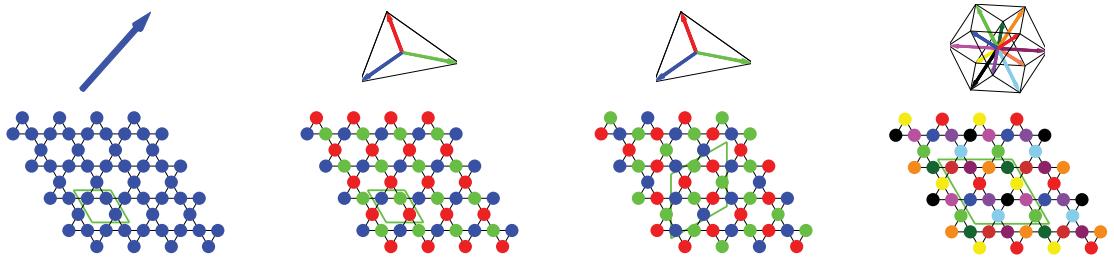

(a) ferromagnetic order (b) $\boldsymbol{q} = 0$ Néel order (c) $\sqrt{3} \times \sqrt{3}$ Néel order (d) cuboc order

Figure 4.2.: Real space representations for the four types of magnetic order which occur on the kagome lattice in the classical J_1-J_2 phase diagram [see Fig. 4.1(b)]: The top row indicates the colour-coded spin directions whereas the bottom row shows their distribution on the lattice. The respective unit cell boundaries are depicted by a green rhombus. (a) The ferromagnetic order features spins which are aligned parallelly. (b) $\boldsymbol{q} = 0$ Néel order is characterised by three different spin orientations within one plane and an angle of 120° between them. (c) The $\sqrt{3} \times \sqrt{3}$ Néel state has a spin alignment similar to the $\boldsymbol{q} = 0$ state. However, the unit cell is now increased from 3 to 9 lattice sites. (d) A spin arrangement in cuboc order needs the largest unit cell which contains 12 sites. The spins are aligned as if they would point from the center of a cuboctahedron into its corners. The $\boldsymbol{k}$-space positions of the dominant susceptibility components for all four types of order can be seen in Fig. 4.5(a). *Figure adapted from Ref. [121].*

According to the Moriya's rules, the vector $\boldsymbol{D}_{ij}$ has to be aligned perpendicularly to the system's mirror plane which in our case requires that $\boldsymbol{D}_{ij} = \pm D\boldsymbol{e}_z$. This assumption implies a global $U(1)$ spin-rotation symmetry around the z axis as compared to the $SU(2)$ symmetry of a pure Heisenberg system which yields a much higher numerical effort for the model at hand, confer App. E.2. Furthermore, $\boldsymbol{D}_{ij} \| \boldsymbol{e}_z$ is a good approximation for *herbertsmithite* in which $\boldsymbol{D}_{ij}$ is only slightly tilted towards the kagome plane [192]. Due to the antisymmetry of the DM interaction, the relation $D_{ij} = -D_{ji}$ must hold and one needs to take care of the correct sign structure for those terms on the entire lattice. Changing the signs of all DM terms simultaneously only amounts to a global spin rotation by an angle of π in the x-z plane. This leaves all those physical quantities invariant which, like the susceptibility, depend on an even number of spin operators. However, the chirality of a spin pattern for example switches sign after such a transformation because it involves three spin operators. For a detailed discussion on spin rotations please also confer App. E.2. In the following, we restrict ourselves to a single convention with $D \geq 0$ as shown in Fig. 4.1(a).

Previous studies have shown that the classical J_1-J_2 Heisenberg model on the kagome lattice features four different magnetically ordered phases, namely, the $\boldsymbol{q} = 0$ and the $\sqrt{3} \times \sqrt{3}$ Néel phases, a cuboc ordered, and a ferromagnetic phase. Here, all phases except for the ferromagnetic one show a non-collinear spin alignment. Their spin structures in real space are illustrated in Fig. 4.2 and the corresponding momentum space positions where

the maximal susceptibility for each type of order is expected can be seen in Fig. 4.5(a). Fig. 4.1(b) provides the classical phase diagram which is already known from Ref. [45].

In the quantum spin-$\frac{1}{2}$ limit, paramagnetic phases around the points $(J_1, J_2) = (1, 0)$ and $(J_1, J_2) = (0, 1)$ appear [18, 60, 90, 103, 173]. Especially the paramagnetic phase around $(J_1, J_2) = (1, 0)$ has gathered a lot of attention in recent years for the sake of (hopefully) finding a quantum spin liquid (QSL) in this regime. The J_1-D model has so far been studied by Cépas *et al.* [27] using exact diagonalisation. They have shown that the magnetically disordered phase of the nearest-neighbour model is driven into a magnetically ordered phase at a critical DM interaction strength of $D/J_1 \gtrsim 0.1$. This was afterwards confirmed by a study of Seman *et al.* [162] investigating the antiferromagnetic J_1-J_2-D model with $J_2 < J_1$. In its paramagnetic regime, they predict a gapped (gapless) QSL for a modest J_2 (D) coupling. We are now going to enhance these preceding works by studying the full model also allowing for ferromagnetic interactions.

4.2. Functional renormalization group for spin systems

The pseudo-fermion functional-renormalisation group (PFFRG) method [125, 147] has so far been successfully applied to various Heisenberg and diagonal anisotropic models in different 2D and 3D lattices [11, 18, 20, 89, 145, 146, 173]. Also, the J_1-J_2 Heisenberg kagome model has been investigated using PFFRG [18, 90, 173]. One of the FRG's strengths lies in the fact that it can describe magnetically ordered as well as disordered phases independent of the number of competing interactions, the lattice geometry, and dimensionality. In this section, we lay the foundation of all later work by deriving the PFFRG flow equations for spin-$\frac{1}{2}$ systems with interactions of Heisenberg and DM type. Throughout this thesis, we frequently utilise the numerically resulting vertex functions as the main subject for all the following physical interpretations, regardless of the actual model. Hence, we start by introducing the general details on how to implement the method that was derived in Chap. 3 for spin systems before turning to the concrete examples of Heisenberg and DM interactions.

4.2.1. General PFFRG approach

As already mentioned in the introduction to this thesis, the starting point of our derivations and what makes this FRG approach being called pseudo-fermion is the Abrikosov decomposition of our local spin operators into

$$S_i^\mu = \frac{1}{2} \sum_{\alpha,\beta} f_{i,\alpha}^\dagger \sigma_{\alpha\beta}^\mu f_{i,\beta} \,. \tag{4.2}$$

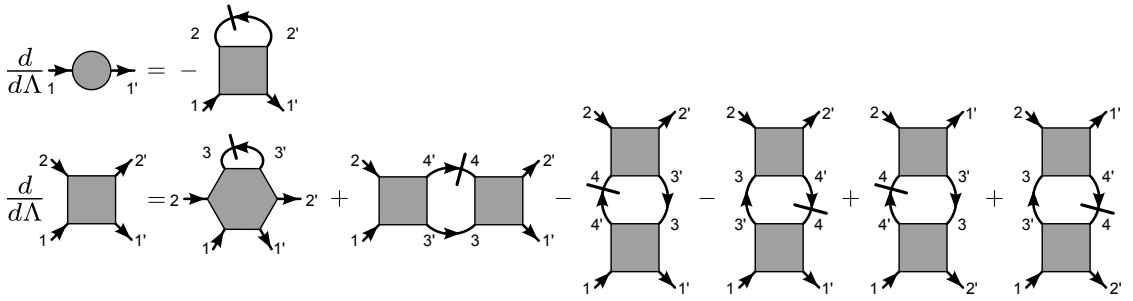

Figure 4.3.: Diagrammatic representation of FRG flow equations: Circles, squares, and hexagons represent 1-, 2-, and 3-particle vertices, respectively. Regular (slashed) arrows denote the fully dressed Green's function G^Λ (single-scale propagator $S^\Lambda = G^\Lambda \dot{\left[G_0^\Lambda\right]}^{-1} G^\Lambda$). Again, it shows that all m-particle vertices couple to all n-particle vertices with $n \leq m+1$ leading to an infinite hierarchy of equations. Note that we do not display the flow equations for m-particle vertices with $m > 2$. The order of terms corresponds to Eqs. (3.25) and (3.30).

Here, the second quantisation operators $f^\dagger_{i,\alpha}$ $(f_{i,\alpha})$[1] create (annihilate) a spin-$\frac{1}{2}$ fermion at lattice site i and the index $\alpha \in \{\uparrow, \downarrow\}$ labels the orientation of their spin. σ^μ with $\mu \in \{x, y, z\}$ are the standard Pauli matrices. If written like this, we are able to employ the standard fermionic Feynman diagram techniques from the previous chapters for our spin Hamiltonian. One issue though arises from representing the spins with Abrikosov fermions, namely, where our physical model has a single spin-$\frac{1}{2}$ degree of freedom (with its only choice being whether to point up or down) we now have four possible states per site with the possible occupations

$$|n_{i,\uparrow}, n_{i,\downarrow}\rangle = \begin{cases} |0,0\rangle_i\,,\ Q_i = 0,\ S_i = 0\,, \\ |1,0\rangle_i\,,\ Q_i = 1,\ S_i = 1/2\,, \\ |0,1\rangle_i\,,\ Q_i = 1,\ S_i = 1/2\,, \\ |1,1\rangle_i\,,\ Q_i = 2,\ S_i = 0\,. \end{cases} \tag{4.3}$$

Obviously, the $S = 0$ states span an unphysical sector of our artificially enlarged Hilbert space. Technically speaking, we would have to enforce the occupation number constraint

$$Q_i \equiv f^\dagger_{i,\uparrow} f_{i,\uparrow} + f^\dagger_{i,\downarrow} f_{i,\downarrow} = 1 \tag{4.4}$$

on every lattice site independently and simultaneously increasing the numerical effort significantly. In the following, we only enforce the average constraint $\langle Q_i \rangle = 1$ which in our particle-hole symmetric and translation invariant models is equivalent to half filling or to

[1] Note that, in contrast to the bosonic *or* fermionic operators a and $a^\dagger$ of Chap. 2, we now use f and $f^\dagger$ to explicitly note the fermionic structure.

setting the chemical potential $\mu = 0$. This method has been shown to be a suitable approximation at $T = 0$ due to a strong suppression of the unphysical occupation numbers $Q_i = 0, 2$ [9].

The decomposition of one spin into two fermions yields a Hamiltonian that is purely quartic in the fermionic operators [cf. Eq. (4.1)]. Due to the lack of kinetic terms, perturbation theory breaks down and we have to employ the FRG method in order to obtain faithful results. According to Chap. 3, the bare Green's function for this system is

$$G_0(\omega) = \frac{-1}{i\omega}\,. \tag{4.5}$$

We note again that this definition of the propagator differs by a factor of -1 in comparison to an alternative convention that is frequently used, confer Sec. 2.1.2. G_0 is regularised using a Heaviside function

$$G_0^\Lambda(\omega) = \theta\left(|\omega| - \Lambda\right) G_0(\omega)\,, \tag{4.6}$$

confer Eq. (3.2). Here, ω denotes a fermionic Matsubara frequency and the cutoff or RG scale Λ determines those low-energy degrees of freedom that are neglected ($G_0^\Lambda(\omega) = 0$ if $|\omega| < \Lambda$). Furthermore, the bare Green's function [Eq. (3.1)] is local in real space and diagonal in spin space because of the special type of purely interacting Hamiltonian. These properties remain intact during the entire flow due to a strictly local and diagonal self energy (see next section).

The flow Eqs. (3.25) and (3.30) from the previous chapter together with their initial conditions [Eqs. (3.32) and (3.34)] and the regularised bare propagator are the starting point for the FRG procedure. A diagrammatic expression of these equations can be seen in Fig. 4.3. Here, we represent the single-scale propagator S^Λ from Eq. (3.26) with a slashed arrow while G^Λ is denoted by a regular arrow. For the correct signs in the second equation, we utilised that $\left[G^\Lambda\right]^T = G^\Lambda$ and the antisymmetry of the two-particle vertex with respect to an exchange of its two incoming or two outgoing arguments. Let us briefly consider the real-space structure of $\Gamma^{(2)\,\Lambda}$. Because of the propagators' locality during the flow, the vertex function effectively only depends on two lattice sites, confer next section. Its antisymmetry upon a single fermionic exchange implies that it can be parameterised as

$$\Gamma^{(2)\,\Lambda}\left(1', 2'|1, 2\right) = \Gamma^{(2)\,\Lambda}_{=\,i_1 i_2}\left(1', 2'|1, 2\right)\delta_{i_{1'} i_1}\delta_{i_{2'} i_2} - \Gamma^{(2)\,\Lambda}_{\times\,i_1 i_2}\left(1', 2'|1, 2\right)\delta_{i_{1'} i_2}\delta_{i_{2'} i_1}\,, \tag{4.7a}$$

$$\Gamma^{(2)\,\Lambda}_{=\,i_1 i_2}\left(1', 2'|1, 2\right) = \Gamma^{(2)\,\Lambda}_{\times\,i_2 i_1}\left(1', 2'|2, 1\right)\,, \tag{4.7b}$$

where $\Gamma^{(2)\,\Lambda}_{=}$ and $\Gamma^{(2)\,\Lambda}_{\times}$ depend on four combined spin and frequency arguments as well as two real-space indices. With this notation, we are able to provide a physical interpretation for the diagrammatic representation of our FRG equations in Fig. 4.3. In the flow equation for the self energy, the term $\propto \Gamma^{(2)\,\Lambda}_{=}$ $\left(\propto \Gamma^{(2)\,\Lambda}_{\times}\right)$ corresponds to Hartree-like (Fock-like) diagrams. For the flow of the two-particle vertex, we can split the contributions into one equation for $\Gamma^{(2)\,\Lambda}_{=}$ and one for $\Gamma^{(2)\,\Lambda}_{\times}$, respectively. Both equations contain the same

information due to Eq. (4.7b). Considering the flow of $\Gamma_{=}^{(2)\,\Lambda}$, the first term in the lower line of Fig. 4.3 represents corrections from the three-particle vertex. The second term in this line contributes the particle-particle channel with ladder diagrams containing propagators pointing in the same direction. Third and fourth (fifth and sixth) term amount to the direct (crossed) particle-hole channel. The crossed particle-hole channel features ladder diagrams with propagators pointing in opposite directions. Very important contributions from the direct particle-hole channel are RPA-like diagrams. Only these diagrams comprise internal fermionic loops where a summation over internal lattice sites is required. In this way, only the RPA-like diagrams can induce long-range correlations and are thereby responsible for magnetic order. All other diagrams couple a vertex with given real-space coordinates to itself and to the onsite vertex. Hence, they are unable to characterise magnetic long-range order. For the flow of $\Gamma_{\times}^{(2)\,\Lambda}$, the diagrammatic representations of direct and crossed particle-hole channels are simply exchanged.

The FRG builds up an infinite hierarchy of coupled differential-integro equations which, in order to be exact, would have to be solved as a complete set. However, that seems to be quite an impossible task and there is the need for a clever truncation scheme allowing us to solve the flow equations approximately. For the entire thesis, this is achieved by truncating the set of equations after the two-particle vertex and employing the Katanin scheme from Eq. (3.35). This is, in a sense, a minimalistic approach since only the two-particle vertex contributes to the initial conditions [cf. Eq. (3.32)] and a truncation already on this level would imply vanishing vertex functions throughout the entire flow. Nevertheless, if one solves the flow equations without the Katanin scheme and thereby neglects all contributions from the flow of the three-particle vertex, one always finds magnetic order as it has been shown in Ref. [147] which is the fundamental article for this quantum-many-body method. Hence, the Katanin truncation is necessary in order to identify paramagnetic phases.

4.2.2. PFFRG for Heisenberg systems

We now summarise the already known implications for the FRG of Heisenberg systems. Due to the high degree of symmetry in this model, the self energy can be parameterised as

$$\Sigma^{\Lambda}(1'|1) = -\Gamma^{(1)\,\Lambda}(1'|1) = -i\gamma_{\mathrm{d}}^{\Lambda}(\omega_1)\delta_{i_{1'}i_1}\delta_{\alpha_{1'}\alpha_1}\delta(\omega_{1'}-\omega_1)\,, \tag{4.8}$$

where the numbers $1 = \{i_1, \alpha_1, \omega_1\}$ label complete sets of quantum numbers with a real-space coordinate, a spin index and a Matsubara frequency each. The diagonal structure in Matsubara (spin) space is caused by the energy (spin) conservation in the language of Feynman diagrams (cf. Sec. 2.3.4) and the locality of propagators induces the proportionality to $\delta_{i_{1'}i_1}$. Because of the $SU(2)$ rotation invariance of our Heisenberg model, the self energy cannot depend on the spin value and it is purely imaginary ($\mathrm{Im}\gamma_{\mathrm{d}}^{\Lambda}(\omega) = 0$) and antisymmetric in its frequency argument [$\gamma_{\mathrm{d}}^{\Lambda}(\omega) = -\gamma_{\mathrm{d}}^{\Lambda}(-\omega)$]. $\gamma_{\mathrm{d}}^{\Lambda}$ can therefore be interpreted as a finite lifetime of our pseudo fermions. For lattices consisting only of equivalent sites, $\Sigma^{\Lambda}(1'|1)$ does also not depend on its real space coordinates. The Dyson equation

[Eq. (2.135a)] yields for the dressed Green's function that

$$G^{\Lambda}(\omega) = \frac{-\theta(|\omega| - \Lambda)}{i\omega + i\gamma_{\mathrm{d}}^{\Lambda}(\omega)} \,. \tag{4.9}$$

To evaluate the single-scale propagator, we have to consider that its definition in Eq. (3.26) includes a Λ derivative of $\left[G_0^{\Lambda}\right]^{-1}$ which needs to be treated with caution. Employing the Dyson equation $G^{\Lambda} = \left[\left(G_0^{\Lambda}\right)^{-1} + \Sigma^{\Lambda}\right]^{-1}$ and that $(\dot{A^{-1}}) = -A^{-1}\dot{A}A^{-1}$ for an arbitrary invertible matrix A, we can derive the general relation

$$\begin{aligned} S^{\Lambda} &= -\left[\left(G_0^{\Lambda}\right)^{-1} + \Sigma^{\Lambda}\right]^{-1} \left(G_0^{\Lambda}\right)^{-1} \dot{G_0^{\Lambda}} \left(G_0^{\Lambda}\right)^{-1} \left[\left(G_0^{\Lambda}\right)^{-1} + \Sigma^{\Lambda}\right]^{-1} \\ &= -\left[\mathbb{1} + \Sigma^{\Lambda} G_0^{\Lambda}\right]^{-1} \dot{G_0^{\Lambda}} \left[\mathbb{1} + G_0^{\Lambda}\Sigma^{\Lambda}\right]^{-1} \,. \end{aligned} \tag{4.10}$$

Here, we used the matrix language from the previous chapter. Inserting the regularised bare and dressed Green's functions from Eqs. (4.6) and (4.9), a product of Heaviside and Dirac delta distributions occurs due to the Λ derivative. Mathematically, this is not well defined. We resolve the issue by using the identity

$$\lim_{\epsilon \to 0} \delta_{\epsilon}(x) f\left(\theta_{\epsilon}(x)\right) = \delta(x) \int_0^1 \mathrm{d}t \, f(t) \tag{4.11}$$

for broadened distributions δ_ϵ, θ_ϵ and an arbitrary continuous function f [130]. With this equation, we arrive at the final expression

$$\begin{aligned} S^{\Lambda}(\omega) &= -\frac{\delta(|\omega| - \Lambda)}{i\omega} \int_0^1 \mathrm{d}t \, \left[1 + \frac{i\gamma_{\mathrm{d}}^{\Lambda}(\omega)}{i\omega} t\right]^{-2} \\ &= \frac{-\delta(|\omega| - \Lambda)}{i\omega + i\gamma_{\mathrm{d}}^{\Lambda}(\omega)} \end{aligned} \tag{4.12}$$

for the single-scale propagator. The delta distribution turns out to be very convenient for us because it renders one frequency integral trivial in each flow equation and thereby decreases the numerical effort considerably.

Turning to the interaction vertex, we can deduce from the $SU(2)$ symmetry that there are exactly two terms that are allowed to contribute, *i.e.*, a spin channel $\Gamma_{\mathrm{s}}^{\Lambda}$ and a density channel $\Gamma_{\mathrm{d}}^{\Lambda}$

$$\begin{aligned} &\Gamma^{\Lambda}\big(1',2'|1,2\big) \equiv \Gamma^{(2)\,\Lambda}\left(1',2'|1,2\right) \\ &\quad = \left[\Gamma^{\Lambda}_{\mathrm{s}\,i_1 i_2}\left(\omega_1',\omega_2'|\omega_1,\omega_2\right) \sum_{\mu} \sigma^{\mu}_{\alpha_{1'}\alpha_1}\sigma^{\mu}_{\alpha_{2'}\alpha_2} + \Gamma^{\Lambda}_{\mathrm{d}\,i_1 i_2}\left(\omega_1',\omega_2'|\omega_1,\omega_2\right) \delta_{\alpha_{1'}\alpha_1}\delta_{\alpha_{2'}\alpha_2}\right] \\ &\qquad \times \delta(\omega_1 + \omega_2 - \omega_{1'} - \omega_{2'})\delta_{i_{1'}i_1}\delta_{i_{2'}i_2} - (\omega_1 \leftrightarrow \omega_2,\, \alpha_1 \leftrightarrow \alpha_2,\, i_1 \leftrightarrow i_2) \,, \end{aligned} \tag{4.13}$$

where the second term ensures the vertex' antisymmetry with respect to an exchange of two fermions, confer also Eqs. (4.7). The locality of the propagators again implies the special real space structure and energy conservation makes it sufficient to only consider the transfer frequencies $s = \omega_{1'} + \omega_{2'}$, $t = \omega_{1'} - \omega_1$, and $u = \omega_{1'} - \omega_2$ such that we only consider

$$\Gamma^{\Lambda}_{\mathrm{s/d}\,i_1 i_2}\left(\omega_1', \omega_2' | \omega_1, \omega_2\right) \longrightarrow \Gamma^{\Lambda}_{\mathrm{s/d}\,i_1 i_2}\left(s, t, u\right) . \tag{4.14}$$

One can show that the two remaining functions $\Gamma^{\Lambda}_{\mathrm{s/d}}$ fulfill the following (anti)symmetries in Matsubara space [147]

$$\Gamma^{\Lambda}_{\mathrm{s/d}\,i_1 i_2}\left(s, t, u\right) = \Gamma^{\Lambda}_{\mathrm{s/d}\,i_2 i_1}\left(-s, t, u\right) , \tag{4.15a}$$

$$\Gamma^{\Lambda}_{\mathrm{s/d}\,i_1 i_2}\left(s, t, u\right) = \Gamma^{\Lambda}_{\mathrm{s/d}\,i_1 i_2}\left(s, -t, u\right) , \tag{4.15b}$$

$$\Gamma^{\Lambda}_{\mathrm{s/d}\,i_1 i_2}\left(s, t, u\right) = \Gamma^{\Lambda}_{\mathrm{s/d}\,i_2 i_1}\left(s, t, -u\right) , \tag{4.15c}$$

$$\Gamma^{\Lambda}_{\mathrm{s/d}\,i_1 i_2}\left(s, t, u\right) = \pm\Gamma^{\Lambda}_{\mathrm{s/d}\,i_1 i_2}\left(u, t, s\right) , \tag{4.15d}$$

where the (anti)symmetry holds for the (density) spin channel in the last line. Hence, we only need to determine the positive frequency sectors of our vertex functions [Eqs. (4.15a–4.15c)] with $u \leq s$ [Eq. (4.15d)] what reduces our numerical effort by a factor of 16.

Inserting our parameterisations for Σ^{Λ} and Γ^{Λ} into the FRG flow Eqs. (3.25) and (3.30), we can derive a set of coupled integro-differential equations for $\gamma^{\Lambda}_{\mathrm{d}}$, $\Gamma^{\Lambda}_{\mathrm{s}}$, and $\Gamma^{\Lambda}_{\mathrm{d}}$. They are provided in App. A and solved using the initial conditions

$$\gamma^{\Lambda\to\infty}_{\mathrm{d}}\left(\omega\right) = 0 , \tag{4.16a}$$

$$\Gamma^{\Lambda\to\infty}_{\mathrm{d}\,i_1 i_2}\left(s, t, u\right) = 0 , \tag{4.16b}$$

$$\Gamma^{\Lambda\to\infty}_{\mathrm{s}\,i_1 i_2}\left(s, t, u\right) = \frac{J_{i_1 i_2}}{4} , \tag{4.16c}$$

where the factor of $\frac{1}{4}$ in the last line remains from Abrikosov decomposition of the spins (confer Eq. (4.2)). For the numerical evaluation, we discretise the three Matsubara frequencies s, t, and u which, in the $T \to 0$ limit, are continuous using 50 discrete points in a combined linear and logarithmic mesh in order to resolve low frequencies appropriately and to enable a sufficiently high initial cutoff value. With the computational power currently available to us, a much higher number of frequency points can be realised if only Heisenberg interactions [18, 173] or anisotropic but diagonal [20] couplings are considered, see also Chaps. 5 and 6. However, due to the much higher complexity of the following equations including DM interactions, we have to limit ourselves to 50 frequency points for comparability also in this section. Even though the FRG, in principle, deals with an infinite and translation invariant lattice, we can only account for correlations of finite cluster sizes. Therefore, we restrict ourselves to a hexagonal plaquette of the kagome lattice reaching 7 nearest-neighbour distances into all high-symmetry directions, *e.g.*, it consists of 125 lattice sites. Since we expect the QSL phases that we are interested in to lack any kind of long-range correlations, this approach seems to be justified. The resulting set of equations

for the real-space-truncated and frequency-discretised vertices is then numerically solved using the Euler method.

We evaluate our vertex functions by computing the Matsubara transformed imaginary-time spin susceptibility $\chi_{ij}^{\mu\nu}(i\Omega)$ as defined in Eq. (2.143). This quantity is related to our vertex and Green's functions via

$$\begin{aligned}\chi_{ij}^{\mu\nu,\,\Lambda}(i\Omega) = &-\frac{1}{4}\frac{1}{2\pi}\int_{-\infty}^{\infty}\mathrm{d}\omega_1\sum_{\alpha_1\alpha_2}G_{\alpha_1}^{\Lambda}(\omega_1)G_{\alpha_2}^{\Lambda}(\omega_1+\Omega)\sigma_{\alpha_1\alpha_2}^{\mu}\sigma_{\alpha_2\alpha_1}^{\nu}\delta_{ij}\\ &-\frac{1}{4}\frac{1}{(2\pi)^2}\int_{-\infty}^{\infty}\mathrm{d}\omega_1\int_{-\infty}^{\infty}\mathrm{d}\omega_2\sum_{\alpha_1,\alpha_{1'},\alpha_2,\alpha_{2'}}\Gamma^{\Lambda}\left(1',2'|1,2\right)\sigma_{\alpha_1\alpha_{1'}}^{\mu}\sigma_{\alpha_2\alpha_{2'}}^{\nu}\\ &\times G_{\alpha_{1'}}^{\Lambda}(\omega_1+\Omega)G_{\alpha_{2'}}^{\Lambda}(\omega_2)G_{\alpha_1}^{\Lambda}(\omega_1)G_{\alpha_2}^{\Lambda}(\omega_2+\Omega)\,,\end{aligned}\tag{4.17}$$

confer Eq. (2.146). For the above representation, we already took the $T\to 0$ limit in which $\frac{2\pi}{\beta}\sum_{\omega_m}\to\int_{-\infty}^{\infty}\mathrm{d}\nu$. We also accounted for the possible spin dependence[2] of the propagators which occurs in the next section and the combined indices are $1'=\{i,\alpha_{1'},\omega_1+\Omega\}$, $2'=\{j,\alpha_{2'},\omega_2\}$, $1=\{i,\alpha_1,\omega_1\}$, and $2=\{j,\alpha_2,\omega_2+\Omega\}$. The static component of the Fourier-transformed susceptibility $\chi^{\mu\nu,\Lambda}(\boldsymbol{k})\equiv\chi^{\mu\nu,\Lambda}(\boldsymbol{k},i\Omega=0)$ as a function of the cutoff Λ is the key quantity for our further investigation. Inserting the defined indices and the parameterisations from Eqs. (4.9), (4.13), and (4.14) into Eq. (4.17), we find that the diagonal static spin susceptibility with $\chi_{ij}^{xx,\,\Lambda}=\chi_{ij}^{yy,\,\Lambda}=\chi_{ij}^{zz,\,\Lambda}$ is given by

$$\begin{aligned}\chi_{ij}^{xx,\,\Lambda}(i\Omega=0) =&\frac{1}{4\pi}\int_{-\infty}^{\infty}\mathrm{d}\omega_1\,\frac{\theta(|\omega_1|-\Lambda)}{\left(\omega_1+\gamma_{\mathrm{d}}^{\Lambda}(\omega_1)\right)^2}\delta_{ij}\\ &-\frac{1}{8\pi^2}\int_{-\infty}^{\infty}\mathrm{d}\omega_1\int_{-\infty}^{\infty}\mathrm{d}\omega_2\,\frac{\theta(|\omega_1|-\Lambda)}{\left(\omega_1+\gamma_{\mathrm{d}}^{\Lambda}(\omega_1)\right)^2}\frac{\theta(|\omega_2|-\Lambda)}{\left(\omega_2+\gamma_{\mathrm{d}}^{\Lambda}(\omega_2)\right)^2}\Big\{2\Gamma_{\mathrm{s}\,ij}^{\Lambda}\left(\omega^+,0,\omega^-\right)\\ &-\left[\Gamma_{\mathrm{d}\,ii}^{\Lambda}\left(\omega^+,\omega^-,0\right)-\Gamma_{\mathrm{s}\,ii}^{\Lambda}\left(\omega^+,\omega^-,0\right)\right]\delta_{ij}\Big\}\,,\end{aligned}\tag{4.18}$$

where $\omega^{\pm}=\omega_1\pm\omega_2$. All details concerning the Fourier transform of this quantity on the kagome lattice are provided in App. D.

As mentioned before, we are mainly interested in finding paramagnetic spin liquids. Since they do not show any magnetic order and therefore also no spontaneous symmetry breaking down to lowest temperatures, such states obey all symmetries of the initial Hamiltonian. In the case of a Heisenberg Hamiltonian ($D=0$), the parameterisation of self energy and two-particle vertex from above stays accurate as the FRG flow smoothly reaches the limit $\Lambda\to 0$. If this is the case, the points in momentum space with the largest susceptibility denote those wave vectors at which dominant short-range spin-spin correlations are found. In contrast, if our system exhibits magnetic order, the spin-rotation symmetry of the initial

[2] In a bare Heisenberg model, the propagators are proportional to unity in spin space.

Hamiltonian is broken spontaneously and, for instance, a certain spin direction is preferred. In that scenario, the $SU(2)$ invariant parameterisations from Eqs. (4.8) and (4.13) become inaccurate and we cannot draw any conclusions for the magnetically ordered state because the flow of the vertex functions breaks down at a finite cutoff $\Lambda_{\text{crit}} > 0$. However, before this breakdown, we can see signs of a diverging susceptibility that is regularised due to finite correlation lengths and the frequency discretisation. This behaviour manifests itself as a kink at Λ_{crit} of the susceptibility at the dominant wave vectors indicating the type of magnetic order.

4.2.3. Modifications of the PFFRG for finite DM interactions

In this paragraph, we summarise the main part of our original work which is the generalisation of the flow equations from App. A that were already derived in Ref. [147] towards systems with finite DM interactions. We still limit ourselves to Eq. (4.1) with a DM term $\boldsymbol{D}_{ij} = \pm D\boldsymbol{e}_z$ and the given sign structure from Fig. 4.1(a). As already pointed out, the global $SU(2)$ spin rotation symmetry of the bare Heisenberg model is then broken down to $U(1)$ rotations around the z axis which has severe consequences.

Let us start by re-parameterising the self energy. Our previous considerations regarding real and Matsubara spaces (locality and energy conservation) remain correct. The only changes occur in spin space where $\Sigma^\Lambda(1'|1)$ before had to be invariant under all spin rotations yielding a proportionality to $\delta_{\alpha_{1'}\alpha_1}$ [cf. Eq. (4.8)]. Now, only rotations around the z axis have to leave the self energy invariant such that it can also depend on the z component of the spin. Hence, we need to account for a spin channel $\gamma_{\text{s}}^\Lambda$ and find

$$\Sigma^\Lambda(1'|1) = \left(-i\gamma_{\text{d}}^\Lambda(\omega_1)\delta_{\alpha_{1'}\alpha_1} + \gamma_{\text{s}}^\Lambda(\omega_1)\sigma^z_{\alpha_{1'}\alpha_1}\right)\delta_{i_{1'}i_1}\delta(\omega_{1'} - \omega_{1'})\,, \tag{4.19}$$

where in addition to the previous considerations for $\gamma_{\text{d}}^\Lambda$ also the spin channel is real ($\text{Im}\gamma_{\text{s}}^\Lambda(\omega) = 0$) and antisymmetric in its frequency argument [$\gamma_{\text{s}}^\Lambda(\omega) = -\gamma_{\text{s}}^\Lambda(-\omega)$]. Therefore, the extra term does not break the time-reversal symmetry of our system unlike, for instance, a magnetic field. It is also directly related to the DM interaction and cannot be generated by diagonal couplings like in the XXZ model, see Chap. 5. Due to $\gamma_{\text{s}}^\Lambda$, our Green's function now acquires a spin sector in addition to its regular density sector

$$G_\alpha^\Lambda(\omega) = G_{\text{d}}^\Lambda(\omega) + G_{\text{s}}^\Lambda(\omega)\sigma^z_{\alpha\alpha}\,, \tag{4.20a}$$

$$G_{\text{d}}^\Lambda(\omega) = \theta(|\omega| - \Lambda)\frac{i\omega + i\gamma_{\text{d}}^\Lambda(\omega)}{\left(\gamma_{\text{s}}^\Lambda(\omega)\right)^2 + \left(\omega + \gamma_{\text{d}}^\Lambda(\omega)\right)^2}\,, \tag{4.20b}$$

$$G_{\text{s}}^\Lambda(\omega) = \theta(|\omega| - \Lambda)\frac{\gamma_{\text{s}}^\Lambda(\omega)}{\left(\gamma_{\text{s}}^\Lambda(\omega)\right)^2 + \left(\omega + \gamma_{\text{d}}^\Lambda(\omega)\right)^2}\,. \tag{4.20c}$$

The same also holds for the single-scale propagator

$$S_\alpha^\Lambda(\omega) = S_\mathrm{d}^\Lambda(\omega) + S_\mathrm{s}^\Lambda(\omega)\sigma^z_{\alpha\alpha}\,, \tag{4.21a}$$

$$S_\mathrm{d}^\Lambda(\omega) = \delta(|\omega|-\Lambda)\frac{i\omega + i\gamma_\mathrm{d}^\Lambda(\omega)}{\left(\gamma_\mathrm{s}^\Lambda(\omega)\right)^2 + \left(\omega+\gamma_\mathrm{d}^\Lambda(\omega)\right)^2}\,, \tag{4.21b}$$

$$S_\mathrm{s}^\Lambda(\omega) = \delta(|\omega|-\Lambda)\frac{\gamma_\mathrm{s}^\Lambda(\omega)}{\left(\gamma_\mathrm{s}^\Lambda(\omega)\right)^2 + \left(\omega+\gamma_\mathrm{d}^\Lambda(\omega)\right)^2}\,, \tag{4.21c}$$

where we again employed Eq. (4.11) for the derivation of $S_\alpha^\Lambda(\omega)$.

For the two-particle vertex, the situation is even more complex since we are now dealing with simultaneous rotations of two spins around the z axis. There are six out of the possible sixteen spin-spin interaction channels which are invariant under such rotations. As discussed in the next chapter for the XXZ model, the spin channel $\Gamma_\mathrm{s}^\Lambda$ splits up into a contribution along the z axis $\Gamma_\mathrm{zz}^\Lambda$ and an in-plane component with $\Gamma_\mathrm{xx}^\Lambda = \Gamma_\mathrm{yy}^\Lambda$. Of course, the density channel $\Gamma_\mathrm{d}^\Lambda$ as well as the DM term $\Gamma_\mathrm{DM}^\Lambda$ with its spin-space structure being $\sigma^x_{\alpha_{1'}\alpha_1}\sigma^y_{\alpha_{2'}\alpha_2} - \sigma^y_{\alpha_{1'}\alpha_1}\sigma^x_{\alpha_{2'}\alpha_2}$ remain invariant under the appropriate rotations as well. Furthermore, two new terms denoted by $\Gamma_\mathrm{zd}^\Lambda$ and $\Gamma_\mathrm{dz}^\Lambda$ which couple the z component of one particle's spin with the spin density of another particle are now allowed and induced by the DM interaction. At this point, we again refer the reader to App. E.2 for a detailed discussion on global spin rotations and their consequences. Combining all of these results, our updated vertex parameterisation reads

$$\begin{aligned}
\Gamma^\Lambda\left(1',2'|1,2\right) = \Bigg[&\Gamma^\Lambda_{\mathrm{xx}\,i_1i_2}(s,t,u)\left(\sigma^x_{\alpha_{1'}\alpha_1}\sigma^x_{\alpha_{2'}\alpha_2} + \sigma^y_{\alpha_{1'}\alpha_1}\sigma^y_{\alpha_{2'}\alpha_2}\right)\\
&+\Gamma^\Lambda_{\mathrm{zz}\,i_1i_2}(s,t,u)\,\sigma^z_{\alpha_{1'}\alpha_1}\sigma^z_{\alpha_{2'}\alpha_2} + \Gamma^\Lambda_{\mathrm{d}\,i_1i_2}(s,t,u)\,\delta_{\alpha_{1'}\alpha_1}\delta_{\alpha_{2'}\alpha_2}\\
&+\Gamma^\Lambda_{\mathrm{DM}\,i_1i_2}(s,t,u)\left(\sigma^x_{\alpha_{1'}\alpha_1}\sigma^y_{\alpha_{2'}\alpha_2} - \sigma^y_{\alpha_{1'}\alpha_1}\sigma^x_{\alpha_{2'}\alpha_2}\right)\\
&+\Gamma^\Lambda_{\mathrm{zd}\,i_1i_2}(s,t,u)\,\sigma^z_{\alpha_{1'}\alpha_1}\delta_{\alpha_{2'}\alpha_2} + \Gamma^\Lambda_{\mathrm{dz}\,i_1i_2}(s,t,u)\,\delta_{\alpha_{1'}\alpha_1}\sigma^z_{\alpha_{2'}\alpha_2}\Bigg]\\
&\times\delta(\omega_1+\omega_2-\omega_{1'}-\omega_{2'})\delta_{i_{1'}i_1}\delta_{i_{2'}i_2} - (\omega_1\leftrightarrow\omega_2,\,\alpha_1\leftrightarrow\alpha_2,\,i_1\leftrightarrow i_2)\,.
\end{aligned} \tag{4.22}$$

The new FRG flow equations couple these six interaction channels with the four different sectors from the propagators and are thus much more complex as compared to the Heisenberg or the XXZ model. We display them in App. B. Additionally, the frequency symmetries of the vertices from Eqs. (4.15) are reduced by the DM interaction such that now only

$$\Gamma^\Lambda_{\mathrm{xx/zz/d}\,i_1i_2}(s,t,u) = \Gamma^\Lambda_{\mathrm{xx/zz/d}\,i_2i_1}(-s,t,u)\,, \tag{4.23a}$$

$$\Gamma^\Lambda_{\mathrm{DM}\,i_1i_2}(s,t,u) = -\Gamma^\Lambda_{\mathrm{DM}\,i_2i_1}(-s,t,u)\,, \tag{4.23b}$$

$$\Gamma^\Lambda_{\mathrm{zd/dz}\,i_1i_2}(s,t,u) = \Gamma^\Lambda_{\mathrm{dz/zd}\,i_2i_1}(-s,t,u)\,, \tag{4.23c}$$

and the two-particle exchange

$$\Gamma^{\Lambda}_{\mathrm{xx/zz/d}\,i_1i_2}(s,t,u) = \Gamma^{\Lambda}_{\mathrm{xx/zz/d}\,i_2i_1}(s,-t,-u)\,, \tag{4.24a}$$

$$\Gamma^{\Lambda}_{\mathrm{DM}\,i_1i_2}(s,t,u) = -\Gamma^{\Lambda}_{\mathrm{DM}\,i_2i_1}(s,-t,-u)\,, \tag{4.24b}$$

$$\Gamma^{\Lambda}_{\mathrm{zd/dz}\,i_1i_2}(s,t,u) = \Gamma^{\Lambda}_{\mathrm{dz/zd}\,i_2i_1}(s,-t,-u)\,, \tag{4.24c}$$

can be utilised for minimising the numerical effort. In Eqs. (4.23c) and (4.24c) one needs to pay attention that the spin-density vertices $\Gamma^{\Lambda}_{\mathrm{dz}}$ and $\Gamma^{\Lambda}_{\mathrm{zd}}$ interchange their roles if the respective symmetry is applied. The two-particle exchange simply amounts to an exchange of the two incoming and the two outgoing indices simultaneously which leaves the entire vertex $\Gamma^{\Lambda}(1',2'|1,2)$ from Eq. (4.22) invariant. Finally, the initial conditions for our vertex functions in the J_1-J_2-D model are (cf. Sec 3.2)

$$\gamma^{\Lambda\to\infty}_{\mathrm{d}}(\omega) = \gamma^{\Lambda\to\infty}_{\mathrm{s}}(\omega) = 0\,, \tag{4.25a}$$

$$\Gamma^{\Lambda\to\infty}_{\mathrm{d}\,i_1i_2}(s,t,u) = \Gamma^{\Lambda\to\infty}_{\mathrm{zd}\,i_1i_2}(s,t,u) = \Gamma^{\Lambda\to\infty}_{\mathrm{dz}\,i_1i_2}(s,t,u) = 0\,, \tag{4.25b}$$

$$\Gamma^{\Lambda\to\infty}_{\mathrm{xx}\,i_1i_2}(s,t,u) = \Gamma^{\Lambda\to\infty}_{\mathrm{zz}\,i_1i_2}(s,t,u) = \frac{J_{i_1i_2}}{4}\,, \tag{4.25c}$$

$$\Gamma^{\Lambda\to\infty}_{\mathrm{DM}\,i_1i_2}(s,t,u) = \frac{D_{i_1i_2}}{4}\,. \tag{4.25d}$$

Using this as an input, we solve the flow equations from App. B as explained in Sec. 4.2.2. The diagonal static spin susceptibility again has to be extracted from the vertex functions. Due to the more complex vertex and self-energy structures as compared to the Heisenberg scenario, it splits into an in-plane and into an out-of-plane component in accordance with our physical system. The biggest impact of the DM interaction is however expected for the in-plane susceptibility because it energetically favours an in-plane alignment of the spins. We therefore only consider the quantity

$$\begin{aligned}\chi^{xx,\,\Lambda}_{ij}(0) =& \frac{1}{4\pi}\int_{-\infty}^{\infty}\mathrm{d}\omega_1\,\frac{\theta(|\omega_1|-\Lambda)}{\left(\gamma^{\Lambda}_{\mathrm{s}}(\omega_1)\right)^2+\left(\omega_1+\gamma^{\Lambda}_{\mathrm{d}}(\omega_1)\right)^2}\delta_{ij}\\ &-\frac{1}{8\pi^2}\int_{-\infty}^{\infty}\mathrm{d}\omega_1\int_{-\infty}^{\infty}\mathrm{d}\omega_2\,\frac{\theta(|\omega_1|-\Lambda)}{\left(\gamma^{\Lambda}_{\mathrm{s}}(\omega_1)\right)^2+\left(\omega_1+\gamma^{\Lambda}_{\mathrm{d}}(\omega_1)\right)^2}\,\frac{\theta(|\omega_2|-\Lambda)}{\left(\gamma^{\Lambda}_{\mathrm{s}}(\omega_2)\right)^2+\left(\omega_2+\gamma^{\Lambda}_{\mathrm{d}}(\omega_2)\right)^2}\\ &\times\left\{2\Gamma^{\Lambda}_{\mathrm{xx}\,ij}\left(\omega^+,0,\omega^-\right)-\left[\Gamma^{\Lambda}_{\mathrm{d}\,ii}\left(\omega^+,\omega^-,0\right)-\Gamma^{\Lambda}_{\mathrm{zz}\,ii}\left(\omega^+,\omega^-,0\right)\right]\delta_{ij}\right\},\end{aligned} \tag{4.26}$$

with $\omega^{\pm}=\omega_1\pm\omega_2$. Note that the formula for $\chi^{zz,\,\Lambda}_{ij}$ is much more complex than the above due to a split-up of the Green's functions' different spin sectors.

This completes the derivation of our new method. We are now ready to investigate the resulting spin susceptibilities for various couplings on the kagome lattice.

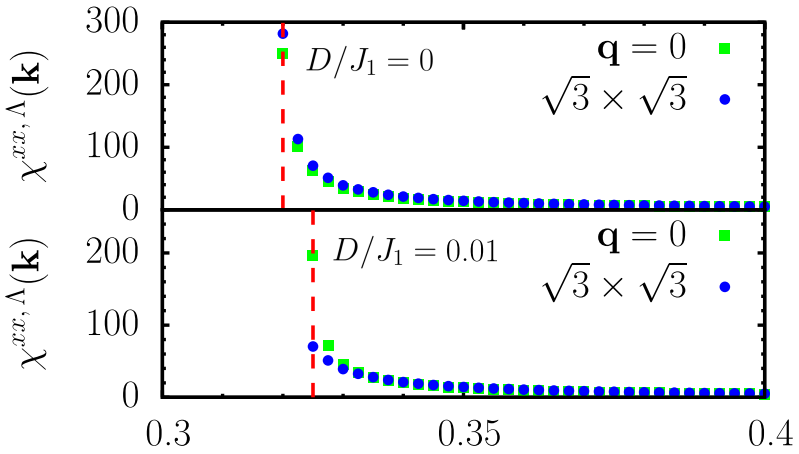

Figure 4.4.: RPA susceptibilities for the J_1-D model at different wave vectors: Blue circles (green squares) represent the susceptibilities for $\sqrt{3} \times \sqrt{3}$ order ($\boldsymbol{q} = 0$ order). Upper panel: In a pure Heisenberg antiferromagnet ($D = 0$), the maximal susceptibility is found at the $\sqrt{3} \times \sqrt{3}$ wave vector. Lower panel: For $D = 0.01\, J_1$, $\boldsymbol{q} = 0$ order is preferred which indicates a phase transition for infinitesimal DM interactions within the accuracy of our FRG procedure. Dashed red lines show the cutoff value at which the flow breaks down. The momentum space coordinates of the corresponding wave vectors are shown in Fig. 4.5(a).

4.3. J_1-D model on the kagome lattice

In this section, we discuss our findings for the nearest-neighbour spin-$\frac{1}{2}$ model with antiferromagnetic Heisenberg and DM interactions. This J_1-D model featuring the Hamiltonian from Eq. (4.1) with $J_1 > 0$, $J_2 = 0$, and $D \geq 0$ was already studied by Cépas *et al.* using exact diagonalisation [27]. Therefore, it seems to be the perfect starting point to benchmark the validity of our method.

4.3.1. PFFRG in the RPA channel

Before we turn to the results of the full PFFRG, we discuss an approximative scheme which treats our vertex functions solely in the direct particle-hole or RPA channel, *i.e.*, only the terms with internal fermionic loops contribute, confer discussion in Sec. 4.2.1. Within this scheme, we neglect all contributions to the flow arising from the self energy which remains zero in the course of this section. Furthermore, all frequency components of the two-particle vertices decouple and we hence only focus on the static vertices at $s = t = u = 0$.

Due to its special structure, the RPA channel is the only term responsible for long-range correlations between spins. In this way, the current approximation amounts to a classical treatment of the system. During the flow, the classical approach manifests itself because of

the vanishing self-energy which amounts to an infinite pseudo-fermion lifetime. Similar to a truncation scheme without the Katanin corrections (cf. Sec. 4.2.1), this always implies the formation of magnetic order in our simulations. However, due to the quite basic structure of the resulting equations, we are capable of finding an analytic solution for them.

Using the initial conditions from Eq. (4.25), one easily verifies that all density-related vertices $\Gamma^{\Lambda}_{\mathrm{d}\,i_1 i_2} = \Gamma^{\Lambda}_{\mathrm{zd}\,i_1 i_2} = \Gamma^{\Lambda}_{\mathrm{dz}\,i_1 i_2} = 0$ vanish during the flow (cf. App. B). The flow equations for the remaining static spin and DM channels simplify to

$$\frac{d}{d\Lambda}\Gamma^{\Lambda}_{\mathrm{xx}\,i_1 i_2} = \frac{2}{\pi\Lambda^2}\sum_j \left(\Gamma^{\Lambda}_{\mathrm{xx}\,i_1 j}\Gamma^{\Lambda}_{\mathrm{xx}\,j i_2} - \Gamma^{\Lambda}_{\mathrm{DM}\,i_1 j}\Gamma^{\Lambda}_{\mathrm{DM}\,j i_2}\right) , \tag{4.27a}$$

$$\frac{d}{d\Lambda}\Gamma^{\Lambda}_{\mathrm{DM}\,i_1 i_2} = \frac{2}{\pi\Lambda^2}\sum_j \left(\Gamma^{\Lambda}_{\mathrm{DM}\,i_1 j}\Gamma^{\Lambda}_{\mathrm{xx}\,j i_2} + \Gamma^{\Lambda}_{\mathrm{xx}\,i_1 j}\Gamma^{\Lambda}_{\mathrm{DM}\,j i_2}\right) , \tag{4.27b}$$

$$\frac{d}{d\Lambda}\Gamma^{\Lambda}_{\mathrm{zz}\,i_1 i_2} = \frac{2}{\pi\Lambda^2}\sum_j \Gamma^{\Lambda}_{\mathrm{zz}\,i_1 j}\Gamma^{\Lambda}_{\mathrm{zz}\,j i_2} . \tag{4.27c}$$

This immediately shows that the DM interaction only affects the in-plane spin vertex whereas the out-of-plane vertex behaves identically to the Heisenberg scenario. In general, we find a larger in-plane vertex for any finite DM interaction. We proceed by decoupling the upper equations using a Fourier transform with respect to the triangular Bravais lattice while keeping the sublattice space encoded in a 3×3 matrix structure.

$$\Gamma^{\Lambda}_{\mathrm{xx/zz/DM}\,a(i)b(j)}(\boldsymbol{k}) = \sum_{\Delta\boldsymbol{R}=\boldsymbol{R}_i-\boldsymbol{R}_j} e^{-i\boldsymbol{k}(\boldsymbol{R}_i-\boldsymbol{R}_j)}\Gamma^{\Lambda}_{\mathrm{xx/zz/DM}\,ij} \tag{4.28}$$

Here, $a(i) = \mathcal{A}, \mathcal{B}, \mathcal{C}$ ($\boldsymbol{R}_i$) labels the sublattice (unit cell) of site i and the same holds for $b(j)$ ($\boldsymbol{R}_j$) and site j. For details on our lattice geometry conventions, please confer App. D. The additional transformation

$$\Gamma^{\Lambda}_{\pm}(\boldsymbol{k}) = \Gamma^{\Lambda}_{\mathrm{xx}}(\boldsymbol{k}) \pm i\Gamma^{\Lambda}_{\mathrm{DM}}(\boldsymbol{k}) , \tag{4.29}$$

further decouples the two flow equations for the (in-plane) spin and DM vertices such that a remarkably simple set of equations can be obtained, *i.e.*,

$$\frac{d}{d\Lambda}\Gamma^{\Lambda}_{\pm}(\boldsymbol{k}) = \frac{2}{\pi\Lambda^2}\Gamma^{\Lambda}_{\pm}(\boldsymbol{k})\Gamma^{\Lambda}_{\pm}(\boldsymbol{k}) , \tag{4.30}$$

were the vertex functions are now 3×3 matrices in sublattice space and the product on the right-hand side denotes a standard matrix product. A plain separation of variables straightforwardly yields

$$\Gamma^{\Lambda}_{\pm}(\boldsymbol{k}) = \pi\Lambda\left[2 + \pi\Lambda\left(\Gamma^{\Lambda\to\infty}_{\pm}(\boldsymbol{k})\right)^{-1}\right]^{-1} . \tag{4.31}$$

We transform back to the spin and DM vertices which ultimately yield our desired susceptibility.

$$\Gamma^{\Lambda}_{\mathrm{xx}}(\boldsymbol{k}) = \frac{1}{2}\left[\frac{\pi\Lambda}{2+\pi\Lambda\left(\Gamma^{\Lambda\to\infty}_{\mathrm{xx}}(\boldsymbol{k})+i\Gamma^{\Lambda\to\infty}_{\mathrm{DM}}(\boldsymbol{k})\right)^{-1}} + \frac{\pi\Lambda}{2+\pi\Lambda\left(\Gamma^{\Lambda\to\infty}_{\mathrm{xx}}(\boldsymbol{k})-i\Gamma^{\Lambda\to\infty}_{\mathrm{DM}}(\boldsymbol{k})\right)^{-1}}\right] \tag{4.32a}$$

$$\Gamma^{\Lambda}_{\mathrm{DM}}(\boldsymbol{k}) = \frac{1}{2}\left[\frac{\pi\Lambda}{2+\pi\Lambda\left(\Gamma^{\Lambda\to\infty}_{\mathrm{xx}}(\boldsymbol{k})+i\Gamma^{\Lambda\to\infty}_{\mathrm{DM}}(\boldsymbol{k})\right)^{-1}} - \frac{\pi\Lambda}{2+\pi\Lambda\left(\Gamma^{\Lambda\to\infty}_{\mathrm{xx}}(\boldsymbol{k})-i\Gamma^{\Lambda\to\infty}_{\mathrm{DM}}(\boldsymbol{k})\right)^{-1}}\right] \tag{4.32b}$$

$$\Gamma^{\Lambda}_{\mathrm{zz}}(\boldsymbol{k}) = \frac{\pi\Lambda}{2+\pi\Lambda\left(\Gamma^{\Lambda\to\infty}_{\mathrm{xx}}(\boldsymbol{k})\right)^{-1}} \tag{4.32c}$$

For the frequency integrals in Eq. (4.26), we replace the finite-frequency components of our vertex functions by their static values at $s = t = u = 0$. Since our self energies vanish and the propagators hence only acquire finite density sectors, our static in-plane susceptibility simplifies to

$$\chi^{xx,\,\Lambda}_{ij}(i\Omega=0) = \frac{1}{2\pi\Lambda}\delta_{ij} - \frac{1}{2\left(\pi\Lambda\right)^2}\left[2\Gamma^{\Lambda}_{\mathrm{xx}\,ij} - \Gamma^{\Lambda}_{\mathrm{zz}\,ii}\delta_{ij}\right] . \tag{4.33}$$

We are only interested in the behaviour of the momentum resolved susceptibility. For this, the local terms ($\propto \delta_{ij}$) do not play an important role because they only yield a constant contribution in $\boldsymbol{k}$ space. This is why we can safely neglect the out-of-plane vertex and therefore find $\chi^{xx,\,\Lambda}(\boldsymbol{k})$ from the different matrix elements of $\Gamma^{\Lambda}_{\mathrm{xx}}(\boldsymbol{k})$ multiplied by phase factors which correspond to their sublattice vectors.

Plotting the susceptibility as a function of the cutoff shows that it always diverges at finite Λ indicating a magnetically ordered system as expected. However, the wave vector for which this occurs at the highest Λ value changes for different initial couplings as shown in Fig. 4.4. At vanishing DM coupling, the $\sqrt{3}\times\sqrt{3}$ Néel order is dominant which coincides with the findings of the semi-classical large-S studies in Refs. [36–38]. For any small but finite $D \gtrsim 0$, the 120° antiferromagnetic $\boldsymbol{q} = 0$ Néel order is preferred and prevails up to $D \to \infty$. That matches precisely the classical result of Elhajal *et al.* [49].

Even though the RPA approach has been used in the context of our PFFRG before, the solution in Eqs. (4.32) was missing so far. Since its discovery, it was already proven to be very useful for the interpretation and further extension of our method. As Baez *et al.* show [9], the large-S limit of the PFFRG is dominated by the RPA channel. The fact that only magnetic order can be found with this method is directly related to our spin system effectively being classical, although this correspondence is not exact due to the breakdown of the flow at $\Lambda > 0$. The dominant wave vectors that are derived from our analytical solutions are identical to those selected as so-called eigenmodes by the Luttinger-Tisza method [9]. This approach minimises the classical spin system's energy with respect to a weak constraint $\sum_{i=1}^{N} |\boldsymbol{S}_i|^2 = NS^2$ [112, 113]. A superposition of the obtained eigenmodes

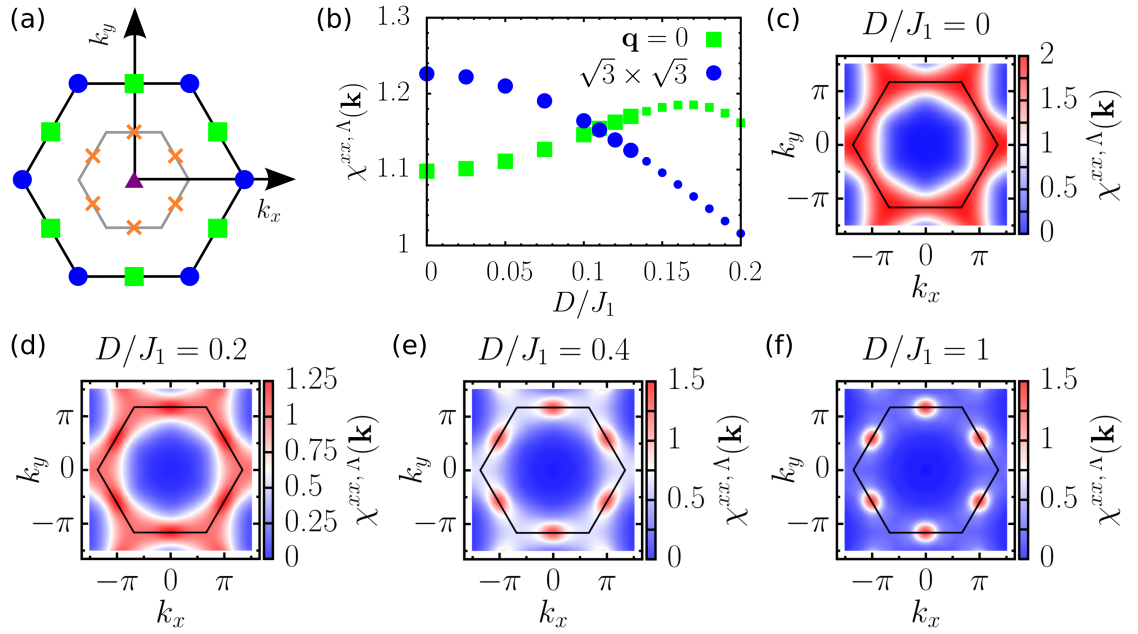

Figure 4.5.: (a) Peak positions for classical types of order in the J_1-J_2 model: $\sqrt{3}\times\sqrt{3}$ (blue circles), $\boldsymbol{q}=0$ (green squares), and cuboc order (orange crosses) [ferromagnetic order (purple triangle)] show susceptibility maxima residing within the extended [first] Brillouin zone marked by a black [grey] hexagon. (b) Competing susceptibilities at $\boldsymbol{q}=0$ (green squares) and $\sqrt{3}\times\sqrt{3}$ (blue circles) wave vectors as function of D at finite $\Lambda\approx 0.19$: Small icons denote that the values were obtained after the critical flow breakdown and hence only provide a guide to the eye. (c)-(f) Static spin susceptibility $\chi^{xx,\Lambda}(\boldsymbol{k})$ for different values of D: The extended Brillouin zone (cf. App. D) is again marked by a black hexagon. In (c), the susceptibility is obtained for the cutoff-free theory at $\Lambda=0$. Otherwise, the plots are shown for a cutoff value just before the breakdown of the flow (see arrows in Fig. 4.6).

can then yield a classically exact result if it also fulfills the strong constraint $|\boldsymbol{S}_i|^2=S^2$, $\forall\, i$ which is always possible for Bravais lattices. Therefore, we now know that the PFFRG yields quite reliable results in the large-S limit.

With this simplified version of our method, we showed that the $\boldsymbol{q}=0$ Néel phase is correctly determined for finite DM interactions. Its appearance for already infinitesimally small values of D as well as the lack of any paramagnetic phase is an artefact of this classical approximation. Hence, we will investigate the effects of quantum fluctuations using our full PFFRG in the next section.

4.3.2. Full PFFRG calculation

Our next benchmark is the critical DM interaction strength at which the $\boldsymbol{q}=0$ Néel order occurs in a nearest-neighbour spin-$\frac{1}{2}$ J_1-D model. Cépas *et al.* determined a value

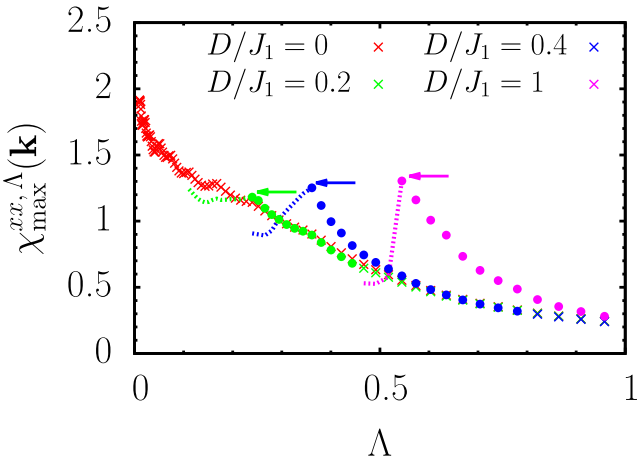

Figure 4.6.: Plot of the $\boldsymbol{k}$-space-resolved maximal susceptibilities as functions of Λ for the nearest-neighbour J_1-D model: Crosses (circles) denote that the maximal value was found at the $\sqrt{3} \times \sqrt{3}$ ($\boldsymbol{q} = 0$) wave vectors. If the flow enters a symmetry-broken phase at a critical Λ, our formalism cannot access the underlying physics which is indicated by dashed lines. The critical cutoff values are indicated by arrows.

of $D = 0.1\,J_1$ using exact diagonalisation [27]. We now employ the full FRG equations from App. B and solve them with the initial conditions $J_1 > 0$, $J_2 = 0$, and $D \geq 0$ [cf. Eq. (4.25)]. Again, the DM interaction favours a spin orientation in the x-y plane and we therefore study the momentum space resolved in-plane susceptibility $\chi^{xx,\Lambda}(\boldsymbol{k})$ for different values of D.

For the bare Heisenberg antiferromagnet ($D = 0$), we reproduce the data that was previously obtained via PFFRG in Ref. [173]. The susceptibility flows smoothly down to the lowest Λ values (see Fig. 4.6) indicating a magnetically disordered phase and the strongest short-range correlations are almost homogeneously spread along the edges of the extended Brillouin zone, see Fig. 4.5 (c). Small maxima are found at the $\sqrt{3} \times \sqrt{3}$ wave vectors which is in agreement with recent DMRG studies [44]. Exact diagonalisation methods on small cluster sizes agree with the homogeneously spread susceptibility profile, but find dominant $\boldsymbol{q} = 0$ correlations at $T = 0$ [106, 164] in contrast to our findings.

Turning on the DM interaction, the wave vectors with maximal susceptibility shift towards the $\boldsymbol{q} = 0$ points. At $D = 0.2\,J_1$, a strong signal along the edges of the extended Brillouin zone remains [Fig. 4.5 (d)] and the $\boldsymbol{q} = 0$ peaks become only more prominent and separated if the DM coupling is further increased, *i.e.*, if $D \gtrsim 0.4\,J_1$ [see Figs. 4.5 (e),(f)]. The corresponding flow of the largest susceptibility as function of Λ can be seen in Fig. 4.6. For interaction strengths $D \geq 0.2\,J_1$, a kink being marked by an arrow is clearly visible indicating the breakdown of our $SU(2)$ spin-rotation invariant flow equations and therefore the onset of magnetic order (see discussion in Sec. 4.2.2).

To further resolve the transition from the paramagnetic phase with dominant $\sqrt{3} \times \sqrt{3}$

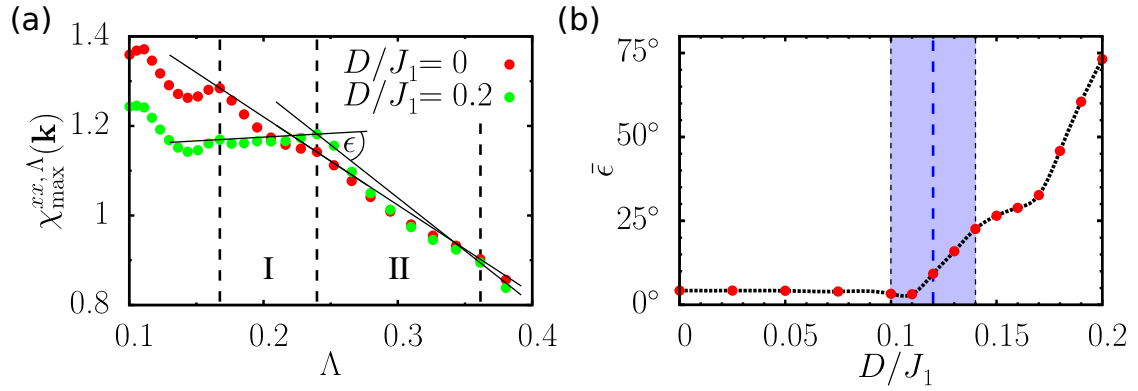

Figure 4.7.: (Color online) (a) Approximation scheme for the Λ-dependent susceptibility: We divide a certain interval into two sectors, I and II, which lie between two adjacent pairs of susceptibility peaks (or susceptibility upturns). Within each sector, $\chi^{xx,\Lambda}(\boldsymbol{k})$ is approximated by a tangent connecting neighboring peaks. While the angle between both tangents is negligible for $D/J_1 = 0$, we find a finite value for $D/J_1 = 0.2$ indicating that both curves belong to different phases. A more quantitative measure for the size of the kink is obtained by considering tangents between additional pairs of adjacent peaks in a fixed Λ interval and calculating the average angle $\bar{\epsilon}$. (b) Averaged angle $\bar{\epsilon}$ as a function of D/J_1. While $\bar{\epsilon}$ is almost constant for $D/J_1 < 0.1$, there is a pronounced increase for higher values. Based on this behavior, we estimate the phase transition of the J_1-D model to be at $D = (0.12 \pm 0.02)\, J_1$ (blue shaded area).

correlations and the 120° antiferromagnetically ordered $\boldsymbol{q} = 0$ Néel phase, we show the values of their respective susceptibility at fixed $\Lambda \approx 0.19$ as a function of D in Fig. 4.5 (b). It can be seen that the coupling from which on the maximal susceptibility is found at the $\boldsymbol{q} = 0$ positions is given by $D = 0.11\, J_1$. In this plot, one has to be aware of the fact that some of the values provided in this plot are obtained in a symmetry-broken phase.

The shift of the peak positions in momentum space is one effect of the DM interaction but not a clear signature for the onset of magnetic order as explained in Sec. 4.2.2. For this subject, we have to resolve a breakdown of the susceptibility flow. Because of the relatively rough discretisation of Matsubara frequencies and small cluster sizes caused by the complexity of our FRG equations, this is a delicate task if some precision is required. For that reason, we developed a method dealing with the issue systematically in the next section.

4.3.3. Detection of magnetic instabilities

This is where we present our method of detecting a magnetic instability in the RG flow. The expected diverging susceptibility signaling the onset of spontaneous symmetry breaking at a critical scale Λ is regularised by two numerical approximations of the PFFRG method, *i.e.*, the finite lattice size and the discretised frequencies. Both approximations reduce the

divergence to a finite maximum or to a kink-like feature. Furthermore, the discretisation of the frequencies induces oscillations in the susceptibility. Here, we propose a scheme to detect instabilities in the RG flow even in the presence of pronounced frequency oscillations and when the magnetisation is small. As an example, we focus on the phase transition from the paramagnetic into the $\boldsymbol{q} = 0$ Néel-ordered phase of the J_1-D model (see Sec. 4.3.2). The same procedure can also be applied to other phase boundaries.

A regularised divergence generally manifests as a change of the slope of the flowing susceptibility if Λ is decreased. A difficulty in defining the slope arises because, as a result of the frequency discretisation, the RG-flow is overlaid by oscillations. We therefore measure the slope in a way that averages out these oscillations. Each discrete frequency grid point leads to a small peak or upturn of the susceptibility. We connect two adjacent peaks by a straight line which represents a tangent of the susceptibility and approximates $\chi^{xx,\Lambda}(\boldsymbol{k})$ between the peaks. A kink during the RG-flow now appears as an angle (*i.e.*, a change of the slope) between two neighboring tangents, as illustrated in Fig. 4.7(a). To find a magnetic instability at an unknown value of Λ, we take the average $\bar{\epsilon}$ of the absolute values of such angles within a certain Λ interval. The angle $\bar{\epsilon}$ then serves as a measure of how much the slope changes within this interval, *e.g.*, how pronounced the kink is. To locate the phase transition, we plot $\bar{\epsilon}$ as a function of the interaction strength D/J_1, see Fig. 4.7(b). For $D/J_1 < 0.1$, we observe a small and constant value of $\bar{\epsilon} \approx 5°$, followed by a sudden increase at $D/J_1 \approx 0.11$ indicating a phase transition. Note that the critical Λ slightly changes as a function of D/J_1. If it coincides with a discrete frequency grid point, this can cause an anomaly in $\bar{\epsilon}$ such as the dip in Fig. 4.7(b) at $D/J_1 \approx 0.16$. Taking into account possible errors due to suchlike effects, a conservative estimate for the critical interaction strength at which the transition from the paramagnetic phase with dominant $\sqrt{3} \times \sqrt{3}$ short-range correlations into the $\boldsymbol{q} = 0$ Néel-ordered phase occurs is $D = (0.12 \pm 0.02)\, J_1$ [blue shaded area in Fig. 4.7(b)]. This is in good agreement with the result from Ref. [27].

We conclude that, besides the correct selection of the $\boldsymbol{q} = 0$ order for finite DM interactions, our method also provides results that are quantitatively reliable. Thus, we continue by investigating the full J_1-J_2-D model which could not yet be accessed via other methods.

4.4. J_1-J_2-D model on the kagome lattice

4.4.1. Phase diagram

In this section, we study the entire spin-$\frac{1}{2}$ model on the kagome lattice governed by the Hamiltonian in Eq. (4.1) with both ferromagnetic and antiferromagnetic couplings J_1 and J_2 as well as $D \geq 0$. This model is motivated by the promising spin liquid candidate *herbertsmithite* for which $J_1 \gg D > J_2 > 0$. For a clear parameterisation across the whole interaction range, we express our Heisenberg couplings using an overall strength J and an

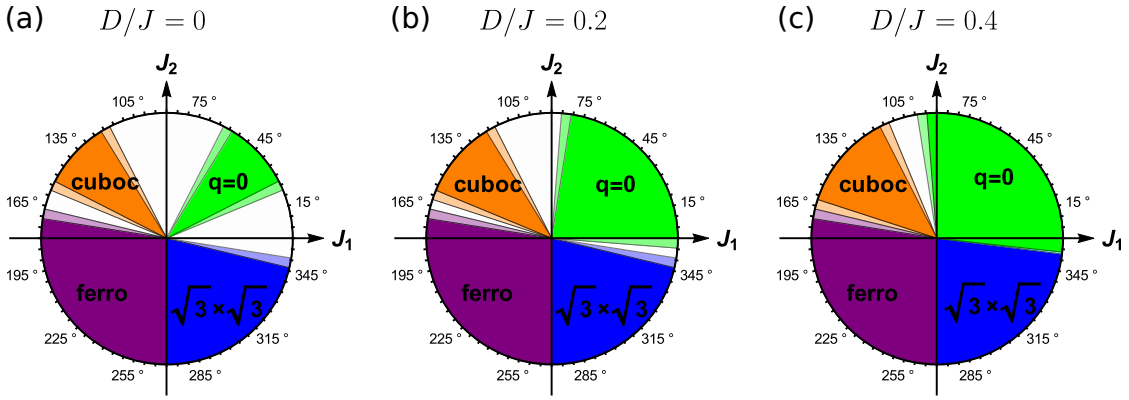

Figure 4.8.: J_1-J_2-D phase diagrams using the angular parameterisation from Eqs. (4.34) and various values of D: The magnetically ordered phases are represented by the colours of their classical analogues from Fig. 4.1(b). White areas indicate a paramagnetic flow behaviour and the numerical uncertainties regarding the boundaries between ordered and disordered phases are indicated by light colours. The precise positions of the phase boundaries are presented in Table 4.1.

angle θ ranging from 0° to 360°.

$$J_1 = J\cos\theta \tag{4.34a}$$

$$J_2 = J\sin\theta \tag{4.34b}$$

For $D = 0$, our model has already been studied in Refs. [18, 173] using the FRG formalism. In agreement with these studies, we can identify the four types of classical order along with additional coupling regimes around $(J_1, J_2) = (1, 0)$ and $(0, 1)$ in which the maximal susceptibility flows smoothly towards the limit $\Lambda \to 0$ signaling a paramagnetic phase. Our findings also admit the existence of a small third paramagnetic phase between the cuboc and the ferromagnetic order. However, due to the relatively small clusters of considered spin correlations and the coarse frequency grid, our numerical implementation might underestimate magnetically ordered phases since magnetic instabilities are less pronounced as compared to the previous study in Ref. [18]. The full phase diagram is depicted in Fig. 4.8(a).

As one would expect through the preceding sections, a finite DM coupling has its largest effect on the $\boldsymbol{q} = 0$ Néel phase which is strongly enlarged as D increases. While this type of order only occurred for both finite and antiferromagnetic $J_1, J_2 > 0$ at $D = 0$, it already touches the positive J_1 axis at $D = 0.2\,J$ [see Fig. 4.8(b)]. Increasing the DM interaction even further eventually leads to a $\boldsymbol{q} = 0$ phase which even allows for either a slightly ferromagnetic nearest-neighbour ($J_1 \gtrsim 0$) or next-nearest-neighbour ($J_2 \gtrsim 0$) Heisenberg interaction. Also, the other two types of non-collinearly ordered phases, *i.e.*, the cuboc and the $\sqrt{3}\times\sqrt{3}$ phase, are augmented by a finite $D > 0$. As a consequence, the non-magnetic phase around $(J_1, J_2) = (1, 0)$ in which also *herbertsmithite* resides has vanished entirely

order type	$\boldsymbol{q} = 0$	cuboc	ferro	$\sqrt{3} \times \sqrt{3}$
$D = 0.0$	$[27, 59]$	$[122, 153]$	$[171, 270]$	$[270, 347]$
$D = 0.2$	$[0, 81]$	$[122, 158]$	$[171, 270]$	$[270, 347]$
$D = 0.4$	$[-6, 95]$	$[117, 162]$	$[171, 270]$	$[270, 353]$

Table 4.1.: Phase boundaries of the differently ordered phases in the J_1-J_2-D model: The Heisenberg interactions can be derived from Eqs. (4.34) and the corresponding θ intervals are given in angular degrees with an accuracy of about $\pm 5°$.

for $D = 0.4J$, confer Fig. 4.8(c). The only phase transition retaining its $D = 0$ position in the entire parameter range studied here is the one between the ferromagnetic and the $\sqrt{3} \times \sqrt{3}$ Néel phase at the negative J_2 axis ($\theta = 270°$). The precise values for the phase boundaries of the magnetically ordered phases are summarised in Tab. 4.1.

In general, a finite DM interaction leads to a shift of the phase boundaries between paramagnetic and non-collinearly ordered phases in favour of the magnetic phases. This tendency can be understood from the fact that a system of three spins on a triangle with only Heisenberg interactions is more frustrated than its analogue containing only DM couplings, *e.g.*, the differences between the energy levels of this three-site model are larger for the DM interaction. Further, at finite D, a spin system can gain energy for an alignment of two adjacent spins with an angle that is (close to) $\frac{\pi}{2}$. This maximises the magnitude of the cross product in the DM interaction and a proper orientation of the (almost) perpendicular spins then lowers the system's energy. A parallel spin arrangement, on the other hand, is not affected by the DM coupling since the cross product and thereby the DM term itself vanish in this case. Hence, the three magnetic types of order with non-collinear spin patterns, *i.e.*, the $\boldsymbol{q} = 0$, the $\sqrt{3} \times \sqrt{3}$, and the cuboc order, are found in enlarged parameter spaces for $D > 0$ while the ferromagnetic order remains uninfluenced. Our results also suggest that magnetically disordered phases might disappear entirely in the J_1-J_2-D model for large enough DM terms.

4.4.2. Implications for *herbertsmithite*

One of the primary motivations for our study of the spin-$\frac{1}{2}$ kagome J_1-J_2-D model is to explore its predictions for the mineral *herbertsmithite* ($ZnCu_3(OH)_6Cl_2$). Experimentally, it exhibits no sign of magnetic long-range order down to very low temperatures until $50\,mK$ [73, 119, 165] and a broad, featureless spin structure factor with its strongest signal along the edges of the extended Brillouin zone [69] and small maxima at the $\boldsymbol{q} = 0$ positions [68]. Considering these finding, *herbertsmithite* appears to be one of the most promising candidates for a QSL with possible spinon excitations, confer Chap. 1. The neutron-scattering data shows a strong correspondence to the momentum-resolved susceptibility profiles for the paramagnetic phase that was earlier found in the antiferromagnetic nearest-neighbour Heisenberg model, confer Fig. 4.5(c). In fact, this seems to be the rel-

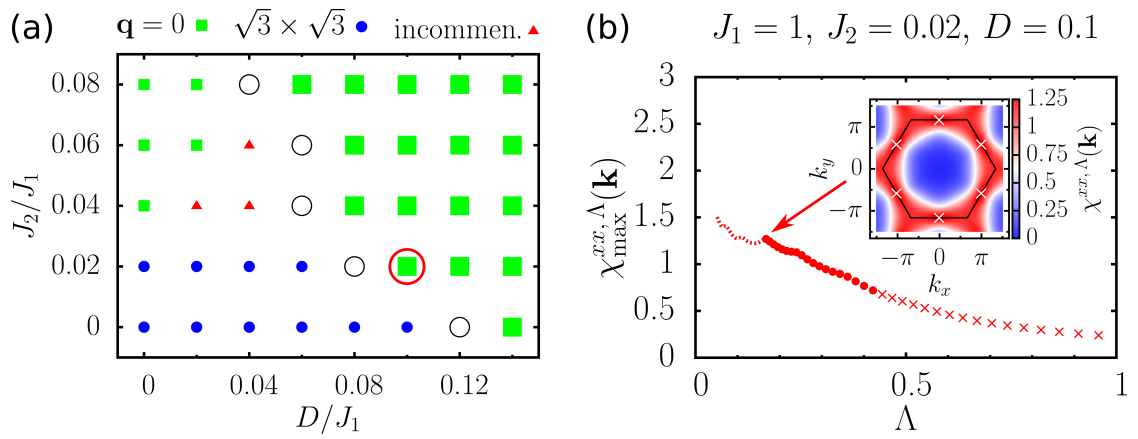

Figure 4.9.: (a) Phase diagram in the parameter range for *herbertsmithite*: The momentum-space position of the maximal susceptibility is denoted by green squares (blue circles) for the $\boldsymbol{q} = 0$ ($\sqrt{3} \times \sqrt{3}$) wave vectors. Red triangles show that incommensurate spin correlations, which do not correspond to any of the classical ordering types, are dominant. Large icons indicate that the system magnetically orders. On the other hand, small icons show a possible spin liquid behaviour. For the parameters with black circles, we cannot reliably determine the magnetic characteristics due to numerical imprecisions. (b) Susceptibility flow for $(J_1, J_2, D) = (1, 0.02, 0.1)$ [see red circle in (a)]: Circles and crosses denote that the largest spin correlations are found at the $\boldsymbol{q} = 0$ and $\sqrt{3} \times \sqrt{3}$ positions, respectively. The arrow marks a breakdown of the flow signaling the onset of magnetic order. The inset provides the susceptibility profile at the corresponding Λ value with maxima at the $\boldsymbol{q} = 0$ positions (highlighted by white crosses) in agreement with Ref. [68].

evant model for *herbertsmithite* and subleading terms were already estimated by DFT simulations yielding an also antiferromagnetic second-neighbour Heisenberg interaction with $J_2/J_1 = 0.019$ [93]. ESR measurements, susceptibility fittings, and the difference in entropy as compared to a bare Heisenberg model determine a nearest-neighbour DM coupling reaching from $D/J_1 \sim 0.08$ to 0.1 [149, 166, 192].

We apply our PFFRG method in a parameter range surrounding those predicted interaction strengths and investigate the resulting susceptibility flows as well as the momentum-space profiles, see Fig. 4.9(a). As one can see, there is a strong competition between a magnetically ordered $\boldsymbol{q} = 0$ Néel phase (large icons) and paramagnetic phase (small icons) with different types of dominant spin correlations ($\boldsymbol{q} = 0$, $\sqrt{3} \times \sqrt{3}$, incommensurate). Due to the challenging numerical implementation, the phase boundary is hard to identify exactly and therefore estimated by the area of numerical uncertainty which is marked by black circles. For our considered couplings, the phase boundary is approximately given by the straight line connecting the points $(D/J_1, J_2/J_1) = (0.04, 0.08)$ and $(0.12, 0)$. It therefore lies in close proximity to the predicted values for *herbertsmithite*. At the point $(D/J_1, J_2/J_1) = (0.1, 0.02)$, which presumably seems to be the experimentally relevant

situation, we find a susceptibility profile showing a strong resemblance to the neutron-scattering data of Ref. [68] with the strongest signal almost continuously spread over the edges of the extended Brillouin zone and small maxima at the $\boldsymbol{q} = 0$ positions, see inset of Fig. 4.9(b). However, as the major plot shows, the FRG flow features a small magnetic instability suggesting the onset of magnetic order, in contrast to the experimental findings. Increasing the number of discrete Matsubara frequencies or enlarging the considered spin-correlation cluster size would expectably amplify the instability feature.

Therefore, we conclude that the J_1-J_2-D model is yet insufficient to completely characterise the magnetic properties of *herbertsmithite*. If the so far predicted values for D/J_1 are too large and $D < 0.1\,J_1$, we find paramagnetic behaviour but we also sacrifice the $\boldsymbol{q} = 0$ maxima for a dominant $\sqrt{3} \times \sqrt{3}$ response in that case. This would require additional spin interactions shifting the peaks in order to reproduce the experimental data. Also, if $(D/J_1, J_2/J_1) \approx (0.1, 0.02)$ accurately describes the investigated mineral, further sources of frustration are needed to suppress its ordering tendencies. In fact, ab-initio calculations predict a plethora of further inter-layer Heisenberg couplings with a magnitude of up to $0.035\,J_1$ [93]. Together with magnetic impurities which are caused by copper ions at zinc lattice sites in the actual material, this might easily increase in-plane fluctuations and thereby destroy the magnetic long-range order.

4.5. Summary, conclusion, and outlook

In this chapter, we extended the well-known PFFRG method in order to investigate spin-$\frac{1}{2}$ models with Heisenberg and DM interactions. The main modifications caused by the additional off-diagonal and anisotropic DM coupling were summarised in Sec. 4.2. Refs. [27, 162] already studied our model of interest and we could benchmark the utilised procedure by confirming their results, *i.e.*, a destabilisation of the paramagnetic phase in the antiferromagnetic J_1-J_2-D model and transition into the $\boldsymbol{q} = 0$ order at $D \geq (0.12 \pm 0.02)\,J_1$ for the nearest-neighbour model. In Sec. 4.4, we applied our numerical simulations to the full model also allowing for ferromagnetic nearest and second-neighbour Heisenberg interactions. As the phase diagrams in Fig. 4.8 show, a finite DM interaction enlarges all non-collinearly ordered phases ($\boldsymbol{q} = 0$, $\sqrt{3} \times \sqrt{3}$, and cuboc orders) while, simultaneously, all surrounding non-magnetic phases are diminished. In particular, the very important paramagnetic phase around $(J_1, J_2) = (1, 0)$ in which the spin-liquid candidate *herbertsmithite* resides completely disappears for a sufficiently strong $D \gtrsim 0.4\,J$. We also find that this mineral lies in the vicinity of a quantum critical point where we are able to obtain susceptibilities that strongly resemble the experimental spin structure factors from Ref. [68] for certain parameter regions. Nevertheless, we argue that, due to signs of weak magnetic order in our simulations, the J_1-J_2-D model is probably insufficient to accurately characterise the magnetic properties of *herbertsmithite* and additional sources of frustration like inter-layer couplings and magnetic impurities might be important for a QSL behaviour.

To conclude, we have shown that the PFFRG for spin systems can be applied to models

with finite DM interactions. The anisotropic and off-diagonal structure of this particular spin coupling with its intrinsically lower degree of symmetry as compared to a bare Heisenberg model complicates the analysis by a non-negligible amount. Considering the complexity of the resulting flow equations, we certainly demonstrated how important it is in theoretical physics to utilise all symmetries that are available. Nevertheless, we could also confirm that an implementation of the PFFRG for systems with reduced symmetries is in general possible.

The anisotropic nature of the DM interaction is caused by spin-orbit coupling which becomes the more important the heavier the magnetic ions are. In addition to the DM interaction which can only occur for lattices with broken inversion symmetry at the center of a bond, Kitaev and XXZ models are also possible consequences of this effect. For many of the currently investigated magnetic materials, these effects are quite sizable and therefore a large number of future applications for even more generalised or stripped-down versions of the PFFRG are conceivable. We will not derive flow equations that are more complex than the ones shown in App. B. Instead, we continue by simply changing their initial conditions in the next chapter. In this way, we can apply our PFFRG implementation to arbitrary XXZ models with a considerable numerical speed-up.

5. XXZ model for spin-1 A-site spinel $NiRh_2O_4$

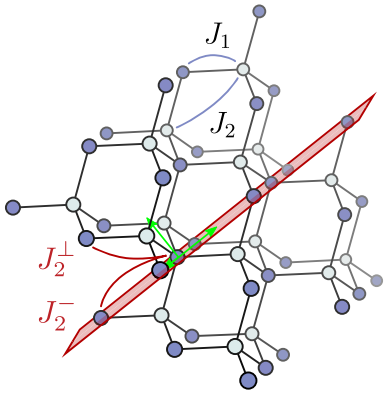

Figure 5.1.: Diamond lattice with tetragonal distortion: The diamond lattice is bipartite and consists of two face-centered cubic lattices stacked into another. Spin frustrations arise due to a combination of nearest (J_1) and next-nearest (J_2) neighbour interactions, the latter of which get split up into eight $J_2^{\perp}$ and four J_2^{-} contributions by a tetragonal distortion as in the case of $NiRh_2O_4$. Cartesian unit vectors are depicted green. *Figure adapted from Ref. [20].*

Now that we proved ourselves being able to investigate frustrated quantum spin models with anisotropic types of interactions, we want to study the just recently synthesised spin-1 A-site spinel $NiRh_2O_4$ which has experimentally shown to exhibit no signs of magnetic order down to $T = 0.1\,K$ [30] making it another promising candidate for finding a quantum spin liquid. The chemical formula for spinels AB_2X_4 distinguishes between the real space coordination of three kinds of ions. In general, chalcogens like oxygen, sulfur, and selenium are found at the X positions and the remaining ions characterise the two distinct types of spinels.

The so-called B-site spinels are characterised by magnetic ions that reside on the B sites of the crystal, such as, for instance, ACr_2O_4 and AV_2O_4. Here, the non-magnetic ions are found at the A sites (A = Mg, Zn, Cd) and the magnetic ones form a pyrochlore lattice with antiferromagnetic Heisenberg interactions. Depending on the spin length of the magnetic ions, these materials are well known to establish spin liquid behaviour [10, 157] in the classical ($S \to \infty$) [127, 128] as well as in the quantum ($S = \frac{1}{2}$) [22, 23] limits and are thus prime examples for finding these desired states in three dimensions. On the other hand, if the positions of magnetic and non-magnetic ions are swapped, one faces A-site spinels with an effective diamond lattice structure for the magnetic moments. For example, the materials $MnSc_2S_4$ [56], $FeSc_2S_4$ [56], and $CoAl_2O_4$ [174, 175] caught large attraction since, despite the non-frustrated nature of the diamond lattice, they also show a strong suppression of their ordering temperature as compared to the Curie-Weiss temperature. This counterintuitive phenomenon was understood shortly after by realising that the frustrations necessary for such a behaviour can be induced by finite second-neighbour interactions [13].

A good starting point for the investigation of our A-site nickel spinel is therefore the Hamiltonian

$$H = J_1 \sum_{\langle i,j \rangle} \boldsymbol{S}_i \cdot \boldsymbol{S}_j + J_2 \sum_{\langle\langle i,j \rangle\rangle} \boldsymbol{S}_i \cdot \boldsymbol{S}_j \,, \tag{5.1}$$

on the diamond lattice from Fig. 5.1. In the classical limit, this model shows the formation of spin-spiral surfaces in the momentum-resolved susceptibilities if $J_2 > |J_1|/8$ [13]. The largest spin correlations are found at degenerate sets of incommensurate wave vectors forming a surface in the three-dimensional Brillouin zone. If there is no ordering mechanism present, the system can vary continuously between the energetically most favourable spin spirals with different wave vectors. Such a phase is often denoted as a *spiral spin liquid*. However, spin-spiral surfaces are unlike Fermi surfaces highly unstable with respect to small perturbations to the Hamiltonian and thermal or quantum fluctuations drive them into an order-by-disorder transition selecting finite sets of ordering wave vectors in $\boldsymbol{k}$ space [13, 14].

While a classical treatment of the model has proven to be sufficient for understanding the magnetic properties of large-S A-site spinels with magnetic Mn ($S = \frac{5}{2}$) and Co ($S = \frac{3}{2}$) ions [57, 108, 158], the behaviour of $FeSc_2S_4$ is dominated by spin-orbit coupling effects [34, 35] which are not captured in Eq. (5.1). Furthermore, the absence of any type of magnetic order in the compound $NiRh_2O_4$ down to lowest temperatures is also not captured by the classical model (confer discussion in previous chapter). This motivated our collaborators from Cologne to study the J_1-J_2 model on the diamond lattice using a generalised version of the FRG flow equations in App. A for arbitrary spin lengths S. It has been shown in Ref. [9] that an extension of the previously derived equations for spin-$\frac{1}{2}$ particles, in essence, amounts to multiplying all diagrams where a sum over real-space coordinates appears with the factor $M = 2S$. Employing these remarkably elegant modifications to the equations for the self energy and the two-particle vertex, a phase diagram for different coupling ratios J_2/J_1 and spin lengths was mapped out which is not part of the original work from this thesis. Its main result is that, beyond an ordered Néel state at $J_1 = 1$ and $0 \leq J_2 \leq 1/8$ for all spin lengths, a sequence of dominant susceptibility wave vectors is found depending on the precise value of J_2/J_1 where magnetic order occurs for $S \geq 2$ and a paramagnetic state (possibly a quantum spiral liquid) is found if $S = \frac{1}{2}$, 1 [20]. A classical to quantum transition occurs precisely at $S = \frac{3}{2}$ where for $0.2 \lesssim J_2/J_1 \lesssim 0.4$ the system still resides in the fluctuation dominated quantum regime with no onset of magnetic order during the flow, and with classical magnetic order for larger J_2 as well as in the Néel phase.

However, the recently synthesised spin liquid candidate $NiRh_2O_4$ undergoes a structural transition at $T = 440\,K$ [30] which induces a tetragonal distortion on the diamond lattice such that the second-neighbour couplings are split up into eight out-of-plane contributions $J_2^{\perp}$ and four in-plane contributions J_2^{-}, see Fig. 5.1. An *arxiv* preprint version of a manuscript by Chamorro *et al.* presents a DFT study yielding the values $(J_1, J_2^{-}, J_2^{\perp}) = (1, 0.73, -0.91)$ [29]. We therefore consider antiferromagnetic $J_1 = 1$ and $J_2^{-} = 0.73$ with a tetragonal distortion determined by the parameter $J_2^{\perp}/J_2^{-}$. Using

Luttinger-Tisza and PFFRG methods with these values, our collaborators found that already for very small second-neighbour splittings the spin liquid phase vanishes giving way to a magnetically ordered Néel phase for all spin lengths S. Since a recent study proposed that an additional single-ion anisotropy drives the system into a trivial quantum paramagnet [33], our goal is now to include this term in the PFFRG framework and to investigate its effects on the modified spin-1 diamond lattice model.

5.1. XXZ model on spin-1 diamond lattice

According to Refs [29] and [33], we investigate the spin-1 Heisenberg model with tetragonal distortion and local single-ion anisotropy. It is governed by the Hamiltonian

$$H = J_1 \sum_{\langle i,j\rangle} \boldsymbol{S}_i \cdot \boldsymbol{S}_j + J_2^{\perp} \sum_{\langle\langle i,j\rangle\rangle_{\perp}} \boldsymbol{S}_i \cdot \boldsymbol{S}_j + J_2^{-} \sum_{\langle\langle i,j\rangle\rangle_{-}} \boldsymbol{S}_i \cdot \boldsymbol{S}_j + D \sum_i S_i^z S_i^z - A \sum_i \boldsymbol{S}_i \boldsymbol{S}_i \,. \quad (5.2)$$

For our purposes of a spin length $S = 1$, it is shown in Ref. [9] that we have to encode our spin operators by

$$\boldsymbol{S}_i = \sum_{\kappa=1}^{2S} \boldsymbol{S}_{i\,\kappa} \,, \quad (5.3)$$

where now there are two different spin-$\frac{1}{2}$ flavours ($\boldsymbol{S}_{i\,1}$ and $\boldsymbol{S}_{i\,2}$) residing at site i which are in turn expressed with the help of the auxiliary fermions from Eq. (4.2). As already mentioned above, in our diagrammatic language that is dealing with vertex functions, this modification of the spins amounts to additional factors of $M = 2S$ for every real-space sum carried-out in the flow equations for Σ^{Λ} and Γ^{Λ}. Furthermore, the anisotropy term $\propto D$ causes a splitting of the spin-spin interaction channel such that our two-particle vertex function is parameterised by

$$\begin{aligned}\Gamma^{\Lambda}(s,t,u) = \Bigg[& \Gamma^{\Lambda}_{\mathrm{xx}\,i_1 i_2}(s,t,u) \left(\sigma^x_{\alpha_{1'}\alpha_1} \sigma^x_{\alpha_{2'}\alpha_2} + \sigma^y_{\alpha_{1'}\alpha_1} \sigma^y_{\alpha_{2'}\alpha_2} \right) + \Gamma^{\Lambda}_{\mathrm{zz}\,i_1 i_2}(s,t,u)\, \sigma^z_{\alpha_{1'}\alpha_1} \sigma^z_{\alpha_{2'}\alpha_2} \\ & + \Gamma^{\Lambda}_{\mathrm{d}\,i_1 i_2}(s,t,u)\, \delta_{\alpha_{1'}\alpha_1} \delta_{\alpha_{2'}\alpha_2} \Bigg] \delta(\omega_1 + \omega_2 - \omega_{1'} - \omega_{2'}) \delta_{i_{1'} i_1} \delta_{i_{2'} i_2} \\ & - (\omega_1 \leftrightarrow \omega_2,\, \alpha_1 \leftrightarrow \alpha_2,\, i_1 \leftrightarrow i_2) \,. \end{aligned} \quad (5.4)$$

Similar to the scenario with Dzyaloshinsky-Moriya interactions from the previous chapter, a global $U(1)$ spin-rotation symmetry around the z axis is present in this model (cf. App. E.2). Since no off-diagonal interactions are present, the self energy remains finite only in the density channel and the propagators are identical to those from the bare Heisenberg case, confer Sec. 4.2.2. The last term $\propto A$ in Eq. (5.2) is an artificially included level repulsion term. This ensures that the $S = 0, \frac{1}{2}$ sectors of our now drastically enlarged Hilbert space are energetically penalised and therefore suppressed during the FRG flow.

The single-ion anisotropy would favour these unphysical spin lengths and the value of A has to be determined empirically, depending on D.

The initial conditions from the Hamiltonian characterising our A-site spinel are hence given by

$$\gamma_{\mathrm{d}}^{\Lambda\to\infty}(\omega) = 0\,, \tag{5.5a}$$

$$\Gamma_{\mathrm{d}\,i_1 i_2}^{\Lambda\to\infty}(s,t,u) = 0\,, \tag{5.5b}$$

$$\Gamma_{\mathrm{xx}\,i_1 i_2}^{\Lambda\to\infty}(s,t,u) = \frac{J_{i_1 i_2}}{4} - \frac{A_{i_1 i_2}}{4}\,, \tag{5.5c}$$

$$\Gamma_{\mathrm{zz}\,i_1 i_2}^{\Lambda\to\infty}(s,t,u) = \frac{J_{i_1 i_2}}{4} + \frac{D_{i_1 i_2} - A_{i_1 i_2}}{4}\,, \tag{5.5d}$$

where $D_{i_1 i_2} = D\delta_{i_1 i_2}$ and $A_{i_1 i_2} = A\delta_{i_1 i_2}$. The flow equations for this XXZ model with arbitrary spin length (represented by the factor $M = 2S$) are given in App. C. Due to the broken $SU(2)$ spin-rotation symmetry, we distinguish the in-plane and out-of-plane susceptibilities

$$\begin{aligned}
\chi_{ij}^{xx,\,\Lambda}(0) = {} & \frac{1}{4\pi}\int_{-\infty}^{\infty} \mathrm{d}\omega_1\, M \frac{\theta(|\omega_1|-\Lambda)}{\left(\omega_1 + \gamma_{\mathrm{d}}^{\Lambda}(\omega_1)\right)^2}\delta_{ij} \\
& - \frac{1}{8\pi^2}\int_{-\infty}^{\infty}\mathrm{d}\omega_1 \int_{-\infty}^{\infty}\mathrm{d}\omega_2\, \frac{\theta(|\omega_1|-\Lambda)}{\left(\omega_1 + \gamma_{\mathrm{d}}^{\Lambda}(\omega_1)\right)^2}\frac{\theta(|\omega_2|-\Lambda)}{\left(\omega_2 + \gamma_{\mathrm{d}}^{\Lambda}(\omega_2)\right)^2}\Big\{2M^2\Gamma_{\mathrm{xx}\,ij}^{\Lambda}\left(\omega^+,0,\omega^-\right) \\
& - M\left[\Gamma_{\mathrm{d}\,ii}^{\Lambda}\left(\omega^+,\omega^-,0\right) - \Gamma_{\mathrm{zz}\,ii}^{\Lambda}\left(\omega^+,\omega^-,0\right)\right]\delta_{ij}\Big\}\,,
\end{aligned} \tag{5.6a}$$

$$\begin{aligned}
\chi_{ij}^{zz,\,\Lambda}(0) = {} & \frac{1}{4\pi}\int_{-\infty}^{\infty} \mathrm{d}\omega_1\, M \frac{\theta(|\omega_1|-\Lambda)}{\left(\omega_1 + \gamma_{\mathrm{d}}^{\Lambda}(\omega_1)\right)^2}\delta_{ij} \\
& - \frac{1}{8\pi^2}\int_{-\infty}^{\infty}\mathrm{d}\omega_1 \int_{-\infty}^{\infty}\mathrm{d}\omega_2\, \frac{\theta(|\omega_1|-\Lambda)}{\left(\omega_1 + \gamma_{\mathrm{d}}^{\Lambda}(\omega_1)\right)^2}\frac{\theta(|\omega_2|-\Lambda)}{\left(\omega_2 + \gamma_{\mathrm{d}}^{\Lambda}(\omega_2)\right)^2}\Big\{2M^2\Gamma_{\mathrm{zz}\,ij}^{\Lambda}\left(\omega^+,0,\omega^-\right) \\
& - M\left[\Gamma_{\mathrm{zz}\,ii}^{\Lambda}\left(\omega^+,\omega^-,0\right) - 2\Gamma_{\mathrm{xx}\,ii}^{\Lambda}\left(\omega^+,\omega^-,0\right) + \Gamma_{\mathrm{d}\,ii}^{\Lambda}\left(\omega^+,\omega^-,0\right)\right]\delta_{ij}\Big\}\,,
\end{aligned} \tag{5.6b}$$

where we defined that $\omega^{\pm} = \omega_1 \pm \omega_2$ and the additional prefactors of M and M^2 arise due to one or two spin flavour summations within the loop diagrams that contribute to the susceptibilities.

5.2. Spin anisotropy versus level repulsion

The spin anisotropy term $\propto D$ in the Hamiltonian from Eq. (5.2) suppresses the out-of-plane susceptibility $\chi_{ij}^{xx,\,\Lambda}$ because it favours a spin alignment within the x-y plane. Nevertheless, we cannot exclude the occupation of unphysical spin sectors with $S < 1$ which is why we also include the level-repulsion term $\propto A$. In essence, we now need

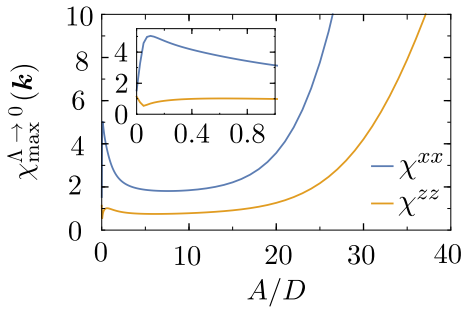

Figure 5.2.: Susceptibility components for different values of A/D in the effective single-ion model: For this decoupled spin-1 system, the vertices show a smooth flow down to zero cutoff at which we calculate the maximal in-plane and out-of-plane susceptibility components in momentum space. As expected, the out-of-plane component $\chi^{zz,\Lambda}(\boldsymbol{k})$ is strongly suppresses as compared to $\chi^{xx,\Lambda}(\boldsymbol{k})$ but remains finite for all values of A/D because of quantum fluctuations. A flat plateau for both curves appears if $3 \lesssim A/D \lesssim 10$ indicating an occupation of the physical sector of the Hilbert space within that range. *Figure adapted from Ref. [20].*

to balance three independent effects. The antiferromagnetic Heisenberg interaction should favour antiparallel spin alignments with maximal and thus physical spin lengths $S = 1$, but due to its sometimes frustrated nature it could locally support an unphysical occupation as well. In addition, the single-ion anisotropy wants to minimise S^z which can also lead to reduced spin lengths. The level-repulsion term, on the other hand, raises the energy of unphysical states and therefore acts as a counterweight for the anisotropy in particular since there are reasons to believe that the PFFRG for bare Heisenberg models already selects the correct spin sectors without the level repulsion [9]. Because the repulsion term is an artificial parameter that is needed in order to overcome certain difficulties of our method, we have to analyse its effect in detail. We want to determine a reliable value for the ratio A/D at which a physical occupation of our augmented Hilbert space is realised. This is, for instance, achieved if the results obtained from PFFRG do not change upon further increasing A. If this is the case, the maximal spin length is already enforced on each site and only the total energy of the systems is lowered if A becomes even larger.

Let us investigate the effectively decoupled single-ion model where $J_1 = J_2^{\perp} = J_2^{-} = 0$ in this section. Considering the initial conditions in Eqs. (5.5), it should be clear that at least for values $A/D > 1$ a suppression of the unphysical spin sector sets in because the isolated ion minimises its energy by maximising all of its spin components. If $A/D < 1$, the in-plane spin component is maximised whereas the out-of-plane component is minimised. Depending on the precise ratio, this might or might not lead to an unphysical occupation. However, the numerical implementation of our flow equations has to utilise a finite frequency mesh and is hence limited to a finite resolution with respect to the initial conditions of the vertices. If we set $D = 1$, this implies that we are not able to gain insights for

$A \gg D$ since the flow breaks down in this case due to an insufficient amount of considered large frequencies. In contrast, by setting $A = 1$ and sending $D \to 0$ in order to investigate the same limit, we are not able to observe the anisotropy's effects any longer because the low frequencies in our numerics have a finite spacing. Hence, we keep $D = 1$ and look for an intermediate range with $A/D \gtrsim 1$ where unphysical occupations are avoided and the effects of the single-ion anisotropy are still noticeable.

We compare the values of $\chi^{xx,\Lambda}(\boldsymbol{k})$ and $\chi^{zz,\Lambda}(\boldsymbol{k})$ in the decoupled single-ion model as a function of A/D, see Fig. 5.2. The different spin sites are independent of each other and therefore add up to a trivial paramagnet with a susceptibility that is completely constant within the Brillouin zone. We directly investigate the results for $\Lambda \to 0$ and see that in a certain parameter range, *i.e.*, $3 \lesssim A/D \lesssim 10$, our results are independent of the precise value of A/D. Any different behaviour suggests that unphysical states are occupied for smaller values and that the numerical PFFRG implementation breaks down for even higher values. We thus determine an intermediate value of $A/D = 4$ for our further calculations. The behaviour of both susceptibility components during the flow for this choice of parameters can be seen in the right-most panel of Fig. 5.3.

5.3. Antiferromagnetic XXZ model without tetragonal splitting

We first investigate the effect of the single-ion anisotropy on the antiferromagnetic XXZ model from Eq. (5.2) without the tetragonal distortion, *i.e.*, $J_2^{\perp} = J_2^{\perp} = 0.73\, J_1$. The flow of the maximal susceptibility values in $\boldsymbol{k}$ space can be seen in Fig 5.3. Without the XXZ splitting due to the anisotropy ($D = 0$), the remaining bare Heisenberg system does not discriminate the susceptibility components $\chi^{xx,\Lambda}(\boldsymbol{k})$ and $\chi^{zz,\Lambda}(\boldsymbol{k})$. In this case, the functions flow smoothly towards $\Lambda = 0$ showing no signs of long-range order and a formation of spiral surfaces in momentum space can be observed for this quantum spiral liquid regime (confer introduction to this chapter). Contrarily, in the $D \to \infty$ limit, our spin system effectively decouples into isolated spins with a favoured orientation in the x-y plane. This implies a maximal suppression of $\chi^{zz,\Lambda}(\boldsymbol{k})$ which is as well as the in-plane response $\chi^{xx,\Lambda}(\boldsymbol{k})$ constant inside the entire Brillouin zone. Interestingly, the out-of-plane susceptibility does not vanish completely, implying a finite expectation value of $(S_i^z)^2$ due to quantum fluctuations. The ratio between both susceptibility components is given by $\frac{\chi^{xx}}{\chi^{zz}} \simeq 4$ for the trivial paramagnet in the $\Lambda \to \infty$ limit. We expect that both this ratio and the pronounced increase of the in-plane susceptibility for low Λ values are upheld within that phase, confer right-most panel of Fig. 5.3. From our plots, we estimate that the crossover between trivial and quantum paramagnet occurs around $D/J_1 \approx 2$ (see middle panel of Fig. 5.3) which is in good agreement with the mean-field result from Ref. [33]. At this point, the RG flows of $\chi^{xx,\Lambda}$ and $\chi^{zz,\Lambda}$ are qualitatively similar to the ones in the $D \to \infty$ limit and their ratio has the same maximal value for $\Lambda \to \infty$ as the trivial

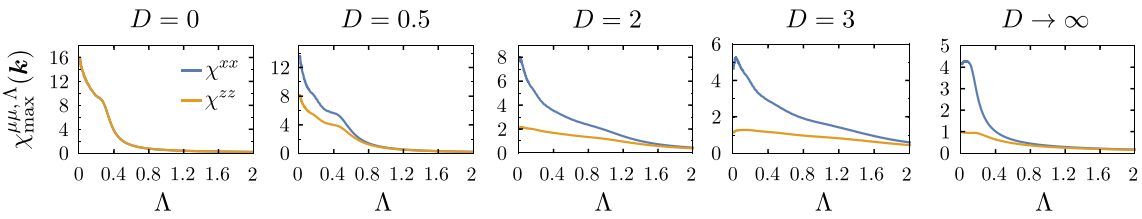

Figure 5.3.: Spin susceptibilities for XXZ model on the diamond lattice without tetragonal distortion ($J_2^{\perp} = J_2^{\perp} = 0.73\,J_1$) and different values of D: Without the anisotropy ($D = 0$), both components are identical [$\chi^{xx,\Lambda}(\boldsymbol{k}) = \chi^{zz,\Lambda}(\boldsymbol{k})$]. The trivial paramagnet is found in the $D \to \infty$ limit where now the out-of-plane component $\chi^{zz,\Lambda}(\boldsymbol{k})$ is maximally suppressed, but not zero. In all plots, the level repulsion is kept at $A/D = 4$. *Figure adapted from Ref. [20].*

paramagnet. For the quantum spiral liquid, we show the momentum resolved susceptibility for the high-symmetry $(h, l, 0)$ and (h, h, l) planes in the top panel of Fig. 5.5. The spiral surfaces are found in the $(h, l, 0)$ and $(0, h, l)$ planes which are identical through lattice symmetries. The spin correlations are almost constant on these surfaces indicating a strong competition between different possible spin arrangements suppressing magnetic long-range order up to the smallest numerically achieved cutoff values. In the other limit of $D \to \infty$, the susceptibility is constant in $\boldsymbol{k}$ space signaling nothing but effectively decoupled lattice sites. We do not plot the susceptibility for this scenario.

5.4. Antiferromagnetic XXZ model with tetragonal splitting

Let us finally turn to the effects of the tetragonal distortion which occurs for $NiRh_2O_4$ at $T = 440\,K$ [30]. As explained in the introduction, the suggested coupling ratios from DFT being $(J_1, J_2^{-}, J_2^{\perp}) = (1, 0.73, -0.91)$ [29] lead to a formation of a Néel antiferromagnet in our PFFRG simulations. If we include these coupling parameters together with a single-ion anisotropy while keeping the level repulsion term such that $A/D = 4$ (confer Sec. 5.2), the out-of-plane spin correlations are again suppressed as in the previous chapter, see Fig. 5.4. However, we rigorously find Néel order state for all considered values of $D \leq 8$, see bottom panel of Fig. 5.5 for an exemplary illustration. Only in the $D \to \infty$ limit, the trivial paramagnet is recovered (right-most panel in Fig. 5.3). The trivial paramagnet of decoupled spins though is of no great interest for finding novel physical phenomena and we are also not seduced to believe that our nickel spinel is entirely dominated by the anisotropy term.

The *arxiv* preprint manuscript Ref. [29] is the only available source for possible coupling strengths in $NiRh_2O_4$ obtained from *ab-initio* calculations. Because we do not find any paramagnetic behaviour with these values, not even with an additional single-ion anisotropy, we now map out a phase diagram where we take the Hamiltonian from Eq. (5.2) and vary the distortion $J_2^{\perp}/J_2^{-}$ as well as the anisotropy D. As before, we fix the level

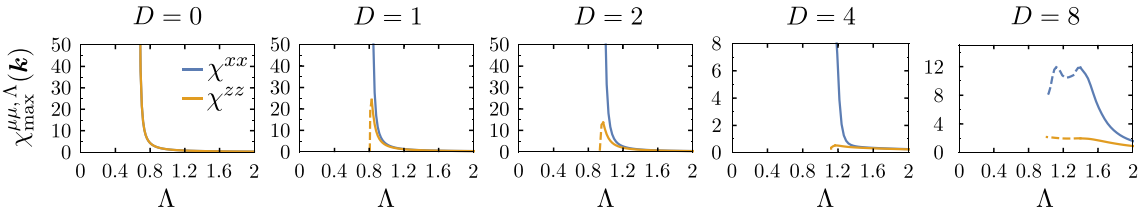

Figure 5.4.: Effects of tetragonal splitting: Shown are identical calculations as in Fig. 5.3, but now with the tetragonal splitting $(J_1, J_2^-, J_2^\perp) = (1, 0.73, -0.91)$ from Ref. [29]. We observe the onset of magnetic order for all values of the single-ion anisotropy up to $D = 8$ in contrast to the experimental findings for $NiRh_2O_4$. Only in the $D \to \infty$ limit, the plot from the right-most panel in Fig. 5.3 is reobtained. *Figure adapted from Ref. [20].*

repulsion to $A/D = 4$. Since different ordered and disordered states can manifest themselves in this model, our main focus is on whether or not the system shows magnetic order. For that reason, in Fig. 5.6, we only show the critical cutoff value Λ_c for which magnetic long-range order is found to set in. If $\Lambda_c = 0$ (white panels in Fig. 5.6), the susceptibility grows smoothly until the end of the flow signaling a paramagnetic and hence possible spin liquid phase. Indeed, we find an extended regime without magnetic long-range order which spans over finite tetragonal distortions $J_2^\perp/J_2^-$ from -0.5 to 1.25 at an anisotropy value of $D/J_1 = 5$. The susceptibility flows along horizontal cuts can be seen for $J_2^\perp/J_2^- = 1$ and $J_2^\perp/J_2^- = -1.25$ in Fig 5.3 and Fig 5.4, respectively. These results are published in Ref. [20] and interpreted therein in the way that some reduction of the tetragonal splitting in combination with a reasonably sized single-ion anisotropy could well explain the experimental observations for $NiRh_2O_4$. A more detailed DFT analysis including the anisotropy term would shine more light onto this situation.

Meanwhile, we take notice though that, in the published version of the aforementioned online preprint, the DFT analysis is completely replaced by a different model where the coupling parameters are determined by fitting linear spin-wave simulations to inelastic neutron-scattering data [30]. This seems to be a bit ambiguous because the spin-wave theory is based on an ordered state and cannot access the presumed spin liquid phase. The reason for this modification in the publication is not known to us. Since our previous analysis is based on the work of this group, we also analyse the Hamiltonian that is estimated in the published article, *i.e.*,

$$H = J_1 \sum_{\langle i,j \rangle} \left(\sigma_i^x \sigma_j^x + \sigma_i^y \sigma_j^y + \Delta \sigma_i^z \sigma_j^z \right) + J_2^\perp \sum_{\langle\langle i,j \rangle\rangle_\perp} \boldsymbol{S}_i \cdot \boldsymbol{S}_j + J_2^- \sum_{\langle\langle i,j \rangle\rangle_-} \boldsymbol{S}_i \cdot \boldsymbol{S}_j \,. \tag{5.7}$$

This is also an effective XXZ model which, due to the lack of the single-ion anisotropy, does not necessarily require the involvement of a level repulsion term because the PFFRG has shown to automatically select the correct sector of the Hilbert space in related Heisenberg models [9]. Despite the conceptual issues of linear spin-wave theory for our spinel material, the neutron-scattering data can allegedly be relatively well reconstructed from

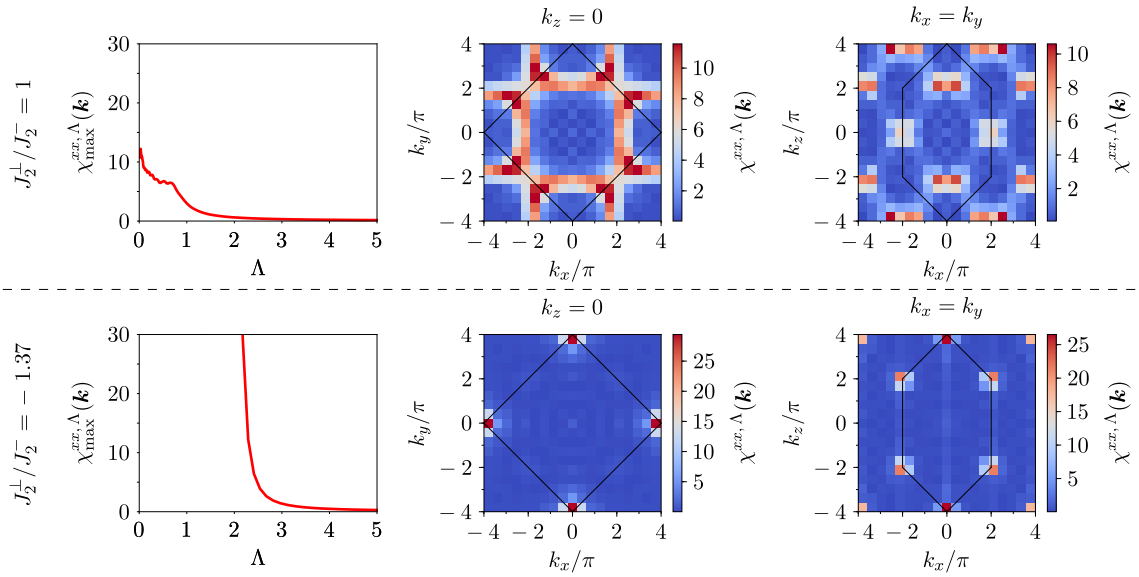

Figure 5.5.: Comparison between XXZ models with and without tetragonal splitting: In the top ($J_2^\perp/J_2^- = 1$) and bottom ($J_2^\perp/J_2^- = -1.37$) panels, we compare susceptibility flow and cuts through the Brillouin zone (black lines) from PFFRG calculations for the Hamiltonian in Eq. (5.2) with $D = A = 0$. Without the splitting, we find a quantum spiral liquid whereas the tetragonal distortion from Ref. [29] induces long-range Néel order. Slight differences to the left panels in Figs. 5.3 and 5.4 are caused by a coarser frequency resolution and different splitting sizes (only bottom panel).

the Hamiltonian in Eq. (5.7) if $(J_1, J_2^-, J_2^\perp) = (1, -0.3, 0.12)$ and $\Delta = 1.1$ what considerably differs from the previous analysis. These couplings are easily implemented via the initial conditions

$$\gamma_{\mathrm{d}}^{\Lambda\to\infty}(\omega) = 0\,, \tag{5.8a}$$

$$\Gamma_{\mathrm{d}\,i_1 i_2}^{\Lambda\to\infty}(s,t,u) = 0\,, \tag{5.8b}$$

$$\Gamma_{\mathrm{xx}\,i_1 i_2}^{\Lambda\to\infty}(s,t,u) = \frac{J_{i_1 i_2}}{4}\,, \tag{5.8c}$$

$$\Gamma_{\mathrm{zz}\,i_1 i_2}^{\Lambda\to\infty}(s,t,u) = \frac{\Delta_{i_1 i_2} J_{i_1 i_2}}{4}\,. \tag{5.8d}$$

Unfortunately, we still find a conventionally ordered Néel state for this model. The resulting susceptibility flow and $\boldsymbol{k}$-space plots do not differ substantially from those of the previous one, confer bottom panel of Fig. 5.5.

5.5. Summary and conclusion

In this chapter, we employed PFFRG formalism with anisotropic, but diagonal spin interactions for the XXZ model with arbitrary spin length S. For the first time, we included

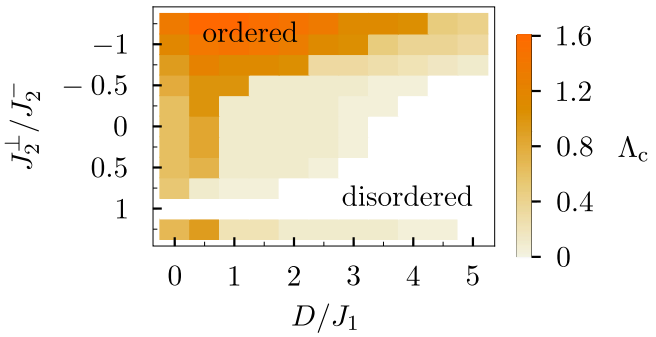

Figure 5.6.: Phase diagram for tetragonal splitting $J_2^\perp/J_2^-$ and single-ion anisotropy D/J_1: The colour scale represents the critical cutoff value Λ_c. Orange, beige, and brown shades indicate the RG scale for the onset of magnetic order. White panels represent a smooth flow with $\Lambda_c = 0$ denoting a paramagnetic regime. The in-plane second-neighbour coupling is kept constant at $J_2^- = 0.73\,J_1$ for this plot. *Figure adapted from Ref. [20].*

a single-ion anisotropy in such a calculation and investigated how to add a level repulsion term in order to avoid the occupation of unphysical spin sectors. The motivation behind all this is that the previously suggested Heisenberg model with tetragonal distortion [29] for the spin-1 *A*-site spinel $NiRh_2O_4$ failed to explain the experimental observation of no magnetic long-range order in this material down to lowest temperatures. Therefore, we also added a single-ion anisotropy as supposed in Ref. [33], which can drive the system into a trivial paramagnet, and the hence required level-repulsion term to that model, see Eq. (5.2).

Even though we are able to confirm the existence of an extended paramagnetic regime once a finite-sized anisotropy is present, we can only identify magnetic order at splitting values as high as $J_2^\perp/J_2^- = -1.25$ for all considered anisotropy strengths. Unfortunately, also the second considered model from Ref. [30] is unable to describe the physics of $NiRh_2O_4$ [confer Eq. (5.7)]. For all coupling parameters that do not reside within the white area of Fig. 5.6, the PFFRG detects conventional antiferromagnetic Néel order as depicted in the bottom panel of Fig. 5.5. This is in strong contrast with the experimental findings for $NiRh_2O_4$ and we therefore conclude once more that precise *ab-initio* calculations which include all symmetry-allowed spin interactions are needed for a further analysis of this remarkable material.

This ends the part of this thesis where we derive new results following solely from the PFFRG. One of the fundamental observations which should be repeated once more at this point is that an efficient evaluation of the flow equations is only possible if certain symmetries remain, especially in three dimensional systems. Otherwise there are trade-offs in the achievable frequency resolution and cluster size. Additionally, it seems rather impossible to us to manually implement the most generally conceivable spin-spin interaction. In such a scenario, some automated script should translate the flow equations into code in order

to avoid mistakes and to save a tremendous amount of time. In the following Chap. 6, we develop a method that uses the vertex functions from a PFFRG analysis for the computation of effective free spinon models for the considered systems. This method is based on a FRG enhanced Fock mean-field equation and self-consistently determines spinon hopping and pairing amplitudes which follow from Xiao-Gang Wen's projective symmetry group considerations [182]. In this way, we hope to acquire fundamental knowledge about the properties of the possibly realised spin liquid states such as their spinon band structure and their stability against the in a PSG classification neglected gauge fluctuations.

6. Characterisation of quantum spin liquids and their spinon band structure via functional renormalisation

In the previous chapters, we have developed methods of implementing the PFFRG formalism for various types of spin interactions on different lattices. The key motivation to this was always the identification of possible spin liquid phases which were recognised by their lack of long-range order. Even though this particular method has proven itself to be an in general well-behaved tool for identifying the phase boundaries between different magnetically ordered and paramagnetic systems for plenty of Hamiltonians, this method is not capable of providing insight into some of physically most relevant properties like excitation spectra, exchange statistics, and topology of the realised state. Instead, it yields imaginary-timed static spin susceptibilities which show resemblance of experimentally obtained neutron-scattering structure factors which are *per se* real-timed entities corresponding to, *e.g.*, the excitation of two spinons at finite frequency.

On the other hand, there is a classification scheme for spin liquids called the projective symmetry group (PSG) developed by X. G. Wen, see Ref. [182]. This method is based on the same Abrikosov decomposition of spin operators into fermions as the PFFRG and identifies the possible spin liquid states that obey all symmetries of lattice and Hamiltonian. The PSG yields effective low-energy theories by providing certain hopping and pairing patterns for spinons on the corresponding lattice which can then be, for instance, compared by a mean-field self-consistency analysis. One downside of a bare mean-field treatment though is that it neglects most contributions from quantum fluctuations and might therefore miss important details of the considered model like spinon-spinon interactions and vison excitations, see Sec. 6.2 for details.

In this chapter, we develop a technique connecting these two pseudo-fermion perspectives by including quantum fluctuations into a PSG mean-field analysis via an insertion of renormalised vertex functions into the self-consistency equations. Such an approach of coalesced FRG mean-field study has so far only been considered for the two-dimensional Hubbard model [143, 179] which is why we try to be thorough in this part of the thesis for the sake of reproducibility. We do not perform any spin liquid classification using the PSG but instead take their results for the considered J_1-J_2 square lattice [182] and the nearest-neighbour kagome lattice [111] Heisenberg models from the existing literature. But before we explain the details of our new method and, at least, introduce the concept of the PSG, we start with laying a solid mathematical foundation for all further considerations.

6.1. Preliminaries

This section is dedicated to the derivation of a mean-field decoupling for Heisenberg Hamiltonians. Even though the finial results can be found in many standard textbooks and well-known publications, we want to extend this theory in Sec. 6.4 by incorporating renormalised Green's and vertex functions. Since the two-particle vertices that follow from a PFFRG analysis are more spread-out in real space as compared to the bare Heisenberg interactions and they additionally are also depending on frequency, our main focus lies on obtaining the correct structures in real space and imaginary time for our self-consistency

equations. Initially, this might appear somewhat unnecessary to the more advanced reader. Some aspects of the basic computations become quite relevant though in the following and, since they are often elegantly neglected, this seems like an appropriate place to define and derive all constituents of our further investigations properly.

6.1.1. Preface to non-interacting fermionic system

We shall start with a non-interacting Hamiltonian H_0 that is diagonal in some fermionic creation and annihilation operators $f_l^\dagger$ and f_l with a set of quantum numbers denoted by l

$$H_0 = \sum_l \omega_l \, f_l^\dagger f_l \,, \tag{6.1}$$

where the single-particle energy is ω_l. In the imaginary-time Heisenberg picture, the time evolution of our operators is determined by the Heisenberg differential equation

$$\begin{aligned}
\frac{\partial}{\partial\tau} f_l(\tau) &= \Big[H_0, f_l\Big]_- \\
&= \sum_k \Big\{\omega_k \, f_k^\dagger f_k f_l - \omega_k \, f_l f_k^\dagger f_k\Big\} \\
&= \sum_k \Big\{\omega_k \, f_k^\dagger f_k f_l - \omega_k \, \Big(\delta_{kl} - f_k^\dagger f_l\Big) \, f_k\Big\} = -\omega_l f_l \,, \qquad (6.2a) \\
\frac{\partial}{\partial\tau} f_l^\dagger(\tau) &= \Big[H_0, f_l^\dagger\Big]_- \\
&= \sum_k \Big\{\omega_k \, f_k^\dagger f_k f_l^\dagger - \omega_k \, f_l^\dagger f_k^\dagger f_k\Big\} \\
&= \sum_k \Big\{\omega_k \, f_k^\dagger f_k f_l^\dagger + \omega_k \, f_k^\dagger \Big(\delta_{kl} - f_k f_l^\dagger\Big)\Big\} = +\omega_l f_l^\dagger \,, \qquad (6.2b)
\end{aligned}$$

where the brackets $[A, B]_- = AB - BA$ denote a standard commutator. Note that different signs appear for creation and annihilation operator. This is the reason why the well-known time evolution

$$f_l(\tau) = e^{-\omega_l \tau} f_l \qquad \text{and} \qquad f_l^\dagger(\tau) = e^{\omega_l \tau} f_l^\dagger \tag{6.3}$$

should be used which implies that $f_l^\dagger(\tau) \neq [f_l(\tau)]^\dagger$.

Let us now trace the effect of this different time evolutions during the calculation of a normal Green's function, *i.e.*, the expectation value of equal numbers of fermionic creation and annihilation operators (cf. Sec. 2.1.2). Even though one can employ standard notations for them, a clear definition is imperative for extending our language towards so-called anomalous Green's functions which do not conserve particle number in the following.

6.1.2. Normal Green's function

Here, we provide the known facts about the non-interacting system for $H_0 = 0$. In our systems of interest, as in the previous chapters, the full set of quantum numbers for any

fermionic operator is labeled by a lattice site i, a spin index $\alpha \in \{\uparrow, \downarrow\}$, and an imaginary time τ. The bare, imaginary-time-ordered Green's function from Eq. (2.24) is then given by

$$G^0_{\alpha\beta}(i,\tau|j,\tau') = \left\langle T_\tau f_\alpha(i,\tau) f^\dagger_\beta(j,\tau') \right\rangle_0 , \tag{6.4}$$

where $\langle \dots \rangle_0$ denotes that the average is taken with respect to H_0. Please note once more that our convention for the fermionic single-particle propagators differs by a factor of -1 from another possible definition which is also frequently used, see Sec. 2.1.2. As explained above, if $H_0 \neq 0$, one obtains a time evolution of the fermionic creation and annihilation operators $f_\alpha(i,\tau) = e^{-\omega_{i,\alpha}\tau} f_\alpha(i,0) = e^{-\omega_{i,\alpha}\tau} f_{i,\alpha}$ and $f^\dagger_\alpha(i,\tau) = e^{\omega_{i,\alpha}\tau} f^\dagger_\alpha(i,0) = e^{\omega_{i,\alpha}\tau} f^\dagger_{i,\alpha}$. For our scenario with no single-particle energies, we have to send $\omega_{i,\alpha} \to 0$ for all i and α. This step will be performed in the end of our calculation in order to keep track of the correct frequency structure. For the regular Green's function, we thus find

$$\begin{aligned} G^0_{\alpha\beta}(i,\tau|j,\tau') &= \left\langle T_\tau f_\alpha(i,\tau) f^\dagger_\beta(j,\tau') \right\rangle_0 \\ &= \theta(\tau-\tau') \left\langle f_\alpha(i,\tau) f^\dagger_\beta(j,\tau') \right\rangle_0 - \theta(\tau'-\tau) \left\langle f^\dagger_\beta(j,\tau') f_\alpha(i,\tau) \right\rangle_0 \\ &= \theta(\tau-\tau') \left\langle e^{\omega_{j,\beta}\tau' - \omega_{i,\alpha}\tau} f_{i,\alpha} f^\dagger_{j,\beta} \right\rangle_0 - \theta(\tau'-\tau) \left\langle e^{\omega_{j,\beta}\tau' - \omega_{i,\alpha}\tau} f^\dagger_{j,\beta} f_{i,\alpha} \right\rangle_0 . \end{aligned} \tag{6.5}$$

Considering the fact that all the frequencies vanish and that, in the non-interacting scenario, the system is in a product state of the decoupled states on all individual lattice sites i, *e.g.*, $|0,0\rangle_i$, $|0,1\rangle_i$, $|1,0\rangle_i$, and $|1,1\rangle_i$ [see Eq. (4.3)], we easily verify that

$$\begin{aligned} G^0_{\alpha\beta}(i,\tau|j,\tau') &= \theta(\tau-\tau') \left\langle f_{i,\alpha} f^\dagger_{j,\beta} \right\rangle_0 - \theta(\tau'-\tau) \left\langle f^\dagger_{j,\beta} f_{i,\alpha} \right\rangle_0 \\ &= \theta(\tau-\tau') \left\langle f_{i,\alpha} f^\dagger_{i,\alpha} \right\rangle_0 \delta_{\alpha\beta}\delta_{ij} - \theta(\tau'-\tau) \left\langle f^\dagger_{i,\alpha} f_{i,\alpha} \right\rangle_0 \delta_{\alpha\beta}\delta_{ij} \\ &= \theta(\tau-\tau') \frac{1}{2} \delta_{\alpha\beta}\delta_{ij} - \theta(\tau'-\tau) \frac{1}{2} \delta_{\alpha\beta}\delta_{ij} . \end{aligned} \tag{6.6}$$

This proves that G^0 only depends on the difference of the two imaginary-time arguments $\tau - \tau'$ as it is required for a time-translation invariant system.

Now, we want to transform this result into the fermionic Matsubara space with $\omega_n = \frac{(2n+1)\pi}{\beta}$

$$\begin{aligned} G^0_{\alpha\beta}(i,j|i\omega_n) &= \int_0^\beta \mathrm{d}\tau \, e^{i\omega_n\tau} G^0_{\alpha\beta}(i,\tau|j,0) = \int_0^\beta \mathrm{d}\tau \, e^{i\omega_n\tau} \frac{1}{2} \delta_{\alpha\beta}\delta_{ij} \\ &= \frac{1}{i\omega_n} \left(e^{i\pi} - e^0 \right) \frac{1}{2} \delta_{\alpha\beta}\delta_{ij} \\ &= -\frac{1}{i\omega_n} \delta_{\alpha\beta}\delta_{ij} . \end{aligned} \tag{6.7}$$

We utilised this result already plenty of times before. It should, however, be noted that the Fourier transform was effectively performed with respect to the time argument of $f_{i,\alpha}$. Going back to the description with two time arguments, we have to define that

$$f_\alpha(i,i\omega_n) = \int_0^\beta \mathrm{d}\tau\, e^{i\omega_n\tau} f_\alpha(i,\tau)\,, \qquad f_\alpha(i,\tau) = \frac{1}{\beta}\sum_n e^{-i\omega_n\tau} f_\alpha(i,i\omega_n)\,, \tag{6.8a}$$

$$f^\dagger_\alpha(i,i\omega_n) = \int_0^\beta \mathrm{d}\tau\, e^{-i\omega_n\tau} f^\dagger_\alpha(i,\tau)\,, \qquad f^\dagger_\alpha(i,\tau) = \frac{1}{\beta}\sum_n e^{i\omega_n\tau} f^\dagger_\alpha(i,i\omega_n)\,, \tag{6.8b}$$

where again the phase factors for creation and annihilation operators have opposite signs. For our normal propagator, this implies

$$\begin{aligned} G^0_{\alpha\beta}(i,i\omega_n|j,i\omega_m) &= \int_0^\beta \mathrm{d}\tau \int_0^\beta \mathrm{d}\tau'\, e^{i\omega_n\tau} e^{-i\omega_m\tau'} G^0_{\alpha\beta}(i,\tau-\tau'|j,0) \\ &= \int_0^\beta \mathrm{d}\tau \int_0^\beta \mathrm{d}\tau'\, e^{i\omega_n\tau} e^{-i\omega_m\tau'} \frac{1}{\beta}\sum_l e^{-i\omega_l(\tau-\tau')} G^0_{\alpha\beta}(i,j|\omega_l) \\ &= \beta\, G^0_{\alpha\beta}(i,j|i\omega_n)\delta_{nm}\,, \end{aligned} \tag{6.9}$$

where $G^0_{\alpha\beta}(i,j|i\omega_n)$ is given in Eq. (6.7). This summarises the known properties of our normal Green's functions. We can hence continue by applying the same thoughts to anomalous propagators which do not preserve our system's particle number.

6.1.3. Propagators in Nambu space

Not only in solid-state physics, there is a strong correspondence between particles and holes which can often be considered as dual perspectives for describing the same concepts. In phases with particle-number conservation, it is sufficient to consider only one of these two possible points of view. Both of them yield identical results. However, we try to characterise quantum spin liquids (QSLs) which might be related to superconductors as argued in Chap. 1. For these systems, particle number is in general not conserved due to the creation of spinon pairs or Cooper pairs, respectively. This requires an analysis in a combined representation of particle and hole channels coupling via pairing terms. In the language of propagators, this can be achieved by introducing the so-called *Nambu space* [134]. The Nambu spinors are defined as

$$a_i(\tau) = \begin{pmatrix} f_{i\uparrow}(\tau) \\ f^\dagger_{i\downarrow}(\tau) \end{pmatrix}, \qquad a^\dagger_i(\tau) = \begin{pmatrix} f^\dagger_{i\uparrow}(\tau)\ ,\ f_{i\downarrow}(\tau) \end{pmatrix}. \tag{6.10}$$

They are used to construct a matrix Green's function via their imaginary-time-ordered expectation value

$$\mathbb{G}(i,\tau|j,\tau') = \left\langle T_\tau a_i(\tau) a_j^\dagger(\tau') \right\rangle = \begin{pmatrix} \left\langle T_\tau f_{i\uparrow}(\tau) f_{j\uparrow}^\dagger(\tau') \right\rangle & \left\langle T_\tau f_{i\uparrow}(\tau) f_{j\downarrow}(\tau') \right\rangle \\ \left\langle T_\tau f_{i\downarrow}^\dagger(\tau) f_{j\uparrow}^\dagger(\tau') \right\rangle & \left\langle T_\tau f_{i\downarrow}^\dagger(\tau) f_{j\downarrow}(\tau') \right\rangle \end{pmatrix} . \tag{6.11}$$

In this representation, the propagators for particles $\langle f f^\dagger \rangle$ and holes $\langle f^\dagger f \rangle$ couple to each other via the pairing amplitudes $\langle f f \rangle$ and $\langle f^\dagger f^\dagger \rangle$ which vanish in phases with conserved particle number. We can identify the above matrix elements in accordance to the last section as

$$G_{\uparrow\uparrow}(i,\tau|j,\tau') = \left\langle T_\tau f_{i\uparrow}(\tau) f_{j\uparrow}^\dagger(\tau') \right\rangle , \tag{6.12a}$$

$$F_{\uparrow\downarrow}(i,\tau|j,\tau') = \left\langle T_\tau f_{i\uparrow}(\tau) f_{j\downarrow}(\tau') \right\rangle . \tag{6.12b}$$

Here, G is the normal Green's function whereas F is named anomalous Green's function or propagator. We will now derive some important relations for the anomalous off-diagonal elements of $\mathbb{G}$ and define their appropriate Matsubara transforms for completeness.

The following calculations are performed in equilibrium. Hence, all functions only depend on the differences of the appearing imaginary-time arguments. In the Heisenberg and the interaction picture ($H_0 = 0$), operators evolve in time as

$$f_{i\alpha}^{(\dagger)}(\tau) = e^{H\tau} f_{i\alpha}^{(\dagger)} e^{-H\tau} , \tag{6.13}$$

which directly implies that

$$\left(f_{i\alpha}(\tau)\right)^\dagger = f_{i\alpha}^\dagger(-\tau) . \tag{6.14}$$

Using Eq. (6.14), we can derive for the second off-diagonal term in Eq. (6.11) that

$$\begin{aligned} \left\langle T_\tau f_{i\downarrow}^\dagger(\tau) f_{j\uparrow}^\dagger(\tau') \right\rangle &= \theta(\tau-\tau') \left\langle f_{i\downarrow}^\dagger(\tau) f_{j\uparrow}^\dagger(\tau') \right\rangle - \theta(\tau'-\tau) \left\langle f_{j\uparrow}^\dagger(\tau') f_{i\downarrow}^\dagger(\tau) \right\rangle \\ &= \theta(\tau-\tau') \left\langle f_{j\uparrow}(-\tau') f_{i\downarrow}(-\tau) \right\rangle^\dagger - \theta(\tau'-\tau) \left\langle f_{i\downarrow}(-\tau) f_{j\uparrow}(-\tau') \right\rangle^\dagger \\ &= \left\langle T_\tau f_{j\uparrow}(-\tau') f_{i\downarrow}(-\tau) \right\rangle^\dagger = - \left\langle T_\tau f_{i\downarrow}(-\tau) f_{j\uparrow}(-\tau') \right\rangle^\dagger \\ &= -F_{\downarrow\uparrow}^\dagger(i,-\tau|j,-\tau') = F_{\uparrow\downarrow}^\dagger(i,-\tau|j,-\tau') \\ &= F_{\uparrow\downarrow}^\dagger(i,\tau'|j,\tau) , \end{aligned} \tag{6.15}$$

where we utilised the appropriate spin-rotation (around the x or y axis) in the second to last line (see App. E.2) and time-translation invariance in the last one. For the other normal Green's function, we find

$$\begin{aligned} \left\langle T_\tau f_{i\downarrow}^\dagger(\tau) f_{j\downarrow}(\tau') \right\rangle &= - \left\langle T_\tau f_{j\downarrow}(\tau') f_{i\downarrow}^\dagger(\tau) \right\rangle \\ &= -G_{\downarrow\downarrow}(j,\tau'|i,\tau) = -G_{\uparrow\uparrow}(j,\tau'|i,\tau) . \end{aligned} \tag{6.16}$$

Again, a proper spin rotation was used. In this way, we showed that

$$\mathbb{G}(i,\tau|j,\tau') = \begin{pmatrix} G_{ij}(\tau|\tau') & F_{ij}(\tau|\tau') \\ F^{\dagger}_{ij}(\tau'|\tau) & -G_{ji}(\tau'|\tau) \end{pmatrix} . \tag{6.17}$$

We dropped the spin index since it should be clear from the respective definitions.

In Matsubara space, the previously derived relations still hold for the normal Green's functions and especially also Eq. (6.9) translates to

$$G_{ij}(i\omega_n|i\omega_m) = \beta\, G_{ij}(i\omega_n)\delta_{nm} \tag{6.18}$$

for the full propagator. However, for the anomalous Green's function, the situation is quite different. Similar thoughts to the previous ones imply for them that

$$\begin{aligned} F_{ij}(i\omega_n|i\omega_m) &= \int_0^\beta \mathrm{d}\tau \int_0^\beta \mathrm{d}\tau'\, e^{-i\omega_n\tau} e^{-i\omega_m\tau'} F_{ij}(\tau|\tau') \\ &= \int_0^\beta \mathrm{d}\tau \int_0^\beta \mathrm{d}\tau'\, e^{-i\omega_n(\tau-\tau')} e^{-i(\omega_m+\omega_n)\tau'} F_{ij}(\tau-\tau'|0) \\ &= \beta\, F_{ij}(i\omega_n)\delta_{n-m}\,, \end{aligned} \tag{6.19a}$$

$$\begin{aligned} F^{\dagger}_{ij}(i\omega_n|i\omega_m) &= \int_0^\beta \mathrm{d}\tau \int_0^\beta \mathrm{d}\tau'\, e^{i\omega_n\tau} e^{i\omega_m\tau'} F^{\dagger}_{ij}(\tau|\tau') \\ &= \int_0^\beta \mathrm{d}\tau \int_0^\beta \mathrm{d}\tau'\, e^{i\omega_n(\tau-\tau')} e^{i(\omega_m+\omega_n)\tau'} F^{\dagger}_{ij}(\tau-\tau'|0) \\ &= \beta\, F^{\dagger}_{ij}(i\omega_n)\delta_{n-m}\,. \end{aligned} \tag{6.19b}$$

This sets the framework for everything forthcoming. In the next section, we will show how to decouple our Hamiltonian in a mean-field manner for further evaluation.

6.1.4. Mean-field Hamiltonian

A mean-field decoupling of an interacting Hamiltonian amounts to the neglection of certain quantum fluctuations. For spin systems, such an approximation is typically justified if the spins interact with many of their neighbours in which case the fluctuating fields of all individual neighbouring spins can be averaged to their combined *mean field*. In this way, the spin degrees of freedom decouple and a solution can usually be obtained from a self-consistency equation. The mean-field approach of our following analysis yields effectively free and spinful particles with finite hopping and pairing amplitudes on particular bonds, *i.e.*, spinon hoppings and pairings.

Even though the results of this section are well known [12], we want to explicitly present the derivation of the mean-field Hamiltonian being utilised by Xiao-Gang Wen [182] and Yuan-Ming Lu [111] for a PSG analysis of possible spin liquid states on the square and the kagome lattice, respectively. Since our new theory is based on the same decoupling scheme and we have to include the additional density-density interaction channel from FRG later on, a solid foundation is indispensable in this regard.

We again replace the spin operators with the usual Abrikosov fermions [see Eq. (1.2) or (4.2)] which goes hand in hand with an enlargement of the Hilbert space into a physical and an unphysical sector (confer Sec. 4.2.1). It is worth mentioning at this point that the Abrikosov decomposition of a single spin operator into two fermionic operators directly corresponds to the fractionalisation of spin-1 excitations into spin-$\frac{1}{2}$ spinons, see Chap. 1 for details. Indeed, one could actually refer to the new operators as spinon operators because they create or annihilate spinons. A Heisenberg Hamiltonian can be rewritten in terms of the spinon operators as

$$\begin{aligned} H &= \sum_{(i,j)} J_{ij} \boldsymbol{S}_i \cdot \boldsymbol{S}_j = \sum_{i,j} \sum_{\alpha,\beta,\gamma,\delta} \sum_{\mu} \frac{J_{ij}}{8} f^\dagger_{i\alpha} \sigma^\mu_{\alpha\beta} f_{i\beta} f^\dagger_{j\gamma} \sigma^\mu_{\gamma\delta} f_{j\delta} \\ &= \sum_{i,j} \sum_{\alpha,\beta,\gamma,\delta} \frac{J_{ij}}{8} f^\dagger_{i\alpha} f_{i\beta} f^\dagger_{j\gamma} f_{j\delta} \left(2\delta_{\alpha\delta}\delta_{\beta\gamma} - \delta_{\alpha\beta}\delta_{\gamma\delta}\right) \\ &= \sum_{i,j} \sum_{\alpha,\beta} -\frac{J_{ij}}{4} \left(f^\dagger_{i\alpha} f_{j\alpha} f^\dagger_{j\beta} f_{i\beta} + \frac{1}{2} f^\dagger_{i\alpha} f_{i\alpha} f^\dagger_{j\beta} f_{j\beta} \right) + \text{const.}\,, \end{aligned} \tag{6.20}$$

where the sum over site pairs (i,j) was transformed into a sum over lattice sites i and j yielding a factor of $\frac{1}{2}$. The constant term in the last line is purely quadratic in the fermionic operators and only amounts to a shift of the considered system's zero energy at least in the physical Hilbert space. Hence, this term has no physical consequences and we neglect it in the following. We now perform our mean-field decoupling according to

$$\eta_{ij}\epsilon_{\alpha\beta} = -2\Big\langle f_{i\alpha} f_{j\beta} \Big\rangle\,, \qquad \eta_{ij} = \eta_{ji}\,, \tag{6.21a}$$

$$\eta^\dagger_{ij}\epsilon_{\alpha\beta} = -2\Big\langle f^\dagger_{j\beta} f^\dagger_{i\alpha} \Big\rangle\,, \qquad \eta^\dagger_{ij} = \eta^\dagger_{ji}\,, \tag{6.21b}$$

$$\chi_{ij}\delta_{\alpha\beta} = 2\Big\langle f^\dagger_{i\alpha} f_{j\beta} \Big\rangle\,, \qquad \chi_{ij} = \chi^\dagger_{ji}\,, \tag{6.21c}$$

$$\chi^\dagger_{ij}\delta_{\alpha\beta} = 2\Big\langle f^\dagger_{j\beta} f_{i\alpha} \Big\rangle\,, \qquad \chi^\dagger_{ij} = \chi_{ji}\,. \tag{6.21d}$$

The completely antisymmetric tensor is defined via $\epsilon_{\uparrow\downarrow} = -\epsilon_{\downarrow\uparrow} = 1$ and $\epsilon_{\uparrow\uparrow} = \epsilon_{\downarrow\downarrow} = 0$. Keeping in mind that $F^{(\dagger)}_{ji}(\tau'|\tau) = F^{(\dagger)}_{ij}(\tau|\tau') = F^{(\dagger)}_{ij}(\tau-\tau'|0)$ and $G^\dagger_{ji}(\tau|\tau') = G^\dagger_{ji}(-\tau'|-\tau)$ $= G_{ij}(\tau|\tau') = G_{ij}(\tau-\tau'|0)$, for our later derivations, we already note here that this substitution can be rewritten as

$$\eta_{ij} = -\lim_{\lambda\to 0} 2F_{ij}(0|\lambda)\,, \qquad \eta^\dagger_{ij} = -\lim_{\lambda\to 0} 2F^\dagger_{ij}(0|\lambda)\,, \tag{6.22a}$$

$$\chi_{ij} = -\lim_{\lambda\to 0} 2G_{ji}(0|\lambda)\,, \qquad \chi^\dagger_{ij} = -\lim_{\lambda\to 0} 2G_{ij}(0|\lambda)\,. \tag{6.22b}$$

Now, we replace the Hamiltonian with its mean-field version by contracting all four possible non-local amplitudes of each of the two terms in Eq. (6.20).

$$\begin{aligned}
H_{\mathrm{MF}} &= \sum_{i,j}\sum_{\alpha,\beta} -\frac{J_{ij}}{4}\Big(\frac{1}{2}\chi_{ij}f^\dagger_{j\beta}f_{i\beta}\delta_{\alpha\alpha} + \frac{1}{2}\chi_{ji}f^\dagger_{i\alpha}f_{j\alpha}\delta_{\beta\beta} + \frac{1}{2}\eta^\dagger_{ji}f_{j\alpha}f_{i\beta}\epsilon_{\beta\alpha} + \frac{1}{2}\eta_{ji}f^\dagger_{i\alpha}f^\dagger_{j\beta}\epsilon_{\alpha\beta} \\
&\qquad + \frac{1}{4}\chi_{ij}f_{i\alpha}f^\dagger_{j\beta}\delta_{\alpha\beta} + \frac{1}{4}\chi_{ji}f_{j\beta}f^\dagger_{i\alpha}\delta_{\alpha\beta} + \frac{1}{4}\eta^\dagger_{ji}f_{i\alpha}f_{j\beta}\epsilon_{\beta\alpha} + \frac{1}{4}\eta_{ij}f^\dagger_{i\alpha}f^\dagger_{j\beta}\epsilon_{\alpha\beta}\Big) \\
&= \sum_{i,j}\sum_{\alpha} -\frac{J_{ij}}{4}\Big(\chi_{ij}f^\dagger_{j\alpha}f_{i\alpha} + \chi^\dagger_{ij}f^\dagger_{i\alpha}f_{j\alpha} + \frac{1}{4}\chi_{ij}f_{i\alpha}f^\dagger_{j\alpha} + \frac{1}{4}\chi^\dagger_{ij}f_{j\alpha}f^\dagger_{i\alpha} \\
&\quad + \sum_{\beta}\epsilon_{\alpha\beta}\left[\frac{1}{2}\eta^\dagger_{ij}f_{i\beta}f_{j\alpha} + \frac{1}{2}\eta_{ij}f^\dagger_{i\alpha}f^\dagger_{j\beta} + \frac{1}{4}\eta^\dagger_{ij}f_{i\beta}f_{j\alpha} + \frac{1}{4}\eta_{ij}f^\dagger_{i\alpha}f^\dagger_{j\beta}\right]\Big) \\
&= \sum_{i,j}\sum_{\alpha} -\frac{3}{16}J_{ij}\left(\chi_{ij}f^\dagger_{j\alpha}f_{i\alpha} + \chi^\dagger_{ij}f^\dagger_{i\alpha}f_{j\alpha} + \sum_{\beta}\epsilon_{\alpha\beta}\left[\eta^\dagger_{ij}f_{i\beta}f_{j\alpha} + \eta_{ij}f^\dagger_{i\alpha}f^\dagger_{j\beta}\right]\right) \\
&= \sum_{i,j} -\frac{3}{16}J_{ij}\Big(\chi_{ij}f^\dagger_{j\uparrow}f_{i\uparrow} + \chi^\dagger_{ij}f^\dagger_{i\uparrow}f_{j\uparrow} + \chi_{ij}f^\dagger_{j\downarrow}f_{i\downarrow} + \chi^\dagger_{ij}f^\dagger_{i\downarrow}f_{j\downarrow} \\
&\qquad + \eta^\dagger_{ij}f_{j\downarrow}f_{i\uparrow} + \eta_{ij}f^\dagger_{i\uparrow}f^\dagger_{j\downarrow} + \eta^\dagger_{ij}f_{i\downarrow}f_{j\uparrow} + \eta_{ij}f^\dagger_{j\uparrow}f^\dagger_{i\downarrow}\Big)
\end{aligned} \tag{6.23}$$

In the second and in the last step, we used that $J_{ij} = J_{ji}$ which always holds for Heisenberg interactions. In order to rewrite H_{MF} in terms of the Nambu spinors a_i and $a_i^\dagger$ from Eq. (6.10), we note that

$$\sum_{i,j} a^\dagger_i \begin{pmatrix} U^{11}_{ij} & U^{12}_{ij} \\ U^{21}_{ij} & U^{22}_{ij} \end{pmatrix} a_j = \sum_{i,j} U^{11}_{ij} f^\dagger_{i\uparrow}f_{j\uparrow} + U^{12}_{ij} f^\dagger_{i\uparrow}f^\dagger_{j\downarrow} + U^{21}_{ij} f_{i\downarrow}f_{j\uparrow} + U^{22}_{ij} f_{i\downarrow}f^\dagger_{j\downarrow}\,. \tag{6.24}$$

Comparing the coefficients of the last two equations, we derive the final form of our Hamiltonian

$$H_{\mathrm{MF}} = \sum_{i,j} -\frac{3}{16}J_{ij}\left[a^\dagger_i \begin{pmatrix} \chi^\dagger_{ij} & \eta_{ij} \\ \eta^\dagger_{ij} & -\chi_{ij} \end{pmatrix} a_j + a^\dagger_j \begin{pmatrix} \chi_{ij} & \eta_{ij} \\ \eta^\dagger_{ij} & -\chi^\dagger_{ij} \end{pmatrix} a_i\right], \tag{6.25}$$

which is hermitian as expected. Employing the so-called Fock approximation, we are ready to explore its implications for the Dyson-Schwinger equations of the matrix Green's function. Before further pursuing this issue in Sec. 6.3, we introduce the concept behind Xiao-Gang Wen's projective symmetry group in the following. This classification scheme for spin liquids provides the necessary mean-field ansätze for the real-space patterns of the χ_{ij} and η_{ij} in Nambu space which are the basis of our upcoming investigations.

6.2. Gauge fluctuations and projective symmetries

Most of the following work relies on the fundamental articles by Xiao-Gang Wen [182] for the square lattice and by Yuan-Ming Lu [111] for the kagome lattice. Even though there are no novel results derived from the projective symmetry group scheme in this thesis, we at least present a brief introduction for the reader to be able to grasp the important concepts behind this method. Furthermore, we also provide a coherent characterisation of all gauge-inequivalent nearest-neighbour $\mathbb{Z}_2$ spin liquids on the square and kagome lattices with great help from Yasir Iqbal and Jonas Sonnenschein.

In the decoupled form of Eq. (6.25), the mean-field Hamiltonian denotes an effective low-energy theory for our system with hopping and pairing amplitudes between spins at different sites, *e.g.*, χ_{ij} (η_{ij}) is a so-called spinon hopping (spinon singlet-pairing) term. The Abrikosov representation from Eqs. (1.2) or (4.2) expresses the local spin operators in terms of pseudo fermions. These fermions can be associated with creation and annihilation operators for spinons as explained in the previous section. We have already notoriously repeated that this decomposition augments the Hilbert space by two unphysical states per site (cf. Sec. 4.2.1). At this point, the Nambu space comes in quite handy because here any type of time-dependent and local $SU(2)$ rotation

$$a_i(\tau) \longrightarrow W_i(\tau) a_i(\tau)\,, \qquad\qquad a_i^\dagger(\tau) \longrightarrow a_i^\dagger(\tau) W_i^\dagger(\tau) \tag{6.26}$$

leaves the physical subspace invariant. Such transformations correspond to local gauge degrees of freedom and can have no effect on physical observables as long as the computation is carried out correctly, see App. E.1 for details. Here, all $W_i(\tau)$ are $SU(2)$ matrices with

$$W_i(\tau) = \alpha_{i\,0}(\tau)\mathbb{1} + i\left[\alpha_{i\,x}(\tau)\sigma^x + \alpha_{i\,y}(\tau)\sigma^y + \alpha_{i\,z}(\tau)\sigma^z\right]\,, \tag{6.27a}$$

$$1 = \sqrt{\left(\alpha_{i\,0}(\tau)\right)^2 + \left(\alpha_{i\,x}(\tau)\right)^2 + \left(\alpha_{i\,y}(\tau)\right)^2 + \left(\alpha_{i\,z}(\tau)\right)^2}\,, \tag{6.27b}$$

where $\mathbb{1}$ denotes a 2×2 unit matrix, the σ^μ with $\mu \in \{x,\, y,\, z\}$ are the standard Pauli matrices, and the prefactors $\alpha_i \in \mathbb{R}$ such that

$$W_i^\dagger(\tau) W_i(\tau) = \mathbb{1}\,, \tag{6.28a}$$

$$\det W_i(\tau) = 1\,. \tag{6.28b}$$

For compatibility to the notation used in the standard literature of the topic, we rewrite Eq. (6.25) once more into

$$H_{\mathrm{MF}} = \sum_{(i,j)} a_i^\dagger u_{ij} a_j\,, \tag{6.29a}$$

$$u_{ij} = -\frac{3}{4} J_{ij} \begin{pmatrix} \chi_{ij}^\dagger & \eta_{ij} \\ \eta_{ij}^\dagger & -\chi_{ij} \end{pmatrix}\,, \tag{6.29b}$$

where we utilised the symmetry relations $\chi_{ij}^\dagger = \chi_{ji}$ and $\eta_{ij} = \eta_{ji}$ as well as the common notation of a sum over pairs of sites [denoted by (i,j)] in order to obtain the correct prefactor for the matrix u_{ij}.

Unlike the original Heisenberg Hamiltonian of our model from Eq. (6.20), this non-interacting mean-field Hamiltonian is not invariant under local $SU(2)$ transformations if the amplitudes χ and η are treated as constants (confer App. E.1). In comparison to the mean-field approach from Eqs. (6.29), a Hubbard-Stratonovich transformation would treat the hopping and pairing amplitudes as locally and temporally fluctuating quantities. In this case, the matrix from Eq. (6.29b) would transform under Eqs. (6.26) as $u_{ij}(\tau) \longrightarrow W_i(\tau)\, u_{ij}\,(\tau) W_j^\dagger(\tau)$. This implies that the Hamiltonian in Eq. (6.29a) would, like the original spin Hamiltonian, not depend on the specific choice of local gauges. Therefore, the Hubbard-Stratonovich transform is mathematically exact and also as challenging as solving the precise interacting model from the start. Nevertheless, we proceed with the initially quite ambiguous assumption of constant u_{ij}. If the solutions obtained from our simplified approach are then robust with respect to local gauge fluctuations, they are expected to describe the effective low-energy theory of the considered system well. We will discuss when this is the case in Sec. 6.2.2.

6.2.1. Projective Symmetry Group

In the current mean-field representation, the physical properties of our system are only characterised by the hopping and pairing amplitudes χ_{ij} and η_{ij}. Our effective low-energy Hamiltonian [Eq. (6.29a)] transforms under local, but now time-independent gauge transformations as

$$H_{\mathrm{MF}} \longrightarrow \sum_{(i,j)} a_i^\dagger W_i^\dagger\, u_{ij}\, W_j a_j\,. \tag{6.30}$$

Hence, every transformation of the type $u_{ij} \longrightarrow W_i\, u_{ij}\, W_j^\dagger$ that is acting on a considered mean-field state should leave the physical state of our original quantum spin model invariant after a so-called Gutzwiller projection [62, 63] onto the appropriate one-particle-per-site subspace.

Apart from local gauge transformations, there are of course other invariances which a projected state has to obey, namely, the system's physical (anti)symmetries (denoted by S), *e.g.*, lattice translations, rotations, mirror symmetries, and time reversal. If we would operate within the physical sector of the Hilbert space only, each of these transformations would have to leave the matrices $S(u_{ij}) \equiv u_{ij}$ unaltered. In our case however, every real symmetry can only be defined up to a local gauge transformation $S(u_{ij}) \equiv W_i u_{ij} W_j^\dagger$. Therefore, one defines a projective symmetry as the composition of a physical symmetry and its associated local gauge transformation that leaves all matrices u_{ij} unchanged. Since S and the set of all local gauge transformations are groups, the projective symmetries likewise form a group. At a first glance, this seems to aggravate calculations even further, but one can classify all possible Gutzwiller-projected states that can result from our mean-

field treatment of a system with given symmetry operations by determining all its distinct groups of allowed projective symmetries. A projective symmetry group (PSG) classification is then based on two important concepts which are the invariant gauge group (IGG) and symmetry relations.

The IGG consists of those (global) gauge transformations being associated with the identity operation which is also a legitimate symmetry in S. Hence, the IGG is given by a group of matrices G that fulfills $W_i u_{ij} W_j^\dagger = u_{ij} \quad \forall \quad i, j$ with $W_i \in G$. If one denotes a PSG with P and its respective symmetry group (IGG) by S (G), the symmetry group can formally be expressed as the quotient of PSG with IGG

$$S = P/G\,. \tag{6.31}$$

In practice, the $W_i \in G$ can depend on the site index but once one of them is fixed, the others follow automatically from $W_i u_{ij} W_j^\dagger = u_{ij}$. Depending on the precise structure of the u_{ij}, the IGG can either be $\{-\mathbb{1}, \mathbb{1}\}$ for $\mathbb{Z}_2$ spin liquids, $e^{i\theta \boldsymbol{n}\boldsymbol{\sigma}}$ with $\boldsymbol{n}$ being a fixed but possibly site-dependent unit vector, $\boldsymbol{\sigma} = (\sigma^x, \sigma^y, \sigma^z)^T$ and $\theta \in [0, 2\pi)$ for $U(1)$ spin liquids, or an arbitrary $SU(2)$ matrix as defined in Eqs. (6.27) for $SU(2)$ spin liquids. Once the IGG is fixed, one can constrain the effects that two symmetry operations S_1, $S_2 \in S$ have on the u matrices if there is a sequence of them that should map all amplitudes back onto themselves. In the PSG scheme, this sequence then has to be an element of the IGG. Let, for instance, S_1 and S_2 be the mirror symmetries with respect to the coordinate axes on the square lattice. In this case, their symmetry relation could formally be denoted by $S_2^{-1} S_1^{-1} S_2 S_1 \in G$. A PSG classification is finally based on the constraints from all possible relations within the system's symmetry group.

6.2.2. IGG and stability of mean-field ansatz

The IGG is peculiarly important within the PSG classification. The reason for this is its close connection to the aforementioned gauge fluctuations. Without providing rigorous proofs, we try to summarise the general arguments for the IGG's importance along the lines of Ref. [126].

Our bare mean-field Hamiltonian neglects the effects of gauge fluctuations as explained in Sec. 6.2. In this way, the previously interacting Hamiltonian is decoupled and now only consists of free spinons that can propagate throughout the considered lattice. Quite obviously, such a decoupling neglects potentially attractive spinon-spinon interactions which could confine the spinons and thereby render our theory invalid *a posteriori*. In terms of a mathematically exact Hubbard-Stratonovich transformation, those interactions are a part of the gauge fluctuations which are acquired by two[1] spinons along the path of their spatial separation. In addition to the mediated spinon interactions, also flux excitations, the so-called *visons* [163] are neglected in a model without gauge fluctuations. Visons correspond

[1] Spinons have to be created in pairs in the physical system due to the one-particle-per-site constraint.

in our formalism to a local excitation that sends $u_{ij} \to -u_{ij}$ on some bond in the case of $\mathbb{Z}_2$ spin liquids.

There are basically only two possible scenarios now, namely that a mean-field state determined from Eqs. (6.29) with a certain set of matrices u_{ij} is or is not stable upon introducing the neglected gauge fluctuations. It can, however, be shown that particular spin liquid states are stable with respect to gauge fluctuations [126] and the IGG is very important for that purpose. A $\mathbb{Z}_2$ spin liquid has gapped gauge fluctuations which, in principle, can be seen by formally integrating out the spinon degrees of freedom to arrive at an effective theory for the gauge modes [102]. The more hand-waving argument which can also be used is that, if the gauge modes would not be gapped, they would most probably obey a higher degree of symmetry like, *e.g.*, Dirac cones obey Lorentz invariance. So if the gauge fluctuations would not be gapped, and a $\mathbb{Z}_2$ IGG would not be possible any longer because the entire spin system would have to be in a larger symmetry group. If all gauge modes are gapped though, the low-energy effective theory for the spinons is unaffected by them since to some point they occur within that gap. Results being derived from the mean-field Hamiltonian can be interpreted with some confidence in this case. A similar statement also holds for chiral spin liquids which break time-reversal symmetry and can therefore be protected by the now allowed Chern-Simons terms which are also able to gap the gauge fluctuations [185]. On the other hand, stability with respect to the gauge fluctuations seems rather to be an exception for $U(1)$ and $SU(2)$ spin liquids, see Ref. [126] for a discussion.

We therefore focus on $\mathbb{Z}_2$ and chiral spin liquids in our following investigations, but might still detect $U(1)$ or $SU(2)$ states, for instance, if allowed hopping or pairing terms vanish or are equal in size. On the other hand, a spin liquid might appear to have a $U(1)$ or $SU(2)$ IGG on nearest-neighbour bonds, but a $\mathbb{Z}_2$ structure is realised on longer-ranged bonds due to, *e.g.*, the presence of a finite-sized pairing term.

In general, we note that the IGG of a certain mean-field ansatz can be determined from computing all different products of u matrices along the possible closed loops $\mathcal{C}$ of a chosen lattice. The resulting so-called plaquette operators

$$P_{\mathcal{C}} = u_{ij} u_{jk} \ldots u_{qi} \tag{6.32}$$

by definition then have to commute with all elements of the IGG. If they are proportional to $\mathbb{1}$, the IGG is $SU(2)$. If, for instance, only one of the Pauli matrices appears, a $U(1)$ spin liquid is found. For arbitrary terms that only commute with the unit matrix, the IGG is $\mathbb{Z}_2$. In this way, it is not difficult to realise that a bare hopping ansatz (the matrices u_{ij} are all diagonal) will always describe a spin liquid with $U(1)$ or even $SU(2)$ gauge structure. Solely, the appearance of an additional pairing term can change this gauge structure. Therefore, $\mathbb{Z}_2$ spin liquids can only occur if both finite hoppings and finite pairings exist in the mean-field ansatz.

6.2.3. Classification scheme

As already mentioned, once the IGG is defined, one needs to constrain the effects that two symmetry operations from S have on the hopping and pairing terms if a sequence of these symmetries maps, up to elements of the IGG, all matrices u_{ij} back onto themselves. Gathering the constraints from all possible symmetry relations, one can then classify the different possible projective symmetry operations and their according action on the u_{ij}. Once these representations are known, one simply fixes the local gauge freedom by defining one of the u_{ij} from which all remaining hopping and pairing amplitudes can be calculated in the respective PSG.

Unfortunately, we have to refer the interested reader to Refs. [182], [111], and [170] for the precise details of this method. Instead, we state one of its most important results which can already be concluded with our current knowledge. The precise pattern of hoppings and pairings in real space is not well defined in the PSG classification scheme due to their local gauge freedom. Therefore, some apparently very different ansätze turn out to yield the same state after projection. However, the traces of the plaquette operators from Eq. (6.32) remain invariant under any local gauge transformation due to $W_i^\dagger W_i = \mathbb{1}$ and the invariance of the trace under cyclic permutations

$$\operatorname{tr} P_{\mathcal{C}} \longrightarrow \operatorname{tr}\left(W_i\, u_{ij}\, W_j^\dagger\, W_j\, u_{jk}\, W_k^\dagger\, \ldots\, W_q\, u_{qi}\, W_i^\dagger\right) = \operatorname{tr} P_{\mathcal{C}}\,. \tag{6.33}$$

We now summarise the results of a PSG classification on the square and the kagome lattice for $\mathbb{Z}_2$ spin liquids on a nearest-neighbour level. For the subsequent investigation of certain models, we also take on-site and longer-ranged terms into account. If not stated otherwise, they are either not generated within our formalism or their influence is marginal. We therefore do not provide a complete classification of them.

6.2.4. PSG on the square lattice

Let us consider the Hamiltonian from Eq. (6.29a) on a square lattice with $u_{ij} \neq 0$ only for nearest-neighbour sites i and j. In that case, the plaquette operators are solely non-zero for an even number of u matrices. They always take the form

$$P_{\mathcal{C}} = u_{ij} u_{jk}\, \ldots\, u_{pq} u_{qi} = \begin{pmatrix} \phi^* & \psi \\ -\psi^* & \phi \end{pmatrix} \tag{6.34}$$

and their trace is hence given by

$$\operatorname{tr} P_{\mathcal{C}} = \phi^* + \phi = 2\mathrm{Re}\,[\phi]\ , \tag{6.35}$$

where ϕ is in general a non-vanishing complex number. We only consider time-reversal symmetric spin liquids that also obey all projective lattice symmetries, *i.e.*, the magnitudes of all nearest-neighbour hopping amplitudes χ are identical independent of the connected lattice sites and the same statement holds for the pairings η separately. In this instance,

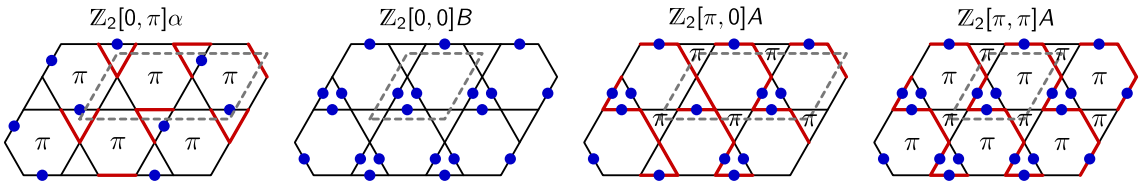

Figure 6.1.: Ansätze for the four time-reversal symmetric, nearest-neighbour $\mathbb{Z}_2$ spin liquids on the kagome lattice: We choose a gauge in which all hopping (pairing) amplitudes χ (η) are real and have the same magnitude on each bond. A black line indicates both positive χ and positive η on a particular bond, whereas red lines or blue dots represent a negative χ or a negative η, respectively. The unit cell of an ansatz is circumscribed by a grey dashed line and a label π denotes a non-vanishing flux through the respective plaquette in the parent $U(1)$ state (confer main text). *Figure created by Johannes Reuther.*

there are only two distinct $\mathbb{Z}_2$ spin liquids, dubbed Z2Azz13 and Z2Bzz13, with the trace of a plaquette operator $P_{\mathcal{C}(\square)}$ around an elementary square loop taking the value

$$\operatorname{tr} P_{\mathcal{C}(\square)} = \begin{cases} 2\left(\chi^2-\eta^2\right)^2 - 8\chi^2\eta^2\,, & \text{Z2A}zz13\,, \\ -2\left(\chi^2-\eta^2\right)^2 + 8\chi^2\eta^2\,, & \text{Z2B}zz13\,. \end{cases} \tag{6.36}$$

The nomenclature of these cases is taken from Ref. [182] and their real space representations for a particular gauge can be seen in the inset of Fig. 6.9. The ratio η/χ is very important since both spin liquids yield the same trace if $(\chi,\eta)=(c,0)$ or $(0,c)$ for the Z2Bzz13 state and if $\chi=\eta=c/\sqrt{2}$ for the Z2Azz13 state. In that scenario, both of these states are gauge equivalent to the so-called $SU(2)$ π-flux state introduced in Refs. [3, 115], *i.e.*, they are identical to it after some local gauge transformation. The π-flux state only consists of equal spinon hopping terms with an enlarged unit cell of two sites. Here, Eq. (6.36) yields the value $-2c^4$ denoting that a spinon picks up a minus sign which is tantamount to a phase of π upon propagating around the elementary square loop. Hence the state's name.

On the nearest-neighbour level for $\mathbb{Z}_2$ spin liquids, this exhausts all possibilities on the square lattice. Since we are now familiar with the PSG concept, we can turn to the more interesting case of the kagome lattice.

6.2.5. PSG on the kagome lattice

For the kagome lattice, there are four distinct $\mathbb{Z}_2$ QSLs on a nearest-neighbour level which are derived in Ref. [111]. Since there are now two distinct elementary triangle loops (up and down triangles) and one elementary hexagonal loop, we do not display all of their plaquette operator traces here. Instead, we provide the corresponding real space patterns of all gauge-inequivalent hopping and pairing amplitudes in Fig. 6.1. The $\mathbb{Z}_2[0,\pi]\alpha$ and the $\mathbb{Z}_2[\pi,0]A$ states feature an increased unit cell including six lattice sites, whereas the $\mathbb{Z}_2[0,0]B$ and the $\mathbb{Z}_2[\pi,\pi]A$ states have the same three-atomic basis as the kagome lattice

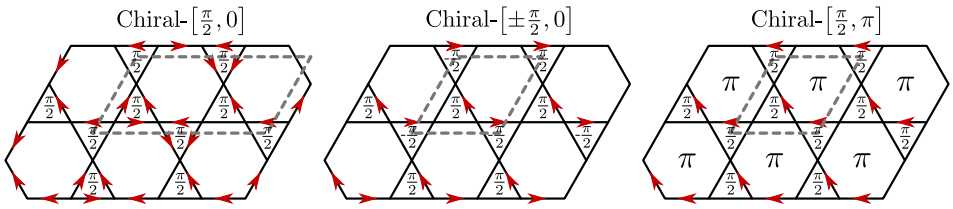

Figure 6.2.: Three selected chiral spin liquids on the kagome lattice: All nearest-neighbour bonds only include hopping terms which can be real (black lines) or imaginary. In the latter case, a red arrow from site j to site i denotes a hopping term $i\chi_{ij}f_i f_j^\dagger$ with $\chi > 0$. The hermitian conjugate of this term now acquires a minus sign and the direction matters. As in Fig. 6.1, the labels $\pm\frac{\pi}{2}$ and π denote all non-zero fluxes that are acquired upon propagation around the elementary loops and grey dashed lines show the respective ansatz' unit cells. *Figure created by Johannes Reuther.*

itself. The names of these different spin liquids arise from their parent $U(1)$ states that are obtained by setting all pairing amplitudes to zero. Then, the IGG is trivially given by a complex exponent rather then just $\pm\mathbb{1}$. For these $U(1)$ hopping models, the flux of an elementary loop is defined as the sign of the product of hopping amplitudes along that loop. If the product is positive, the spinons do not pick up additional minus signs after a propagation around the loop and its flux is 0. If the product is negative though as for the π-flux state on the square lattice, a minus sign occurs which is identical to a flux of π. The first (second) number in the square brackets of the above nomenclature identifies the flux through down triangles (hexagons) for the respective $U(1)$ parent states, confer Fig. 6.1.

In addition to the time-reversal symmetric spin liquids considered so far, we are also interested in chiral states on the kagome lattice. As predicted by variational Monte Carlo (VMC) studies, some of these chiral states are energetically very compatible to the most promising $\mathbb{Z}_2$ candidates [140]. They break time-reversal symmetry which, in our language, is denoted by plaquette fluxes that are fractions of π implying the pick-up of a complex phase upon propagation around elementary loops. In Sec. 6.5.4, we investigate those three chiral spin liquids that posses the lowest variational energies in VMC calculations. In correspondence to the $\mathbb{Z}_2$ states, they are called Chiral-$[\frac{\pi}{2},0]$, Chiral-$[\pm\frac{\pi}{2},0]$, and Chiral-$[\frac{\pi}{2},\pi]$ respectively and are shown together with their flux patterns in Fig. 6.2.

This concludes our section about the PSG. Again, for more important details on the precise computations, the reader is referred to the essential articles in this topic [111, 182]. We now continue by deriving a method that aims at self-consistently calculating the low-energy effective theory in Eqs. (6.29) from FRG vertex functions.

$$G_{ij}(\tau|\tau') = \left\langle T_\tau f_{i\uparrow}(\tau) f^\dagger_{j\uparrow}(\tau') \right\rangle =$$

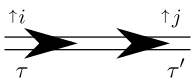

$$F^\dagger_{ij}(\tau'|\tau) = \left\langle T_\tau f^\dagger_{i\downarrow}(\tau) f^\dagger_{j\uparrow}(\tau') \right\rangle =$$

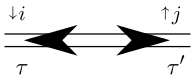

$$F_{ij}(\tau|\tau') = \left\langle T_\tau f_{i\uparrow}(\tau) f_{j\downarrow}(\tau') \right\rangle =$$

$$-G_{ji}(\tau'|\tau) = \left\langle T_\tau f^\dagger_{i\downarrow}(\tau) f_{j\downarrow}(\tau') \right\rangle =$$

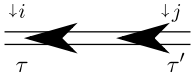

Figure 6.3.: Diagrammatic representation of the normal and the anomalous Green's functions G and F in imaginary time and real space: Ingoing arrows represent annihilation operators, whereas outgoing ones denote creation operators.

6.3. Dyson-Schwinger equations in Fock approximation

Our entire approach for this chapter is based on the self-consistent Dyson-Schwinger equation which is deduced from an approximation of the propagators to first order in the Hamiltonian. This approximation corresponds to a self-consistent mean-field scheme in order to determine the hopping and pairing amplitudes of Eq. (6.29b). We compute the Dyson-Schwinger equations for the normal and the anomalous Green's functions in the so far utilised imaginary-time and real-space formalism first.

6.3.1. Imaginary-time and real-space formalism

Let us start by reminding ourselves how to actually compute an imaginary-time ordered Green's function. In the interaction picture where operators evolve with respect to the non-interacting Hamiltonian, it is given by

$$\begin{aligned} G_{AB}(\tau_1|\tau_2) &= \left\langle T_\tau A(\tau_1) B(\tau_2) \right\rangle \\ &= \frac{\left\langle T_\tau e^{-\int_0^\beta \mathrm{d}\tau\, H(\tau)} A(\tau_1) B(\tau_2) \right\rangle_0}{\left\langle T_\tau e^{-\int_0^\beta \mathrm{d}\tau\, H(\tau)} \right\rangle_0} \\ &= \frac{1}{\mathcal{Z}} \left\langle T_\tau e^{-\int_0^\beta \mathrm{d}\tau\, H(\tau)} A(\tau_1) B(\tau_2) \right\rangle_0 . \end{aligned} \tag{6.37}$$

The operators A and B do not need to be specified here and $\hbar = 1$. For our mean-field Hamiltonian from Eq. (6.25), we expand $e^{-\int_0^\beta \mathrm{d}\tau\, H(\tau)} \simeq 1 - \int_0^\beta \mathrm{d}\tau\, H(\tau)$ in numerator and denominator separately. This first-order perturbation amounts to a Fock approximation of the self energy. Higher-order terms are later included by replacing bare propagators with dressed ones in the final set of equations. This will also render our scheme self-consistent

in the end. For the partition function, we hence find

$$\begin{aligned}
\mathcal{Z} &= \left\langle T_\tau e^{-\int_0^\beta \mathrm{d}\tau\, H_{\mathrm{MF}}(\tau)} \right\rangle_0 \\
&\simeq \left\langle T_\tau 1 \right\rangle_0 - \int_0^\beta \mathrm{d}\tau \left\langle T_\tau H_{\mathrm{MF}}(\tau) \right\rangle_0 \\
&= 1 + \frac{3}{16} \sum_{i,j} \int_0^\beta \mathrm{d}\tau\, J_{ij} \Big\langle T_\tau \Big(\chi_{ij} f^\dagger_{j\uparrow}(\tau) f_{i\uparrow}(\tau) + \chi^\dagger_{ij} f^\dagger_{i\uparrow}(\tau) f_{j\uparrow}(\tau) \\
&\quad + \chi_{ij} f^\dagger_{j\downarrow}(\tau) f_{i\downarrow}(\tau) + \chi^\dagger_{ij} f^\dagger_{i\downarrow}(\tau) f_{j\downarrow}(\tau) + \eta^\dagger_{ij} f_{j\downarrow}(\tau) f_{i\uparrow}(\tau) \\
&\quad + \eta_{ij} f^\dagger_{i\uparrow}(\tau) f^\dagger_{j\downarrow}(\tau) + \eta^\dagger_{ij} f_{i\downarrow}(\tau) f_{j\uparrow}(\tau) + \eta_{ij} f^\dagger_{j\uparrow}(\tau) f^\dagger_{i\downarrow}(\tau) \Big) \Big\rangle_0 \\
&= 1 - \frac{3}{8} \sum_{i,j} \int_0^\beta \mathrm{d}\tau\, J_{ij} \left(\chi_{ij} G^0_{ij}(\tau,\tau) + \chi^\dagger_{ij} G^0_{ji}(\tau,\tau) + \eta^\dagger_{ij} F^0_{ij}(\tau,\tau) + \eta_{ij} F^{\dagger\,0}_{ji}(\tau,\tau) \right) .
\end{aligned} \tag{6.38}$$

It should be clear that $F^0 \equiv F^{\dagger\,0} \equiv 0$. We keep those terms for now in order to derive the correct Dyson equation. In the next steps, we have to proceed analogously for the numerators of the different propagators while utilising Wick's theorem. We begin with the normal Green's function.

$$\begin{aligned}
\mathcal{Z} G_{ij}(\tau_1|\tau_2) &= \left\langle T_\tau e^{-\int_0^\beta \mathrm{d}\tau\, H_{\mathrm{MF}}(\tau)} f_{i\uparrow}(\tau_1) f^\dagger_{j\uparrow}(\tau_2) \right\rangle_0 \\
&\simeq \left\langle T_\tau \left(1 - \int_0^\beta \mathrm{d}\tau\, H_{\mathrm{MF}}(\tau) \right) f_{i\uparrow}(\tau_1) f^\dagger_{j\uparrow}(\tau_2) \right\rangle_0 \\
&= G^0_{ij}(\tau_1|\tau_2) + \frac{3}{16} \sum_{k,l} \int_0^\beta \mathrm{d}\tau\, J_{kl} \Big\langle T_\tau \Big(\chi_{kl} f^\dagger_{l\uparrow}(\tau) f_{k\uparrow}(\tau) + \chi^\dagger_{kl} f^\dagger_{k\uparrow}(\tau) f_{l\uparrow}(\tau) \\
&\quad + \chi_{kl} f^\dagger_{l\downarrow}(\tau) f_{k\downarrow}(\tau) + \chi^\dagger_{kl} f^\dagger_{k\downarrow}(\tau) f_{l\downarrow}(\tau) + \eta^\dagger_{kl} f_{l\downarrow}(\tau) f_{k\uparrow}(\tau) \\
&\quad + \eta_{kl} f^\dagger_{k\uparrow}(\tau) f^\dagger_{l\downarrow}(\tau) + \eta^\dagger_{kl} f_{k\downarrow}(\tau) f_{l\uparrow}(\tau) + \eta_{kl} f^\dagger_{l\uparrow}(\tau) f^\dagger_{k\downarrow}(\tau) \Big) f_{i\uparrow}(\tau_1) f^\dagger_{j\uparrow}(\tau_2) \Big\rangle_0 \\
&= G^0_{ij}(\tau_1|\tau_2) + \frac{3}{16} \sum_{k,l} \int_0^\beta \mathrm{d}\tau\, J_{kl} \Bigg[\Big(\chi_{kl} G^0_{kl}(\tau|\tau) + \chi^\dagger_{kl} G^0_{lk}(\tau|\tau) \\
&\quad + \eta^\dagger_{kl} F^0_{kl}(\tau|\tau) + \eta_{kl} F^{\dagger\,0}_{lk}(\tau|\tau) \Big) (-2) G^0_{ij}(\tau_1|\tau_2) + \big(\chi_{kl} G^0_{il}(\tau_1|\tau) G^0_{kj}(\tau|\tau_2) \\
&\quad + \chi^\dagger_{kl} G^0_{ik}(\tau_1|\tau) G^0_{lj}(\tau|\tau_2) + \eta^\dagger_{kl} F^0_{il}(\tau_1|\tau) G^0_{kj}(\tau|\tau_2) + \eta_{kl} G^0_{ik}(\tau_1|\tau) F^{\dagger\,0}_{lj}(\tau_2|\tau) \\
&\quad + \eta^\dagger_{kl} F^0_{ik}(\tau_1|\tau) G^0_{lj}(\tau|\tau_2) + \eta_{kl} G^0_{il}(\tau_1|\tau) F^{\dagger\,0}_{kj}(\tau_2|\tau) \Big) \\
&\quad - \chi_{kl} F^{\dagger\,0}_{lj}(\tau_2|\tau) F^0_{ik}(\tau_1|\tau) - \chi^\dagger_{kl} F^{\dagger\,0}_{kj}(\tau_2|\tau) F^0_{il}(\tau_1|\tau) \Bigg]
\end{aligned} \tag{6.39}$$

Using that $1/(1+x) \simeq 1-x$, we see that dividing by the partition function precisely cancels the disconnected diagrams. Hence, we find up to first order in our interaction that

$$\begin{aligned} G_{ij}(\tau_1|\tau_2) \simeq G^0_{ij}(\tau_1|\tau_2) + \frac{3}{16}\sum_{k,l}\int_0^\beta \mathrm{d}\tau\, J_{kl}\Big[&\chi_{kl}G^0_{il}(\tau_1|\tau)G^0_{kj}(\tau|\tau_2) + \chi^\dagger_{kl}G^0_{ik}(\tau_1|\tau)G^0_{lj}(\tau|\tau_2) \\ &+ \eta^\dagger_{kl}F^0_{il}(\tau_1|\tau)G^0_{kj}(\tau|\tau_2) + \eta_{kl}G^0_{ik}(\tau_1|\tau)F^{\dagger\,0}_{lj}(\tau_2|\tau) + \eta^\dagger_{kl}F^0_{ik}(\tau_1|\tau)G^0_{lj}(\tau|\tau_2) \\ &+ \eta_{kl}G^0_{il}(\tau_1|\tau)F^{\dagger\,0}_{kj}(\tau_2|\tau) - \chi_{kl}F^{\dagger\,0}_{lj}(\tau_2|\tau)F^0_{ik}(\tau_1|\tau) - \chi^\dagger_{kl}F^{\dagger\,0}_{kj}(\tau_2|\tau)F^0_{il}(\tau_1|\tau)\Big]. \end{aligned} \tag{6.40}$$

Together with the previously derived symmetries for χ and η [Eqs. (6.21)], and the fact that $J_{kl} = J_{lk}$ for the considered Heisenberg system, we can finally show that

$$\begin{aligned} G_{ij}(\tau_1|\tau_2) \simeq G^0_{ij}(\tau_1|\tau_2) + \frac{3}{8}\sum_{k,l}\int_0^\beta \mathrm{d}\tau\, J_{kl}\Big(&\chi^\dagger_{kl}G^0_{ik}(\tau_1|\tau)G^0_{lj}(\tau|\tau_2) + \eta^\dagger_{kl}F^0_{ik}(\tau_1|\tau)G^0_{lj}(\tau|\tau_2) \\ &+ \eta_{kl}G^0_{ik}(\tau_1|\tau)F^{\dagger\,0}_{lj}(\tau_2|\tau) - \chi_{kl}F^0_{ik}(\tau_1|\tau)F^{\dagger\,0}_{lj}(\tau_2|\tau)\Big). \end{aligned} \tag{6.41}$$

Concerning the matrix Green's function, this already suffices in order to calculate the diagonal elements. For the off-diagonals, we now continue by deriving the Dyson-Schwinger equations for both anomalous Green's function.

$$\begin{aligned} \mathcal{Z}F_{ij}(\tau_1|\tau_2) &= \Big\langle T_\tau e^{-\int_0^\beta \mathrm{d}\tau\, H_{\mathrm{MF}}(\tau)} f_{i\uparrow}(\tau_1) f_{j\downarrow}(\tau_2)\Big\rangle_0 \\ &\simeq F^0_{ij}(\tau_1|\tau_2) + \frac{3}{16}\sum_{k,l}\int_0^\beta \mathrm{d}\tau\, J_{kl}\Big[\Big(\chi_{kl}G^0_{kl}(\tau|\tau) + \chi^\dagger_{kl}G^0_{lk}(\tau|\tau) \\ &\quad + \eta^\dagger_{kl}F^0_{kl}(\tau|\tau) + \eta_{kl}F^{\dagger\,0}_{lk}(\tau|\tau)\Big)(-2)F^0_{ij}(\tau_1|\tau_2) + \chi_{kl}G^0_{il}(\tau_1|\tau)F^0_{kj}(\tau|\tau_2) \\ &\quad + \chi^\dagger_{kl}G^0_{ik}(\tau_1|\tau)F^0_{lj}(\tau|\tau_2) + \eta^\dagger_{kl}F^0_{il}(\tau_1|\tau)F^0_{kj}(\tau|\tau_2) - \eta_{kl}G^0_{ik}(\tau_1|\tau)G^0_{jl}(\tau_2|\tau) \\ &\quad + \eta^\dagger_{kl}F^0_{ik}(\tau_1|\tau)F^0_{lj}(\tau|\tau_1) - \eta_{kl}G^0_{il}(\tau_1|\tau)G^0_{jk}(\tau_2|\tau) \\ &\quad + \chi_{kl}G^0_{jl}(\tau_2|\tau)F^0_{ik}(\tau_1|\tau) + \chi^\dagger_{kl}G^0_{jk}(\tau_2|\tau)F^0_{il}(\tau_1,\tau)\Big] \end{aligned} \tag{6.42}$$

Again, our partition function cancels the disconnected diagrams and employing the usual symmetries yields that

$$\begin{aligned} F_{ij}(\tau_1|\tau_2) \simeq F^0_{ij}(\tau_1|\tau_2) + \frac{3}{8}\sum_{k,l}\int_0^\beta \mathrm{d}\tau\, J_{kl}\Big(&\chi^\dagger_{kl}G^0_{ik}(\tau_1|\tau)F^0_{lj}(\tau|\tau_2) + \eta^\dagger_{kl}F^0_{ik}(\tau_1|\tau)F^0_{lj}(\tau|\tau_2) \\ &- \eta_{kl}G^0_{ik}(\tau_1|\tau)G^0_{jl}(\tau_2|\tau) + \chi_{kl}F^0_{ik}(\tau_1|\tau)G^0_{jl}(\tau_2|\tau)\Big). \end{aligned} \tag{6.43}$$

For the other off-diagonal element, we find

$$\begin{aligned}\mathcal{Z}F^{\dagger\,0}_{ij}(\tau_2|\tau_1) &= \left\langle T_\tau e^{-\int_0^\beta \mathrm{d}\tau\, H_{\mathrm{MF}}(\tau)} f^\dagger_{i\downarrow}(\tau_1) f^\dagger_{j\uparrow}(\tau_2)\right\rangle_0 \\ &\simeq F^{\dagger\,0}_{ij}(\tau_1|\tau_2) + \frac{3}{16}\sum_{k,l}\int_0^\beta \mathrm{d}\tau\, J_{kl}\Bigg[\Big(\chi_{kl}G^0_{kl}(\tau|\tau) + \chi^\dagger_{kl}G^0_{lk}(\tau|\tau) \\ &\quad +\eta^\dagger_{kl}F^0_{kl}(\tau|\tau) + \eta_{kl}F^{\dagger\,0}_{lk}(\tau|\tau)\Big)(-2)F^{\dagger\,0}_{ij}(\tau_2|\tau_1) + \chi_{kl}F^{\dagger\,0}_{il}(\tau|\tau_1)G^0_{kj}(\tau|\tau_2) \\ &\quad + \chi^\dagger_{kl}F^{\dagger\,0}_{ik}(\tau|\tau_1)G^0_{lj}(\tau|\tau_2) - \eta^\dagger_{kl}G^0_{li}(\tau|\tau_1)G^0_{kj}(\tau|\tau_2) + \eta_{kl}F^{\dagger\,0}_{ik}(\tau|\tau_1)F^{\dagger\,0}_{lj}(\tau_2|\tau) \\ &\quad - \eta^\dagger_{kl}G^0_{ki}(\tau|\tau_1)G^0_{lj}(\tau|\tau_2) + \eta_{kl}F^{\dagger\,0}_{il}(\tau|\tau_1)F^{\dagger\,0}_{kj}(\tau_2|\tau) \\ &\quad + \chi_{kl}F^{\dagger\,0}_{lj}(\tau_2|\tau)G^0_{ki}(\tau|\tau_1) + \chi^\dagger_{kl}F^{\dagger\,0}_{kj}(\tau_2|\tau)G^0_{li}(\tau|\tau_1)\Bigg]. \end{aligned} \tag{6.44}$$

Inserting Eqs. (6.21) and Eq. (6.38), the last missing equation reads

$$\begin{aligned}F^\dagger_{ij}(\tau_2|\tau_1) \simeq F^{\dagger\,0}_{ij}(\tau_2|\tau_1) + \frac{3}{8}\sum_{k,l}\int_0^\beta \mathrm{d}\tau\, J_{kl}\Big(&\chi^\dagger_{kl}F^{\dagger\,0}_{ik}(\tau|\tau_1)G^0_{lj}(\tau|\tau_2) - \eta^\dagger_{kl}G^0_{ki}(\tau|\tau_1)G^0_{lj}(\tau|\tau_2) \\ &+ \eta_{kl}F^{\dagger\,0}_{ik}(\tau|\tau_1)F^{\dagger\,0}_{lj}(\tau_2|\tau) + \chi_{kl}G^0_{ki}(\tau|\tau_1)F^{\dagger\,0}_{lj}(\tau_2|\tau)\Big). \end{aligned} \tag{6.45}$$

It is straightforward to derive the last missing, however symmetry-related Green's function from Eq. (6.41).

$$\begin{aligned}-G_{ji}(\tau_2|\tau_1) &\simeq -G^0_{ji}(\tau_2|\tau_1) - \frac{3}{8}\sum_{k,l}\int_0^\beta \mathrm{d}\tau\, J_{kl}\Big(\chi_{kl}G^0_{jl}(\tau_2|\tau)G^0_{ki}(\tau|\tau_1) + \eta^\dagger_{kl}F^0_{jl}(\tau_2|\tau)G^0_{ki}(\tau|\tau_1) \\ &\quad + \eta_{kl}G^0_{jl}(\tau_2|\tau)F^{\dagger\,0}_{ki}(\tau_1|\tau) - \chi^\dagger_{kl}F^0_{jl}(\tau_2|\tau)F^{\dagger\,0}_{ki}(\tau_1|\tau)\Big) \\ &= -G^0_{ji}(\tau_2|\tau_1) - \frac{3}{8}\sum_{k,l}\int_0^\beta \mathrm{d}\tau\, J_{kl}\Big(\chi_{kl}G^0_{ki}(\tau|\tau_1)G^0_{jl}(\tau_2|\tau) + \eta^\dagger_{kl}G^0_{ki}(\tau|\tau_1)F^0_{lj}(\tau|\tau_2) \\ &\quad + \eta_{kl}F^{\dagger\,0}_{ik}(\tau|\tau_1)G^0_{jl}(\tau_2|\tau) - \chi^\dagger_{kl}F^{\dagger\,0}_{ik}(\tau|\tau_1)F^0_{lj}(\tau|\tau_2)\Big) \end{aligned} \tag{6.46}$$

In the second line, we employed that $F^{(\dagger)}_{ji}(\tau'|\tau) = F^{(\dagger)}_{ij}(\tau|\tau')$.

This finally enables us to write down all approximations for our propagators in the single matrix equation

$$\mathbb{G}_{ij}(\tau_1|\tau_2) = \mathbb{G}^0_{ij}(\tau_1|\tau_2) + \frac{3}{8}\sum_{k,l}\int_0^\beta \mathrm{d}\tau\, J_{kl}\,\mathbb{G}^0_{ik}(\tau_1|\tau)\begin{pmatrix}\chi^\dagger_{kl} & \eta_{kl}\\ \eta^\dagger_{kl} & -\chi_{kl}\end{pmatrix}\mathbb{G}^0_{lj}(\tau|\tau_2) \tag{6.47a}$$

$$= \mathbb{G}^0_{ij}(\tau_1|\tau_2) - \sum_{(k,l)}\int_0^\beta \mathrm{d}\tau\, \mathbb{G}^0_{ik}(\tau_1|\tau)\,u_{kl}\,\mathbb{G}^0_{lj}(\tau|\tau_2)\,, \tag{6.47b}$$

where we have inserted the definition from Eq. (6.29b) and made use of the sum notation for pairs of sites (k,l) in the second line. The last remaining step is to plug in the original Green's function representation of our hopping and pairing amplitudes from Eqs. (6.22) into Eq. (6.47a).

$$\mathbb{G}_{ij}(\tau_1|\tau_2) = \mathbb{G}^0_{ij}(\tau_1|\tau_2) - \lim_{\lambda\to 0}\frac{3}{4}\sum_{k,l}\int_0^\beta \mathrm{d}\tau\, J_{kl}\,\mathbb{G}^0_{ik}(\tau_1|\tau)\mathbb{G}^\lambda_{kl}(\tau|\tau)\mathbb{G}^0_{lj}(\tau|\tau_2) \tag{6.48a}$$

$$\mathbb{G}^\lambda_{ij}(\tau|\tau) = \begin{pmatrix} G_{ij}(\tau|\tau+\lambda) & F_{ij}(\tau|\tau+\lambda) \\ F^\dagger_{ij}(\tau|\tau+\lambda) & -G_{ji}(\tau|\tau+\lambda) \end{pmatrix} \tag{6.48b}$$

Here, the infinitesimal imaginary time λ has to be inserted for the correct order of spinon operators in the equal-time Green's functions of Eqs. (6.22). The according Dyson-Schwinger equation can now be generated by omitting the zero superscript of the right-most propagator and thereby replacing it with the dressed propagator $\mathbb{G}$.

$$\mathbb{G}_{ij}(\tau_1|\tau_2) = \mathbb{G}^0_{ij}(\tau_1|\tau_2) - \lim_{\lambda\to 0}\frac{3}{4}\sum_{k,l}\int_0^\beta \mathrm{d}\tau\, J_{kl}\,\mathbb{G}^0_{ik}(\tau_1|\tau)\mathbb{G}^\lambda_{kl}(\tau|\tau)\mathbb{G}_{lj}(\tau|\tau_2) \tag{6.49}$$

Diagrammatically, we represent our propagators according to Fig. 6.3. The Dyson-Schwinger equation can be visualised for each component individually (see Fig. 6.4).

Due to its special real-space structure, this self-consistency equation has a very important property. The matrix u_{kl} in Eq. (6.47b) transforms under local and time-independent gauge transformations as $u_{kl} \longrightarrow W_k\, u_{kl}\, W_l^\dagger$. Therefore, to first order in u, the dressed propagator transforms as

$$\begin{aligned}\mathbb{G}_{ij}(\tau_1|\tau_2) \longrightarrow\ & \mathbb{G}^0_{ij}(\tau_1|\tau_2) - \sum_{(k,l)}\int_0^\beta \mathrm{d}\tau\, \mathbb{G}^0_{ik}(\tau_1|\tau)\, W_k\, u_{kl}\, W_l^\dagger\, \mathbb{G}^0_{lj}(\tau|\tau_2) \\ =& W_i\left(\mathbb{G}^0_{ij}(\tau_1|\tau_2) - \sum_{(k,l)}\int_0^\beta \mathrm{d}\tau\, \mathbb{G}^0_{ik}(\tau_1|\tau)\, u_{kl}\, \mathbb{G}^0_{lj}(\tau|\tau_2)\right) W_j^\dagger \\ =& W_i\, \mathbb{G}_{ij}(\tau_1|\tau_2)\, W_j^\dagger\,. \end{aligned} \tag{6.50}$$

In the second line, we employed that $\mathbb{G}^0_{ij} \propto \delta_{ij}$ and that $W_i\, W_i^\dagger = \mathbb{1}$. Considering the self-consistency Eq. (6.49), one can now verify that also in general

$$\mathbb{G}_{ij} \longrightarrow W_i\, \mathbb{G}_{ij}\, W_j^\dagger \tag{6.51}$$

must hold. To first order in u, this is shown in Eq. (6.50). To second order in u, we have to insert the first-order result into the right-hand side of Eq. (6.49) and repeat the same calculation as in Eq. (6.50) once more. In this way, Eq. (6.51) can be proven via mathematical induction. For Eq. (6.49), it implies that both left-hand and right-hand

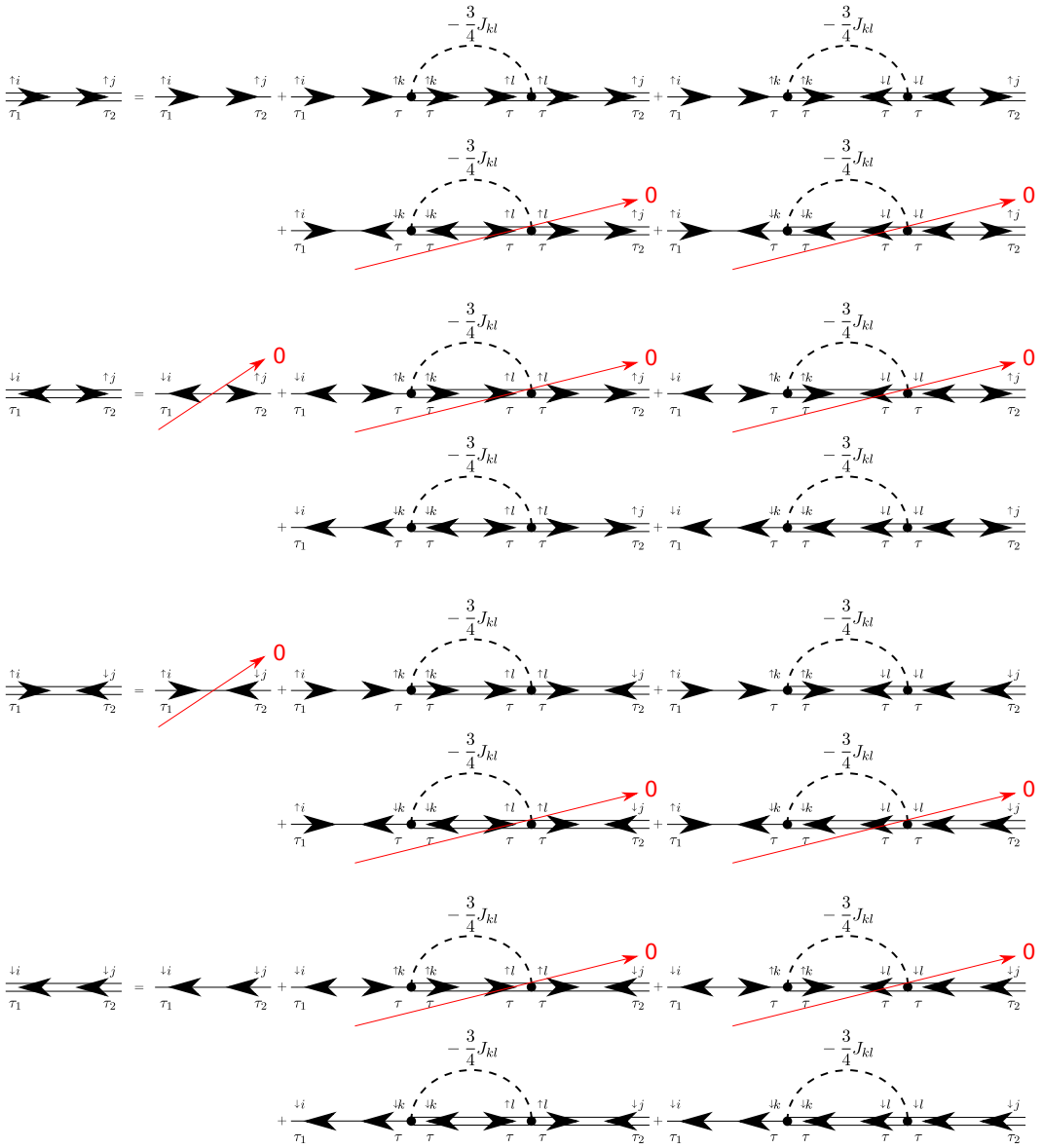

Figure 6.4.: Dyson equations for G and F in imaginary time and real space: The double line corresponds to a dressed Green's function and a single line denotes the bare propagator. All minus signs are correctly incorporated in the definitions of our propagators. A sum or, respectively, an integral needs to be performed over all internal times and lattice sites. Note that the crossed-out terms equal zero because the bare anomalous Green's functions vanishes.

side transform under local and time-independent gauge transformations as demanded by Eq. (6.51).

$$\begin{aligned} & W_i\, \mathbb{G}_{ij}(\tau_1|\tau_2)\, W_j^\dagger \\ & \quad = \mathbb{G}^0_{ij}(\tau_1|\tau_2) - \lim_{\lambda\to 0} \frac{3}{4} \sum_{k,l} \int_0^\beta \mathrm{d}\tau\, J_{kl}\, \mathbb{G}^0_{ik}(\tau_1|\tau)\, W_k\, \mathbb{G}^\lambda_{kl}(\tau|\tau)\, W_l^\dagger\, W_l\, \mathbb{G}_{lj}(\tau|\tau_2)\, W_j^\dagger \\ & \quad = W_i\, \mathbb{G}^0_{ij}(\tau_1|\tau_2)\, W_j^\dagger - \lim_{\lambda\to 0} \frac{3}{4} \sum_{k,l} \int_0^\beta \mathrm{d}\tau\, J_{kl}\, W_i\, \mathbb{G}^0_{ik}(\tau_1|\tau)\, \mathbb{G}^\lambda_{kl}(\tau|\tau)\, \mathbb{G}_{lj}(\tau|\tau_2)\, W_j^\dagger \\ & \quad = W_i \left(\mathbb{G}^0_{ij}(\tau_1|\tau_2) - \lim_{\lambda\to 0} \frac{3}{4} \sum_{k,l} \int_0^\beta \mathrm{d}\tau\, J_{kl}\, \mathbb{G}^0_{ik}(\tau_1|\tau) \mathbb{G}^\lambda_{kl}(\tau|\tau) \mathbb{G}_{lj}(\tau|\tau_2) \right) W_j^\dagger \end{aligned} \tag{6.52}$$

This form invariance of the defining equation implies that a specific choice of local gauges is preserved within our mean-field approach. All gauge-invariant and therefore physical quantities of a particular PSG are computed irrespective of the chosen hopping and pairing pattern which is not uniquely defined, confer Sec. 6.2.1.

6.3.2. Transforming into Matsubara space

Due to the internal sums and the convolution integral, the different channels of our matrix propagator in Eq. (6.49) can be decoupled by means of Fourier transforms for temporally and spatially translation invariant systems. For the models considered during this chapter, these symmetry assumptions (mostly) hold and we discuss the necessary modifications to our equations once they are needed.

There is no meaningful way of defining the Fourier transforms identically for all entries of $\mathbb{G}$. The reason for this is that a true constituent of a diagrammatic expansion should conserve energy and later also momentum. Furthermore, our matrices should all obey the same hermitian structure as their original definitions. With the definitions from Secs. 6.1.2 and 6.1.3, one can, however, transform the four components of Eq. (6.49) separately into Matsubara space. In so doing, one recognises that a new matrix structure can be realised by rewriting the resulting equations in terms of $G_{ij}(\omega_n)$, $-G_{ji}(-\omega_n)$, $F_{ij}(\omega_n)$, and $F^\dagger_{ij}(\omega_n)$. A rather elaborate but otherwise elementary calculation then shows that

$$\begin{aligned} \mathbb{G}_{ij}(\omega_n) &= \begin{pmatrix} G_{ij}(\omega_n) & F_{ij}(\omega_n) \\ F^\dagger_{ij}(\omega_n) & -G_{ji}(-\omega_n) \end{pmatrix} \\ &= \mathbb{G}^0_{ij}(\omega_n) - \lim_{\lambda\to 0} \frac{3}{4\beta} \sum_{k,l} \sum_{\omega_m} J_{kl}\, \mathbb{G}^0_{ik}(\omega_n) \mathbb{G}^\lambda_{kl}(\omega_m) \mathbb{G}_{lj}(\omega_n)\,, \end{aligned} \tag{6.53}$$

where we defined

$$\mathbb{G}^\lambda_{kl}(\omega_m) = \begin{pmatrix} G_{kl}(\omega_m) e^{i\omega_m\lambda} & F_{kl}(\omega_m) e^{i\omega_m\lambda} \\ F^\dagger_{kl}(\omega_m) e^{-i\omega_m\lambda} & -G_{kl}(-\omega_m) e^{-i\omega_m\lambda} \end{pmatrix} = e^{i\omega_m\lambda\sigma^z}\, \mathbb{G}_{kl}(\omega_m)\,. \tag{6.54}$$

An analogous transformation has now to be performed for the real-space coordinates.

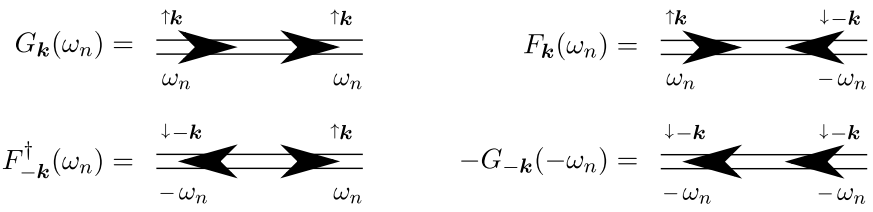

Figure 6.5.: Normal and anomalous Green's functions in Matsubara and momentum space: The diagrammatic representation corresponds to the one in Fig. 6.3. Please note, however, the different indices that are involved for the two spinon operators of each propagator.

6.3.3. Fourier transform of real space

Let us, at the moment, consider a spin system on a two-dimensional Bravais lattice and extend the derived theory later in Sec. 6.3.4 for lattices with poly-atomic unit cells. In a translational invariant Bravais lattice, all entities can only depend on coordinate differences. In analogy to the Matsubara transform, we define

$$f_\alpha(\boldsymbol{r}_i) = \frac{1}{V}\sum_{\boldsymbol{k}} e^{-i\boldsymbol{k}\boldsymbol{r}_i} f_\alpha(\boldsymbol{k})\,, \qquad f^\dagger_\alpha(\boldsymbol{r}_i) = \frac{1}{V}\sum_{\boldsymbol{k}} e^{i\boldsymbol{k}\boldsymbol{r}_i} f^\dagger_\alpha(\boldsymbol{k})\,, \tag{6.55a}$$

$$f_\alpha(\boldsymbol{k}) = \sum_{\boldsymbol{r}_i} e^{i\boldsymbol{k}\boldsymbol{r}_i} f_\alpha(\boldsymbol{r}_i)\,, \qquad f^\dagger_\alpha(\boldsymbol{k}) = \sum_{\boldsymbol{r}_i} e^{-i\boldsymbol{k}\boldsymbol{r}_i} f^\dagger_\alpha(\boldsymbol{r}_i)\,. \tag{6.55b}$$

The according diagrammatic building blocks in Matsubara and momentum space are shown in Fig. 6.5. With them, we find for the Green's functions

$$\begin{aligned} G(\boldsymbol{k}|\boldsymbol{k'}) &= \sum_{\boldsymbol{r}_i,\boldsymbol{r}_j} e^{i(\boldsymbol{k}\boldsymbol{r}_i - \boldsymbol{k'}\boldsymbol{r}_j)} G(\boldsymbol{r}_i|\boldsymbol{r}_j) = \sum_{\boldsymbol{r}_i,\boldsymbol{r}_j} e^{i(\boldsymbol{k}(\boldsymbol{r}_i-\boldsymbol{r}_j)-(\boldsymbol{k'}-\boldsymbol{k})\boldsymbol{r}_j)} G(\boldsymbol{r}_i-\boldsymbol{r}_j|0) \\ &= V G(\boldsymbol{k})\delta_{\boldsymbol{k},\boldsymbol{k'}}\,, \end{aligned} \tag{6.56a}$$

$$\begin{aligned} F^\dagger(\boldsymbol{k}|\boldsymbol{k'}) &= \sum_{\boldsymbol{r}_i,\boldsymbol{r}_j} e^{-i(\boldsymbol{k}\boldsymbol{r}_i + \boldsymbol{k'}\boldsymbol{r}_j)} F^\dagger(\boldsymbol{r}_i|\boldsymbol{r}_j) = \sum_{\boldsymbol{r}_i,\boldsymbol{r}_j} e^{-i(\boldsymbol{k}(\boldsymbol{r}_i-\boldsymbol{r}_j)+(\boldsymbol{k'}+\boldsymbol{k})\boldsymbol{r}_j)} F^\dagger(\boldsymbol{r}_i-\boldsymbol{r}_j|0) \\ &= V F^\dagger(\boldsymbol{k})\delta_{\boldsymbol{k},-\boldsymbol{k'}}\,, \end{aligned} \tag{6.56b}$$

$$\begin{aligned} F(\boldsymbol{k'}|\boldsymbol{k}) &= \sum_{\boldsymbol{r}_i,\boldsymbol{r}_j} e^{i(\boldsymbol{k}\boldsymbol{r}_i + \boldsymbol{k'}\boldsymbol{r}_j)} F(\boldsymbol{r}_i|\boldsymbol{r}_j) = \sum_{\boldsymbol{r}_i,\boldsymbol{r}_j} e^{i(\boldsymbol{k}(\boldsymbol{r}_i-\boldsymbol{r}_j)+(\boldsymbol{k'}+\boldsymbol{k})\boldsymbol{r}_j)} F(\boldsymbol{r}_i-\boldsymbol{r}_j|0) \\ &= V F(\boldsymbol{k})\delta_{\boldsymbol{k},-\boldsymbol{k'}}\,, \end{aligned} \tag{6.56c}$$

where we explicitly kept the spatial coordinates as an argument and not as an index for clarity. The interaction J_{ij} transforms like G_{ij}. In complete analogy to the Matsubara transform from before, Eq. (6.53) can be rewritten as

$$\begin{aligned} \mathbb{G}_{\boldsymbol{k}}(\omega_n) &= \begin{pmatrix} G_{\boldsymbol{k}}(\omega_n) & F_{\boldsymbol{k}}(\omega_n) \\ F^\dagger_{-\boldsymbol{k}}(\omega_n) & -G_{-\boldsymbol{k}}(-\omega_n) \end{pmatrix} \\ &= \mathbb{G}^0_{\boldsymbol{k}}(\omega_n) - \lim_{\lambda\to 0}\frac{3}{4\beta V}\sum_{\boldsymbol{q}}\sum_{\omega_m} J_{\boldsymbol{k}-\boldsymbol{q}}\,\mathbb{G}^0_{\boldsymbol{k}}(\omega_n)\mathbb{G}^\lambda_{\boldsymbol{q}}(\omega_m)\mathbb{G}_{\boldsymbol{k}}(\omega_n)\,. \end{aligned} \tag{6.57}$$

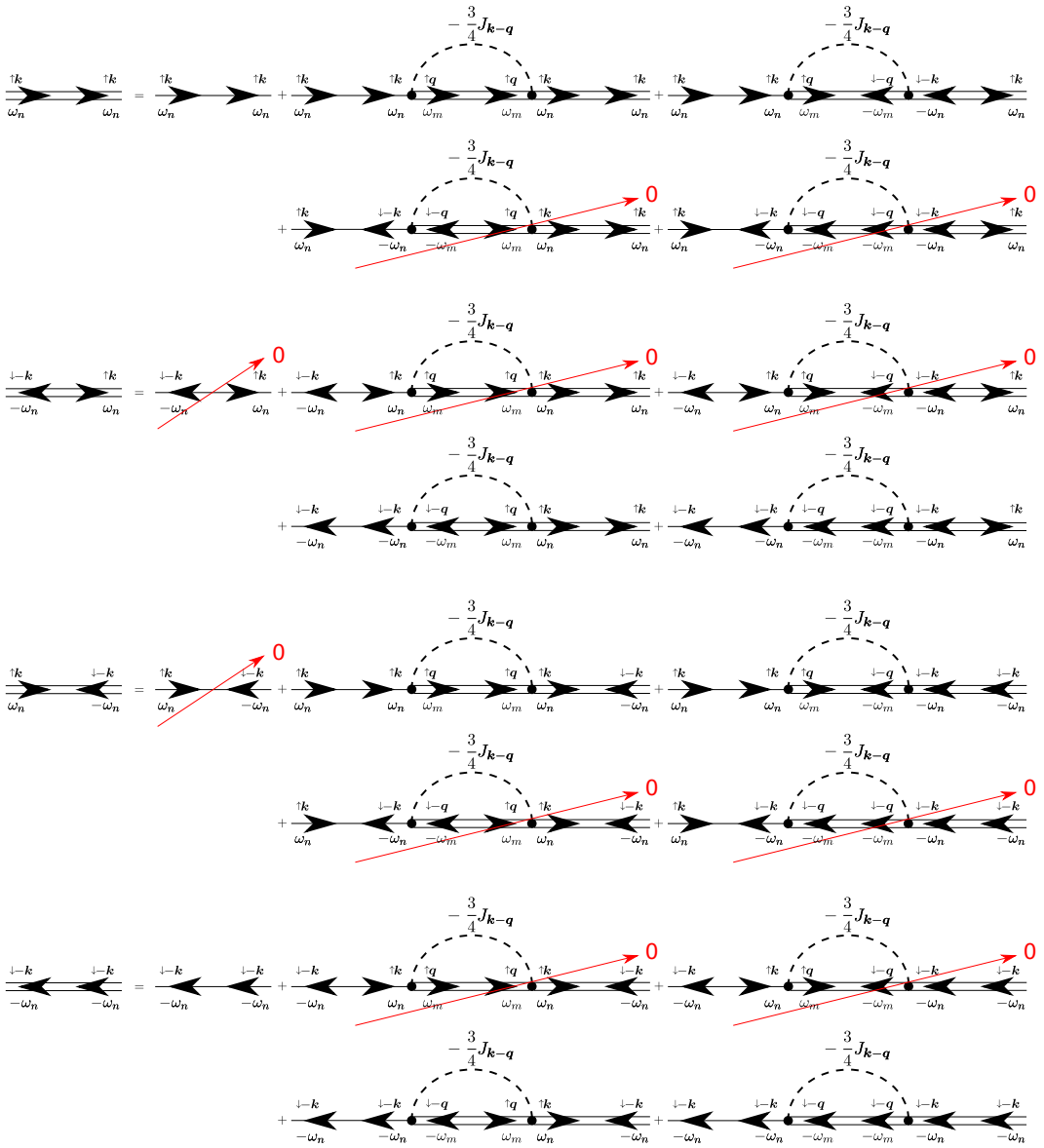

Figure 6.6.: Dyson equations for G and F in Matsubara and momentum space: The diagrammatic conventions are identical to those in Fig. 6.4. Again, the crossed-out diagrams vanish due to $F^{(\dagger)} = 0$.

One should be aware at this point that, due to $F^0_{\boldsymbol{k}}(\omega_n) = F^{\dagger\,0}_{\boldsymbol{k}}(\omega_n) = 0$, the bare matrix Green's function is given by

$$\mathbb{G}^0_{\boldsymbol{k}}(\omega_n) = -\frac{1}{i\omega_n}\mathbb{1}. \tag{6.58}$$

Using this last piece of information, we are able to derive our final self-consistent mean-field equation

$$\mathbb{G}_{\boldsymbol{k}}(\omega_n) = -\left(i\omega_n\mathbb{1} + \bar{\Sigma}_{\boldsymbol{k}}\right)^{-1}, \tag{6.59a}$$

$$\bar{\Sigma}_{\boldsymbol{k}} = -\lim_{\lambda\to 0}\frac{3}{4\beta V}\sum_{\boldsymbol{q}}\sum_{\omega_m} J_{\boldsymbol{k}-\boldsymbol{q}}\mathbb{G}^{\lambda}_{\boldsymbol{q}}(\omega_m), \tag{6.59b}$$

$$\mathbb{G}^{\lambda}_{\boldsymbol{q}}(\omega_m) = e^{i\omega_m\lambda\sigma^z}\mathbb{G}_{\boldsymbol{q}}(\omega_m). \tag{6.59c}$$

We note for the last time that the equations presented here can be rewritten for an alternative definition of the fermionic single-particle propagators by sending $\mathbb{G} \longrightarrow -\mathbb{G}$, confer Sec. 2.1.2. A diagrammatic representation of all four equations can be seen in Fig. 6.6. Half of the diagrams do not contribute due to the vanishing bare anomalous Green's functions. The occurring Matsubara sum for the matrix self energy $\bar{\Sigma}_{\boldsymbol{k}}$ can be evaluate for bare Heisenberg couplings using the residue theorem. Later on in Sec. 6.4 for the renormalised vertices, we have to perform a continuous integral for $T \to 0$ as we do it anyway for the momentum space limit $V^{-1} \to 0$.

6.3.4. Extensions for non-Bravais lattices or translation invariance breaking amplitudes

So far, we assumed that our Heisenberg Hamiltonian from Eq. (6.25) sums over Bravais-lattice sites and that the mean-field ansatz from the considered PSG does not break any translation invariance of this model. Even if the assumption that all considered entities only depend on coordinate differences is broken by the fact that we are no longer dealing with a Bravais lattice or by the fact that our hopping and pairing amplitudes are not necessarily translation invariant [111, 182], we can solve the resulting self-consistency equation by employing an extended matrix structure. There are no changes in our previous Dyson equation for real and Matsubara space [see Eq. (6.53)]. The only remaining challenge is the Fourier transform into $\boldsymbol{k}$ space which is a bit more cumbersome due to the (presumably) lost symmetry. However, Eqs. (6.59) can be formally restored by defining a more complex matrix structure for our Green's function which also incorporates a sublattice index.

Conceptually, we assume that our system can be understood as a problem on a Bravais lattice by introducing the distinct sublattices $\mathcal{A}$, $\mathcal{B}$, $\mathcal{C}$, ... (for the kagome lattice, please

also confer Sec. 4.3.1 and App. D). We rewrite our matrix Green's function as

$$\mathbb{G}(i|j) = \begin{pmatrix} G_{\mathcal{A}\mathcal{A}}(i|j) & G_{\mathcal{A}\mathcal{B}}(i|j) & \cdots & F_{\mathcal{A}\mathcal{A}}(i|j) & F_{\mathcal{A}\mathcal{B}}(i|j) & \cdots \\ G_{\mathcal{B}\mathcal{A}}(i|j) & G_{\mathcal{B}\mathcal{B}}(i|j) & \cdots & F_{\mathcal{B}\mathcal{A}}(i|j) & F_{\mathcal{B}\mathcal{B}}(i|j) & \cdots \\ \vdots & \vdots & \ddots & \vdots & \vdots & \ddots \\ F^\dagger_{\mathcal{A}\mathcal{A}}(i|j) & F^\dagger_{\mathcal{A}\mathcal{B}}(i|j) & \cdots & -G_{\mathcal{A}\mathcal{A}}(j|i) & -G_{\mathcal{B}\mathcal{A}}(j|i) & \cdots \\ F^\dagger_{\mathcal{B}\mathcal{A}}(i|j) & F^\dagger_{\mathcal{B}\mathcal{B}}(i|j) & \cdots & -G_{\mathcal{A}\mathcal{B}}(j|i) & -G_{\mathcal{B}\mathcal{B}}(j|i) & \cdots \\ \vdots & \vdots & \ddots & \vdots & \vdots & \ddots \end{pmatrix}, \tag{6.60}$$

and the matrix self energy

$$\bar{\Sigma}(i|j) = \begin{pmatrix} \chi^\dagger_{\mathcal{A}\mathcal{A}}(i|j) & \chi^\dagger_{\mathcal{A}\mathcal{B}}(i|j) & \cdots & \eta_{\mathcal{A}\mathcal{A}}(i|j) & \eta_{\mathcal{A}\mathcal{B}}(i|j) & \cdots \\ \chi^\dagger_{\mathcal{B}\mathcal{A}}(i|j) & \chi^\dagger_{\mathcal{B}\mathcal{B}}(i|j) & \cdots & \eta_{\mathcal{B}\mathcal{A}}(i|j) & \eta_{\mathcal{B}\mathcal{B}}(i|j) & \cdots \\ \vdots & \vdots & \ddots & \vdots & \vdots & \ddots \\ \eta^\dagger_{\mathcal{A}\mathcal{A}}(i|j) & \eta^\dagger_{\mathcal{A}\mathcal{B}}(i|j) & \cdots & -\chi_{\mathcal{A}\mathcal{A}}(i|j) & -\chi_{\mathcal{A}\mathcal{B}}(i|j) & \cdots \\ \eta^\dagger_{\mathcal{B}\mathcal{A}}(i|j) & \eta^\dagger_{\mathcal{B}\mathcal{B}}(i|j) & \cdots & -\chi_{\mathcal{B}\mathcal{A}}(i|j) & -\chi_{\mathcal{B}\mathcal{B}}(i|j) & \cdots \\ \vdots & \vdots & \ddots & \vdots & \vdots & \ddots \end{pmatrix}, \tag{6.61}$$

where the indices i and j each now only label a unit cell of the system. One has to pay attention at this point to the exchanged sublattice indices in the lower-right sector of $\mathbb{G}(i|j)$. Green's function and self energy are again translation invariant, meaning that they only depend on the coordinate differences between the unit cells labeled by i and j. Using these definitions, one derives completely identical equations as compared to Eqs. (6.59). Only the matrix structure of self energy and Green's function has changed from 2×2 to $2n \times 2n$ if n is the number of atoms within one unit cell. This has the effect that the necessary matrix inversion increases our numerical effort by a factor of $\simeq n^3$. On the other hand, the Brillouin zone is diminished in its size by a factor of n which also reduces the number of discrete $\boldsymbol{k}$-space points for the momentum integral in the self-consistency equation yielding a total increase of computational time by a factor of $\simeq n^2$.

All statements from this section are also valid if the FRG vertex functions are incorporated into our theory, see Sec. 6.4. In the next section, we describe how to solve the self-consistency equations analytically for spin systems on a Bravais lattice without renormalisation effects.

6.3.5. Mean-field solution for bare interaction

We now present the analytical solution for a minimal example of Eqs. (6.59), meaning that we consider a spin-$\frac{1}{2}$ Heisenberg Bravais-lattice model with translation invariant pairing and hopping amplitudes. This has the effect that our equations keep their 2×2 matrix structure and can therefore still be inverted in a decently visualisable way. Furthermore, we suppose that the hoppings and pairings are instantaneous in imaginary time, *i.e.*, χ_{ij}, $\eta_{ij} \propto$

$\delta(\tau - \tau')$. This renders the self energy, which is the key quantity of our investigation, constant in Matsubara space and we rely on that assumption for the rest of this chapter.

The set of equations from above is self-consistent in the self energy. It can be computed via

$$\bar{\Sigma}_{\boldsymbol{k}} = \lim_{\lambda\to 0} \frac{3}{4\beta V} \sum_{\boldsymbol{q}} \sum_{\omega_m} J_{\boldsymbol{k}-\boldsymbol{q}} e^{i\omega_m \lambda \sigma^z} \left(i\omega_m \mathbb{1} + \bar{\Sigma}_{\boldsymbol{q}} \right)^{-1} \tag{6.62}$$

and carries the units of J. We therefore replace the propagator's hopping and pairing amplitudes as $J_{ij}\chi_{ij} \to \chi_{ij}$ and $J_{ij}\eta_{ij} \to \eta_{ij}$. Then we can rewrite the self energy in terms of the different mean-field ansätze which are provided by X.-G. Wen [182] via

$$\bar{\Sigma}_{ij} = \begin{pmatrix} J_{ij}\chi_{ij}^\dagger & J_{ij}\eta_{ij} \\ J_{ij}\eta_{ij}^\dagger & -J_{ij}\chi_{ij} \end{pmatrix} \longrightarrow \begin{pmatrix} \chi_{ij}^\dagger & \eta_{ij} \\ \eta_{ij}^\dagger & -\chi_{ij} \end{pmatrix} . \tag{6.63}$$

Substituting this into Eq. (6.62), inverting the matrix structure and taking the limit $\frac{1}{V}\sum_{\boldsymbol{q}} \to \int_{\text{B.Z.}} \frac{\mathrm{d}\boldsymbol{q}}{(2\pi)^2}$, we find that

$$\begin{aligned} \begin{pmatrix} \chi_{\boldsymbol{k}}^\dagger & \eta_{\boldsymbol{k}} \\ \eta_{-\boldsymbol{k}}^\dagger & -\chi_{-\boldsymbol{k}} \end{pmatrix} &= \lim_{\lambda\to 0} \frac{3}{16\pi^2\beta} \int_{\text{B.Z.}} \mathrm{d}\boldsymbol{q} \sum_{\omega_m} J_{\boldsymbol{k}-\boldsymbol{q}} e^{i\omega_m\lambda\sigma^z} \begin{pmatrix} i\omega_m + \chi_{\boldsymbol{q}}^\dagger & \eta_{\boldsymbol{q}} \\ \eta_{-\boldsymbol{q}}^\dagger & i\omega_m - \chi_{-\boldsymbol{q}} \end{pmatrix}^{-1} \\ &= \lim_{\lambda\to 0} \frac{3}{16\pi^2\beta} \int_{\text{B.Z.}} \mathrm{d}\boldsymbol{q} \sum_{\omega_m} J_{\boldsymbol{k}-\boldsymbol{q}} \frac{1}{(i\omega_m)^2 - \chi_{\boldsymbol{q}}^\dagger\chi_{-\boldsymbol{q}} - \eta_{-\boldsymbol{q}}^\dagger\eta_{\boldsymbol{q}}} \\ &\qquad \times e^{i\omega_m\lambda\sigma^z} \begin{pmatrix} i\omega_m - \chi_{-\boldsymbol{q}} & -\eta_{\boldsymbol{q}} \\ -\eta_{-\boldsymbol{q}}^\dagger & i\omega_m + \chi_{\boldsymbol{q}}^\dagger \end{pmatrix} , \end{aligned} \tag{6.64}$$

where we already used that $\chi_{\boldsymbol{k}}^\dagger = \chi_{-\boldsymbol{k}}$ holds due to $\chi_{ij}^\dagger = \chi_{ji}$ and, in the same way, also $\eta_{\boldsymbol{k}}^{(\dagger)} = \eta_{-\boldsymbol{k}}^{(\dagger)}$. The denominator in this equation has $i\omega_m$ poles at $\pm A_{\boldsymbol{q}} = \pm\sqrt{\chi_{\boldsymbol{q}}^\dagger\chi_{-\boldsymbol{q}} + \eta_{-\boldsymbol{q}}^\dagger\eta_{\boldsymbol{q}}}$ and we are thus able to rewrite the Matsubara sum according to

$$\frac{1}{\beta}\sum_m F(i\omega_m) = \sum_n \mathrm{Res}\left[F(z)f^\pm(z)\right]\Big|_{z=z_n} , \tag{6.65a}$$

$$f^\pm(z) = \pm\frac{1}{e^{\pm\beta z}+1} . \tag{6.65b}$$

Here, $\mathrm{Res}\left[g(z)\right]\Big|_{z=z_n}$ denotes the residue of the complex function $g(z)$ at its pole z_n and $z_{1,2} = A_{\boldsymbol{q}}, -A_{\boldsymbol{q}}$ in our case. For the evaluation of the residue, the function $f^+(z)$ ($f^-(z)$) has to be used when the σ^z term yields $+1$ (-1) in the exponent of Eq. (6.64). The only remaining step is to rewrite the denominator from above as

$$\frac{1}{(i\omega_m)^2 - (A_{\boldsymbol{q}})^2} = \frac{1}{2A_{\boldsymbol{q}}}\left(\frac{1}{(i\omega_m - A_{\boldsymbol{q}})} - \frac{1}{(i\omega_m + A_{\boldsymbol{q}})}\right) . \tag{6.66}$$

Combining all this, we are able to write down a formal expression for our self energy, *i.e.*,

$$\begin{pmatrix} \chi_{\boldsymbol{k}}^\dagger & \eta_{\boldsymbol{k}} \\ \eta_{-\boldsymbol{k}}^\dagger & -\chi_{-\boldsymbol{k}} \end{pmatrix} = \frac{3}{8} \int_{\text{B.Z.}} \frac{\mathrm{d}\boldsymbol{q}}{(2\pi)^2} \frac{J_{\boldsymbol{k}-\boldsymbol{q}}}{A_{\boldsymbol{q}}} \left\{ \begin{pmatrix} f^+(A_{\boldsymbol{q}}) & 0 \\ 0 & f^-(A_{\boldsymbol{q}}) \end{pmatrix} \begin{pmatrix} A_{\boldsymbol{q}} - \chi_{-\boldsymbol{q}} & -\eta_{\boldsymbol{q}} \\ -\eta_{-\boldsymbol{q}}^\dagger & A_{\boldsymbol{q}} + \chi_{\boldsymbol{q}}^\dagger \end{pmatrix} + \begin{pmatrix} f^+(-A_{\boldsymbol{q}}) & 0 \\ 0 & f^-(-A_{\boldsymbol{q}}) \end{pmatrix} \begin{pmatrix} A_{\boldsymbol{q}} + \chi_{-\boldsymbol{q}} & \eta_{\boldsymbol{q}} \\ \eta_{-\boldsymbol{q}}^\dagger & A_{\boldsymbol{q}} - \chi_{\boldsymbol{q}}^\dagger \end{pmatrix} \right\}, \tag{6.67}$$

where we already performed the limit $\lambda \to 0$. Technically, one should be careful about the fact that, if $\eta = 0$, the pole structure is slightly different. It turns out, however, that the terms which should vanish due to this circumstance also vanish in the final result in Eq. (6.67). Because of the Fermi function, the $\boldsymbol{k}$-space integral depends not only on the chosen PSG but also on temperature. It should be evaluated numerically and features all necessary momentum-space and gauge symmetries. The results for different mean-field ansätze on the square lattice are provided in Sec. 6.5.

6.4. Including renormalised vertex functions from FRG

The previous pure mean-field description is known for more than three decades and has been applied to several related systems in the past [3, 12, 104, 176, 181, 182], even though it is usually not formulated in a diagrammatic way like presented above. As we explained in Sec. 6.2, this approach neglects the important effects of gauge fluctuations which are responsible for spinon-spinon interactions as well as vison excitations. We will now incorporate these effects implicitly by inserting the renormalised Green's and vertex functions from a PFFRG analysis into the self-consistency equations. In this way, we go beyond mean-field theory because consider additional Feynman diagrams as summarised in Sec. 4.2.1. In the current equations, we can replace the former coupling constant $J_{ij}/4$ with its FRG analogue $\Gamma^\Lambda_{\mathrm{s}\,ij}$. This is, however, a frequency-dependent entity and we need to select the correct modes for our calculations which is one of the reasons for the extensive previous considerations. Additionally, in the FRG scheme, there is an effective density-density interaction $\Gamma^\Lambda_{\mathrm{d}\,ij}$ appearing during the flow (confer Sec. 4.2.2) for which we do not yet know how it contributes to the self-consistency equations. To that end, we consider the Feynman diagrams for the self energy once more, see Fig. 6.7.

6.4.1. Mean-field decoupled density-density interaction

Using the Abrikosov fermions from before, we should rewrite a spin-density operator as

$$n_i = \frac{1}{2} \sum_{\alpha,\beta} f_{i\alpha}^\dagger \delta_{\alpha\beta} f_{i\beta} = \frac{1}{2} \sum_{\alpha} f_{i\alpha}^\dagger f_{i\alpha} \,. \tag{6.68}$$

It yields the same absolute value as an S_z operator but with a positive sign regardless of the spin's orientation for any physical state. A (fictitious) density-density Hamiltonian can then be represented by

$$\begin{aligned} H^{\mathrm{d}} &= \sum_{(i,j)} D_{ij} n_i n_j = \sum_{i,j} \frac{D_{ij}}{2} n_i n_j \\ &= \sum_{i,j} \sum_{\alpha,\beta} \frac{D_{ij}}{8} f^\dagger_{i\alpha} f_{i\alpha} f^\dagger_{j\beta} f_{j\beta} \,. \end{aligned} \tag{6.69}$$

How such a term decouples in a mean-field treatment is already known from Sec. 6.1.4. We proceed by contracting all four possible non-local amplitudes of this Hamiltonian.

$$\begin{aligned} H^{\mathrm{d}}_{\mathrm{MF}} &= \sum_{i,j} \sum_{\alpha,\beta} \frac{D_{ij}}{8} \left(\frac{1}{2} \chi_{ij} f_{i\alpha} f^\dagger_{j\beta} \delta_{\alpha\beta} + \frac{1}{2} \chi_{ji} f_{j\beta} f^\dagger_{i\alpha} \delta_{\alpha\beta} + \frac{1}{2} \eta^\dagger_{ji} f_{i\alpha} f_{j\beta} \epsilon_{\beta\alpha} + \frac{1}{2} \eta_{ij} f^\dagger_{i\alpha} f^\dagger_{j\beta} \epsilon_{\alpha\beta} \right) \\ &= \sum_{i,j} \sum_{\alpha} \frac{D_{ij}}{8} \left(\frac{1}{2} \chi_{ij} f_{i\alpha} f^\dagger_{j\alpha} + \frac{1}{2} \chi^\dagger_{ij} f_{j\alpha} f^\dagger_{i\alpha} + \sum_{\beta} \epsilon_{\alpha\beta} \left[\frac{1}{2} \eta^\dagger_{ij} f_{i\beta} f_{j\alpha} + \frac{1}{2} \eta_{ij} f^\dagger_{i\alpha} f^\dagger_{j\beta} \right] \right) \\ &= \sum_{i,j} \sum_{\alpha} -\frac{1}{16} D_{ij} \left(\chi_{ij} f^\dagger_{j\alpha} f_{i\alpha} + \chi^\dagger_{ij} f^\dagger_{i\alpha} f_{j\alpha} - \sum_{\beta} \epsilon_{\alpha\beta} \left[\eta^\dagger_{ij} f_{i\beta} f_{j\alpha} + \eta_{ij} f^\dagger_{i\alpha} f^\dagger_{j\beta} \right] \right) \\ &= \sum_{i,j} -\frac{1}{16} D_{ij} \Big(\chi_{ij} f^\dagger_{j\uparrow} f_{i\uparrow} + \chi^\dagger_{ij} f^\dagger_{i\uparrow} f_{j\uparrow} + \chi_{ij} f^\dagger_{j\downarrow} f_{i\downarrow} + \chi^\dagger_{ij} f^\dagger_{i\downarrow} f_{j\downarrow} \\ &\qquad - \eta^\dagger_{ij} f_{j\downarrow} f_{i\uparrow} - \eta_{ij} f^\dagger_{i\uparrow} f^\dagger_{j\downarrow} - \eta^\dagger_{ij} f_{i\downarrow} f_{j\uparrow} - \eta_{ij} f^\dagger_{j\uparrow} f^\dagger_{i\downarrow} \Big) \end{aligned} \tag{6.70}$$

In the second and in the last step, we used that $D_{ij} = D_{ji}$. Rewriting this in the known matrix form [cf. Eq. (6.25)], we find that

$$H^{\mathrm{d}}_{\mathrm{MF}} = -\frac{1}{16} \sum_{i,j} D_{ij} \left[a^\dagger_i \begin{pmatrix} \chi^\dagger_{ij} & -\eta_{ij} \\ -\eta^\dagger_{ij} & -\chi_{ij} \end{pmatrix} a_j + a^\dagger_j \begin{pmatrix} \chi_{ij} & -\eta_{ij} \\ -\eta^\dagger_{ij} & -\chi^\dagger_{ij} \end{pmatrix} a_i \right] . \tag{6.71}$$

This Hamiltonian is hermitian. In comparison to the one presented in Eq. (6.25), an additional minus sign appears in its off-diagonal elements. Soon, we will see that this is in fact not a mistake but a rather important result. It actually enables us to include the density vertex from PFFRG into our self-consistency equations without losing the necessary property that these equations preserve a specific choice of gauge as discussed in the end of Sec. 6.3.1.

6.4.2. Incorporating the FRG vertices

We now want to insert the renormalised Green's function as well as the spin and density vertex resulting from a PFFRG analysis of our Heisenberg system (confer Sec. 4.2.2) into Eqs. (6.59). Therefor, we replace the bare propagator G_0 by its regularised version G_0^Λ

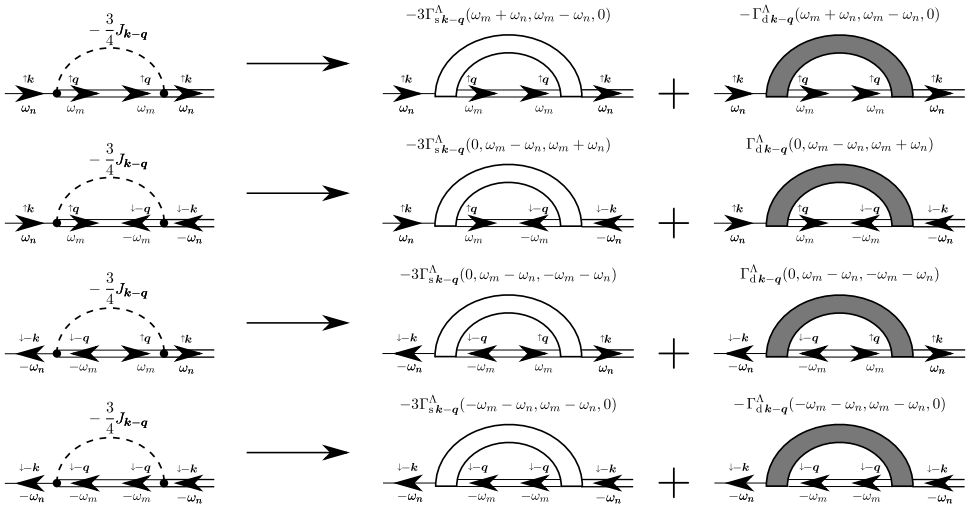

Figure 6.7.: Replacement scheme for the Fock self-energy diagram to obtain correct frequency structure of the FRG renormalised vertex functions: The first frequency argument s of Γ^Λ is the out-going frequency on the left side plus the out-going one on the right. Out-going on the left minus in-going on the left frequency equals the second argument t. The third frequency u is the out-going frequency on the left minus the in-going one on the right side. A white box corresponds to the spin-spin interaction channel, whereas a grey box complies with the density-density interaction.

from Eq. (4.6), add the pseudo-fermion lifetime $\gamma_\mathrm{d}^\Lambda$ from Eq. (4.8) to the self energy, and substitute the bare Heisenberg interaction in the self-consistency equations with the frequency-dependent vertices $\Gamma_\mathrm{s}^\Lambda$ and $\Gamma_\mathrm{d}^\Lambda$. The FRG formalism implies that we are now investigating the $T \to 0$ limit and that our equations have to be formulated in terms of the RG scale Λ which can be seen as an effective temperature.

Let us start by considering the replacement scheme for the Heisenberg interaction. As seen in the previous section, we not only have to replace $\frac{3}{4}J_{ij}$ by $3\Gamma_{\mathrm{s}\,ij}^\Lambda$, but we must also add an additional density term $\pm\Gamma_{\mathrm{d}\,ij}^\Lambda$. The + (−) sign has to be used for the (off-)diagonal elements of the self energy. In order to identify the correct real-space and frequency structures of the renormalised vertex functions, it is now sufficient to read off the respective entries from the propagators being connected to the Fock-like self-energy diagrams (see Fig. 6.7). This is only possible due to the preliminary work in this chapter. In Fig. 6.7, one immediately realises that spin and momentum-space are unaffected by this procedure. On the other hand, summarising the diagrammatically achieved frequency structures, we spot seemingly different contributions to the four self-energy components. These components can, however, be rewritten for a Heisenberg system using the symmetries for the transfer frequencies s, t, and u from Eqs. (4.15). In real space, these symmetries include exchanges of the two real-space coordinates $i \leftrightarrow j$ which, in momentum space, corresponds to the

inversion $\boldsymbol{k} \leftrightarrow -\boldsymbol{k}$. Nevertheless, for the Bravais lattices considered exclusively so far, the entire system has to be symmetric with respect to this transformation and therefore $\Gamma^{\Lambda}_{\mathrm{s/d}\,\boldsymbol{k}} = \Gamma^{\Lambda}_{\mathrm{s/d}\,-\boldsymbol{k}}$. We are thus able to rewrite the vertex contributions from the replacement scheme in Fig. 6.7 as follows.

$$\Gamma^{\Lambda}_{\mathrm{s}\,\boldsymbol{k}-\boldsymbol{q}}(\omega_m+\omega_n,\omega_m-\omega_n,0) = \Gamma^{\Lambda}_{\mathrm{s}\,\boldsymbol{k}-\boldsymbol{q}}(\omega_m+\omega_n,\omega_m-\omega_n,0) \tag{6.72a}$$
$$\Gamma^{\Lambda}_{\mathrm{s}\,\boldsymbol{k}-\boldsymbol{q}}(0,\omega_m-\omega_n,\omega_m+\omega_n) = \Gamma^{\Lambda}_{\mathrm{s}\,\boldsymbol{k}-\boldsymbol{q}}(\omega_m+\omega_n,\omega_m-\omega_n,0) \tag{6.72b}$$
$$\Gamma^{\Lambda}_{\mathrm{s}\,\boldsymbol{k}-\boldsymbol{q}}(0,\omega_m-\omega_n,-\omega_m-\omega_n) = \Gamma^{\Lambda}_{\mathrm{s}\,\boldsymbol{k}-\boldsymbol{q}}(\omega_m+\omega_n,\omega_m-\omega_n,0) \tag{6.72c}$$
$$\Gamma^{\Lambda}_{\mathrm{s}\,\boldsymbol{k}-\boldsymbol{q}}(-\omega_m-\omega_n,\omega_m-\omega_n,0) = \Gamma^{\Lambda}_{\mathrm{s}\,\boldsymbol{k}-\boldsymbol{q}}(\omega_m+\omega_n,\omega_m-\omega_n,0) \tag{6.72d}$$

$$\Gamma^{\Lambda}_{\mathrm{d}\,\boldsymbol{k}-\boldsymbol{q}}(\omega_m+\omega_n,\omega_m-\omega_n,0) = \Gamma^{\Lambda}_{\mathrm{d}\,\boldsymbol{k}-\boldsymbol{q}}(\omega_m+\omega_n,\omega_m-\omega_n,0) \tag{6.73a}$$
$$-\Gamma^{\Lambda}_{\mathrm{d}\,\boldsymbol{k}-\boldsymbol{q}}(0,\omega_m-\omega_n,\omega_m+\omega_n) = \Gamma^{\Lambda}_{\mathrm{d}\,\boldsymbol{k}-\boldsymbol{q}}(\omega_m+\omega_n,\omega_m-\omega_n,0) \tag{6.73b}$$
$$-\Gamma^{\Lambda}_{\mathrm{d}\,\boldsymbol{k}-\boldsymbol{q}}(0,\omega_m-\omega_n,-\omega_m-\omega_n) = \Gamma^{\Lambda}_{\mathrm{d}\,\boldsymbol{k}-\boldsymbol{q}}(\omega_m+\omega_n,\omega_m-\omega_n,0) \tag{6.73c}$$
$$\Gamma^{\Lambda}_{\mathrm{d}\,\boldsymbol{k}-\boldsymbol{q}}(-\omega_m-\omega_n,\omega_m-\omega_n,0) = \Gamma^{\Lambda}_{\mathrm{d}\,\boldsymbol{k}-\boldsymbol{q}}(\omega_m+\omega_n,\omega_m-\omega_n,0) \tag{6.73d}$$

Now, we can see how important the minus signs in the off-diagonal elements from Eq. (6.71) are. They precisely cancel the signs that appear because of the density vertices' antisymmetry with respect to the frequency exchange $s \leftrightarrow u$, see Eq. (4.15d). Therefore, we do not obtain an extra matrix structure from including the renormalised vertices and can simply replace

$$\frac{3}{4}J_{\boldsymbol{k}-\boldsymbol{q}} \longrightarrow 3\Gamma^{\Lambda}_{\mathrm{s}\,\boldsymbol{k}-\boldsymbol{q}}(\omega_m+\omega_n,\omega_m-\omega_n,0) + \Gamma^{\Lambda}_{\mathrm{d}\,\boldsymbol{k}-\boldsymbol{q}}(\omega_m+\omega_n,\omega_m-\omega_n,0) \tag{6.74}$$

in Eqs. (6.59).

To also account for the finite lifetime $\gamma^{\Lambda}_{\mathrm{d}}$ of our pseudo fermions from Sec. 4.2.2, we have to add it to the self energy contributions for the normal Green's functions. This finally enables us to provide a set of self-consistent equations for the self-energy which incorporates all considered FRG vertices, *i.e.*,

$$\mathbb{G}^{\Lambda}_{\boldsymbol{k}}(\omega_n) = -\,\theta(|\omega|-\Lambda)\left(i(\omega_n+\gamma^{\Lambda}_{\mathrm{d}}(\omega_n))\mathbb{1}+\bar{\Sigma}_{\boldsymbol{k}}(\omega_n)\right)^{-1}, \tag{6.75a}$$
$$\begin{aligned}\bar{\Sigma}^{\Lambda}_{\boldsymbol{k}}(\omega_n) = &-\frac{1}{\beta V}\sum_{\boldsymbol{q}}\sum_{\omega_m}\big(3\Gamma^{\Lambda}_{\mathrm{s}\,\boldsymbol{k}-\boldsymbol{q}}(\omega_m+\omega_n,\omega_m-\omega_n,0)\\ &+\Gamma^{\Lambda}_{\mathrm{d}\,\boldsymbol{k}-\boldsymbol{q}}(\omega_m+\omega_n,\omega_m-\omega_n,0)\big)\mathbb{G}^{\Lambda}_{\boldsymbol{q}}(\omega_m)\,.\end{aligned} \tag{6.75b}$$

Our last step for solving the above equation is to require again that all hoppings and pairings are instantaneous in imaginary time which results in a self energy being constant in Matsubara space ($\bar{\Sigma}^{\Lambda}_{\boldsymbol{k}}(\omega_n) \equiv \bar{\Sigma}^{\Lambda}_{\boldsymbol{k}}$). Employing this assumption, we can rearrange Eqs. (6.75)

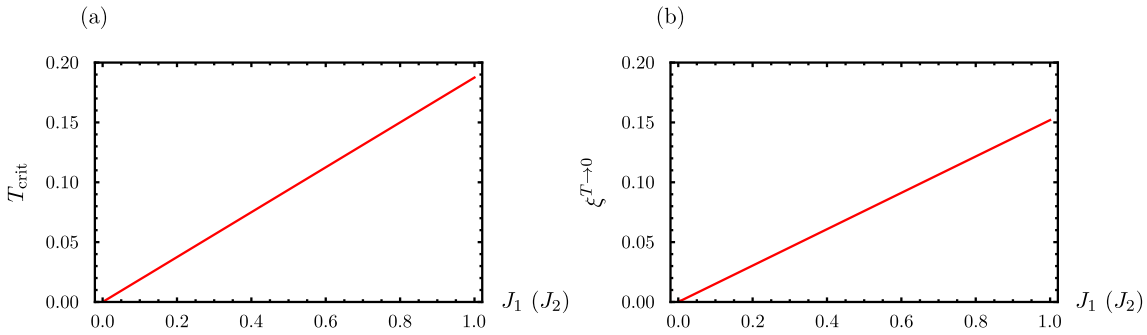

Figure 6.8.: Dependence of (a) critical temperature and (b) maximal amplitude for isotropic nearest (second-nearest) neighbour hopping on J_1 (J_2): On the square lattice, the results for an isotropic nearest-neighbour hopping and second-neighbour hopping model are identical if considered as functions of J_1 and J_2, respectively. The temperature at which the first non-vanishing amplitude is found T_{crit} as well as the amplitude in the zero-temperature limit $\xi^{T\to 0}$ depend linearly on the coupling strength, see Eqs. (6.79).

as

$$\mathbb{G}^{\Lambda}_{\boldsymbol{k}}(\nu) = -\theta(|\nu| - \Lambda)\left(i(\nu + \gamma^{\Lambda}_{\mathrm{d}}(\nu))\mathbb{1} + \bar{\Sigma}_{\boldsymbol{k}}\right)^{-1}, \tag{6.76a}$$

$$\bar{\Sigma}^{\Lambda}_{\boldsymbol{k}} = -\frac{1}{8\pi^3}\int_{-\infty}^{\infty} \mathrm{d}\nu \int_{\mathrm{B.Z.}} \mathrm{d}\boldsymbol{q}\, \left(3\Gamma^{\Lambda}_{\mathrm{s}\,\boldsymbol{k}-\boldsymbol{q}}(\nu,\nu,0) + \Gamma^{\Lambda}_{\mathrm{d}\,\boldsymbol{k}-\boldsymbol{q}}(\nu,\nu,0)\right) \mathbb{G}^{\Lambda}_{\boldsymbol{q}}(\nu)\,, \tag{6.76b}$$

where we already performed the $T \to 0$, $\left(\frac{2\pi}{\beta}\sum_{\omega_m} \to \int_{-\infty}^{\infty}\mathrm{d}\nu\right)$ and the $V \to \infty$, $\left(\frac{4\pi^2}{V}\sum_{\boldsymbol{q}} \to \int_{\mathrm{B.Z.}}\mathrm{d}\boldsymbol{q}\right)$ limits in accordance to the FRG formalism.

The most general definitions from Eqs. (6.60) and (6.61) together with Eqs. (6.59) or (6.76) now define our new functional-renormalisation and projective-symmetry-group Fock-like self-consistency scheme. In principle, we only need to plug in the appropriate mean-field ansätze, investigate and interpret the obtained results. This will be performed in the next sections.

6.5. J_1-J_2 Heisenberg model on the square lattice

We now turn to the results for the J_1-J_2 Heisenberg model on the square lattice. In order to get an intuition for the mathematical details of our method and to verify its applicability, we first investigate the system with bare couplings in which case our results should agree with the mean-field treatment from Ref. [182]. As explained for this scenario in Sec. 6.3.5, we need to solve Eq. (6.67) for a given mean-field ansatz with a numerical evaluation of the occurring $\boldsymbol{k}$-space integral.

Before we discuss the results for those $\mathbb{Z}_2$ spin liquids, let us acquire some fundamental understanding by examining the model for real isotropic hopping amplitudes on either nearest or second-neighbour bonds. If treated separately, they are gauge equivalent to isotropic pairings and we hence only consider the gauge-invariant quantity

$$\xi_{ij} = \sqrt{|\chi_{ij}|^2 + |\eta_{ij}|^2} \tag{6.77}$$

as a measure of the combined hopping and pairing strength on a considered bond type in the following.

6.5.1. Results for isotropic hoppings or pairings

The two simplest mean-field ansätze on a square lattice are a real and isotropic hopping $u_{ij} = \chi_{ij}\sigma^z$ on all nearest or all second-nearest neighbour bonds. The according functions that have to be plugged into Eq. (6.67) for those ansätze are

$$\left(\chi_{1\,\boldsymbol{k}}, \eta_{1\,\boldsymbol{k}}\right) = \left(2\xi_1 \left(\cos(k_x) + \cos(k_y)\right), 0\right), \tag{6.78a}$$

$$\left(\chi_{2\,\boldsymbol{k}}, \eta_{2\,\boldsymbol{k}}\right) = \left(4\xi_2 \cos(k_x)\cos(k_y), 0\right), \tag{6.78b}$$

where we set the lattice constant $a = 1$. After solving the self-consistency equations for those ansätze, we determine how the critical temperature T_{crit} at which a non-zero amplitude occurs first and the maximal amplitude in the $T \to 0$ limit $\xi^{T\to 0}$ depend on the coupling strengths J_1 and J_2. An immediate observation is that the plots for ξ_1 and ξ_2 are identical if treated as a function of J_1 and J_2, respectively. The opposite coupling does not affect these quantities on the other hand, see Fig. 6.8. Such results are not surprising if one considers that the self-energy $\bar{\Sigma}_{ij} \propto J_{ij}$ [cf. Eqs. (6.49)] and that a bare second-neighbour model decouples into two identical nearest-neighbour square lattice models. We fit the plots from above with linear functions and find for isotropic hoppings on the square lattice

$$T_{\text{crit}} = 0.1875\, J\,, \tag{6.79a}$$

$$\xi^{T\to 0} = 0.1520\, J\,, \tag{6.79b}$$

independent of the specific bond type. Note again that $\hbar = 1$ and $k_B = 1$.

The ansätze from above both have a $SU(2)$ gauge structure because they are bare hopping models and all constructible plaquette operators contain even numbers of u matrices, confer Eq. (6.32) and the discussion in Sec. 6.2.2. This is why they are unlikely to be stable upon introducing gauge fluctuations. However, these simple first observations can guide us throughout the following sections. In whichever considered model, we start with the spin system at a finite temperature above all existing T_{crit} and ask ourselves what happens to it if we cool it down. At the largest T_{crit}, the system develops a finite corresponding hopping or pairing amplitude and thereby lower its own energy. In the typical mean-field procedure, this amplitude then only increases if one further lowers the temperature. Any additional

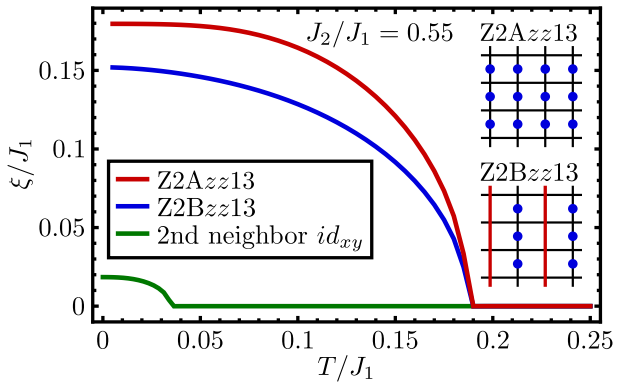

Figure 6.9.: Results for nearest-neighbour $\mathbb{Z}_2$ spin liquids on the square lattice from bare mean-field approach [Eqs. (6.59)]: The coupling ratio $J_2/J_1 = 0.55$ ensures maximal frustration and we plot the overall amplitude ξ_{ij} from Eq. (6.77) for the Z2Azz13 and the Z2Bzz13 state [182]. Additionally, we plot the time-reversal-breaking second-neighbour pairing that is found for the Z2Azz13 state (see Sec. 6.5.3). The inset shows ansätze for both spin liquids in a certain gauge. Here, black lines denote both positive χ and η, whereas red lines (blue) dots illustrate negative hoppings (pairings). *Figure created by Johannes Reuther.*

amplitudes are then generated on top of the first one and we present an according hierarchy of critical temperatures if necessary. The system's PSG and band structure can then be extracted from the corresponding χ_{ij} and η_{ij} in the $T \to 0$ limit. In addition, we are only interested in phases without the occurrence of magnetic order because the concept of deconfined spinons is not suitable otherwise. For the spin-$\frac{1}{2}$ Heisenberg square-lattice model, a paramagnetic phase exists around $J_2/J_1 \simeq 0.5$ implying that the amplitude occurring at the highest temperature is of nearest-neighbour type. A similar statement is true for the kagome lattice at $J_2/J_1 \approx 0$. Hence, we always initiate our analysis by discussing the different scenarios for nearest-neighbour $\mathbb{Z}_2$ spin liquids.

6.5.2. Nearest-neighbour amplitudes

Let us proceed with nearest-neighbour hopping and pairing amplitudes on the square lattice that follow from a bare mean-field treatment [Eqs. (6.59)]. The objective now is to determine which of the gauge-inequivalent $\mathbb{Z}_2$ ansätze is preferably realised by the system. The two possible $\mathbb{Z}_2$ states found by Ref. [182] are characterised in Sec. 6.2.4 and shown in the inset of Fig. 6.9. Here, the Z2Azz13 state features a real and isotropic (s-wave) hopping and real d-wave pairing on nearest-neighbour bonds. For the Z2Bzz13 state on the other hand, translation invariance is broken in terms of one lattice (not the projective) symmetry and we have to extend the unit cell as described in Sec. 6.3.4. Their

momentum-space representations are given by

$$\left(\chi_{\mathrm{A}\,\boldsymbol{k}}, \eta_{\mathrm{A}\,\boldsymbol{k}}\right) = \left(2\chi_{\mathrm{A}}\left(\cos(k_x)+\cos(k_y)\right), 2\eta_{\mathrm{A}}\left(\cos(k_x)-\cos(k_y)\right)\right) \tag{6.80}$$

for the Z2Azz13 state, and by

$$\left(\chi^{\mathcal{A}}_{\mathrm{B}\,\boldsymbol{k}}, \eta^{\mathcal{A}}_{\mathrm{B}\,\boldsymbol{k}}\right) = \left(2\chi_{\mathrm{B}}\left(\cos(k_x)-\cos(k_y)\right), 2\eta_{\mathrm{B}}\left(\cos(k_x)+\cos(k_y)\right)\right) \tag{6.81a}$$

$$\left(\chi^{\mathcal{B}}_{\mathrm{B}\,\boldsymbol{k}}, \eta^{\mathcal{B}}_{\mathrm{B}\,\boldsymbol{k}}\right) = \left(2\chi_{\mathrm{B}}\left(\cos(k_x)+\cos(k_y)\right), 2\eta_{\mathrm{B}}\left(\cos(k_x)-\cos(k_y)\right)\right) \tag{6.81b}$$

for the Z2Bzz13 state where the square lattice is now split into two sublattices $\mathcal{A}$ and $\mathcal{B}$ due to the staggered nature of this mean-field ansatz.

Our results for the maximally frustrated regime at $J_2/J_1 = 0.55$ are shown in Fig. 6.9 where we again plot the overall amplitude ξ as defined in Eq. (6.77) for the nearest-neighbour bonds as a function of temperature T. We find that for both states non-vanishing amplitudes solve Eqs. (6.59) if $T \lesssim 0.1875\,J_1$ as it is the case for an isotropic hopping ansatz. Quite remarkably, this result is independent of the considered state and therefore the critical temperature T_{crit} is not sufficient in order to characterise the preferred state of the system. Also, hopping and pairing amplitudes are equal in size $\chi = \eta = \xi/\sqrt{2}$ for both cases. Fortunately though, this is where the similarities between the Z2Azz13 and the Z2Bzz13 state end. For temperatures below T_{crit}, the Z2Azz13 state ($\xi^{T\to 0} \simeq 0.18\,J_1$) is clearly dominant and develops a significantly higher amplitude ξ compared to the Z2Bzz13 state ($\xi^{T\to 0} \simeq 0.15\,J_1$) as can be seen in Fig. 6.9.

Therefore, we conclude that on a bare mean-field level the system prefers the formation of an effective low-energy theory with spinon hopping and pairing terms characterised by Eq. (6.80) where $\chi_{\mathrm{A}} = \eta_{\mathrm{A}}$. However, since nearest-neighbour hopping and pairing are equal in size, the Z2Azz13 is in fact gauge equivalent to the aforementioned $SU(2)$ π-flux state which is labeled SU2Bn0 in Ref. [182] (also confer Sec. 6.2.4). A similar statement holds for the Z2Bzz13 state and the isotropic hopping model from Eq. (6.78a). As discussed in the previous section, these results do not depend on the value of the second-neighbour Heisenberg coupling J_2. Even though we identify a possibly unstable $SU(2)$ spin liquid in this simple nearest-neighbour model, it has been argued that the predicted π-flux state can withstand gauge fluctuations, at least in the large-N limit for $SU(N)$ spins [75]. Hence, we continue by analysing all possible second-neighbour hopping and pairing terms that can coexist with the Z2Azz13 state in a PSG classification.

6.5.3. Including second-neighbour amplitudes

As previously seen, finite next-nearest-neighbour mean-field amplitudes occur at temperatures $T \leq 0.19\,J_2$ if treated solitarily. Again, the critical temperature and the maximal amplitude in the $T \to 0$ limit $\xi^{T\to 0} \simeq 0.15\,J_2$ are independent of the real space patterns for non-staggered ansätze, *i.e.*, those that do not break the translation invariance of the lattice. There are only two possible second-neighbour terms that are allowed by the PSG

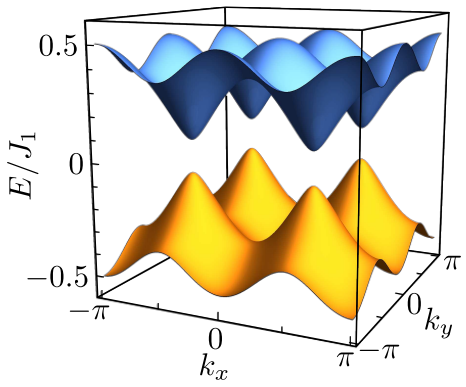

Figure 6.10.: Band structure of the chiral spin liquid [Eq. (6.83)] found for $J_2/J_1 = 0.55$ in the $T \to 0$ limit: There are two spinon bands, one below and one above zero energy. These bands are completely gapped due to the finite second-neighbour pairing. The respective mean-field amplitudes correspond to those in Fig. 6.9.

of the state Z2Azz13. For our nearest-neighbour ansatz from Eq. (6.80), they are either given by real s-wave or by p-wave hoppings

$$(\chi_{\mathrm{A}s\,\boldsymbol{k}}, \eta_{\mathrm{A}\,\boldsymbol{k}}) = (\chi_{\mathrm{A}\,\boldsymbol{k}} + 4\chi_2 \cos(k_x)\cos(k_y), \eta_{\mathrm{A}\,\boldsymbol{k}}) \ , \tag{6.82a}$$

$$(\chi_{\mathrm{A}p\,\boldsymbol{k}}, \eta_{\mathrm{A}\,\boldsymbol{k}}) = (\chi_{\mathrm{A}\,\boldsymbol{k}} + 4\chi_2 \sin(k_x)\sin(k_y), \eta_{\mathrm{A}\,\boldsymbol{k}}) \ . \tag{6.82b}$$

At $J_2/J_1 = 0.55$ however, both of them are not induced within the mean-field formalism down to zero temperature in the presence of nearest-neighbour amplitudes with higher T_{crit}. This difference to the results from Sec. 6.5.1 shows that they must be suppressed by the existence of the shorter-ranged amplitudes.

In fact only because $\chi_{\mathrm{A}} = \eta_{\mathrm{A}} = \xi_{\mathrm{A}}/\sqrt{2}$, the sole PSG-allowed second-neighbour amplitude that we can find to coexist with the state from Eq. (6.80) is an imaginary p-wave pairing, yielding a total state of

$$(\chi_{\mathrm{A}\,\boldsymbol{k}}, \eta_{\mathrm{Ac}\,\boldsymbol{k}}) = (\chi_{\mathrm{A}\,\boldsymbol{k}}, \eta_{\mathrm{A}\,\boldsymbol{k}} + 4i\eta_{\mathrm{c}} \sin(k_x)\sin(k_y)) \ . \tag{6.83}$$

This ansatz breaks time-reversal invariance and therefore represents a chiral spin liquid. We show the corresponding amplitudes for $J_2/J_1 = 0.55$ in Fig 6.9 and the corresponding zero-temperature band structure in Fig. 6.10. In contrast to the band structure of the π-flux state [see Fig. 6.12(a)], all spinons of the chiral spin liquid are gapped due to the finite second-neighbour pairing term. Unlike χ_{A} and η_{A}, the magnitude of η_{c} strongly depends on J_2. It vanishes if $J_2 \leq 0.45\,J_1$ and then only increases within the regime that is believed by most theories to house a paramagnetic phase, *e.g.*, $0.4 \lesssim J_2/J_1 \lesssim 0.65$ [61, 64, 96, 114, 147, 160, 161].

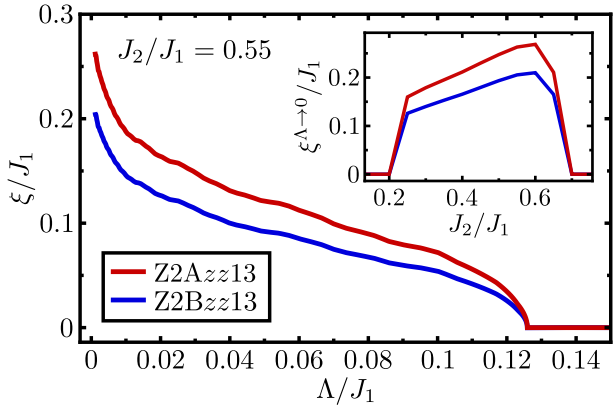

Figure 6.11.: Overall amplitudes $\xi_{ij} = \sqrt{|\chi_{ij}|^2 + |\eta_{ij}|^2}$ from FRG [see Eqs. (6.76)] for $\mathbb{Z}_2$ spin liquids on the square lattice with $J_2/J_1 = 0.55$: The system favours the Z2Azz13 state in comparison to the Z2Bzz13 state which is expressed by a larger ξ during the Λ flow. How the maximal amplitudes ξ in the $\Lambda \to 0$ limit change as a function of the coupling ratio J_2/J_1 is presented in the inset (confer main text for interpretations). *Figure created by Johannes Reuther.*

The gapped chiral spin liquid is the same state that is found by Xiao-Gang Wen for coupling ratios $J_2/J_1 \approx 0.5 \ldots 1.0$ whereas for lower values the gapless π-flux state is supposedly realised [182]. This exactly[2] coincides with our findings and we can therefore apply our method with some confidence since it yields identical results as a plain mean-field analysis if bare Heisenberg couplings are used. We continue with the incorporation of the renormalised vertex functions in the next section.

6.5.4. Results from FRG vertices

So far, we treated our square lattice Heisenberg spin system on the basis of instantaneous interactions and bare propagators. This technique has shown to agree with the results of Xiao-Gang Wen who compares the mean-field energies of the respective states but makes no statement about the magnitudes of hoppings and pairings which we determine self-consistently. As shown in Sec. 6.4, we are also capable of incorporating the frequency-renormalised vertex functions (including a density-density vertex) and pseudo-fermion life-time from a FRG formalism into our theory. This effectively adds more diagrams to the self-consistency scheme the lower the cutoff value Λ is set. We already saw in Chap. 4 that those diagrams are required for finding magnetically disordered phases at zero temperature and hence should be accounted for in an effective low-energy theory for QSLs. Since most of these contributions were neglected in the previous section, they now account for the

[2] Ref. [182] does not provide tabulated values of the phase boundaries and the ones given here were extracted from a plotted phase diagram.

missing gauge fluctuations up to some point and the effects of spinon-spinon interactions and vison excitations are implicitly incorporated in our study. Due to the frequency cutoff, Λ takes in addition the role of an effective temperature and we therefore now look for those amplitudes first that are induced at the highest Λ values. Despite this, the results for the physical system should be derived from the cutoff-free theory in the $\Lambda \to 0$ limit.

We perform pseudo-fermion FRG calculations on the J_1-J_2 Heisenberg square lattice model using clusters of 441 lattice sites and 120 points for the discretisation of the Matsubara frequencies. In comparison to the Dzyaloshinsky-Moriya Heisenberg model from Chap. 4 or the 3D material from Chap. 5, this model is numerically far less challenging and a higher precision in spatial and frequency resolution can thus be achieved. Using the obtained, frequency-dependent vertex functions, we are able to solve Eq. (6.76) by means of a numerical momentum and Matsubara space integration.

In a regime around $J_2/J_1 = 0.55$, the first important result is that only nearest-neighbour amplitudes can exist by themselves. This is in strong contrast to the results obtained with bare couplings (see Sec. 6.5.1) and indicates that one effect of the FRG procedure is a reduction of the effective second-neighbour interaction strength. From Sec. 6.5.3, we know that the induced nearest-neighbour amplitudes suppress the possibility for existence of second-neighbour hoppings and pairings even further. Hence, there is no evidence for second-neighbour terms in a FRG analysis of the relevant coupling range.

Comparing the two different $\mathbb{Z}_2$ spin liquids from Eqs. (6.80) and (6.81), we observe once more a self-consistent solution with equal-sized hopping and pairing for both states. This is a fundamental property of our approach which cannot distinguish between two states that have identical flux patterns and are therefore gauge-equivalent. If treated solitarily, the hopping and the pairing patterns from each of the states Z2Azz13 or Z2Bzz13 have the same PSG and therefore must yield identical results. If considered together, the method still does not discriminate them and returns identical magnitudes as a consequence. In Fig. 6.11, we show the according self-consistent solutions for the overall amplitudes ξ [see Eq. (6.77)] as a function of Λ for $J_2/J_1 = 0.55$. Comparing the Λ dependence to the one on temperature in Fig. 6.9, we see that the curves appear qualitatively similar if $\Lambda \gtrsim 0.06\, J_1$ and $T \gtrsim 0.1\, J_1$. Only for smaller Λ, we observe a pronounced increase of both overall amplitudes obtained from the renormalised vertices. This increase is not present at low temperatures in the mean-field treatment. Again, the Z2Azz13 state is found to be dominant due to its larger amplitude in the entire investigated parameter range. We show how the maximal amplitudes in the limit $\Lambda \to 0$ of both considered states depend on J_2/J_1 in the inset of Fig. 6.11. In addition to the system's preference of the Z2Azz13 state, one verifies that both states remain stable throughout the paramagnetic regime, *i.e.*, $0.4 \lesssim J_2/J_1 \lesssim 0.6$. Outside this range, the maximal amplitudes start to become more and more suppressed until they vanish if $J_2/J_1 \leq 0.2$ or if $J_2/J_1 \geq 0.7$ which shows that their existence has to be directly connected to the presence of strong quantum fluctuations within our approach.

Due to the absence of the time-reversal symmetry breaking second neighbour pairing

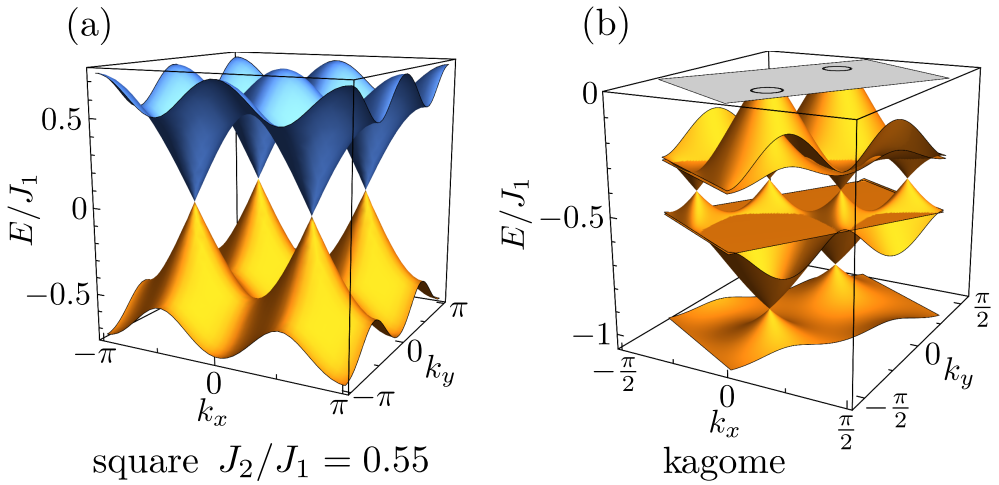

Figure 6.12.: Band structures from self-consistent Fock equations with FRG vertices in the limit $\Lambda \to 0$ for (a) J_1-J_2 Heisenberg model on the square lattice with $J_2/J_1 = 0.55$ and (b) nearest-neighbour Heisenberg model on the kagome lattice: We show the states dubbed Z2Azz13 for the square lattice and $\mathbb{Z}_2[0,\pi]\alpha$ for the kagome lattice which are preferred by our analysis. Both spectra are by definition particle-hole symmetric. In (b), we only show the six bands with negative energies to avoid confusion. Here, the first Brillouin zone (of an ansatz with a six-atomic unit cell) is indicated by a grey area on top of which black rings mark two small circular Fermi surfaces. *Figure created by Johannes Reuther.*

from Sec. 6.5.3, we conclude that the prediction of a chiral spin liquid is an artefact of the previous bare mean-field study. The FRG method yields the familiar $SU(2)$ π-flux state with four Dirac cones in the spinon dispersion at the wave vectors $\boldsymbol{k} = (\pm\pi/2, \pm\pi/2)$ indicating that the opening of a gap is suppressed by gauge fluctuations, see Fig. 6.12(a) for the corresponding band structure. A comparison to variational Monte Carlo studies shows a very good agreement on the nearest-neighbour level where the Z2Azz13 state also yields the best variational energies. On the other hand, for longer-ranged terms differences arise and VMC does predict an additional d-wave pairing term on fifth-neighbour bonds where our FRG procedure does not [52, 76]. In a very recent spin cluster perturbation and VMC study by Yu *et al.*, this result is confirmed in terms of the additional pairings. The paper however also indicates that nearest-neighbour hoppings and pairings differ in magnitude [191]. Despite these facts, all approaches so far verified the existence and the aforementioned positions of four Dirac cones in the frustrated J_1-J_2 Heisenberg model on the square lattice.

6.6. Nearest-neighbour Heisenberg model on the kagome lattice

Let us conclude this chapter by applying the newly developed FRG plus Fock mean-field method on the currently intensively discussed nearest-neighbour Heisenberg antiferromagnet on the kagome lattice which for spin-$\frac{1}{2}$ particles lies in a magnetically disordered phase, confer Fig. 4.8(a). While the existence of a paramagnetic phase is widely agreed on for more than three decades [107, 153, 173], the precise nature of its emergent spinon excitations as well as their associated gauge structure is a topic of ongoing debates until today. For instance, first DMRG studies predicted a gapped $\mathbb{Z}_2$ spin liquid [44, 94, 190], but rather recently the same method identified a gapless $U(1)$ Dirac spin liquid to be the realised state [71]. Similarly, tensor network studies do not yield conclusive results [110, 118]. From a third perspective, VMC simulations seem to agree that indeed the $U(1)$ Dirac spin liquid is realised [83, 85, 86, 140]. However, a strong energetic competition with the gapped $\mathbb{Z}_2$ spin liquid from DMRG is confirmed by this method as well [88].

In Sec. 6.2.5, we have already summarised the four $\mathbb{Z}_2$ and the three chiral states that on one hand can be stable against gauge fluctuations and on the other hand show compatible variational energies [83, 84, 140]. They were previously dubbed $\mathbb{Z}_2[0,0]B$, $\mathbb{Z}_2[\pi,0]A$, $\mathbb{Z}_2[0,\pi]\alpha$, $\mathbb{Z}_2[\pi,\pi]A$, Chiral-$[\frac{\pi}{2},0]$, Chiral-$[\pm\frac{\pi}{2},0]$, and Chiral-$[\frac{\pi}{2},\pi]$ and their real-space representations for specific gauges are shown in Figs. 6.1 and 6.2, respectively. In order to gain more knowledge about the effects of quantum fluctuations which are captured by the frequency renormalisation of the FRG vertex functions, we start our analysis of the kagome Heisenberg antiferromagnet with a stripped-down self-consistency method which still incorporates the bare interactions.

6.6.1. Bare vertex approximation

Due to the large unit cell of up to six atoms for the $\mathbb{Z}_2[\pi,0]A$, $\mathbb{Z}_2[0,\pi]\alpha$, and the Chiral-$[\frac{\pi}{2},0]$ ansätze with a resulting 12×12 matrix structure in Nambu space, an analytic treatment of the Matsubara sums as in the bare mean-field description of the square-lattice Heisenberg model in Sec. 6.3.5 is neither feasible nor would it provide any physical intuition for the system. Instead, we apply a reduced version of the final FRG mean-field formalism from Eqs. (6.76) in which the vertex functions are replaced with their parent expressions from a bare Heisenberg theory, *e.g.*, the expression $3\Gamma^{\Lambda\,\mathrm{s}}_{\boldsymbol{k}}+\Gamma^{\Lambda\,\mathrm{d}}_{\boldsymbol{k}}$ is set to $\frac{3J_{\boldsymbol{k}}}{4}$ in all frequency modes and the single-particle vertex $\gamma^{\Lambda}_{\mathrm{d}}(\omega)=0$ for the Green's function. This amounts to a plain mean-field analysis in the $T\to0$ limit where an artificial effective temperature Λ is generated via the propagator's Heaviside function.

The results of the bare vertex approximation can be seen in Fig. 6.13(a), where the overall nearest-neighbour amplitudes for the seven $\mathbb{Z}_2$ and chiral spin liquids are plotted as a function of Λ in the top panel. Our first and most important observation which also holds during the next sections is that, apart from the $\mathbb{Z}_2[0,\pi]\alpha$ state, all $\mathbb{Z}_2$ ansätze

do not develop a finite nearest-neighbour pairing η such that their gauge structure is in fact $U(1)$. For the $\mathbb{Z}_2[0,\pi]\alpha$ state, the ratio of nearest-neighbour hopping and pairing is $\frac{\chi}{\eta} \approx 2.13$ in the $\Lambda \to 0$ limit. Since a plethora of methods identify that state's $U(1)$ parent state denoted by U(1)$[0,\pi]$ as the preferred state for our model, we also compute the corresponding amplitude by setting $\eta = 0$ in the $\mathbb{Z}_2[0,\pi]\alpha$ ansatz. The result is also shown in Fig. 6.13. For a better visibility, we plot the differences in amplitude to the lowest one found, *i.e.*, the $\mathbb{Z}_2[\pi,\pi]A$ amplitude, in the lower panel of the figure. Here, we determine the $\mathbb{Z}_2[0,\pi]\alpha$ as the preferred state due to its largest amplitude. It is followed by the Chiral-$[\frac{\pi}{2},0]$ ansatz which interestingly shows a crossover with the U(1)$[0,\pi]$ and the $\mathbb{Z}_2[0,0]B$ state at finite Λ. However, since Λ is not a temperature, we can only interpret our results in the $\Lambda \to 0$ limit for the physical system. They agree with the findings of Refs. [70, 116] which suggest lower mean-field energies for the Chiral-$[\frac{\pi}{2},0]$ state than for the U(1)$[0,\pi]$ state. The sequence of remaining ansätze with descending amplitude is Chiral-$[\pm\frac{\pi}{2},0]$, Chiral-$[\frac{\pi}{2},\pi]$, $\mathbb{Z}_2[\pi,0]A$, and $\mathbb{Z}_2[\pi,\pi]A$ where the last three lie close together in the bottom range. How these observations are influenced by the effects of quantum fluctuations is investigated in the following section.

6.6.2. Results from FRG

We finally apply the PFFRG method on a hexagonal kagome lattice segment containing 251 lattice sites for finding the renormalised and frequency-resolved vertex functions $\Gamma_{\mathrm{s}}^{\Lambda}$ and $\Gamma_{\mathrm{d}}^{\Lambda}$. We use 120 discrete points for modeling the continuous Matsubara frequencies and set the initial conditions of the vertex functions to $\left(\Gamma_{\mathrm{s}}^{\Lambda\to\infty}, \Gamma_{\mathrm{d}}^{\Lambda\to\infty}\right) = \left(\frac{1}{4}, 0\right)$ for nearest neighbours and $\left(\Gamma_{\mathrm{s}}^{\Lambda\to\infty}, \Gamma_{\mathrm{d}}^{\Lambda\to\infty}\right) = (0,0)$ otherwise as described in Sec. 4.2.2. Note that again the resolution of the FRG numerics can be chosen much higher than in Chap. 4 because of the pure Heisenberg interaction and the resulting frequency symmetries as well as the reduced number of vertex functions. We then apply Eqs. (6.76) to the four $\mathbb{Z}_2$, the three chiral, and the sole parent $U(1)$ mean-field ansätze that were previously considered within the bare vertex approximation. The resulting nearest-neighbour amplitudes (amplitude differences with respect to $\mathbb{Z}_2[\pi,\pi]A$) can be seen in the top (bottom) panel of Fig. 6.13(b). A first comparison to the results from the previous section shows that the amplitudes now lie closer together indicating that quantum fluctuations lead to an increased competition between the different possible mean-field states. This is in good agreement with the observation of a plethora of competing low-energy states in Ref. [139].

Again, only the $\mathbb{Z}_2[0,\pi]\alpha$ state develops a finite nearest-neighbour pairing term with a similar ratio $\frac{\chi}{\eta} \approx 2.48$ as before. This ansatz also develops the largest amplitude within our method such that we identify it as the preferred state of the spin-$\frac{1}{2}$ kagome Heisenberg antiferromagnet. Its band structure can be seen in Fig. 6.12(b) where we only plot that part of the spectrum which has a negative energy in order to avoid confusion. Most remarkably, the $\mathbb{Z}_2[0,\pi]\alpha$ state with the suggested ratio of nearest-neighbour hopping and pairing is gapless but not Dirac like. Instead, the spectrum shows approximate Dirac cones with

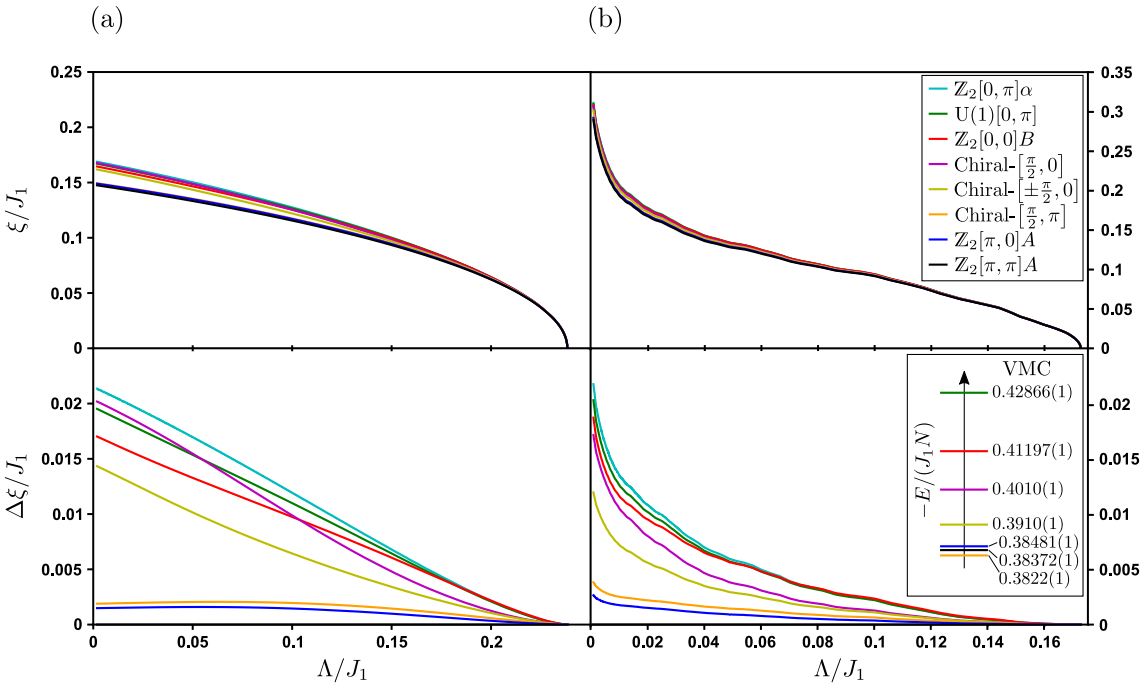

Figure 6.13.: Self-consistent results for chiral and non-chiral ansätze on the kagome lattice for (a) the bare vertex approximation and (b) the full FRG Fock mean-field treatment: In the top panel, we show the overall nearest-neighbour amplitude ξ as a function of Λ. Due to the very similar magnitudes, we plot the differences to the smallest ξ found for PSG $\mathbb{Z}_2[\pi,\pi]A$ in the lower panel. The corresponding gauge structures are discussed in Sec. 6.6.1. The inset shows the variational energies determined by VMC[83, 84, 140]. In this analysis, the $\mathbb{Z}_2[0,\pi]\alpha$ state is absent, confer main text. *Inset created by Johannes Reuther.*

method	BVA $\left[\frac{\xi^{\Lambda\to 0}}{J_1}\right]$	FRG $\left[\frac{\xi^{\Lambda\to 0}}{J_1}\right]$	VMC $\left[-\frac{E}{J_1 N}\right]$
$\mathbb{Z}_2[0,\pi]\alpha$	0.169	0.312	-
U(1)$[0,\pi]$	0.167	0.310	0.428
$\mathbb{Z}_2[0,0]B$	0.165	0.308	0.412
Chiral-$[\frac{\pi}{2},0]$	0.168	0.307	0.401
Chiral-$[\pm\frac{\pi}{2},0]$	0.162	0.301	0.391
Chiral-$[\frac{\pi}{2},\pi]$	0.150	0.293	0.382
$\mathbb{Z}_2[\pi,0]A$	0.149	0.292	0.384
$\mathbb{Z}_2[\pi,\pi]A$	0.148	0.289	0.383

Table 6.1.: Overall amplitudes in the $\Lambda \to 0$ limit and variational energies for the eight considered nearest-neighbour PSGs on the kagome lattice: The results are obtained via the bare vertex approximation (BVA), the full FRG plus Fock mean-field analysis (FRG), and VMC simulations from Refs. [83, 84, 140], respectively. A very good agreement is especially found between the FRG and VMC methods. Note that the best variational energy for the $\mathbb{Z}_2[0,\pi]\alpha$ state is achieved if $\eta = 0$, *i.e.*, for the U(1)$[0,\pi]$ state.

rounded tips for energies $E \lesssim 0.2\,J_1$. Unlike in the π-flux state in Fig. 6.12(a), these cones do not touch at the Fermi level but rather intersect with it. As a result, we find two small circular Fermi surfaces within the appropriately reduced Brillouin zone at zero energy which were not predicted so far by any other method.

The remaining states have a chiral or a $U(1)$ gauge structure and the sequence of descending overall amplitudes remains relatively unchanged as compared to the previous section. Only the crossover at finite Λ for the Chiral-$[\frac{\pi}{2},0]$ amplitude is now absent and seems to be an artefact of the bare vertex approximation. This state is now slightly less favourable than the $\mathbb{Z}_2[0,0]B$ state in agreement with VMC results [83, 84, 140]. In fact, the similarities between the magnitudes of our amplitudes and the variational energies from VMC are impressive and not expected *a priori* due to the quite distinct philosophies behind both methods (see Sec. 6.7 for a detailed discussion). Both methods identify almost the same hierarchy of states. One minor discrepancy is that VMC identifies the Chiral-$[\frac{\pi}{2},\pi]$ ansatz as the least probable one. Within our approach, it resides above the two $\mathbb{Z}_2$ ansätze in its close proximity though. More importantly, the PFFRG plus mean-field analysis determines a finite nearest-neighbour pairing term on top of the U(1)$[0,\pi]$ Dirac spin liquid which VMC does not find. This pairing not only yields an increased overall amplitude in our formalism, but it also limits possible gauge fluctuations to a $\mathbb{Z}_2$ type which might stabilise the according spin liquid (confer Sec. 6.2.2). The overall amplitudes at $\Lambda \approx 0$ from this and the previous section as well as the according variational energies per lattice site are summarised in Tab. 6.1.

6.6.3. Long-range terms on the kagome Heisenberg antiferromagnet

For the PSGs on the kagome lattice considered so far, there are plenty of allowed long-range and onsite terms [111] which, in principle, can follow from our self-consistency analysis. Due to the real-space structure of our Fock equations, they all vanish in the bare Heisenberg model since the J_{ij} are zero on the according lattice bonds. Despite the more spread-out structure of our FRG vertices, long-range and onsite terms are also not generated once the renormalised interactions are utilised because of a rapid decay in the interaction strength on longer-ranged bonds within the FRG. However, finite hoppings are found to be generated on such bonds in the presence of a finite nearest-neighbour hopping. The same statement holds separately for pairings as well. Considering our different PSGs, this implies that the gauge structure cannot be altered by onsite or longer-ranged terms within our approach since this would require finite pairing terms in a pure hopping model or *vice versa*. In addition, the new terms are two orders of magnitude smaller than the nearest-neighbour amplitudes and their effect on the spinon band structure can therefore be safely neglected. For completeness, we note that also onsite hoppings (pairings) are found with our method if allowed by the PSG. In complete analogy to the long-range terms, they are induced by finite nearest-neighbour hoppings (pairings), cannot alter the gauge structure of an ansatz, and their impact on the band structure is negligible.

6.7. Summary, discussion, and outlook

In this chapter, we unified two approaches for the investigation of frustrated quantum magnets which are both based on the Abrikosov decomposition of spin operators into pseudo fermions (spinons). Different $\mathbb{Z}_2$ and chiral spin liquid ansätze were obtained from a PSG classification [111, 182] and we compared their hopping and pairing amplitudes determined from a Fock-like self-consistency approach based on renormalised Green's functions and vertices. The defining Eq. (6.49) is form invariant under local gauge transformations [cf. Eq. (6.52)] such that all possible ansätze within one PSG yield identical physical results. This proves that our combined FRG plus Fock mean-field scheme is consistent with both utilised methods. In contrast to a plain mean-field analysis, the newly developed technique incorporates the effects of gauge fluctuations implicitly due to certain sets of Feynman diagrams that are additionally generated during the RG flow, see Sec. 4.2.1. Therefore, even though we are not directly computing the spinon-spinon interactions or the vison spectra of our models, these effects may still have an influence on the acquired results due to the incorporation of the frequency-resolved vertex functions Γ^Λ and Σ^Λ in the defining equations.

For the J_1-J_2 model on the square lattice, we identified the $SU(2)$ π-flux state [Fig. 6.12(a)] to be preferred over the chiral spin liquid found by the mean-field treatment of Ref. [182]. Therefore, we can conclude that the time-symmetry-breaking pairing term responsible for the finite spinon gap in Fig. 6.10 is an artefact arising from the negligence of gauge fluctu-

ations in the bare mean-field approach. Our numerics show that the π-flux state is realised in the entire paramagnetic regime of the spin-$\frac{1}{2}$ Heisenberg square lattice model whereas no finite hopping or pairing terms are found deep in the magnetically ordered phases. Hence, there seems to be a strong connection between magnetic frustration and quantum fluctuations on one side and effective free spinon models on the other side. A comparison with VMC studies shows good agreement on the nearest-neighbour level where VMC also finds the π-flux state to be preferred [76]. However, on longer-ranged bonds, we do strictly not observe finite amplitudes whereas VMC finds additional pairing terms on fifth-neighbour bonds [52, 76, 191].

On the kagome lattice, the $\mathbb{Z}_2[0,\pi]\alpha$ state with a ratio of $\frac{\chi}{\eta} \approx 2.48$ between nearest-neighbour hopping and pairing is found to be most likely realised. In the considered model, we also identify finite, but small additional terms on other bonds. Their influence on the spinon dispersion can be safely neglected though because they are two orders of magnitude smaller than the nearest-neighbour terms and they are also not capable of altering the IGG of the respective state. The band structure of the identified $\mathbb{Z}_2[0,\pi]\alpha$ state [Fig. 6.12(b)] features two small circular Fermi surfaces within the Brillouin zone which have not been reported by any other method so far. A comparison to VMC results shows strong similarities between the hierarchy of variational energies and the sequence of overall amplitudes derived from our method, confer lower panel of Fig. 6.13(b). This agreement is *a priori* unexpected since both methods explore rather distinct quantities. The combined PFFRG plus mean-field analysis calculates the spinon hoppings and pairings self consistently. This conceptually amounts to integrating out high-energy degrees of freedom in the FRG fashion and a subsequent determination of a matching low-energy theory for the renormalised vertex functions. On the other hand, VMC considers all distinct Hamiltonians which arise from a PSG classification. It then compares the respective ground-state energies after a Gutzwiller projection whilst optimising them with respect to the ratios of considered amplitudes. We do not compute spinon interactions and vison excitations explicitly which is why the results that are obtained with the new FRG mean-field scheme do not necessarily have competitive variational energies. The overall good agreement with VMC methods may therefore hint at possibly small corrections induced by gauge fluctuations as one would expect for $\mathbb{Z}_2$ and chiral spin liquids, see Sec. 6.2.2.

Overall, we have shown that the method developed in this chapter is generally a powerful tool for the characterisation of spinon band structures in magnetically disordered phases. Due to the fact that the FRG can access a large class of spin models, an extension to other lattices and interaction types is not only feasible but also desirable. For instance, a recent mean-field study by Laura Messio *et al.* suggests the realisation of a gapped chiral spin liquid in the Heisenberg-DM model on the kagome lattice (cf. Chap. 4) [123]. This work claims to reproduce the spin-structure factor by Han *et al.* [69] and it would be interesting to observe if and how this result is modified once renormalised vertices are included. Furthermore, the J_1-J_2-J_3 model on the square lattice is known to house a large paramagnetic and thus possible spin liquid phase [148] and there is evidence that a $\mathbb{Z}_2$

spin liquid might be realised for finite J_3/J_1 [24, 141, 154] instead of the π-flux state that we identified for the J_1-J_2 model. Remarkably, also the spin-$\frac{1}{2}$ J_1-J_2-J_3 Heisenberg model on the triangular lattice has attracted renewed interest in the seemingly unrelated context of twisted bilayer graphene [188]. In these systems, there seems to be a strong connection between spin liquids and superconductivity, and both phenomena might descend from the same physical principles at different filling factors. There are hence excellent perspectives for future applications of the combined PFFRG plus mean-field method, especially since PSG classifications of $\mathbb{Z}_2$ and chiral spin liquids already exist for the square, triangular, and kagome lattices [15, 122, 178, 182]. For frustrated three-dimensional lattices such as the pyrochlore or the hyper-hyper[3]-kagome lattice, an extension of the FRG has yet been accomplished. Unfortunately however, there are currently no PSG analyses available for these constructs and they might as well be very cumbersome due to the complexity of the involved loop structures in real space. Nevertheless, the newly derived method therefore provides us with a large class of interesting and explorable research topics for the near and also the distant future.

[3]It is astonishing how far people have made it with these two words in the past.

7. Summary and outlook

We extended the existing PFFRG framework [144, 147] for frustrated quantum spin systems in two important aspects during this thesis. After an introduction in Chap. 2 to all theoretical concepts relevant for our purposes, we derived the FRG flow equations for one and two-particle vertex functions in Chap. 3 which, in combination with a representation of spin operators in terms of Abrikosov pseudo fermions, are essential for the presented studies.

The first main part of our original work is the implementation of DM interactions within PFFRG, see Chap. 4. For the first time, we were able to incorporate off-diagonal spin couplings into the theory and showed that an extension of this method towards more realistic spin models is indeed possible. Apart from the resulting flow equations in App. B, one of the main results from this chapter is that a sizable DM coupling enlarges non-collinearly ordered phases [in particular the $\boldsymbol{q} = 0$ phase, cf. Fig. 4.2(b)] while shirking the paramagnetic phases of the underlying spin-$\frac{1}{2}$ J_1-J_2 Heisenberg model on the kagome lattice, see Fig. 4.8. Especially, the possible quantum spin liquid (QSL) phase of the nearest-neighbour antiferromagnet vanishes and $\boldsymbol{q} = 0$ Néel order is found for DM couplings $D \gtrsim 0.1\, J_1$. On one hand, this study is a proof of principle for the PFFRG's applicability to systems with arbitrary spin-spin interactions. On the other hand, the experimental motivation for this work is the investigation of the mineral *herbertsmithite* for which we obtain qualitatively good results by comparing the computed static spin susceptibility with the experimentally observed spin structure factor. Quantitatively, we find that the minimal model from Eq. (4.1) is insufficient to accurately describe this material due to the presence of magnetic impurities and inter-layer couplings. Our simulations suggest that *herbertsmithite* is, in fact, in close proximity to a quantum critical point. Furthermore, the analytic RPA solution from Sec. 4.3.1 has meanwhile provided more insight into the PFFRG procedure itself. It was shown by Laura Baez *et al.* that this solution corresponds to the large-S limit of our theory and that it yields the same results as the Luttinger-Tisza method which is exact in that limit for Bravais lattices. Together with the observation that the PFFRG for spin systems is also accurate in the large-N limit [19, 150], there is now much more evidence for the reliability of this method and also a clearer understanding of its working principle. Namely, it is based on a simultaneous and relatively unbiased incorporation of those sets of Feynman diagrams that are mainly responsible for magnetic long-range correlations and quantum fluctuations.

In Chap. 5, we used a combination of the PFFRG's arbitrary-S generalisation from Ref. [9] together with a simplified version of the aforementioned flow equations (confer App. C) in order to study the spin-1 XXZ model which is relevant for the A-site spinel $NiRh_2O_4$. Similar to *herbertsmithite* [73, 119, 165], also this substance shows no sign of magnetic long-range order down to lowest temperatures [30]. Hence, both materials are amongst the most promising candidates for finding a realistic QSL at the moment. Because the currently proposed spin couplings for $NiRh_2O_4$ are not yet reliably determined, we investigated two different model Hamiltonians [see Eqs. (5.2) and (5.7)] on the diamond lattice in order to characterise the paramagnetic phase which is the reason for the above

mentioned experimental observations. Both considered Hamiltonians amount to effective XXZ models with tetragonally split-up second-neighbour Heisenberg couplings which are required due to a lattice distortion at $T = 440\,K$ [30]. The Hamiltonian in Eq. (5.2) features an antiferromagnetic nearest-neighbour Heisenberg interaction and a single-ion anisotropy which has been implemented in this context for the first within PFFRG. For this model which was inspired by an online preprint of Ref. [30], we do observe an extended paramagnetic regime for finite, albeit small tetragonal splittings if a significant single-ion anisotropy is present, see Fig. 5.6. However, for strong splittings such as suggested by the motivating DFT analysis [29], we can only identify a conventionally Néel ordered state in the presence of reasonably-sized anisotropies. The same holds for the Hamiltonian in Eq. (5.7) which does not include single-ion terms and instead has an anisotropic XXZ interaction on first-neighbour bonds. Here, we did not map out an entire phase diagram and only considered the coupling strengths from Ref. [30]. Even though, our study confirmed the existence of a possible QSL phase within a wide parameter range of the spin-1 XXZ diamond lattice model with tetragonal splitting and single-ion anisotropy, we could not observe such a behaviour for the couplings that were estimated by the DFT and spin-wave analyses available momentarily. Therefore, we conclude that a more detailed analysis from first principles is desired in order to gain more knowledge about the promising properties of $NiRh_2O_4$.

The second main part of this thesis is contained in Chap. 6. Here, we utilised the important vertex functions which arise from a PFFRG analysis in order to determine the effective low-energy theory for the considered quantum spin models. This work is motivated by one of the most significant articles in the field by Xiao-Gang Wen [182]. Wen's PSG classification scheme which has been summarised in Sec. 6.2 provides different gauge-inequivalent free spinon models whose so-called IGGs are critical. As explained in Sec. 6.2.2, some of these effective models can be destabilised by gauge fluctuations which are neglected within the PSG approach. Only for $\mathbb{Z}_2$ and chiral spin liquids that follow from PSG considerations, there seems to be a general consensus about the fact that they are, at low energies, stable against such gauge fluctuations which are gapped for these models. Therefore, we developed a Fock-like mean-field method based on renormalised vertices that is capable of self-consistently computing spinon hopping and pairing amplitudes. Our approach is form invariant under time-independent local gauge transformations and therefore yields faithful physical results. The final set of equations can be seen in Eqs. (6.76). It was applied to all distinguishable $\mathbb{Z}_2$ spin liquids and a selection of relevant chiral spin liquids in the J_1-J_2 Heisenberg model on the square lattice and the nearest-neighbour Heisenberg model on the kagome lattice. In a simplified version of our method [Eqs. (6.59)], we were able to reproduce the results from a bare mean-field study in Ref. [182] for the square lattice model, see Fig. 6.9. The identified chiral spin liquid is fully gapped (Fig. 6.10), breaks time-reversal symmetry, and prevails if the antiferromagnetic second-neighbour Heisenberg interaction $J_2 > 0.45\,J_1$. The spinon gap and the chirality of this spin liquid are induced by a finite imaginary second-neighbour pairing. This term is absent in our simulations once the effects

of gauge fluctuations are implicitly included by considering the renormalised Green's and vertex functions. In this case, the $SU(2)$ π-flux state is preferred for all coupling ratios and the development of finite spinon hoppings is observed for $J_2/J_1 \in (0.2, 0.7)$. Because the mean-field amplitudes vanish deep inside the magnetically ordered phases, we are able to confirm that the existence of finite hoppings and pairings is related to the strong quantum fluctuations in magnetically frustrated systems. However, for a direct investigation of a confinement-deconfinement transition, spinon-spinon interactions and vison excitations should be considered explicitly. In the nearest-neighbour kagome lattice model, we found that most likely the $\mathbb{Z}_2[0,\pi]\alpha$ state accurately describes the system's low-energy properties since it develops the largest overall amplitudes. This state has two Dirac-like cones in its reduced Brillouin zone at energies $E \lesssim 0.2\,J_1$. In this range, the dispersion is almost linear, but the cones do not touch and rather intersect at zero energy which results in small circular Fermi surfaces at half filling, see Fig. 6.12(b). This has not yet been reported before. For the kagome lattice model, we observe a certain hierarchy of the overall amplitudes for different PSGs. Quite interestingly, this hierarchy agrees very well with the sequence of variational energies determined via VMC, confer bottom panel of Fig. 6.13(b). In fact, there are apparently only two important differences in the results obtained from both methods. The first one is that the Chiral-$[\frac{\pi}{2},\pi]$ state, which has the largest variational energy, occurs as the third-most unlikely state in our approach. The second significant difference between the PFFRG plus mean-field scheme and VMC lies in the results for the $\mathbb{Z}_2[0,\pi]\alpha$ state. Where our new analysis clearly favours this state with finite nearest-neighbour hoppings and pairings, VMC finds that its lowest variational energy is obtained for vanishing pairings in which case the parent state called $\mathrm{U}(1)[0,\pi]$ is realised. A detailed discussion on the differences of the two methods is given in Sec. 6.7. Even though the $\mathbb{Z}_2[0,\pi]\alpha$ spin liquid has already been classified by Lu *et al.* [111], we report, for the first time, that this state with a given ratio between nearest-neighbour hopping and pairing of $\frac{\chi}{\eta} \approx 2.48$ and the resulting band structure in Fig. 6.12(b) is found for the still debated kagome antiferromagnet. According to its IGG, this particular spin liquid should be more robust against gauge fluctuations than the $\mathrm{U}(1)[0,\pi]$ spin liquid identified by VMC or the $SU(2)$ π-flux state of the square lattice model. Thus, we can infer that the frustrated spin-$\frac{1}{2}$ kagome antiferromagnet is, to this day, one of the most promising systems in which a QSL might actually be realised. An extension of the theory to other lattices as well as to finite DM interactions should be pursued in the near future in order to characterise even more spin liquids in a, for the moment, fairly unbiased way. Additionally, one also should investigate how to experimentally verify or falsify the existence of small (circular) Fermi surfaces in an effective free spinon model and thereby check the validity of our method.

In total, we have shown that the PFFRG is a very flexible tool for the investigation of frustrated spin systems and that it also offers plenty of possibilities for further extensions and applications. With our studies of the spin models which approximately describe the materials *herbertsmithite* and $NiRh_2O_4$, we hopefully provided a small contribution to

the understanding of those phenomena that are responsible for a QSL behaviour. In future, this might be helpful to design more efficient high-T_c superconductors [6, 7] and quantum memory with higher fidelity [101]. Especially due to our implementation of more general spin interactions and the formulation of the self-consistency scheme for spinon band structures, we have given a novel perspective to prospectively seek and identify even more *new states of matter in strongly frustrated quantum magnets*.

A. Flow equations for Heisenberg vertices

Here, we summarise the PFFRG flow equations for the vertex functions of a bare spin-$\frac{1}{2}$ Heisenberg Hamiltonian [Eq. (1.1)]. The flow equations are obtained by inserting the parameterisations from Eqs. (4.8) and (4.13) into Eqs. (3.25) and (3.30), and by subsequently performing all Matsubara integrals that are trivial due to the proportionality of S^Λ to the Dirac delta distribution, see Eq. (4.12).

Let us start by providing the flow equation for the pseudo-fermion lifetime which determines the self energy [cf. Eq. (4.8)] and hence the single-particle propagators. It reads

$$\begin{aligned}\frac{\mathrm{d}}{\mathrm{d}\Lambda}\gamma^\Lambda_{\mathrm{d}\,i_1}(\omega_1) = -\frac{1}{2\pi}\sum_{\omega_2=\pm\Lambda}\Bigg\{\sum_j\left[2\Gamma^\Lambda_{\mathrm{d}\,i_1 j}(\omega_1,\omega_2;\omega_1,\omega_2)\left(\frac{1}{\omega_2+\gamma^\Lambda_{\mathrm{d}\,j}(\omega_2)}\right)\right]\\ -\left(\Gamma^\Lambda_{\mathrm{d}\,i_1 i_1}(\omega_1,\omega_2;\omega_2,\omega_1)+3\Gamma^\Lambda_{\mathrm{s}\,i_1 i_1}(\omega_1,\omega_2;\omega_2,\omega_1)\right)\left(\frac{1}{\omega_2+\gamma^\Lambda_{\mathrm{d}\,i_1}(\omega_2)}\right)\Bigg\}.\end{aligned} \tag{A.1}$$

Note that $\gamma^\Lambda_{\mathrm{d}}$ does not depend on its real-space index because we only consider a lattice of equivalent sites and i_1 can thus be chosen arbitrarily, confer Sec. 4.2.2.

For the flow of the two-particle vertex [Eq. (4.13)], we divide the contributions into spin and density channel. The following flow equations are more complex than the previous one, but in principle can still be presented in a rather compact form. For a compatibility with the equations for Heisenberg and DM interactions in App. B which involve a drastically increased number of vertex functions, we present a notation that groups all vertices with identical frequencies and indices into square brackets. The right-hand sides of these brackets then carry real-space and frequency arguments which are valid for all parenthesised vertex functions $\Gamma^\Lambda_{\mathrm{s/d}}$. Please note, that the order of arguments does matter. The exchanges, *e.g.*, $\Big[\omega_3 \leftrightarrow \omega_{2'}+\omega_3-\omega_2\Big]$, only act on the frequencies of the vertices, not on those of the propagators.

For the flow of the two-particle vertex' spin channel, we find that

$$
\begin{aligned}
\frac{\mathrm{d}}{\mathrm{d}\Lambda}\Gamma^{\Lambda}_{\mathrm{s}\,i_1 i_2}(\omega_{1'},\omega_{2'};\omega_1,\omega_2) = \frac{1}{2\pi}\int_{-\infty}^{\infty}\mathrm{d}\omega_3 \Big\{ & \\
& S^{\Lambda}(\omega_1+\omega_2-\omega_3)G^{\Lambda}(\omega_3)\Big[\Gamma^{\Lambda}_{\mathrm{s}}\Gamma^{\Lambda}_{\mathrm{d}}+\Gamma^{\Lambda}_{\mathrm{d}}\Gamma^{\Lambda}_{\mathrm{s}}-2\Gamma^{\Lambda}_{\mathrm{s}}\Gamma^{\Lambda}_{\mathrm{s}} \\
& \Big]_{(i_1,i_2)(i_1,i_2)}(\omega_{1'},\omega_{2'};\omega_3,\omega_1+\omega_2-\omega_3)(\omega_3,\omega_1+\omega_2-\omega_3;\omega_1,\omega_2) \\
& +\Big[\omega_3 \leftrightarrow \omega_1+\omega_2-\omega_3\Big] \\
& -2\sum_j S^{\Lambda}(\omega_{2'}+\omega_3-\omega_2)G^{\Lambda}(\omega_3)\Big[\Gamma^{\Lambda}_{\mathrm{s}}\Gamma^{\Lambda}_{\mathrm{s}} \\
& \Big]_{(i_1,j)(j,i_2)}(\omega_{1'},\omega_{2'}+\omega_3-\omega_2;\omega_1,\omega_3)(\omega_3,\omega_{2'};\omega_{2'}+\omega_3-\omega_2,\omega_2) \\
& -\Big[\omega_3 \leftrightarrow \omega_{2'}+\omega_3-\omega_2\Big] \\
& +S^{\Lambda}(\omega_{2'}+\omega_3-\omega_2)G^{\Lambda}(\omega_3)\Big[\Gamma^{\Lambda}_{\mathrm{s}}\Gamma^{\Lambda}_{\mathrm{d}}-\Gamma^{\Lambda}_{\mathrm{s}}\Gamma^{\Lambda}_{\mathrm{s}} \\
& \Big]_{(i_1,i_2)(i_2,i_2)}(\omega_{1'},\omega_{2'}+\omega_3-\omega_2;\omega_1,\omega_3)(\omega_3,\omega_{2'};\omega_2,\omega_{2'}+\omega_3-\omega_2) \\
& +\Big[\omega_3 \leftrightarrow \omega_{2'}+\omega_3-\omega_2\Big] \\
& +S^{\Lambda}(\omega_{2'}+\omega_3-\omega_2)G^{\Lambda}(\omega_3)\Big[\Gamma^{\Lambda}_{\mathrm{d}}\Gamma^{\Lambda}_{\mathrm{s}}-\Gamma^{\Lambda}_{\mathrm{s}}\Gamma^{\Lambda}_{\mathrm{s}} \\
& \Big]_{(i_1,i_1)(i_1,i_2)}(\omega_{1'},\omega_{2'}+\omega_3-\omega_2;\omega_3,\omega_1)(\omega_3,\omega_{2'};\omega_{2'}+\omega_3-\omega_2,\omega_2) \\
& +\Big[\omega_3 \leftrightarrow \omega_{2'}+\omega_3-\omega_2\Big] \\
& +S^{\Lambda}(\omega_{1'}+\omega_3-\omega_2)G^{\Lambda}(\omega_3)\Big[\Gamma^{\Lambda}_{\mathrm{s}}\Gamma^{\Lambda}_{\mathrm{d}}+\Gamma^{\Lambda}_{\mathrm{d}}\Gamma^{\Lambda}_{\mathrm{s}}+2\Gamma^{\Lambda}_{\mathrm{s}}\Gamma^{\Lambda}_{\mathrm{s}} \\
& \Big]_{(i_2,i_1)(i_2,i_1)}(\omega_{2'},\omega_{1'}+\omega_3-\omega_2;\omega_3,\omega_1)(\omega_3,\omega_{1'};\omega_2,\omega_{1'}+\omega_3-\omega_2) \\
& +\Big[\omega_3 \leftrightarrow \omega_{1'}+\omega_3-\omega_2\Big]\Big\}. \qquad \text{(A.2)}
\end{aligned}
$$

The flow equation of the corresponding density channel reads

$$\begin{aligned}
\frac{\mathrm{d}}{\mathrm{d}\Lambda}\Gamma^{\Lambda}_{\mathrm{d}\,i_1 i_2}(\omega_{1'},\omega_{2'};\omega_1,\omega_2) = \frac{1}{2\pi}\int_{-\infty}^{\infty}\mathrm{d}\omega_3 \Big\{ \\
& S^{\Lambda}(\omega_1+\omega_2-\omega_3)G^{\Lambda}(\omega_3)\Big[\Gamma^{\Lambda}_{\mathrm{d}}\Gamma^{\Lambda}_{\mathrm{d}} + 3\Gamma^{\Lambda}_{\mathrm{s}}\Gamma^{\Lambda}_{\mathrm{s}} \\
& \Big]_{(i_1,i_2)(i_1,i_2)}(\omega_{1'},\omega_{2'};\omega_3,\omega_1+\omega_2-\omega_3)(\omega_3,\omega_1+\omega_2-\omega_3;\omega_1,\omega_2) \\
& + \Big[\omega_3 \leftrightarrow \omega_1+\omega_2-\omega_3\Big] \\
& -2\sum_j S^{\Lambda}(\omega_{2'}+\omega_3-\omega_2)G^{\Lambda}(\omega_3)\Big[\Gamma^{\Lambda}_{\mathrm{d}}\Gamma^{\Lambda}_{\mathrm{d}} \\
& \Big]_{(i_1,j)(j,i_2)}(\omega_{1'},\omega_{2'}+\omega_3-\omega_2;\omega_1,\omega_3)(\omega_3,\omega_{2'};\omega_{2'}+\omega_3-\omega_2,\omega_2) \\
& - \Big[\omega_3 \leftrightarrow \omega_{2'}+\omega_3-\omega_2\Big] \\
& + S^{\Lambda}(\omega_{2'}+\omega_3-\omega_2)G^{\Lambda}(\omega_3)\Big[\Gamma^{\Lambda}_{\mathrm{d}}\left(\Gamma^{\Lambda}_{\mathrm{d}}+3\Gamma^{\Lambda}_{\mathrm{s}}\right) \\
& \Big]_{(i_1,i_2)(i_2,i_2)}(\omega_{1'},\omega_{2'}+\omega_3-\omega_2;\omega_1,\omega_3)(\omega_3,\omega_{2'};\omega_2,\omega_{2'}+\omega_3-\omega_2) \\
& + \Big[\omega_3 \leftrightarrow \omega_{2'}+\omega_3-\omega_2\Big] \\
& + S^{\Lambda}(\omega_{2'}+\omega_3-\omega_2)G^{\Lambda}(\omega_3)\Big[\left(\Gamma^{\Lambda}_{\mathrm{d}}+3\Gamma^{\Lambda}_{\mathrm{s}}\right)\Gamma^{\Lambda}_{\mathrm{d}} \\
& \Big]_{(i_1,i_1)(i_1,i_2)}(\omega_{1'},\omega_{2'}+\omega_3-\omega_2;\omega_3,\omega_1)(\omega_3,\omega_{2'};\omega_{2'}+\omega_3-\omega_2,\omega_2) \\
& + \Big[\omega_3 \leftrightarrow \omega_{2'}+\omega_3-\omega_2\Big] \\
& + S^{\Lambda}(\omega_{1'}+\omega_3-\omega_2)G^{\Lambda}(\omega_3)\Big[\Gamma^{\Lambda}_{\mathrm{d}}\Gamma^{\Lambda}_{\mathrm{d}} + 3\Gamma^{\Lambda}_{\mathrm{s}}\Gamma^{\Lambda}_{\mathrm{s}} \\
& \Big]_{(i_2,i_1)(i_2,i_1)}(\omega_{2'},\omega_{1'}+\omega_3-\omega_2;\omega_3,\omega_1)(\omega_3,\omega_{1'};\omega_2,\omega_{1'}+\omega_3-\omega_2) \\
& + \Big[\omega_3 \leftrightarrow \omega_{1'}+\omega_3-\omega_2\Big]\Big\}. \qquad \text{(A.3)}
\end{aligned}$$

These equations are already known since 2010 [144, 147]. Their extension to systems with Heisenberg and DM interactions is given in App. B.

B. Flow equations for Heisenberg and DM vertices

In this appendix, we provide the flow equations for the two different self-energy channels and the six vertex functions from the parameterisations in Eqs. (4.19) and (4.22) for a spin-$\frac{1}{2}$ model with Heisenberg and DM interactions. These equations are derived in the same way as the ones in App. A and we stick to the notation that is introduced there. The FRG equations for the self energy contributions are given by

$$\begin{aligned}
\frac{\mathrm{d}}{\mathrm{d}\Lambda}\gamma^{\Lambda}_{\mathrm{d}\,i_1}(\omega_1) = \frac{1}{2\pi}\sum_{\omega_2=\pm\Lambda}\Bigg\{\sum_j\Bigg[&-2\Gamma^{\Lambda}_{\mathrm{d}\,i_1 j}(\omega_1,\omega_2;\omega_1,\omega_2)\left(\frac{\omega_2+\gamma^{\Lambda}_{\mathrm{d}\,j}(\omega_2)}{(\gamma^{\Lambda}_{\mathrm{s}\,j}(\omega_2))^2+(\omega_2+\gamma^{\Lambda}_{\mathrm{d}\,j}(\omega_2))^2}\right)\\
&+2i\Gamma^{\Lambda}_{\mathrm{dz}i_1 j}(\omega_1,\omega_2;\omega_1,\omega_2)\left(\frac{\gamma^{\Lambda}_{\mathrm{s}\,j}(\omega_2)}{(\gamma^{\Lambda}_{\mathrm{s}\,j}(\omega_2))^2+(\omega_2+\gamma^{\Lambda}_{\mathrm{d}\,j}(\omega_2))^2}\right)\Bigg]\\
&+\Big[\Gamma^{\Lambda}_{\mathrm{d}\,i_1 i_1}(\omega_1,\omega_2;\omega_2,\omega_1)+2\Gamma^{\Lambda}_{\mathrm{xx}i_1 i_1}(\omega_1,\omega_2;\omega_2,\omega_1)+\Gamma^{\Lambda}_{\mathrm{zz}i_1 i_1}(\omega_1,\omega_2;\omega_2,\omega_1)\Big]\\
&\times\left(\frac{\omega_2+\gamma^{\Lambda}_{\mathrm{d}\,i_1}(\omega_2)}{(\gamma^{\Lambda}_{\mathrm{s}\,i_1}(\omega_2))^2+(\omega_2+\gamma^{\Lambda}_{\mathrm{d}\,i_1}(\omega_2))^2}\right)\\
&-\Big[i\Gamma^{\Lambda}_{\mathrm{zd}i_1 i_1}(\omega_1,\omega_2;\omega_2,\omega_1)+i\Gamma^{\Lambda}_{\mathrm{dz}i_1 i_1}(\omega_1,\omega_2;\omega_2,\omega_1)+2\Gamma^{\Lambda}_{s\times i_1 i_1}(\omega_1,\omega_2;\omega_2,\omega_1)\Big]\\
&\times\left(\frac{\gamma^{\Lambda}_{\mathrm{s}\,i_1}(\omega_2)}{(\gamma^{\Lambda}_{\mathrm{s}\,i_1}(\omega_2))^2+(\omega_2+\gamma^{\Lambda}_{\mathrm{d}\,i_1}(\omega_2))^2}\right)\Bigg\},
\end{aligned}\tag{B.1a}$$

$$\begin{aligned}
\frac{\mathrm{d}}{\mathrm{d}\Lambda}\gamma^{\Lambda}_{\mathrm{s}\,i_1}(\omega_1) = \frac{1}{2\pi}\sum_{\omega_2=\pm\Lambda}\Bigg\{\sum_j\Bigg[&2i\Gamma^{\Lambda}_{\mathrm{zd}i_1 j}(\omega_1,\omega_2;\omega_1,\omega_2)\left(\frac{\omega_2+\gamma^{\Lambda}_{\mathrm{d}\,j}(\omega_2)}{(\gamma^{\Lambda}_{\mathrm{s}\,j}(\omega_2))^2+(\omega_2+\gamma^{\Lambda}_{\mathrm{d}\,j}(\omega_2))^2}\right)\\
&+2\Gamma^{\Lambda}_{\mathrm{zz}i_1 j}(\omega_1,\omega_2;\omega_1,\omega_2)\left(\frac{\gamma^{\Lambda}_{\mathrm{s}\,j}(\omega_2)}{(\gamma^{\Lambda}_{\mathrm{s}\,j}(\omega_2))^2+(\omega_2+\gamma^{\Lambda}_{\mathrm{d}\,j}(\omega_2))^2}\right)\Bigg]\\
&-\Big[i\Gamma^{\Lambda}_{\mathrm{zd}i_1 i_1}(\omega_1,\omega_2;\omega_2,\omega_1)+i\Gamma^{\Lambda}_{\mathrm{dz}i_1 i_1}(\omega_1,\omega_2;\omega_2,\omega_1)-2\Gamma^{\Lambda}_{s\times i_1 i_1}(\omega_1,\omega_2;\omega_2,\omega_1)\Big]\\
&\times\left(\frac{\omega_2+\gamma^{\Lambda}_{\mathrm{d}\,i_1}(\omega_2)}{(\gamma^{\Lambda}_{\mathrm{s}\,i_1}(\omega_2))^2+(\omega_2+\gamma^{\Lambda}_{\mathrm{d}\,i_1}(\omega_2))^2}\right)\\
&-\Big[\Gamma^{\Lambda}_{\mathrm{d}\,i_1 i_1}(\omega_1,\omega_2;\omega_2,\omega_1)-2\Gamma^{\Lambda}_{\mathrm{xx}i_1 i_1}(\omega_1,\omega_2;\omega_2,\omega_1)+\Gamma^{\Lambda}_{\mathrm{zz}i_1 i_1}(\omega_1,\omega_2;\omega_2,\omega_1)\Big]\\
&\times\left(\frac{\gamma^{\Lambda}_{\mathrm{s}\,i_1}(\omega_2)}{(\gamma^{\Lambda}_{\mathrm{s}\,i_1}(\omega_2))^2+(\omega_2+\gamma^{\Lambda}_{\mathrm{d}\,i_1}(\omega_2))^2}\right)\Bigg\},
\end{aligned}\tag{B.1b}$$

As for a Heisenberg system, $\gamma^{\Lambda}_{\mathrm{d}}$ and $\gamma^{\Lambda}_{\mathrm{s}}$ do not depend on the specific choice of i_1 for the considered lattices of equivalent sites.

Due to the two self-energy sectors, the propagators G^{Λ} and S^{Λ} acquire a spin and a density channel, confer Eqs. (4.20a) and (4.21a). Therefore, the frequency arguments of the propagators are now gathered on the left-hand side of each square bracket. Here, we denote the frequencies of $S^{\Lambda}_{\mathrm{d/s}}$ and $G^{\Lambda}_{\mathrm{d/s}}$ in that order. As in App. A, the right-hand side denotes the arguments for the different vertices. Again, one should pay attention to the

fact that the order matters. The exchanges $\left[\omega_3 \leftrightarrow \omega_{2'}+\omega_3-\omega_2\right]$ only act on the frequencies of the vertices and have no effect on the propagators.

The FRG analysis yields for the different vertex functions from (4.22) the following results (turn page).

$$
\begin{aligned}
\frac{\mathrm{d}}{\mathrm{d}\Lambda}\Gamma^{\Lambda}_{\mathrm{d}\,i_1 i_2}(\omega_{1'},\omega_{2'};\omega_1,\omega_2) = \frac{1}{2\pi}\int_{-\infty}^{\infty}\mathrm{d}\omega_3 \Bigg\{ & (\omega_1+\omega_2-\omega_3)(\omega_3)\Big[\\
& S^{\Lambda}_{\mathrm{d}} G^{\Lambda}_{\mathrm{d}} \left(\Gamma^{\Lambda}_{\mathrm{d}}\Gamma^{\Lambda}_{\mathrm{d}} + \Gamma^{\Lambda}_{\mathrm{zd}}\Gamma^{\Lambda}_{\mathrm{zd}} + \Gamma^{\Lambda}_{\mathrm{dz}}\Gamma^{\Lambda}_{\mathrm{dz}} + \Gamma^{\Lambda}_{\mathrm{zz}}\Gamma^{\Lambda}_{\mathrm{zz}} + 2\Gamma^{\Lambda}_{\mathrm{xx}}\Gamma^{\Lambda}_{\mathrm{xx}} + 2\Gamma^{\Lambda}_{\mathrm{DM}}\Gamma^{\Lambda}_{\mathrm{DM}}\right) \\
& + S^{\Lambda}_{\mathrm{d}} G^{\Lambda}_{\mathrm{s}} \left(\Gamma^{\Lambda}_{\mathrm{zd}}\Gamma^{\Lambda}_{\mathrm{d}} + \Gamma^{\Lambda}_{\mathrm{d}}\Gamma^{\Lambda}_{\mathrm{zd}} + \Gamma^{\Lambda}_{\mathrm{zz}}\Gamma^{\Lambda}_{\mathrm{dz}} + \Gamma^{\Lambda}_{\mathrm{dz}}\Gamma^{\Lambda}_{\mathrm{zz}} - 2i\Gamma^{\Lambda}_{\mathrm{DM}}\Gamma^{\Lambda}_{\mathrm{xx}} + 2i\Gamma^{\Lambda}_{\mathrm{xx}}\Gamma^{\Lambda}_{\mathrm{DM}}\right) \\
& + S^{\Lambda}_{\mathrm{s}} G^{\Lambda}_{\mathrm{d}} \left(\Gamma^{\Lambda}_{\mathrm{dz}}\Gamma^{\Lambda}_{\mathrm{d}} + \Gamma^{\Lambda}_{\mathrm{d}}\Gamma^{\Lambda}_{\mathrm{dz}} + \Gamma^{\Lambda}_{\mathrm{zz}}\Gamma^{\Lambda}_{\mathrm{zd}} + \Gamma^{\Lambda}_{\mathrm{zd}}\Gamma^{\Lambda}_{\mathrm{zz}} + 2i\Gamma^{\Lambda}_{\mathrm{DM}}\Gamma^{\Lambda}_{\mathrm{xx}} - 2i\Gamma^{\Lambda}_{\mathrm{xx}}\Gamma^{\Lambda}_{\mathrm{DM}}\right) \\
& + S^{\Lambda}_{\mathrm{s}} G^{\Lambda}_{\mathrm{s}} \left(\Gamma^{\Lambda}_{\mathrm{dz}}\Gamma^{\Lambda}_{\mathrm{zd}} + \Gamma^{\Lambda}_{\mathrm{zd}}\Gamma^{\Lambda}_{\mathrm{dz}} + \Gamma^{\Lambda}_{\mathrm{zz}}\Gamma^{\Lambda}_{\mathrm{d}} + \Gamma^{\Lambda}_{\mathrm{d}}\Gamma^{\Lambda}_{\mathrm{zz}} - 2\Gamma^{\Lambda}_{\mathrm{xx}}\Gamma^{\Lambda}_{\mathrm{xx}} - 2\Gamma^{\Lambda}_{\mathrm{DM}}\Gamma^{\Lambda}_{\mathrm{DM}}\right) \\
& \Big]_{(i_1,i_2)(i_1,i_2)}(\omega_{1'},\omega_{2'};\omega_3,\omega_1+\omega_2-\omega_3)(\omega_3,\omega_1+\omega_2-\omega_3;\omega_1,\omega_2) \\
& + (\omega_1+\omega_2-\omega_3)(\omega_3)\Big[\\
& S^{\Lambda}_{\mathrm{d}} G^{\Lambda}_{\mathrm{d}} \left(\Gamma^{\Lambda}_{\mathrm{d}}\Gamma^{\Lambda}_{\mathrm{d}} + \Gamma^{\Lambda}_{\mathrm{zd}}\Gamma^{\Lambda}_{\mathrm{zd}} + \Gamma^{\Lambda}_{\mathrm{dz}}\Gamma^{\Lambda}_{\mathrm{dz}} + \Gamma^{\Lambda}_{\mathrm{zz}}\Gamma^{\Lambda}_{\mathrm{zz}} + 2\Gamma^{\Lambda}_{\mathrm{xx}}\Gamma^{\Lambda}_{\mathrm{xx}} + 2\Gamma^{\Lambda}_{\mathrm{DM}}\Gamma^{\Lambda}_{\mathrm{DM}}\right) \\
& + S^{\Lambda}_{\mathrm{d}} G^{\Lambda}_{\mathrm{s}} \left(\Gamma^{\Lambda}_{\mathrm{dz}}\Gamma^{\Lambda}_{\mathrm{d}} + \Gamma^{\Lambda}_{\mathrm{d}}\Gamma^{\Lambda}_{\mathrm{dz}} + \Gamma^{\Lambda}_{\mathrm{zz}}\Gamma^{\Lambda}_{\mathrm{zd}} + \Gamma^{\Lambda}_{\mathrm{zd}}\Gamma^{\Lambda}_{\mathrm{zz}} + 2i\Gamma^{\Lambda}_{\mathrm{DM}}\Gamma^{\Lambda}_{\mathrm{xx}} - 2i\Gamma^{\Lambda}_{\mathrm{xx}}\Gamma^{\Lambda}_{\mathrm{DM}}\right) \\
& + S^{\Lambda}_{\mathrm{s}} G^{\Lambda}_{\mathrm{d}} \left(\Gamma^{\Lambda}_{\mathrm{zd}}\Gamma^{\Lambda}_{\mathrm{d}} + \Gamma^{\Lambda}_{\mathrm{d}}\Gamma^{\Lambda}_{\mathrm{zd}} + \Gamma^{\Lambda}_{\mathrm{zz}}\Gamma^{\Lambda}_{\mathrm{dz}} + \Gamma^{\Lambda}_{\mathrm{dz}}\Gamma^{\Lambda}_{\mathrm{zz}} - 2i\Gamma^{\Lambda}_{\mathrm{DM}}\Gamma^{\Lambda}_{\mathrm{xx}} + 2i\Gamma^{\Lambda}_{\mathrm{xx}}\Gamma^{\Lambda}_{\mathrm{DM}}\right) \\
& + S^{\Lambda}_{\mathrm{s}} G^{\Lambda}_{\mathrm{s}} \left(\Gamma^{\Lambda}_{\mathrm{dz}}\Gamma^{\Lambda}_{\mathrm{zd}} + \Gamma^{\Lambda}_{\mathrm{zd}}\Gamma^{\Lambda}_{\mathrm{dz}} + \Gamma^{\Lambda}_{\mathrm{zz}}\Gamma^{\Lambda}_{\mathrm{d}} + \Gamma^{\Lambda}_{\mathrm{d}}\Gamma^{\Lambda}_{\mathrm{zz}} - 2\Gamma^{\Lambda}_{\mathrm{xx}}\Gamma^{\Lambda}_{\mathrm{xx}} - 2\Gamma^{\Lambda}_{\mathrm{DM}}\Gamma^{\Lambda}_{\mathrm{DM}}\right) \\
& \Big]_{(i_1,i_2)(i_1,i_2)}(\omega_{1'},\omega_{2'};\omega_1+\omega_2-\omega_3,\omega_3)(\omega_1+\omega_2-\omega_3,\omega_3;\omega_1,\omega_2) \\
& - 2\sum_j (\omega_{2'}+\omega_3-\omega_2)(\omega_3)\Big[\\
& S^{\Lambda}_{\mathrm{d}} \Big(G^{\Lambda}_{\mathrm{d}} \left(\Gamma^{\Lambda}_{\mathrm{d}}\Gamma^{\Lambda}_{\mathrm{d}} + \Gamma^{\Lambda}_{\mathrm{dz}}\Gamma^{\Lambda}_{\mathrm{zd}}\right) + G^{\Lambda}_{\mathrm{s}} \left(\Gamma^{\Lambda}_{\mathrm{d}}\Gamma^{\Lambda}_{\mathrm{zd}} + \Gamma^{\Lambda}_{\mathrm{dz}}\Gamma^{\Lambda}_{\mathrm{d}}\right) \Big) \\
& + S^{\Lambda}_{\mathrm{s}} \Big(G^{\Lambda}_{\mathrm{d}} \left(\Gamma^{\Lambda}_{\mathrm{d}}\Gamma^{\Lambda}_{\mathrm{zd}} + \Gamma^{\Lambda}_{\mathrm{dz}}\Gamma^{\Lambda}_{\mathrm{d}}\right) + G^{\Lambda}_{\mathrm{s}} \left(\Gamma^{\Lambda}_{\mathrm{d}}\Gamma^{\Lambda}_{\mathrm{d}} + \Gamma^{\Lambda}_{\mathrm{dz}}\Gamma^{\Lambda}_{\mathrm{zd}}\right) \Big) \\
& \Big]_{(i_1,j)(j,i_2)}(\omega_{1'},\omega_{2'}+\omega_3-\omega_2;\omega_1,\omega_3)(\omega_3,\omega_{2'};\omega_{2'}+\omega_3-\omega_2,\omega_2) \\
& - \Big[\omega_3 \leftrightarrow \omega_{2'}+\omega_3-\omega_2\Big] \\
& + (\omega_{2'}+\omega_3-\omega_2)(\omega_3)\Big[\\
& S^{\Lambda}_{\mathrm{d}} G^{\Lambda}_{\mathrm{d}} \left(\Gamma^{\Lambda}_{\mathrm{d}}(\Gamma^{\Lambda}_{\mathrm{d}} + \Gamma^{\Lambda}_{\mathrm{zz}} + 2\Gamma^{\Lambda}_{\mathrm{xx}}) + \Gamma^{\Lambda}_{\mathrm{dz}}(\Gamma^{\Lambda}_{\mathrm{zd}} + \Gamma^{\Lambda}_{\mathrm{dz}} + 2i\Gamma^{\Lambda}_{\mathrm{DM}})\right) \\
& + S^{\Lambda}_{\mathrm{d}} G^{\Lambda}_{\mathrm{s}} \left(\Gamma^{\Lambda}_{\mathrm{dz}}(\Gamma^{\Lambda}_{\mathrm{d}} + \Gamma^{\Lambda}_{\mathrm{zz}} + 2\Gamma^{\Lambda}_{\mathrm{xx}}) + \Gamma^{\Lambda}_{\mathrm{d}}(\Gamma^{\Lambda}_{\mathrm{zd}} + \Gamma^{\Lambda}_{\mathrm{dz}} + 2i\Gamma^{\Lambda}_{\mathrm{DM}})\right) \\
& + S^{\Lambda}_{\mathrm{s}} G^{\Lambda}_{\mathrm{d}} \left(\Gamma^{\Lambda}_{\mathrm{dz}}(\Gamma^{\Lambda}_{\mathrm{d}} + \Gamma^{\Lambda}_{\mathrm{zz}} + 2\Gamma^{\Lambda}_{\mathrm{xx}}) + \Gamma^{\Lambda}_{\mathrm{d}}(\Gamma^{\Lambda}_{\mathrm{zd}} + \Gamma^{\Lambda}_{\mathrm{dz}} + 2i\Gamma^{\Lambda}_{\mathrm{DM}})\right) \\
& + S^{\Lambda}_{\mathrm{s}} G^{\Lambda}_{\mathrm{s}} \left(\Gamma^{\Lambda}_{\mathrm{d}}(\Gamma^{\Lambda}_{\mathrm{d}} + \Gamma^{\Lambda}_{\mathrm{zz}} + 2\Gamma^{\Lambda}_{\mathrm{xx}}) + \Gamma^{\Lambda}_{\mathrm{dz}}(\Gamma^{\Lambda}_{\mathrm{zd}} + \Gamma^{\Lambda}_{\mathrm{dz}} + 2i\Gamma^{\Lambda}_{\mathrm{DM}})\right) \\
& \Big]_{(i_1,i_2)(i_2,i_2)}(\omega_{1'},\omega_{2'}+\omega_3-\omega_2;\omega_1,\omega_3)(\omega_3,\omega_{2'};\omega_2,\omega_{2'}+\omega_3-\omega_2) \\
& + \Big[\omega_3 \leftrightarrow \omega_{2'}+\omega_3-\omega_2\Big]
\end{aligned}
$$

$$
\begin{aligned}
&+(\omega_{2'}+\omega_3-\omega_2)(\omega_3)\Big[\\
&\quad S_{\mathrm{d}}^{\Lambda}G_{\mathrm{d}}^{\Lambda}\left((\Gamma_{\mathrm{d}}^{\Lambda}+\Gamma_{\mathrm{zz}}^{\Lambda}+2\Gamma_{\mathrm{xx}}^{\Lambda})\Gamma_{\mathrm{d}}^{\Lambda}+(\Gamma_{\mathrm{zd}}^{\Lambda}+\Gamma_{\mathrm{dz}}^{\Lambda}-2i\Gamma_{\mathrm{DM}}^{\Lambda})\Gamma_{\mathrm{zd}}^{\Lambda}\right)\\
&+S_{\mathrm{d}}^{\Lambda}G_{\mathrm{s}}^{\Lambda}\left((\Gamma_{\mathrm{d}}^{\Lambda}+\Gamma_{\mathrm{zz}}^{\Lambda}+2\Gamma_{\mathrm{xx}}^{\Lambda})\Gamma_{\mathrm{zd}}^{\Lambda}+(\Gamma_{\mathrm{zd}}^{\Lambda}+\Gamma_{\mathrm{dz}}^{\Lambda}-2i\Gamma_{\mathrm{DM}}^{\Lambda})\Gamma_{\mathrm{d}}^{\Lambda}\right)\\
&+S_{\mathrm{s}}^{\Lambda}G_{\mathrm{d}}^{\Lambda}\left((\Gamma_{\mathrm{d}}^{\Lambda}+\Gamma_{\mathrm{zz}}^{\Lambda}+2\Gamma_{\mathrm{xx}}^{\Lambda})\Gamma_{\mathrm{zd}}^{\Lambda}+(\Gamma_{\mathrm{zd}}^{\Lambda}+\Gamma_{\mathrm{dz}}^{\Lambda}-2i\Gamma_{\mathrm{DM}}^{\Lambda})\Gamma_{\mathrm{d}}^{\Lambda}\right)\\
&+S_{\mathrm{s}}^{\Lambda}G_{\mathrm{s}}^{\Lambda}\left((\Gamma_{\mathrm{d}}^{\Lambda}+\Gamma_{\mathrm{zz}}^{\Lambda}+2\Gamma_{\mathrm{xx}}^{\Lambda})\Gamma_{\mathrm{d}}^{\Lambda}+(\Gamma_{\mathrm{zd}}^{\Lambda}+\Gamma_{\mathrm{dz}}^{\Lambda}-2i\Gamma_{\mathrm{DM}}^{\Lambda})\Gamma_{\mathrm{zd}}^{\Lambda}\right)\\
&\quad\Big]_{(i_1,i_1)(i_1,i_2)}(\omega_{1'},\omega_{2'}+\omega_3-\omega_2;\omega_3,\omega_1)(\omega_3,\omega_{2'};\omega_{2'}+\omega_3-\omega_2,\omega_2)\\
&+\Big[\omega_3\leftrightarrow\omega_{2'}+\omega_3-\omega_2\Big]\\
&+(\omega_{1'}+\omega_3-\omega_2)(\omega_3)\Big[\\
&\quad S_{\mathrm{d}}^{\Lambda}G_{\mathrm{d}}^{\Lambda}\left(\Gamma_{\mathrm{d}}^{\Lambda}\Gamma_{\mathrm{d}}^{\Lambda}+\Gamma_{\mathrm{zd}}^{\Lambda}\Gamma_{\mathrm{zd}}^{\Lambda}+\Gamma_{\mathrm{dz}}^{\Lambda}\Gamma_{\mathrm{dz}}^{\Lambda}+\Gamma_{\mathrm{zz}}^{\Lambda}\Gamma_{\mathrm{zz}}^{\Lambda}+2\Gamma_{\mathrm{xx}}^{\Lambda}\Gamma_{\mathrm{xx}}^{\Lambda}+2\Gamma_{\mathrm{DM}}^{\Lambda}\Gamma_{\mathrm{DM}}^{\Lambda}\right)\\
&+S_{\mathrm{d}}^{\Lambda}G_{\mathrm{s}}^{\Lambda}\left(\Gamma_{\mathrm{zd}}^{\Lambda}\Gamma_{\mathrm{d}}^{\Lambda}+\Gamma_{\mathrm{d}}^{\Lambda}\Gamma_{\mathrm{zd}}^{\Lambda}+\Gamma_{\mathrm{zz}}^{\Lambda}\Gamma_{\mathrm{dz}}^{\Lambda}+\Gamma_{\mathrm{dz}}^{\Lambda}\Gamma_{\mathrm{zz}}^{\Lambda}-2i\Gamma_{\mathrm{DM}}^{\Lambda}\Gamma_{\mathrm{xx}}^{\Lambda}+2i\Gamma_{\mathrm{xx}}^{\Lambda}\Gamma_{\mathrm{DM}}^{\Lambda}\right)\\
&+S_{\mathrm{s}}^{\Lambda}G_{\mathrm{d}}^{\Lambda}\left(\Gamma_{\mathrm{dz}}^{\Lambda}\Gamma_{\mathrm{d}}^{\Lambda}+\Gamma_{\mathrm{d}}^{\Lambda}\Gamma_{\mathrm{dz}}^{\Lambda}+\Gamma_{\mathrm{zz}}^{\Lambda}\Gamma_{\mathrm{zd}}^{\Lambda}+\Gamma_{\mathrm{zd}}^{\Lambda}\Gamma_{\mathrm{zz}}^{\Lambda}-2i\Gamma_{\mathrm{DM}}^{\Lambda}\Gamma_{\mathrm{xx}}^{\Lambda}+2i\Gamma_{\mathrm{xx}}^{\Lambda}\Gamma_{\mathrm{DM}}^{\Lambda}\right)\\
&+S_{\mathrm{s}}^{\Lambda}G_{\mathrm{s}}^{\Lambda}\left(\Gamma_{\mathrm{dz}}^{\Lambda}\Gamma_{\mathrm{zd}}^{\Lambda}+\Gamma_{\mathrm{zd}}^{\Lambda}\Gamma_{\mathrm{dz}}^{\Lambda}+\Gamma_{\mathrm{zz}}^{\Lambda}\Gamma_{\mathrm{d}}^{\Lambda}+\Gamma_{\mathrm{d}}^{\Lambda}\Gamma_{\mathrm{zz}}^{\Lambda}+2\Gamma_{\mathrm{xx}}^{\Lambda}\Gamma_{\mathrm{xx}}^{\Lambda}+2\Gamma_{\mathrm{DM}}^{\Lambda}\Gamma_{\mathrm{DM}}^{\Lambda}\right)\\
&\quad\Big]_{(i_2,i_1)(i_2,i_1)}(\omega_{2'},\omega_{1'}+\omega_3-\omega_2;\omega_3,\omega_1)(\omega_3,\omega_{1'};\omega_2,\omega_{1'}+\omega_3-\omega_2)\\
&+(\omega_{1'}+\omega_3-\omega_2)(\omega_3)\Big[\\
&\quad S_{\mathrm{d}}^{\Lambda}G_{\mathrm{d}}^{\Lambda}\left(\Gamma_{\mathrm{d}}^{\Lambda}\Gamma_{\mathrm{d}}^{\Lambda}+\Gamma_{\mathrm{zd}}^{\Lambda}\Gamma_{\mathrm{zd}}^{\Lambda}+\Gamma_{\mathrm{dz}}^{\Lambda}\Gamma_{\mathrm{dz}}^{\Lambda}+\Gamma_{\mathrm{zz}}^{\Lambda}\Gamma_{\mathrm{zz}}^{\Lambda}+2\Gamma_{\mathrm{xx}}^{\Lambda}\Gamma_{\mathrm{xx}}^{\Lambda}+2\Gamma_{\mathrm{DM}}^{\Lambda}\Gamma_{\mathrm{DM}}^{\Lambda}\right)\\
&+S_{\mathrm{d}}^{\Lambda}G_{\mathrm{s}}^{\Lambda}\left(\Gamma_{\mathrm{dz}}^{\Lambda}\Gamma_{\mathrm{d}}^{\Lambda}+\Gamma_{\mathrm{d}}^{\Lambda}\Gamma_{\mathrm{dz}}^{\Lambda}+\Gamma_{\mathrm{zz}}^{\Lambda}\Gamma_{\mathrm{zd}}^{\Lambda}+\Gamma_{\mathrm{zd}}^{\Lambda}\Gamma_{\mathrm{zz}}^{\Lambda}-2i\Gamma_{\mathrm{DM}}^{\Lambda}\Gamma_{\mathrm{xx}}^{\Lambda}+2i\Gamma_{\mathrm{xx}}^{\Lambda}\Gamma_{\mathrm{DM}}^{\Lambda}\right)\\
&+S_{\mathrm{s}}^{\Lambda}G_{\mathrm{d}}^{\Lambda}\left(\Gamma_{\mathrm{zd}}^{\Lambda}\Gamma_{\mathrm{d}}^{\Lambda}+\Gamma_{\mathrm{d}}^{\Lambda}\Gamma_{\mathrm{zd}}^{\Lambda}+\Gamma_{\mathrm{zz}}^{\Lambda}\Gamma_{\mathrm{dz}}^{\Lambda}+\Gamma_{\mathrm{dz}}^{\Lambda}\Gamma_{\mathrm{zz}}^{\Lambda}-2i\Gamma_{\mathrm{DM}}^{\Lambda}\Gamma_{\mathrm{xx}}^{\Lambda}+2i\Gamma_{\mathrm{xx}}^{\Lambda}\Gamma_{\mathrm{DM}}^{\Lambda}\right)\\
&+S_{\mathrm{s}}^{\Lambda}G_{\mathrm{s}}^{\Lambda}\left(\Gamma_{\mathrm{dz}}^{\Lambda}\Gamma_{\mathrm{zd}}^{\Lambda}+\Gamma_{\mathrm{zd}}^{\Lambda}\Gamma_{\mathrm{dz}}^{\Lambda}+\Gamma_{\mathrm{zz}}^{\Lambda}\Gamma_{\mathrm{d}}^{\Lambda}+\Gamma_{\mathrm{d}}^{\Lambda}\Gamma_{\mathrm{zz}}^{\Lambda}+2\Gamma_{\mathrm{xx}}^{\Lambda}\Gamma_{\mathrm{xx}}^{\Lambda}+2\Gamma_{\mathrm{DM}}^{\Lambda}\Gamma_{\mathrm{DM}}^{\Lambda}\right)\\
&\quad\Big]_{(i_2,i_1)(i_2,i_1)}(\omega_{2'},\omega_3;\omega_{1'}+\omega_3-\omega_2,\omega_1)(\omega_{1'}+\omega_3-\omega_2,\omega_{1'};\omega_2,\omega_3)\Bigg\}
\end{aligned}
\tag{B.2}
$$

$$
\begin{aligned}
\frac{\mathrm{d}}{\mathrm{d}\Lambda}\Gamma^{\Lambda}_{\mathrm{zd}i_1i_2}(\omega_{1'},\omega_{2'};\omega_1,\omega_2) = \frac{1}{2\pi}\int_{-\infty}^{\infty}\mathrm{d}\omega_3 \Big\{ & (\omega_1+\omega_2-\omega_3)(\omega_3)\Big[\\
& S^{\Lambda}_{\mathrm{d}}G^{\Lambda}_{\mathrm{d}}\left(\Gamma^{\Lambda}_{\mathrm{zd}}\Gamma^{\Lambda}_{\mathrm{d}}+\Gamma^{\Lambda}_{\mathrm{d}}\Gamma^{\Lambda}_{\mathrm{zd}}+\Gamma^{\Lambda}_{\mathrm{zz}}\Gamma^{\Lambda}_{\mathrm{dz}}+\Gamma^{\Lambda}_{\mathrm{dz}}\Gamma^{\Lambda}_{\mathrm{zz}}+2i\Gamma^{\Lambda}_{\mathrm{DM}}\Gamma^{\Lambda}_{\mathrm{xx}}-2i\Gamma^{\Lambda}_{\mathrm{xx}}\Gamma^{\Lambda}_{\mathrm{DM}}\right) \\
& +S^{\Lambda}_{\mathrm{d}}G^{\Lambda}_{\mathrm{s}}\left(\Gamma^{\Lambda}_{\mathrm{d}}\Gamma^{\Lambda}_{\mathrm{d}}+\Gamma^{\Lambda}_{\mathrm{zd}}\Gamma^{\Lambda}_{\mathrm{zd}}+\Gamma^{\Lambda}_{\mathrm{dz}}\Gamma^{\Lambda}_{\mathrm{dz}}+\Gamma^{\Lambda}_{\mathrm{zz}}\Gamma^{\Lambda}_{\mathrm{zz}}-2\Gamma^{\Lambda}_{\mathrm{xx}}\Gamma^{\Lambda}_{\mathrm{xx}}-2\Gamma^{\Lambda}_{\mathrm{DM}}\Gamma^{\Lambda}_{\mathrm{DM}}\right) \\
& +S^{\Lambda}_{\mathrm{s}}G^{\Lambda}_{\mathrm{d}}\left(\Gamma^{\Lambda}_{\mathrm{dz}}\Gamma^{\Lambda}_{\mathrm{zd}}+\Gamma^{\Lambda}_{\mathrm{zd}}\Gamma^{\Lambda}_{\mathrm{dz}}+\Gamma^{\Lambda}_{\mathrm{zz}}\Gamma^{\Lambda}_{\mathrm{d}}+\Gamma^{\Lambda}_{\mathrm{d}}\Gamma^{\Lambda}_{\mathrm{zz}}+2\Gamma^{\Lambda}_{\mathrm{xx}}\Gamma^{\Lambda}_{\mathrm{xx}}+2\Gamma^{\Lambda}_{\mathrm{DM}}\Gamma^{\Lambda}_{\mathrm{DM}}\right) \\
& +S^{\Lambda}_{\mathrm{s}}G^{\Lambda}_{\mathrm{s}}\left(\Gamma^{\Lambda}_{\mathrm{dz}}\Gamma^{\Lambda}_{\mathrm{d}}+\Gamma^{\Lambda}_{\mathrm{d}}\Gamma^{\Lambda}_{\mathrm{dz}}+\Gamma^{\Lambda}_{\mathrm{zz}}\Gamma^{\Lambda}_{\mathrm{zd}}+\Gamma^{\Lambda}_{\mathrm{zd}}\Gamma^{\Lambda}_{\mathrm{zz}}-2i\Gamma^{\Lambda}_{\mathrm{DM}}\Gamma^{\Lambda}_{\mathrm{xx}}+2i\Gamma^{\Lambda}_{\mathrm{xx}}\Gamma^{\Lambda}_{\mathrm{DM}}\right) \\
& \Big]_{(i_1,i_2)(i_1,i_2)}(\omega_{1'},\omega_{2'};\omega_3,\omega_1+\omega_2-\omega_3)(\omega_3,\omega_1+\omega_2-\omega_3;\omega_1,\omega_2) \\
& +(\omega_1+\omega_2-\omega_3)(\omega_3)\Big[\\
& S^{\Lambda}_{\mathrm{d}}G^{\Lambda}_{\mathrm{d}}\left(\Gamma^{\Lambda}_{\mathrm{zd}}\Gamma^{\Lambda}_{\mathrm{d}}+\Gamma^{\Lambda}_{\mathrm{d}}\Gamma^{\Lambda}_{\mathrm{zd}}+\Gamma^{\Lambda}_{\mathrm{zz}}\Gamma^{\Lambda}_{\mathrm{dz}}+\Gamma^{\Lambda}_{\mathrm{dz}}\Gamma^{\Lambda}_{\mathrm{zz}}+2i\Gamma^{\Lambda}_{\mathrm{DM}}\Gamma^{\Lambda}_{\mathrm{xx}}-2i\Gamma^{\Lambda}_{\mathrm{xx}}\Gamma^{\Lambda}_{\mathrm{DM}}\right) \\
& +S^{\Lambda}_{\mathrm{d}}G^{\Lambda}_{\mathrm{s}}\left(\Gamma^{\Lambda}_{\mathrm{dz}}\Gamma^{\Lambda}_{\mathrm{zd}}+\Gamma^{\Lambda}_{\mathrm{zd}}\Gamma^{\Lambda}_{\mathrm{dz}}+\Gamma^{\Lambda}_{\mathrm{zz}}\Gamma^{\Lambda}_{\mathrm{d}}+\Gamma^{\Lambda}_{\mathrm{d}}\Gamma^{\Lambda}_{\mathrm{zz}}+2\Gamma^{\Lambda}_{\mathrm{xx}}\Gamma^{\Lambda}_{\mathrm{xx}}+2\Gamma^{\Lambda}_{\mathrm{DM}}\Gamma^{\Lambda}_{\mathrm{DM}}\right) \\
& +S^{\Lambda}_{\mathrm{s}}G^{\Lambda}_{\mathrm{d}}\left(\Gamma^{\Lambda}_{\mathrm{d}}\Gamma^{\Lambda}_{\mathrm{d}}+\Gamma^{\Lambda}_{\mathrm{zd}}\Gamma^{\Lambda}_{\mathrm{zd}}+\Gamma^{\Lambda}_{\mathrm{dz}}\Gamma^{\Lambda}_{\mathrm{dz}}+\Gamma^{\Lambda}_{\mathrm{zz}}\Gamma^{\Lambda}_{\mathrm{zz}}-2\Gamma^{\Lambda}_{\mathrm{xx}}\Gamma^{\Lambda}_{\mathrm{xx}}-2\Gamma^{\Lambda}_{\mathrm{DM}}\Gamma^{\Lambda}_{\mathrm{DM}}\right) \\
& +S^{\Lambda}_{\mathrm{s}}G^{\Lambda}_{\mathrm{s}}\left(\Gamma^{\Lambda}_{\mathrm{dz}}\Gamma^{\Lambda}_{\mathrm{d}}+\Gamma^{\Lambda}_{\mathrm{d}}\Gamma^{\Lambda}_{\mathrm{dz}}+\Gamma^{\Lambda}_{\mathrm{zz}}\Gamma^{\Lambda}_{\mathrm{zd}}+\Gamma^{\Lambda}_{\mathrm{zd}}\Gamma^{\Lambda}_{\mathrm{zz}}-2i\Gamma^{\Lambda}_{\mathrm{DM}}\Gamma^{\Lambda}_{\mathrm{xx}}+2i\Gamma^{\Lambda}_{\mathrm{xx}}\Gamma^{\Lambda}_{\mathrm{DM}}\right) \\
& \Big]_{(i_1,i_2)(i_1,i_2)}(\omega_{1'},\omega_{2'};\omega_1+\omega_2-\omega_3,\omega_3)(\omega_1+\omega_2-\omega_3,\omega_3;\omega_1,\omega_2) \\
& -2\sum_j(\omega_{2'}+\omega_3-\omega_2)(\omega_3)\Big[\\
& S^{\Lambda}_{\mathrm{d}}\Big(G^{\Lambda}_{\mathrm{d}}\left(\Gamma^{\Lambda}_{\mathrm{zd}}\Gamma^{\Lambda}_{\mathrm{d}}+\Gamma^{\Lambda}_{\mathrm{zz}}\Gamma^{\Lambda}_{\mathrm{zd}}\right)+G^{\Lambda}_{\mathrm{s}}\left(\Gamma^{\Lambda}_{\mathrm{zd}}\Gamma^{\Lambda}_{\mathrm{zd}}+\Gamma^{\Lambda}_{\mathrm{zz}}\Gamma^{\Lambda}_{\mathrm{d}}\right)\Big) \\
& +S^{\Lambda}_{\mathrm{s}}\Big(G^{\Lambda}_{\mathrm{d}}\left(\Gamma^{\Lambda}_{\mathrm{zd}}\Gamma^{\Lambda}_{\mathrm{zd}}+\Gamma^{\Lambda}_{\mathrm{zz}}\Gamma^{\Lambda}_{\mathrm{d}}\right)+G^{\Lambda}_{\mathrm{s}}\left(\Gamma^{\Lambda}_{\mathrm{zd}}\Gamma^{\Lambda}_{\mathrm{d}}+\Gamma^{\Lambda}_{\mathrm{zz}}\Gamma^{\Lambda}_{\mathrm{zd}}\right)\Big) \\
& \Big]_{(i_1,j)(j,i_2)}(\omega_{1'},\omega_{2'}+\omega_3-\omega_2;\omega_1,\omega_3)(\omega_3,\omega_{2'};\omega_{2'}+\omega_3-\omega_2,\omega_2) \\
& -\Big[\omega_3\leftrightarrow\omega_{2'}+\omega_3-\omega_2\Big] \\
& +(\omega_{2'}+\omega_3-\omega_2)(\omega_3)\Big[\\
& S^{\Lambda}_{\mathrm{d}}G^{\Lambda}_{\mathrm{d}}\left(\Gamma^{\Lambda}_{\mathrm{zd}}(\Gamma^{\Lambda}_{\mathrm{d}}+\Gamma^{\Lambda}_{\mathrm{zz}}+2\Gamma^{\Lambda}_{\mathrm{xx}})+\Gamma^{\Lambda}_{\mathrm{zz}}(\Gamma^{\Lambda}_{\mathrm{zd}}+\Gamma^{\Lambda}_{\mathrm{dz}}+2i\Gamma^{\Lambda}_{\mathrm{DM}})\right) \\
& +S^{\Lambda}_{\mathrm{d}}G^{\Lambda}_{\mathrm{s}}\left(\Gamma^{\Lambda}_{\mathrm{zz}}(\Gamma^{\Lambda}_{\mathrm{d}}+\Gamma^{\Lambda}_{\mathrm{zz}}+2\Gamma^{\Lambda}_{\mathrm{xx}})+\Gamma^{\Lambda}_{\mathrm{zd}}(\Gamma^{\Lambda}_{\mathrm{zd}}+\Gamma^{\Lambda}_{\mathrm{dz}}+2i\Gamma^{\Lambda}_{\mathrm{DM}})\right) \\
& +S^{\Lambda}_{\mathrm{s}}G^{\Lambda}_{\mathrm{d}}\left(\Gamma^{\Lambda}_{\mathrm{zz}}(\Gamma^{\Lambda}_{\mathrm{d}}+\Gamma^{\Lambda}_{\mathrm{zz}}+2\Gamma^{\Lambda}_{\mathrm{xx}})+\Gamma^{\Lambda}_{\mathrm{zd}}(\Gamma^{\Lambda}_{\mathrm{zd}}+\Gamma^{\Lambda}_{\mathrm{dz}}+2i\Gamma^{\Lambda}_{\mathrm{DM}})\right) \\
& +S^{\Lambda}_{\mathrm{s}}G^{\Lambda}_{\mathrm{s}}\left(\Gamma^{\Lambda}_{\mathrm{zd}}(\Gamma^{\Lambda}_{\mathrm{d}}+\Gamma^{\Lambda}_{\mathrm{zz}}+2\Gamma^{\Lambda}_{\mathrm{xx}})+\Gamma^{\Lambda}_{\mathrm{zz}}(\Gamma^{\Lambda}_{\mathrm{zd}}+\Gamma^{\Lambda}_{\mathrm{dz}}+2i\Gamma^{\Lambda}_{\mathrm{DM}})\right) \\
& \Big]_{(i_1,i_2)(i_2,i_2)}(\omega_{1'},\omega_{2'}+\omega_3-\omega_2;\omega_1,\omega_3)(\omega_3,\omega_{2'};\omega_2,\omega_{2'}+\omega_3-\omega_2) \\
& +\Big[\omega_3\leftrightarrow\omega_{2'}+\omega_3-\omega_2\Big]
\end{aligned}
$$

$$
\begin{aligned}
&+(\omega_{2'}+\omega_3-\omega_2)(\omega_3)\Big[\\
&\quad S_{\mathrm{d}}^{\Lambda}G_{\mathrm{d}}^{\Lambda}\left((\Gamma_{\mathrm{d}}^{\Lambda}+\Gamma_{\mathrm{zz}}^{\Lambda}-2\Gamma_{\mathrm{xx}}^{\Lambda})\Gamma_{\mathrm{zd}}^{\Lambda}+(\Gamma_{\mathrm{zd}}^{\Lambda}+\Gamma_{\mathrm{dz}}^{\Lambda}+2i\Gamma_{\mathrm{DM}}^{\Lambda})\Gamma_{\mathrm{d}}^{\Lambda}\right)\\
&+S_{\mathrm{d}}^{\Lambda}G_{\mathrm{s}}^{\Lambda}\left((\Gamma_{\mathrm{d}}^{\Lambda}+\Gamma_{\mathrm{zz}}^{\Lambda}-2\Gamma_{\mathrm{xx}}^{\Lambda})\Gamma_{\mathrm{d}}^{\Lambda}+(\Gamma_{\mathrm{zd}}^{\Lambda}+\Gamma_{\mathrm{dz}}^{\Lambda}+2i\Gamma_{\mathrm{DM}}^{\Lambda})\Gamma_{\mathrm{zd}}^{\Lambda}\right)\\
&+S_{\mathrm{s}}^{\Lambda}G_{\mathrm{d}}^{\Lambda}\left((\Gamma_{\mathrm{d}}^{\Lambda}+\Gamma_{\mathrm{zz}}^{\Lambda}-2\Gamma_{\mathrm{xx}}^{\Lambda})\Gamma_{\mathrm{d}}^{\Lambda}+(\Gamma_{\mathrm{zd}}^{\Lambda}+\Gamma_{\mathrm{dz}}^{\Lambda}+2i\Gamma_{\mathrm{DM}}^{\Lambda})\Gamma_{\mathrm{zd}}^{\Lambda}\right)\\
&+S_{\mathrm{s}}^{\Lambda}G_{\mathrm{s}}^{\Lambda}\left((\Gamma_{\mathrm{d}}^{\Lambda}+\Gamma_{\mathrm{zz}}^{\Lambda}-2\Gamma_{\mathrm{xx}}^{\Lambda})\Gamma_{\mathrm{zd}}^{\Lambda}+(\Gamma_{\mathrm{zd}}^{\Lambda}+\Gamma_{\mathrm{dz}}^{\Lambda}+2i\Gamma_{\mathrm{DM}}^{\Lambda})\Gamma_{\mathrm{d}}^{\Lambda}\right)\\
&\quad\Big]_{(i_1,i_1)(i_1,i_2)}(\omega_{1'},\omega_{2'}+\omega_3-\omega_2;\omega_3,\omega_1)(\omega_3,\omega_{2'};\omega_{2'}+\omega_3-\omega_2,\omega_2)\\
&+\Big[\omega_3\leftrightarrow\omega_{2'}+\omega_3-\omega_2\Big]\\
&+(\omega_{1'}+\omega_3-\omega_2)(\omega_3)\Big[\\
&\quad S_{\mathrm{d}}^{\Lambda}G_{\mathrm{d}}^{\Lambda}\left(\Gamma_{\mathrm{dz}}^{\Lambda}\Gamma_{\mathrm{d}}^{\Lambda}+\Gamma_{\mathrm{d}}^{\Lambda}\Gamma_{\mathrm{dz}}^{\Lambda}+\Gamma_{\mathrm{zz}}^{\Lambda}\Gamma_{\mathrm{zd}}^{\Lambda}+\Gamma_{\mathrm{zd}}^{\Lambda}\Gamma_{\mathrm{zz}}^{\Lambda}+2i\Gamma_{\mathrm{DM}}^{\Lambda}\Gamma_{\mathrm{xx}}^{\Lambda}-2i\Gamma_{\mathrm{xx}}^{\Lambda}\Gamma_{\mathrm{DM}}^{\Lambda}\right)\\
&+S_{\mathrm{d}}^{\Lambda}G_{\mathrm{s}}^{\Lambda}\left(\Gamma_{\mathrm{dz}}^{\Lambda}\Gamma_{\mathrm{zd}}^{\Lambda}+\Gamma_{\mathrm{zd}}^{\Lambda}\Gamma_{\mathrm{dz}}^{\Lambda}+\Gamma_{\mathrm{zz}}^{\Lambda}\Gamma_{\mathrm{d}}^{\Lambda}+\Gamma_{\mathrm{d}}^{\Lambda}\Gamma_{\mathrm{zz}}^{\Lambda}-2\Gamma_{\mathrm{xx}}^{\Lambda}\Gamma_{\mathrm{xx}}^{\Lambda}-2\Gamma_{\mathrm{DM}}^{\Lambda}\Gamma_{\mathrm{DM}}^{\Lambda}\right)\\
&+S_{\mathrm{s}}^{\Lambda}G_{\mathrm{d}}^{\Lambda}\left(\Gamma_{\mathrm{d}}^{\Lambda}\Gamma_{\mathrm{d}}^{\Lambda}+\Gamma_{\mathrm{zd}}^{\Lambda}\Gamma_{\mathrm{zd}}^{\Lambda}+\Gamma_{\mathrm{dz}}^{\Lambda}\Gamma_{\mathrm{dz}}^{\Lambda}+\Gamma_{\mathrm{zz}}^{\Lambda}\Gamma_{\mathrm{zz}}^{\Lambda}-2\Gamma_{\mathrm{xx}}^{\Lambda}\Gamma_{\mathrm{xx}}^{\Lambda}-2\Gamma_{\mathrm{DM}}^{\Lambda}\Gamma_{\mathrm{DM}}^{\Lambda}\right)\\
&+S_{\mathrm{s}}^{\Lambda}G_{\mathrm{s}}^{\Lambda}\left(\Gamma_{\mathrm{zd}}^{\Lambda}\Gamma_{\mathrm{d}}^{\Lambda}+\Gamma_{\mathrm{d}}^{\Lambda}\Gamma_{\mathrm{zd}}^{\Lambda}+\Gamma_{\mathrm{zz}}^{\Lambda}\Gamma_{\mathrm{dz}}^{\Lambda}+\Gamma_{\mathrm{dz}}^{\Lambda}\Gamma_{\mathrm{zz}}^{\Lambda}+2i\Gamma_{\mathrm{DM}}^{\Lambda}\Gamma_{\mathrm{xx}}^{\Lambda}-2i\Gamma_{\mathrm{xx}}^{\Lambda}\Gamma_{\mathrm{DM}}^{\Lambda}\right)\\
&\quad\Big]_{(i_2,i_1)(i_2,i_1)}(\omega_{2'},\omega_{1'}+\omega_3-\omega_2;\omega_3,\omega_1)(\omega_3,\omega_{1'};\omega_2,\omega_{1'}+\omega_3-\omega_2)\\
&+(\omega_{1'}+\omega_3-\omega_2)(\omega_3)\Big[\\
&\quad S_{\mathrm{d}}^{\Lambda}G_{\mathrm{d}}^{\Lambda}\left(\Gamma_{\mathrm{dz}}^{\Lambda}\Gamma_{\mathrm{d}}^{\Lambda}+\Gamma_{\mathrm{d}}^{\Lambda}\Gamma_{\mathrm{dz}}^{\Lambda}+\Gamma_{\mathrm{zz}}^{\Lambda}\Gamma_{\mathrm{zd}}^{\Lambda}+\Gamma_{\mathrm{zd}}^{\Lambda}\Gamma_{\mathrm{zz}}^{\Lambda}+2i\Gamma_{\mathrm{DM}}^{\Lambda}\Gamma_{\mathrm{xx}}^{\Lambda}-2i\Gamma_{\mathrm{xx}}^{\Lambda}\Gamma_{\mathrm{DM}}^{\Lambda}\right)\\
&+S_{\mathrm{d}}^{\Lambda}G_{\mathrm{s}}^{\Lambda}\left(\Gamma_{\mathrm{dz}}^{\Lambda}\Gamma_{\mathrm{zd}}^{\Lambda}+\Gamma_{\mathrm{zd}}^{\Lambda}\Gamma_{\mathrm{dz}}^{\Lambda}+\Gamma_{\mathrm{zz}}^{\Lambda}\Gamma_{\mathrm{d}}^{\Lambda}+\Gamma_{\mathrm{d}}^{\Lambda}\Gamma_{\mathrm{zz}}^{\Lambda}-2\Gamma_{\mathrm{xx}}^{\Lambda}\Gamma_{\mathrm{xx}}^{\Lambda}-2\Gamma_{\mathrm{DM}}^{\Lambda}\Gamma_{\mathrm{DM}}^{\Lambda}\right)\\
&+S_{\mathrm{s}}^{\Lambda}G_{\mathrm{d}}^{\Lambda}\left(\Gamma_{\mathrm{d}}^{\Lambda}\Gamma_{\mathrm{d}}^{\Lambda}+\Gamma_{\mathrm{zd}}^{\Lambda}\Gamma_{\mathrm{zd}}^{\Lambda}+\Gamma_{\mathrm{dz}}^{\Lambda}\Gamma_{\mathrm{dz}}^{\Lambda}+\Gamma_{\mathrm{zz}}^{\Lambda}\Gamma_{\mathrm{zz}}^{\Lambda}-2\Gamma_{\mathrm{xx}}^{\Lambda}\Gamma_{\mathrm{xx}}^{\Lambda}-2\Gamma_{\mathrm{DM}}^{\Lambda}\Gamma_{\mathrm{DM}}^{\Lambda}\right)\\
&+S_{\mathrm{s}}^{\Lambda}G_{\mathrm{s}}^{\Lambda}\left(\Gamma_{\mathrm{zd}}^{\Lambda}\Gamma_{\mathrm{d}}^{\Lambda}+\Gamma_{\mathrm{d}}^{\Lambda}\Gamma_{\mathrm{zd}}^{\Lambda}+\Gamma_{\mathrm{zz}}^{\Lambda}\Gamma_{\mathrm{dz}}^{\Lambda}+\Gamma_{\mathrm{dz}}^{\Lambda}\Gamma_{\mathrm{zz}}^{\Lambda}+2i\Gamma_{\mathrm{DM}}^{\Lambda}\Gamma_{\mathrm{xx}}^{\Lambda}-2i\Gamma_{\mathrm{xx}}^{\Lambda}\Gamma_{\mathrm{DM}}^{\Lambda}\right)\\
&\quad\Big]_{(i_2,i_1)(i_2,i_1)}(\omega_{2'},\omega_3;\omega_{1'}+\omega_3-\omega_2,\omega_1)(\omega_{1'}+\omega_3-\omega_2,\omega_{1'};\omega_2,\omega_3)\Bigg\}
\end{aligned}
\tag{B.3}
$$

$$
\begin{aligned}
\frac{\mathrm{d}}{\mathrm{d}\Lambda}\Gamma^{\Lambda}_{\mathrm{dz}i_1i_2}(\omega_{1'},\omega_{2'};\omega_1,\omega_2) = \frac{1}{2\pi}\int_{-\infty}^{\infty}\mathrm{d}\omega_3 \Big\{ & (\omega_1+\omega_2-\omega_3)(\omega_3)\Big[\\
& S^{\Lambda}_{\mathrm{d}}G^{\Lambda}_{\mathrm{d}}\left(\Gamma^{\Lambda}_{\mathrm{dz}}\Gamma^{\Lambda}_{\mathrm{d}}+\Gamma^{\Lambda}_{\mathrm{d}}\Gamma^{\Lambda}_{\mathrm{dz}}+\Gamma^{\Lambda}_{\mathrm{zz}}\Gamma^{\Lambda}_{\mathrm{zd}}+\Gamma^{\Lambda}_{\mathrm{zd}}\Gamma^{\Lambda}_{\mathrm{zz}}-2i\Gamma^{\Lambda}_{\mathrm{DM}}\Gamma^{\Lambda}_{\mathrm{xx}}+2i\Gamma^{\Lambda}_{\mathrm{xx}}\Gamma^{\Lambda}_{\mathrm{DM}}\right) \\
& +S^{\Lambda}_{\mathrm{d}}G^{\Lambda}_{\mathrm{s}}\left(\Gamma^{\Lambda}_{\mathrm{dz}}\Gamma^{\Lambda}_{\mathrm{zd}}+\Gamma^{\Lambda}_{\mathrm{zd}}\Gamma^{\Lambda}_{\mathrm{dz}}+\Gamma^{\Lambda}_{\mathrm{zz}}\Gamma^{\Lambda}_{\mathrm{d}}+\Gamma^{\Lambda}_{\mathrm{d}}\Gamma^{\Lambda}_{\mathrm{zz}}+2\Gamma^{\Lambda}_{\mathrm{xx}}\Gamma^{\Lambda}_{\mathrm{xx}}+2\Gamma^{\Lambda}_{\mathrm{DM}}\Gamma^{\Lambda}_{\mathrm{DM}}\right) \\
& +S^{\Lambda}_{\mathrm{s}}G^{\Lambda}_{\mathrm{d}}\left(\Gamma^{\Lambda}_{\mathrm{d}}\Gamma^{\Lambda}_{\mathrm{d}}+\Gamma^{\Lambda}_{\mathrm{zd}}\Gamma^{\Lambda}_{\mathrm{zd}}+\Gamma^{\Lambda}_{\mathrm{dz}}\Gamma^{\Lambda}_{\mathrm{dz}}+\Gamma^{\Lambda}_{\mathrm{zz}}\Gamma^{\Lambda}_{\mathrm{zz}}-2\Gamma^{\Lambda}_{\mathrm{xx}}\Gamma^{\Lambda}_{\mathrm{xx}}-2\Gamma^{\Lambda}_{\mathrm{DM}}\Gamma^{\Lambda}_{\mathrm{DM}}\right) \\
& +S^{\Lambda}_{\mathrm{s}}G^{\Lambda}_{\mathrm{s}}\left(\Gamma^{\Lambda}_{\mathrm{zd}}\Gamma^{\Lambda}_{\mathrm{d}}+\Gamma^{\Lambda}_{\mathrm{d}}\Gamma^{\Lambda}_{\mathrm{zd}}+\Gamma^{\Lambda}_{\mathrm{zz}}\Gamma^{\Lambda}_{\mathrm{dz}}+\Gamma^{\Lambda}_{\mathrm{dz}}\Gamma^{\Lambda}_{\mathrm{zz}}+2i\Gamma^{\Lambda}_{\mathrm{DM}}\Gamma^{\Lambda}_{\mathrm{xx}}-2i\Gamma^{\Lambda}_{\mathrm{xx}}\Gamma^{\Lambda}_{\mathrm{DM}}\right) \\
& \Big]_{(i_1,i_2)(i_1,i_2)}(\omega_{1'},\omega_{2'};\omega_3,\omega_1+\omega_2-\omega_3)(\omega_3,\omega_1+\omega_2-\omega_3;\omega_1,\omega_2) \\
& +(\omega_1+\omega_2-\omega_3)(\omega_3)\Big[\\
& S^{\Lambda}_{\mathrm{d}}G^{\Lambda}_{\mathrm{d}}\left(\Gamma^{\Lambda}_{\mathrm{dz}}\Gamma^{\Lambda}_{\mathrm{d}}+\Gamma^{\Lambda}_{\mathrm{d}}\Gamma^{\Lambda}_{\mathrm{dz}}+\Gamma^{\Lambda}_{\mathrm{zz}}\Gamma^{\Lambda}_{\mathrm{zd}}+\Gamma^{\Lambda}_{\mathrm{zd}}\Gamma^{\Lambda}_{\mathrm{zz}}-2i\Gamma^{\Lambda}_{\mathrm{DM}}\Gamma^{\Lambda}_{\mathrm{xx}}+2i\Gamma^{\Lambda}_{\mathrm{xx}}\Gamma^{\Lambda}_{\mathrm{DM}}\right) \\
& +S^{\Lambda}_{\mathrm{d}}G^{\Lambda}_{\mathrm{s}}\left(\Gamma^{\Lambda}_{\mathrm{d}}\Gamma^{\Lambda}_{\mathrm{d}}+\Gamma^{\Lambda}_{\mathrm{zd}}\Gamma^{\Lambda}_{\mathrm{zd}}+\Gamma^{\Lambda}_{\mathrm{dz}}\Gamma^{\Lambda}_{\mathrm{dz}}+\Gamma^{\Lambda}_{\mathrm{zz}}\Gamma^{\Lambda}_{\mathrm{zz}}-2\Gamma^{\Lambda}_{\mathrm{xx}}\Gamma^{\Lambda}_{\mathrm{xx}}-2\Gamma^{\Lambda}_{\mathrm{DM}}\Gamma^{\Lambda}_{\mathrm{DM}}\right) \\
& +S^{\Lambda}_{\mathrm{s}}G^{\Lambda}_{\mathrm{d}}\left(\Gamma^{\Lambda}_{\mathrm{dz}}\Gamma^{\Lambda}_{\mathrm{zd}}+\Gamma^{\Lambda}_{\mathrm{zd}}\Gamma^{\Lambda}_{\mathrm{dz}}+\Gamma^{\Lambda}_{\mathrm{zz}}\Gamma^{\Lambda}_{\mathrm{d}}+\Gamma^{\Lambda}_{\mathrm{d}}\Gamma^{\Lambda}_{\mathrm{zz}}+2\Gamma^{\Lambda}_{\mathrm{xx}}\Gamma^{\Lambda}_{\mathrm{xx}}+2\Gamma^{\Lambda}_{\mathrm{DM}}\Gamma^{\Lambda}_{\mathrm{DM}}\right) \\
& +S^{\Lambda}_{\mathrm{s}}G^{\Lambda}_{\mathrm{s}}\left(\Gamma^{\Lambda}_{\mathrm{zd}}\Gamma^{\Lambda}_{\mathrm{d}}+\Gamma^{\Lambda}_{\mathrm{d}}\Gamma^{\Lambda}_{\mathrm{zd}}+\Gamma^{\Lambda}_{\mathrm{zz}}\Gamma^{\Lambda}_{\mathrm{dz}}+\Gamma^{\Lambda}_{\mathrm{dz}}\Gamma^{\Lambda}_{\mathrm{zz}}+2i\Gamma^{\Lambda}_{\mathrm{DM}}\Gamma^{\Lambda}_{\mathrm{xx}}-2i\Gamma^{\Lambda}_{\mathrm{xx}}\Gamma^{\Lambda}_{\mathrm{DM}}\right) \\
& \Big]_{(i_1,i_2)(i_1,i_2)}(\omega_{1'},\omega_{2'};\omega_1+\omega_2-\omega_3,\omega_3)(\omega_1+\omega_2-\omega_3,\omega_3;\omega_1,\omega_2) \\
& -2\sum_j(\omega_{2'}+\omega_3-\omega_2)(\omega_3)\Big[\\
& S^{\Lambda}_{\mathrm{d}}\Big(G^{\Lambda}_{\mathrm{d}}\left(\Gamma^{\Lambda}_{\mathrm{d}}\Gamma^{\Lambda}_{\mathrm{dz}}+\Gamma^{\Lambda}_{\mathrm{dz}}\Gamma^{\Lambda}_{\mathrm{zz}}\right)+G^{\Lambda}_{\mathrm{s}}\left(\Gamma^{\Lambda}_{\mathrm{dz}}\Gamma^{\Lambda}_{\mathrm{dz}}+\Gamma^{\Lambda}_{\mathrm{d}}\Gamma^{\Lambda}_{\mathrm{zz}}\right)\Big) \\
& +S^{\Lambda}_{\mathrm{s}}\Big(G^{\Lambda}_{\mathrm{d}}\left(\Gamma^{\Lambda}_{\mathrm{dz}}\Gamma^{\Lambda}_{\mathrm{dz}}+\Gamma^{\Lambda}_{\mathrm{d}}\Gamma^{\Lambda}_{\mathrm{zz}}\right)+G^{\Lambda}_{\mathrm{s}}\left(\Gamma^{\Lambda}_{\mathrm{d}}\Gamma^{\Lambda}_{\mathrm{dz}}+\Gamma^{\Lambda}_{\mathrm{dz}}\Gamma^{\Lambda}_{\mathrm{zz}}\right)\Big) \\
& \Big]_{(i_1,j)(j,i_2)}(\omega_{1'},\omega_{2'}+\omega_3-\omega_2;\omega_1,\omega_3)(\omega_3,\omega_{2'};\omega_{2'}+\omega_3-\omega_2,\omega_2) \\
& -\Big[\omega_3\leftrightarrow\omega_{2'}+\omega_3-\omega_2\Big] \\
& +(\omega_{2'}+\omega_3-\omega_2)(\omega_3)\Big[\\
& S^{\Lambda}_{\mathrm{d}}G^{\Lambda}_{\mathrm{d}}\left(\Gamma^{\Lambda}_{\mathrm{dz}}(\Gamma^{\Lambda}_{\mathrm{d}}+\Gamma^{\Lambda}_{\mathrm{zz}}-2\Gamma^{\Lambda}_{\mathrm{xx}})+\Gamma^{\Lambda}_{\mathrm{d}}(\Gamma^{\Lambda}_{\mathrm{zd}}+\Gamma^{\Lambda}_{\mathrm{dz}}-2i\Gamma^{\Lambda}_{\mathrm{DM}})\right) \\
& +S^{\Lambda}_{\mathrm{d}}G^{\Lambda}_{\mathrm{s}}\left(\Gamma^{\Lambda}_{\mathrm{d}}(\Gamma^{\Lambda}_{\mathrm{d}}+\Gamma^{\Lambda}_{\mathrm{zz}}-2\Gamma^{\Lambda}_{\mathrm{xx}})+\Gamma^{\Lambda}_{\mathrm{dz}}(\Gamma^{\Lambda}_{\mathrm{zd}}+\Gamma^{\Lambda}_{\mathrm{dz}}-2i\Gamma^{\Lambda}_{\mathrm{DM}})\right) \\
& +S^{\Lambda}_{\mathrm{s}}G^{\Lambda}_{\mathrm{d}}\left(\Gamma^{\Lambda}_{\mathrm{d}}(\Gamma^{\Lambda}_{\mathrm{d}}+\Gamma^{\Lambda}_{\mathrm{zz}}-2\Gamma^{\Lambda}_{\mathrm{xx}})+\Gamma^{\Lambda}_{\mathrm{dz}}(\Gamma^{\Lambda}_{\mathrm{zd}}+\Gamma^{\Lambda}_{\mathrm{dz}}-2i\Gamma^{\Lambda}_{\mathrm{DM}})\right) \\
& +S^{\Lambda}_{\mathrm{s}}G^{\Lambda}_{\mathrm{s}}\left(\Gamma^{\Lambda}_{\mathrm{dz}}(\Gamma^{\Lambda}_{\mathrm{d}}+\Gamma^{\Lambda}_{\mathrm{zz}}-2\Gamma^{\Lambda}_{\mathrm{xx}})+\Gamma^{\Lambda}_{\mathrm{d}}(\Gamma^{\Lambda}_{\mathrm{zd}}+\Gamma^{\Lambda}_{\mathrm{dz}}-2i\Gamma^{\Lambda}_{\mathrm{DM}})\right) \\
& \Big]_{(i_1,i_2)(i_2,i_2)}(\omega_{1'},\omega_{2'}+\omega_3-\omega_2;\omega_1,\omega_3)(\omega_3,\omega_{2'};\omega_2,\omega_{2'}+\omega_3-\omega_2) \\
& +\Big[\omega_3\leftrightarrow\omega_{2'}+\omega_3-\omega_2\Big]
\end{aligned}
$$

$$
\begin{aligned}
&+(\omega_{2'}+\omega_3-\omega_2)(\omega_3)\Big[\\
&\quad S_{\mathrm{d}}^{\Lambda}G_{\mathrm{d}}^{\Lambda}\left((\Gamma_{\mathrm{d}}^{\Lambda}+\Gamma_{\mathrm{zz}}^{\Lambda}+2\Gamma_{\mathrm{xx}}^{\Lambda})\Gamma_{\mathrm{dz}}^{\Lambda}+(\Gamma_{\mathrm{zd}}^{\Lambda}+\Gamma_{\mathrm{dz}}^{\Lambda}-2i\Gamma_{\mathrm{DM}}^{\Lambda})\Gamma_{\mathrm{zz}}^{\Lambda}\right)\\
&+S_{\mathrm{d}}^{\Lambda}G_{\mathrm{s}}^{\Lambda}\left((\Gamma_{\mathrm{d}}^{\Lambda}+\Gamma_{\mathrm{zz}}^{\Lambda}+2\Gamma_{\mathrm{xx}}^{\Lambda})\Gamma_{\mathrm{zz}}^{\Lambda}+(\Gamma_{\mathrm{zd}}^{\Lambda}+\Gamma_{\mathrm{dz}}^{\Lambda}-2i\Gamma_{\mathrm{DM}}^{\Lambda})\Gamma_{\mathrm{dz}}^{\Lambda}\right)\\
&+S_{\mathrm{s}}^{\Lambda}G_{\mathrm{d}}^{\Lambda}\left((\Gamma_{\mathrm{d}}^{\Lambda}+\Gamma_{\mathrm{zz}}^{\Lambda}+2\Gamma_{\mathrm{xx}}^{\Lambda})\Gamma_{\mathrm{zz}}^{\Lambda}+(\Gamma_{\mathrm{zd}}^{\Lambda}+\Gamma_{\mathrm{dz}}^{\Lambda}-2i\Gamma_{\mathrm{DM}}^{\Lambda})\Gamma_{\mathrm{dz}}^{\Lambda}\right)\\
&+S_{\mathrm{s}}^{\Lambda}G_{\mathrm{s}}^{\Lambda}\left((\Gamma_{\mathrm{d}}^{\Lambda}+\Gamma_{\mathrm{zz}}^{\Lambda}+2\Gamma_{\mathrm{xx}}^{\Lambda})\Gamma_{\mathrm{dz}}^{\Lambda}+(\Gamma_{\mathrm{zd}}^{\Lambda}+\Gamma_{\mathrm{dz}}^{\Lambda}-2i\Gamma_{\mathrm{DM}}^{\Lambda})\Gamma_{\mathrm{zz}}^{\Lambda}\right)\\
&\quad\Big]_{(i_1,i_1)(i_1,i_2)}(\omega_{1'},\omega_{2'}+\omega_3-\omega_2;\omega_3,\omega_1)(\omega_3,\omega_{2'};\omega_{2'}+\omega_3-\omega_2,\omega_2)\\
&+\Big[\omega_3\leftrightarrow\omega_{2'}+\omega_3-\omega_2\Big]\\
&+(\omega_{1'}+\omega_3-\omega_2)(\omega_3)\Big[\\
&\quad S_{\mathrm{d}}^{\Lambda}G_{\mathrm{d}}^{\Lambda}\left(\Gamma_{\mathrm{zd}}^{\Lambda}\Gamma_{\mathrm{d}}^{\Lambda}+\Gamma_{\mathrm{d}}^{\Lambda}\Gamma_{\mathrm{zd}}^{\Lambda}+\Gamma_{\mathrm{zz}}^{\Lambda}\Gamma_{\mathrm{dz}}^{\Lambda}+\Gamma_{\mathrm{dz}}^{\Lambda}\Gamma_{\mathrm{zz}}^{\Lambda}+2i\Gamma_{\mathrm{DM}}^{\Lambda}\Gamma_{\mathrm{xx}}^{\Lambda}-2i\Gamma_{\mathrm{xx}}^{\Lambda}\Gamma_{\mathrm{DM}}^{\Lambda}\right)\\
&+S_{\mathrm{d}}^{\Lambda}G_{\mathrm{s}}^{\Lambda}\left(\Gamma_{\mathrm{d}}^{\Lambda}\Gamma_{\mathrm{d}}^{\Lambda}+\Gamma_{\mathrm{zd}}^{\Lambda}\Gamma_{\mathrm{zd}}^{\Lambda}+\Gamma_{\mathrm{dz}}^{\Lambda}\Gamma_{\mathrm{dz}}^{\Lambda}+\Gamma_{\mathrm{zz}}^{\Lambda}\Gamma_{\mathrm{zz}}^{\Lambda}-2\Gamma_{\mathrm{xx}}^{\Lambda}\Gamma_{\mathrm{xx}}^{\Lambda}-2\Gamma_{\mathrm{DM}}^{\Lambda}\Gamma_{\mathrm{DM}}^{\Lambda}\right)\\
&+S_{\mathrm{s}}^{\Lambda}G_{\mathrm{d}}^{\Lambda}\left(\Gamma_{\mathrm{dz}}^{\Lambda}\Gamma_{\mathrm{zd}}^{\Lambda}+\Gamma_{\mathrm{zd}}^{\Lambda}\Gamma_{\mathrm{dz}}^{\Lambda}+\Gamma_{\mathrm{zz}}^{\Lambda}\Gamma_{\mathrm{d}}^{\Lambda}+\Gamma_{\mathrm{d}}^{\Lambda}\Gamma_{\mathrm{zz}}^{\Lambda}-2\Gamma_{\mathrm{xx}}^{\Lambda}\Gamma_{\mathrm{xx}}^{\Lambda}-2\Gamma_{\mathrm{DM}}^{\Lambda}\Gamma_{\mathrm{DM}}^{\Lambda}\right)\\
&+S_{\mathrm{s}}^{\Lambda}G_{\mathrm{s}}^{\Lambda}\left(\Gamma_{\mathrm{dz}}^{\Lambda}\Gamma_{\mathrm{d}}^{\Lambda}+\Gamma_{\mathrm{d}}^{\Lambda}\Gamma_{\mathrm{dz}}^{\Lambda}+\Gamma_{\mathrm{zz}}^{\Lambda}\Gamma_{\mathrm{zd}}^{\Lambda}+\Gamma_{\mathrm{zd}}^{\Lambda}\Gamma_{\mathrm{zz}}^{\Lambda}+2i\Gamma_{\mathrm{DM}}^{\Lambda}\Gamma_{\mathrm{xx}}^{\Lambda}-2i\Gamma_{\mathrm{xx}}^{\Lambda}\Gamma_{\mathrm{DM}}^{\Lambda}\right)\\
&\quad\Big]_{(i_2,i_1)(i_2,i_1)}(\omega_{2'},\omega_{1'}+\omega_3-\omega_2;\omega_3,\omega_1)(\omega_3,\omega_{1'};\omega_2,\omega_{1'}+\omega_3-\omega_2)\\
&+(\omega_{1'}+\omega_3-\omega_2)(\omega_3)\Big[\\
&\quad S_{\mathrm{d}}^{\Lambda}G_{\mathrm{d}}^{\Lambda}\left(\Gamma_{\mathrm{zd}}^{\Lambda}\Gamma_{\mathrm{d}}^{\Lambda}+\Gamma_{\mathrm{d}}^{\Lambda}\Gamma_{\mathrm{zd}}^{\Lambda}+\Gamma_{\mathrm{zz}}^{\Lambda}\Gamma_{\mathrm{dz}}^{\Lambda}+\Gamma_{\mathrm{dz}}^{\Lambda}\Gamma_{\mathrm{zz}}^{\Lambda}+2i\Gamma_{\mathrm{DM}}^{\Lambda}\Gamma_{\mathrm{xx}}^{\Lambda}-2i\Gamma_{\mathrm{xx}}^{\Lambda}\Gamma_{\mathrm{DM}}^{\Lambda}\right)\\
&+S_{\mathrm{d}}^{\Lambda}G_{\mathrm{s}}^{\Lambda}\left(\Gamma_{\mathrm{dz}}^{\Lambda}\Gamma_{\mathrm{zd}}^{\Lambda}+\Gamma_{\mathrm{zd}}^{\Lambda}\Gamma_{\mathrm{dz}}^{\Lambda}+\Gamma_{\mathrm{zz}}^{\Lambda}\Gamma_{\mathrm{d}}^{\Lambda}+\Gamma_{\mathrm{d}}^{\Lambda}\Gamma_{\mathrm{zz}}^{\Lambda}-2\Gamma_{\mathrm{xx}}^{\Lambda}\Gamma_{\mathrm{xx}}^{\Lambda}-2\Gamma_{\mathrm{DM}}^{\Lambda}\Gamma_{\mathrm{DM}}^{\Lambda}\right)\\
&+S_{\mathrm{s}}^{\Lambda}G_{\mathrm{d}}^{\Lambda}\left(\Gamma_{\mathrm{d}}^{\Lambda}\Gamma_{\mathrm{d}}^{\Lambda}+\Gamma_{\mathrm{zd}}^{\Lambda}\Gamma_{\mathrm{zd}}^{\Lambda}+\Gamma_{\mathrm{dz}}^{\Lambda}\Gamma_{\mathrm{dz}}^{\Lambda}+\Gamma_{\mathrm{zz}}^{\Lambda}\Gamma_{\mathrm{zz}}^{\Lambda}-2\Gamma_{\mathrm{xx}}^{\Lambda}\Gamma_{\mathrm{xx}}^{\Lambda}-2\Gamma_{\mathrm{DM}}^{\Lambda}\Gamma_{\mathrm{DM}}^{\Lambda}\right)\\
&+S_{\mathrm{s}}^{\Lambda}G_{\mathrm{s}}^{\Lambda}\left(\Gamma_{\mathrm{dz}}^{\Lambda}\Gamma_{\mathrm{d}}^{\Lambda}+\Gamma_{\mathrm{d}}^{\Lambda}\Gamma_{\mathrm{dz}}^{\Lambda}+\Gamma_{\mathrm{zz}}^{\Lambda}\Gamma_{\mathrm{zd}}^{\Lambda}+\Gamma_{\mathrm{zd}}^{\Lambda}\Gamma_{\mathrm{zz}}^{\Lambda}+2i\Gamma_{\mathrm{DM}}^{\Lambda}\Gamma_{\mathrm{xx}}^{\Lambda}-2i\Gamma_{\mathrm{xx}}^{\Lambda}\Gamma_{\mathrm{DM}}^{\Lambda}\right)\\
&\quad\Big]_{(i_2,i_1)(i_2,i_1)}(\omega_{2'},\omega_3;\omega_{1'}+\omega_3-\omega_2,\omega_1)(\omega_{1'}+\omega_3-\omega_2,\omega_{1'};\omega_2,\omega_3)\Bigg\}
\end{aligned}
\tag{B.4}
$$

$$
\begin{aligned}
\frac{\mathrm{d}}{\mathrm{d}\Lambda}\Gamma^{\Lambda}_{\mathrm{zz}i_1i_2}(\omega_{1'},\omega_{2'};\omega_1,\omega_2) = \frac{1}{2\pi}\int_{-\infty}^{\infty}\mathrm{d}\omega_3 \Big\{ & (\omega_1+\omega_2-\omega_3)(\omega_3)\Big[\\
& S^{\Lambda}_{\mathrm{d}}G^{\Lambda}_{\mathrm{d}}\left(\Gamma^{\Lambda}_{\mathrm{dz}}\Gamma^{\Lambda}_{\mathrm{zd}}+\Gamma^{\Lambda}_{\mathrm{zd}}\Gamma^{\Lambda}_{\mathrm{dz}}+\Gamma^{\Lambda}_{\mathrm{zz}}\Gamma^{\Lambda}_{\mathrm{d}}+\Gamma^{\Lambda}_{\mathrm{d}}\Gamma^{\Lambda}_{\mathrm{zz}}-2\Gamma^{\Lambda}_{\mathrm{xx}}\Gamma^{\Lambda}_{\mathrm{xx}}-2\Gamma^{\Lambda}_{\mathrm{DM}}\Gamma^{\Lambda}_{\mathrm{DM}}\right) \\
& +S^{\Lambda}_{\mathrm{d}}G^{\Lambda}_{\mathrm{s}}\left(\Gamma^{\Lambda}_{\mathrm{dz}}\Gamma^{\Lambda}_{\mathrm{d}}+\Gamma^{\Lambda}_{\mathrm{d}}\Gamma^{\Lambda}_{\mathrm{dz}}+\Gamma^{\Lambda}_{\mathrm{zz}}\Gamma^{\Lambda}_{\mathrm{zd}}+\Gamma^{\Lambda}_{\mathrm{zd}}\Gamma^{\Lambda}_{\mathrm{zz}}+2i\Gamma^{\Lambda}_{\mathrm{DM}}\Gamma^{\Lambda}_{\mathrm{xx}}-2i\Gamma^{\Lambda}_{\mathrm{xx}}\Gamma^{\Lambda}_{\mathrm{DM}}\right) \\
& +S^{\Lambda}_{\mathrm{s}}G^{\Lambda}_{\mathrm{d}}\left(\Gamma^{\Lambda}_{\mathrm{zd}}\Gamma^{\Lambda}_{\mathrm{d}}+\Gamma^{\Lambda}_{\mathrm{d}}\Gamma^{\Lambda}_{\mathrm{zd}}+\Gamma^{\Lambda}_{\mathrm{zz}}\Gamma^{\Lambda}_{\mathrm{dz}}+\Gamma^{\Lambda}_{\mathrm{dz}}\Gamma^{\Lambda}_{\mathrm{zz}}-2i\Gamma^{\Lambda}_{\mathrm{DM}}\Gamma^{\Lambda}_{\mathrm{xx}}+2i\Gamma^{\Lambda}_{\mathrm{xx}}\Gamma^{\Lambda}_{\mathrm{DM}}\right) \\
& +S^{\Lambda}_{\mathrm{s}}G^{\Lambda}_{\mathrm{s}}\left(\Gamma^{\Lambda}_{\mathrm{d}}\Gamma^{\Lambda}_{\mathrm{d}}+\Gamma^{\Lambda}_{\mathrm{zd}}\Gamma^{\Lambda}_{\mathrm{zd}}+\Gamma^{\Lambda}_{\mathrm{dz}}\Gamma^{\Lambda}_{\mathrm{dz}}+\Gamma^{\Lambda}_{\mathrm{zz}}\Gamma^{\Lambda}_{\mathrm{zz}}+2\Gamma^{\Lambda}_{\mathrm{xx}}\Gamma^{\Lambda}_{\mathrm{xx}}+2\Gamma^{\Lambda}_{\mathrm{DM}}\Gamma^{\Lambda}_{\mathrm{DM}}\right) \\
& \Big]_{(i_1,i_2)(i_1,i_2)}(\omega_{1'},\omega_{2'};\omega_3,\omega_1+\omega_2-\omega_3)(\omega_3,\omega_1+\omega_2-\omega_3;\omega_1,\omega_2) \\
& +(\omega_1+\omega_2-\omega_3)(\omega_3)\Big[\\
& S^{\Lambda}_{\mathrm{d}}G^{\Lambda}_{\mathrm{d}}\left(\Gamma^{\Lambda}_{\mathrm{dz}}\Gamma^{\Lambda}_{\mathrm{zd}}+\Gamma^{\Lambda}_{\mathrm{zd}}\Gamma^{\Lambda}_{\mathrm{dz}}+\Gamma^{\Lambda}_{\mathrm{zz}}\Gamma^{\Lambda}_{\mathrm{d}}+\Gamma^{\Lambda}_{\mathrm{d}}\Gamma^{\Lambda}_{\mathrm{zz}}-2\Gamma^{\Lambda}_{\mathrm{xx}}\Gamma^{\Lambda}_{\mathrm{xx}}-2\Gamma^{\Lambda}_{\mathrm{DM}}\Gamma^{\Lambda}_{\mathrm{DM}}\right) \\
& +S^{\Lambda}_{\mathrm{d}}G^{\Lambda}_{\mathrm{s}}\left(\Gamma^{\Lambda}_{\mathrm{zd}}\Gamma^{\Lambda}_{\mathrm{d}}+\Gamma^{\Lambda}_{\mathrm{d}}\Gamma^{\Lambda}_{\mathrm{zd}}+\Gamma^{\Lambda}_{\mathrm{zz}}\Gamma^{\Lambda}_{\mathrm{dz}}+\Gamma^{\Lambda}_{\mathrm{dz}}\Gamma^{\Lambda}_{\mathrm{zz}}-2i\Gamma^{\Lambda}_{\mathrm{DM}}\Gamma^{\Lambda}_{\mathrm{xx}}+2i\Gamma^{\Lambda}_{\mathrm{xx}}\Gamma^{\Lambda}_{\mathrm{DM}}\right) \\
& +S^{\Lambda}_{\mathrm{s}}G^{\Lambda}_{\mathrm{d}}\left(\Gamma^{\Lambda}_{\mathrm{dz}}\Gamma^{\Lambda}_{\mathrm{d}}+\Gamma^{\Lambda}_{\mathrm{d}}\Gamma^{\Lambda}_{\mathrm{dz}}+\Gamma^{\Lambda}_{\mathrm{zz}}\Gamma^{\Lambda}_{\mathrm{zd}}+\Gamma^{\Lambda}_{\mathrm{zd}}\Gamma^{\Lambda}_{\mathrm{zz}}+2i\Gamma^{\Lambda}_{\mathrm{DM}}\Gamma^{\Lambda}_{\mathrm{xx}}-2i\Gamma^{\Lambda}_{\mathrm{xx}}\Gamma^{\Lambda}_{\mathrm{DM}}\right) \\
& +S^{\Lambda}_{\mathrm{s}}G^{\Lambda}_{\mathrm{s}}\left(\Gamma^{\Lambda}_{\mathrm{d}}\Gamma^{\Lambda}_{\mathrm{d}}+\Gamma^{\Lambda}_{\mathrm{zd}}\Gamma^{\Lambda}_{\mathrm{zd}}+\Gamma^{\Lambda}_{\mathrm{dz}}\Gamma^{\Lambda}_{\mathrm{dz}}+\Gamma^{\Lambda}_{\mathrm{zz}}\Gamma^{\Lambda}_{\mathrm{zz}}+2\Gamma^{\Lambda}_{\mathrm{xx}}\Gamma^{\Lambda}_{\mathrm{xx}}+2\Gamma^{\Lambda}_{\mathrm{DM}}\Gamma^{\Lambda}_{\mathrm{DM}}\right) \\
& \Big]_{(i_1,i_2)(i_1,i_2)}(\omega_{1'},\omega_{2'};\omega_1+\omega_2-\omega_3,\omega_3)(\omega_1+\omega_2-\omega_3,\omega_3;\omega_1,\omega_2) \\
& -2\sum_j(\omega_{2'}+\omega_3-\omega_2)(\omega_3)\Big[\\
& S^{\Lambda}_{\mathrm{d}}\Big(G^{\Lambda}_{\mathrm{d}}\left(\Gamma^{\Lambda}_{\mathrm{zd}}\Gamma^{\Lambda}_{\mathrm{dz}}+\Gamma^{\Lambda}_{\mathrm{zz}}\Gamma^{\Lambda}_{\mathrm{zz}}\right)+G^{\Lambda}_{\mathrm{s}}\left(\Gamma^{\Lambda}_{\mathrm{zz}}\Gamma^{\Lambda}_{\mathrm{dz}}+\Gamma^{\Lambda}_{\mathrm{zd}}\Gamma^{\Lambda}_{\mathrm{zz}}\right)\Big) \\
& +S^{\Lambda}_{\mathrm{s}}\Big(G^{\Lambda}_{\mathrm{d}}\left(\Gamma^{\Lambda}_{\mathrm{zz}}\Gamma^{\Lambda}_{\mathrm{dz}}+\Gamma^{\Lambda}_{\mathrm{zd}}\Gamma^{\Lambda}_{\mathrm{zz}}\right)+G^{\Lambda}_{\mathrm{s}}\left(\Gamma^{\Lambda}_{\mathrm{zd}}\Gamma^{\Lambda}_{\mathrm{dz}}+\Gamma^{\Lambda}_{\mathrm{zz}}\Gamma^{\Lambda}_{\mathrm{zz}}\right)\Big) \\
& \Big]_{(i_1,j)(j,i_2)}(\omega_{1'},\omega_{2'}+\omega_3-\omega_2;\omega_1,\omega_3)(\omega_3,\omega_{2'};\omega_{2'}+\omega_3-\omega_2,\omega_2) \\
& -\Big[\omega_3\leftrightarrow\omega_{2'}+\omega_3-\omega_2\Big] \\
& +(\omega_{2'}+\omega_3-\omega_2)(\omega_3)\Big[\\
& S^{\Lambda}_{\mathrm{d}}G^{\Lambda}_{\mathrm{d}}\left(\Gamma^{\Lambda}_{\mathrm{zz}}(\Gamma^{\Lambda}_{\mathrm{d}}+\Gamma^{\Lambda}_{\mathrm{zz}}-2\Gamma^{\Lambda}_{\mathrm{xx}})+\Gamma^{\Lambda}_{\mathrm{zd}}(\Gamma^{\Lambda}_{\mathrm{zd}}+\Gamma^{\Lambda}_{\mathrm{dz}}-2i\Gamma^{\Lambda}_{\mathrm{DM}})\right) \\
& +S^{\Lambda}_{\mathrm{d}}G^{\Lambda}_{\mathrm{s}}\left(\Gamma^{\Lambda}_{\mathrm{zd}}(\Gamma^{\Lambda}_{\mathrm{d}}+\Gamma^{\Lambda}_{\mathrm{zz}}-2\Gamma^{\Lambda}_{\mathrm{xx}})+\Gamma^{\Lambda}_{\mathrm{zz}}(\Gamma^{\Lambda}_{\mathrm{zd}}+\Gamma^{\Lambda}_{\mathrm{dz}}-2i\Gamma^{\Lambda}_{\mathrm{DM}})\right) \\
& +S^{\Lambda}_{\mathrm{s}}G^{\Lambda}_{\mathrm{d}}\left(\Gamma^{\Lambda}_{\mathrm{zd}}(\Gamma^{\Lambda}_{\mathrm{d}}+\Gamma^{\Lambda}_{\mathrm{zz}}-2\Gamma^{\Lambda}_{\mathrm{xx}})+\Gamma^{\Lambda}_{\mathrm{zz}}(\Gamma^{\Lambda}_{\mathrm{zd}}+\Gamma^{\Lambda}_{\mathrm{dz}}-2i\Gamma^{\Lambda}_{\mathrm{DM}})\right) \\
& +S^{\Lambda}_{\mathrm{s}}G^{\Lambda}_{\mathrm{s}}\left(\Gamma^{\Lambda}_{\mathrm{zz}}(\Gamma^{\Lambda}_{\mathrm{d}}+\Gamma^{\Lambda}_{\mathrm{zz}}-2\Gamma^{\Lambda}_{\mathrm{xx}})+\Gamma^{\Lambda}_{\mathrm{zd}}(\Gamma^{\Lambda}_{\mathrm{zd}}+\Gamma^{\Lambda}_{\mathrm{dz}}-2i\Gamma^{\Lambda}_{\mathrm{DM}})\right) \\
& \Big]_{(i_1,i_2)(i_2,i_2)}(\omega_{1'},\omega_{2'}+\omega_3-\omega_2;\omega_1,\omega_3)(\omega_3,\omega_{2'};\omega_2,\omega_{2'}+\omega_3-\omega_2) \\
& +\Big[\omega_3\leftrightarrow\omega_{2'}+\omega_3-\omega_2\Big]
\end{aligned}
$$

$$
\begin{aligned}
&+(\omega_{2'}+\omega_3-\omega_2)(\omega_3)\Big[\\
&\quad S_{\mathrm{d}}^{\Lambda}G_{\mathrm{d}}^{\Lambda}\left((\Gamma_{\mathrm{d}}^{\Lambda}+\Gamma_{\mathrm{zz}}^{\Lambda}-2\Gamma_{\mathrm{xx}}^{\Lambda})\Gamma_{\mathrm{zz}}^{\Lambda}+(\Gamma_{\mathrm{zd}}^{\Lambda}+\Gamma_{\mathrm{dz}}^{\Lambda}+2i\Gamma_{\mathrm{DM}}^{\Lambda})\Gamma_{\mathrm{dz}}^{\Lambda}\right)\\
&+S_{\mathrm{d}}^{\Lambda}G_{\mathrm{s}}^{\Lambda}\left((\Gamma_{\mathrm{d}}^{\Lambda}+\Gamma_{\mathrm{zz}}^{\Lambda}-2\Gamma_{\mathrm{xx}}^{\Lambda})\Gamma_{\mathrm{dz}}^{\Lambda}+(\Gamma_{\mathrm{zd}}^{\Lambda}+\Gamma_{\mathrm{dz}}^{\Lambda}+2i\Gamma_{\mathrm{DM}}^{\Lambda})\Gamma_{\mathrm{zz}}^{\Lambda}\right)\\
&+S_{\mathrm{s}}^{\Lambda}G_{\mathrm{d}}^{\Lambda}\left((\Gamma_{\mathrm{d}}^{\Lambda}+\Gamma_{\mathrm{zz}}^{\Lambda}-2\Gamma_{\mathrm{xx}}^{\Lambda})\Gamma_{\mathrm{dz}}^{\Lambda}+(\Gamma_{\mathrm{zd}}^{\Lambda}+\Gamma_{\mathrm{dz}}^{\Lambda}+2i\Gamma_{\mathrm{DM}}^{\Lambda})\Gamma_{\mathrm{zz}}^{\Lambda}\right)\\
&+S_{\mathrm{s}}^{\Lambda}G_{\mathrm{s}}^{\Lambda}\left((\Gamma_{\mathrm{d}}^{\Lambda}+\Gamma_{\mathrm{zz}}^{\Lambda}-2\Gamma_{\mathrm{xx}}^{\Lambda})\Gamma_{\mathrm{zz}}^{\Lambda}+(\Gamma_{\mathrm{zd}}^{\Lambda}+\Gamma_{\mathrm{dz}}^{\Lambda}+2i\Gamma_{\mathrm{DM}}^{\Lambda})\Gamma_{\mathrm{dz}}^{\Lambda}\right)\\
&\quad\Big]_{(i_1,i_1)(i_1,i_2)}(\omega_{1'},\omega_{2'}+\omega_3-\omega_2;\omega_3,\omega_1)(\omega_3,\omega_{2'};\omega_{2'}+\omega_3-\omega_2,\omega_2)\\
&+\Big[\omega_3\leftrightarrow\omega_{2'}+\omega_3-\omega_2\Big]\\
&+(\omega_{1'}+\omega_3-\omega_2)(\omega_3)\Big[\\
&\quad S_{\mathrm{d}}^{\Lambda}G_{\mathrm{d}}^{\Lambda}\left(\Gamma_{\mathrm{dz}}^{\Lambda}\Gamma_{\mathrm{zd}}^{\Lambda}+\Gamma_{\mathrm{zd}}^{\Lambda}\Gamma_{\mathrm{dz}}^{\Lambda}+\Gamma_{\mathrm{zz}}^{\Lambda}\Gamma_{\mathrm{d}}^{\Lambda}+\Gamma_{\mathrm{d}}^{\Lambda}\Gamma_{\mathrm{zz}}^{\Lambda}+2\Gamma_{\mathrm{xx}}^{\Lambda}\Gamma_{\mathrm{xx}}^{\Lambda}+2\Gamma_{\mathrm{DM}}^{\Lambda}\Gamma_{\mathrm{DM}}^{\Lambda}\right)\\
&+S_{\mathrm{d}}^{\Lambda}G_{\mathrm{s}}^{\Lambda}\left(\Gamma_{\mathrm{dz}}^{\Lambda}\Gamma_{\mathrm{d}}^{\Lambda}+\Gamma_{\mathrm{d}}^{\Lambda}\Gamma_{\mathrm{dz}}^{\Lambda}+\Gamma_{\mathrm{zz}}^{\Lambda}\Gamma_{\mathrm{zd}}^{\Lambda}+\Gamma_{\mathrm{zd}}^{\Lambda}\Gamma_{\mathrm{zz}}^{\Lambda}-2i\Gamma_{\mathrm{DM}}^{\Lambda}\Gamma_{\mathrm{xx}}^{\Lambda}+2i\Gamma_{\mathrm{xx}}^{\Lambda}\Gamma_{\mathrm{DM}}^{\Lambda}\right)\\
&+S_{\mathrm{s}}^{\Lambda}G_{\mathrm{d}}^{\Lambda}\left(\Gamma_{\mathrm{zd}}^{\Lambda}\Gamma_{\mathrm{d}}^{\Lambda}+\Gamma_{\mathrm{d}}^{\Lambda}\Gamma_{\mathrm{zd}}^{\Lambda}+\Gamma_{\mathrm{zz}}^{\Lambda}\Gamma_{\mathrm{dz}}^{\Lambda}+\Gamma_{\mathrm{dz}}^{\Lambda}\Gamma_{\mathrm{zz}}^{\Lambda}-2i\Gamma_{\mathrm{DM}}^{\Lambda}\Gamma_{\mathrm{xx}}^{\Lambda}+2i\Gamma_{\mathrm{xx}}^{\Lambda}\Gamma_{\mathrm{DM}}^{\Lambda}\right)\\
&+S_{\mathrm{s}}^{\Lambda}G_{\mathrm{s}}^{\Lambda}\left(\Gamma_{\mathrm{d}}^{\Lambda}\Gamma_{\mathrm{d}}^{\Lambda}+\Gamma_{\mathrm{zd}}^{\Lambda}\Gamma_{\mathrm{zd}}^{\Lambda}+\Gamma_{\mathrm{dz}}^{\Lambda}\Gamma_{\mathrm{dz}}^{\Lambda}+\Gamma_{\mathrm{zz}}^{\Lambda}\Gamma_{\mathrm{zz}}^{\Lambda}+2\Gamma_{\mathrm{xx}}^{\Lambda}\Gamma_{\mathrm{xx}}^{\Lambda}+2\Gamma_{\mathrm{DM}}^{\Lambda}\Gamma_{\mathrm{DM}}^{\Lambda}\right)\\
&\quad\Big]_{(i_2,i_1)(i_2,i_1)}(\omega_{2'},\omega_{1'}+\omega_3-\omega_2;\omega_3,\omega_1)(\omega_3,\omega_{1'};\omega_2,\omega_{1'}+\omega_3-\omega_2)\\
&+(\omega_{1'}+\omega_3-\omega_2)(\omega_3)\Big[\\
&\quad S_{\mathrm{d}}^{\Lambda}G_{\mathrm{d}}^{\Lambda}\left(\Gamma_{\mathrm{dz}}^{\Lambda}\Gamma_{\mathrm{zd}}^{\Lambda}+\Gamma_{\mathrm{zd}}^{\Lambda}\Gamma_{\mathrm{dz}}^{\Lambda}+\Gamma_{\mathrm{zz}}^{\Lambda}\Gamma_{\mathrm{d}}^{\Lambda}+\Gamma_{\mathrm{d}}^{\Lambda}\Gamma_{\mathrm{zz}}^{\Lambda}+2\Gamma_{\mathrm{xx}}^{\Lambda}\Gamma_{\mathrm{xx}}^{\Lambda}+2\Gamma_{\mathrm{DM}}^{\Lambda}\Gamma_{\mathrm{DM}}^{\Lambda}\right)\\
&+S_{\mathrm{d}}^{\Lambda}G_{\mathrm{s}}^{\Lambda}\left(\Gamma_{\mathrm{zd}}^{\Lambda}\Gamma_{\mathrm{d}}^{\Lambda}+\Gamma_{\mathrm{d}}^{\Lambda}\Gamma_{\mathrm{zd}}^{\Lambda}+\Gamma_{\mathrm{zz}}^{\Lambda}\Gamma_{\mathrm{dz}}^{\Lambda}+\Gamma_{\mathrm{dz}}^{\Lambda}\Gamma_{\mathrm{zz}}^{\Lambda}-2i\Gamma_{\mathrm{DM}}^{\Lambda}\Gamma_{\mathrm{xx}}^{\Lambda}+2i\Gamma_{\mathrm{xx}}^{\Lambda}\Gamma_{\mathrm{DM}}^{\Lambda}\right)\\
&+S_{\mathrm{s}}^{\Lambda}G_{\mathrm{d}}^{\Lambda}\left(\Gamma_{\mathrm{d}}^{\Lambda}\Gamma_{\mathrm{dz}}^{\Lambda}+\Gamma_{\mathrm{d}}^{\Lambda}\Gamma_{\mathrm{dz}}^{\Lambda}+\Gamma_{\mathrm{zz}}^{\Lambda}\Gamma_{\mathrm{zd}}^{\Lambda}+\Gamma_{\mathrm{zd}}^{\Lambda}\Gamma_{\mathrm{zz}}^{\Lambda}-2i\Gamma_{\mathrm{DM}}^{\Lambda}\Gamma_{\mathrm{xx}}^{\Lambda}+2i\Gamma_{\mathrm{xx}}^{\Lambda}\Gamma_{\mathrm{DM}}^{\Lambda}\right)\\
&+S_{\mathrm{s}}^{\Lambda}G_{\mathrm{s}}^{\Lambda}\left(\Gamma_{\mathrm{d}}^{\Lambda}\Gamma_{\mathrm{d}}^{\Lambda}+\Gamma_{\mathrm{zd}}^{\Lambda}\Gamma_{\mathrm{zd}}^{\Lambda}+\Gamma_{\mathrm{dz}}^{\Lambda}\Gamma_{\mathrm{dz}}^{\Lambda}+\Gamma_{\mathrm{zz}}^{\Lambda}\Gamma_{\mathrm{zz}}^{\Lambda}+2\Gamma_{\mathrm{xx}}^{\Lambda}\Gamma_{\mathrm{xx}}^{\Lambda}+2\Gamma_{\mathrm{DM}}^{\Lambda}\Gamma_{\mathrm{DM}}^{\Lambda}\right)\\
&\quad\Big]_{(i_2,i_1)(i_2,i_1)}(\omega_{2'},\omega_3;\omega_{1'}+\omega_3-\omega_2,\omega_1)(\omega_{1'}+\omega_3-\omega_2,\omega_{1'};\omega_2,\omega_3)\Bigg\}
\end{aligned}
\tag{B.5}
$$

$$
\begin{aligned}
\frac{\mathrm{d}}{\mathrm{d}\Lambda}\Gamma^{\Lambda}_{\mathrm{xx}i_1i_2}(\omega_{1'},\omega_{2'};\omega_1,\omega_2) = \frac{1}{2\pi}\int_{-\infty}^{\infty}\mathrm{d}\omega_3 \Big\{ & (\omega_1+\omega_2-\omega_3)(\omega_3)\Big[\\
& S^{\Lambda}_{\mathrm{d}}G^{\Lambda}_{\mathrm{d}}\left(\Gamma^{\Lambda}_{\mathrm{xx}}(\Gamma^{\Lambda}_{\mathrm{d}}-\Gamma^{\Lambda}_{\mathrm{zz}})+(\Gamma^{\Lambda}_{\mathrm{d}}-\Gamma^{\Lambda}_{\mathrm{zz}})\Gamma^{\Lambda}_{\mathrm{xx}}+i\Gamma^{\Lambda}_{\mathrm{DM}}(\Gamma^{\Lambda}_{\mathrm{dz}}-\Gamma^{\Lambda}_{\mathrm{zd}})+i(\Gamma^{\Lambda}_{\mathrm{zd}}-\Gamma^{\Lambda}_{\mathrm{dz}})\Gamma^{\Lambda}_{\mathrm{DM}}\right) \\
& +S^{\Lambda}_{\mathrm{d}}G^{\Lambda}_{\mathrm{s}}\left(\Gamma^{\Lambda}_{\mathrm{xx}}(\Gamma^{\Lambda}_{\mathrm{zd}}-\Gamma^{\Lambda}_{\mathrm{dz}})+(\Gamma^{\Lambda}_{\mathrm{zd}}-\Gamma^{\Lambda}_{\mathrm{dz}})\Gamma^{\Lambda}_{\mathrm{xx}}+i\Gamma^{\Lambda}_{\mathrm{DM}}(\Gamma^{\Lambda}_{\mathrm{zz}}-\Gamma^{\Lambda}_{\mathrm{d}})+i(\Gamma^{\Lambda}_{\mathrm{d}}-\Gamma^{\Lambda}_{\mathrm{zz}})\Gamma^{\Lambda}_{\mathrm{DM}}\right) \\
& +S^{\Lambda}_{\mathrm{s}}G^{\Lambda}_{\mathrm{d}}\left(\Gamma^{\Lambda}_{\mathrm{xx}}(\Gamma^{\Lambda}_{\mathrm{dz}}-\Gamma^{\Lambda}_{\mathrm{zd}})+(\Gamma^{\Lambda}_{\mathrm{dz}}-\Gamma^{\Lambda}_{\mathrm{zd}})\Gamma^{\Lambda}_{\mathrm{xx}}+i\Gamma^{\Lambda}_{\mathrm{DM}}(\Gamma^{\Lambda}_{\mathrm{d}}-\Gamma^{\Lambda}_{\mathrm{zz}})+i(\Gamma^{\Lambda}_{\mathrm{zz}}-\Gamma^{\Lambda}_{\mathrm{d}})\Gamma^{\Lambda}_{\mathrm{DM}}\right) \\
& +S^{\Lambda}_{\mathrm{s}}G^{\Lambda}_{\mathrm{s}}\left(\Gamma^{\Lambda}_{\mathrm{xx}}(\Gamma^{\Lambda}_{\mathrm{zz}}-\Gamma^{\Lambda}_{\mathrm{d}})+(\Gamma^{\Lambda}_{\mathrm{zz}}-\Gamma^{\Lambda}_{\mathrm{d}})\Gamma^{\Lambda}_{\mathrm{xx}}+i\Gamma^{\Lambda}_{\mathrm{DM}}(\Gamma^{\Lambda}_{\mathrm{zd}}-\Gamma^{\Lambda}_{\mathrm{dz}})+i(\Gamma^{\Lambda}_{\mathrm{dz}}-\Gamma^{\Lambda}_{\mathrm{zd}})\Gamma^{\Lambda}_{\mathrm{DM}}\right) \\
& \Big]_{(i_1,i_2)(i_1,i_2)}(\omega_{1'},\omega_{2'};\omega_3,\omega_1+\omega_2-\omega_3)(\omega_3,\omega_1+\omega_2-\omega_3;\omega_1,\omega_2) \\
& +(\omega_1+\omega_2-\omega_3)(\omega_3)\Big[\\
& S^{\Lambda}_{\mathrm{d}}G^{\Lambda}_{\mathrm{d}}\left(\Gamma^{\Lambda}_{\mathrm{xx}}(\Gamma^{\Lambda}_{\mathrm{d}}-\Gamma^{\Lambda}_{\mathrm{zz}})+(\Gamma^{\Lambda}_{\mathrm{d}}-\Gamma^{\Lambda}_{\mathrm{zz}})\Gamma^{\Lambda}_{\mathrm{xx}}+i\Gamma^{\Lambda}_{\mathrm{DM}}(\Gamma^{\Lambda}_{\mathrm{dz}}-\Gamma^{\Lambda}_{\mathrm{zd}})+i(\Gamma^{\Lambda}_{\mathrm{zd}}-\Gamma^{\Lambda}_{\mathrm{dz}})\Gamma^{\Lambda}_{\mathrm{DM}}\right) \\
& +S^{\Lambda}_{\mathrm{d}}G^{\Lambda}_{\mathrm{s}}\left(\Gamma^{\Lambda}_{\mathrm{xx}}(\Gamma^{\Lambda}_{\mathrm{dz}}-\Gamma^{\Lambda}_{\mathrm{zd}})+(\Gamma^{\Lambda}_{\mathrm{dz}}-\Gamma^{\Lambda}_{\mathrm{zd}})\Gamma^{\Lambda}_{\mathrm{xx}}+i\Gamma^{\Lambda}_{\mathrm{DM}}(\Gamma^{\Lambda}_{\mathrm{d}}-\Gamma^{\Lambda}_{\mathrm{zz}})+i(\Gamma^{\Lambda}_{\mathrm{zz}}-\Gamma^{\Lambda}_{\mathrm{d}})\Gamma^{\Lambda}_{\mathrm{DM}}\right) \\
& +S^{\Lambda}_{\mathrm{s}}G^{\Lambda}_{\mathrm{d}}\left(\Gamma^{\Lambda}_{\mathrm{xx}}(\Gamma^{\Lambda}_{\mathrm{zd}}-\Gamma^{\Lambda}_{\mathrm{dz}})+(\Gamma^{\Lambda}_{\mathrm{zd}}-\Gamma^{\Lambda}_{\mathrm{dz}})\Gamma^{\Lambda}_{\mathrm{xx}}+i\Gamma^{\Lambda}_{\mathrm{DM}}(\Gamma^{\Lambda}_{\mathrm{zz}}-\Gamma^{\Lambda}_{\mathrm{d}})+i(\Gamma^{\Lambda}_{\mathrm{d}}-\Gamma^{\Lambda}_{\mathrm{zz}})\Gamma^{\Lambda}_{\mathrm{DM}}\right) \\
& +S^{\Lambda}_{\mathrm{s}}G^{\Lambda}_{\mathrm{s}}\left(\Gamma^{\Lambda}_{\mathrm{xx}}(\Gamma^{\Lambda}_{\mathrm{zz}}-\Gamma^{\Lambda}_{\mathrm{d}})+(\Gamma^{\Lambda}_{\mathrm{zz}}-\Gamma^{\Lambda}_{\mathrm{d}})\Gamma^{\Lambda}_{\mathrm{xx}}+i\Gamma^{\Lambda}_{\mathrm{DM}}(\Gamma^{\Lambda}_{\mathrm{zd}}-\Gamma^{\Lambda}_{\mathrm{dz}})+i(\Gamma^{\Lambda}_{\mathrm{dz}}-\Gamma^{\Lambda}_{\mathrm{zd}})\Gamma^{\Lambda}_{\mathrm{DM}}\right) \\
& \Big]_{(i_1,i_2)(i_1,i_2)}(\omega_{1'},\omega_{2'};\omega_1+\omega_2-\omega_3,\omega_3)(\omega_1+\omega_2-\omega_3,\omega_3;\omega_1,\omega_2) \\
& -2\sum_j(\omega_{2'}+\omega_3-\omega_2)(\omega_3)\Big[\\
& S^{\Lambda}_{\mathrm{d}}\Big(G^{\Lambda}_{\mathrm{d}}\left(\Gamma^{\Lambda}_{\mathrm{xx}}\Gamma^{\Lambda}_{\mathrm{xx}}-\Gamma^{\Lambda}_{\mathrm{DM}}\Gamma^{\Lambda}_{\mathrm{DM}}\right)+iG^{\Lambda}_{\mathrm{s}}\left(\Gamma^{\Lambda}_{\mathrm{DM}}\Gamma^{\Lambda}_{\mathrm{xx}}+\Gamma^{\Lambda}_{\mathrm{xx}}\Gamma^{\Lambda}_{\mathrm{DM}}\right)\Big) \\
& +S^{\Lambda}_{\mathrm{s}}\Big(-iG^{\Lambda}_{\mathrm{d}}\left(\Gamma^{\Lambda}_{\mathrm{DM}}\Gamma^{\Lambda}_{\mathrm{xx}}+\Gamma^{\Lambda}_{\mathrm{xx}}\Gamma^{\Lambda}_{\mathrm{DM}}\right)+G^{\Lambda}_{\mathrm{s}}\left(\Gamma^{\Lambda}_{\mathrm{DM}}\Gamma^{\Lambda}_{\mathrm{DM}}-\Gamma^{\Lambda}_{\mathrm{xx}}\Gamma^{\Lambda}_{\mathrm{xx}}\right)\Big) \\
& \Big]_{(i_1,j)(j,i_2)}(\omega_{1'},\omega_{2'}+\omega_3-\omega_2;\omega_1,\omega_3)(\omega_3,\omega_{2'};\omega_{2'}+\omega_3-\omega_2,\omega_2) \\
& -2\sum_j(\omega_{2'}+\omega_3-\omega_2)(\omega_3)\Big[\\
& S^{\Lambda}_{\mathrm{d}}\Big(G^{\Lambda}_{\mathrm{d}}\left(\Gamma^{\Lambda}_{\mathrm{xx}}\Gamma^{\Lambda}_{\mathrm{xx}}-\Gamma^{\Lambda}_{\mathrm{DM}}\Gamma^{\Lambda}_{\mathrm{DM}}\right)-iG^{\Lambda}_{\mathrm{s}}\left(\Gamma^{\Lambda}_{\mathrm{DM}}\Gamma^{\Lambda}_{\mathrm{xx}}+\Gamma^{\Lambda}_{\mathrm{xx}}\Gamma^{\Lambda}_{\mathrm{DM}}\right)\Big) \\
& +S^{\Lambda}_{\mathrm{s}}\Big(iG^{\Lambda}_{\mathrm{d}}\left(\Gamma^{\Lambda}_{\mathrm{DM}}\Gamma^{\Lambda}_{\mathrm{xx}}+\Gamma^{\Lambda}_{\mathrm{xx}}\Gamma^{\Lambda}_{\mathrm{DM}}\right)+G^{\Lambda}_{\mathrm{s}}\left(\Gamma^{\Lambda}_{\mathrm{DM}}\Gamma^{\Lambda}_{\mathrm{DM}}-\Gamma^{\Lambda}_{\mathrm{xx}}\Gamma^{\Lambda}_{\mathrm{xx}}\right)\Big) \\
& \Big]_{(i_1,j)(j,i_2)}(\omega_{1'},\omega_3;\omega_1,\omega_{2'}+\omega_3-\omega_2)(\omega_{2'}+\omega_3-\omega_2,\omega_{2'};\omega_3,\omega_2) \\
& +(\omega_{2'}+\omega_3-\omega_2)(\omega_3)\Big[\\
& S^{\Lambda}_{\mathrm{d}}G^{\Lambda}_{\mathrm{d}}\left(\Gamma^{\Lambda}_{\mathrm{xx}}(\Gamma^{\Lambda}_{\mathrm{d}}-\Gamma^{\Lambda}_{\mathrm{zz}})+i\Gamma^{\Lambda}_{\mathrm{DM}}(\Gamma^{\Lambda}_{\mathrm{zd}}-\Gamma^{\Lambda}_{\mathrm{dz}})\right) \\
& +S^{\Lambda}_{\mathrm{d}}G^{\Lambda}_{\mathrm{s}}\left(\Gamma^{\Lambda}_{\mathrm{xx}}(\Gamma^{\Lambda}_{\mathrm{zd}}-\Gamma^{\Lambda}_{\mathrm{dz}})+i\Gamma^{\Lambda}_{\mathrm{DM}}(\Gamma^{\Lambda}_{\mathrm{d}}-\Gamma^{\Lambda}_{\mathrm{zz}})\right) \\
& +S^{\Lambda}_{\mathrm{s}}G^{\Lambda}_{\mathrm{d}}\left(\Gamma^{\Lambda}_{\mathrm{xx}}(\Gamma^{\Lambda}_{\mathrm{dz}}-\Gamma^{\Lambda}_{\mathrm{zd}})-i\Gamma^{\Lambda}_{\mathrm{DM}}(\Gamma^{\Lambda}_{\mathrm{d}}-\Gamma^{\Lambda}_{\mathrm{zz}})\right) \\
& +S^{\Lambda}_{\mathrm{s}}G^{\Lambda}_{\mathrm{s}}\left(\Gamma^{\Lambda}_{\mathrm{xx}}(\Gamma^{\Lambda}_{\mathrm{zz}}-\Gamma^{\Lambda}_{\mathrm{d}})-i\Gamma^{\Lambda}_{\mathrm{DM}}(\Gamma^{\Lambda}_{\mathrm{zd}}-\Gamma^{\Lambda}_{\mathrm{dz}})\right) \\
& \Big]_{(i_1,i_2)(i_2,i_2)}(\omega_{1'},\omega_{2'}+\omega_3-\omega_2;\omega_1,\omega_3)(\omega_3,\omega_{2'};\omega_2,\omega_{2'}+\omega_3-\omega_2)
\end{aligned}
$$

$$
\begin{aligned}
&+(\omega_{2'}+\omega_3-\omega_2)(\omega_3)\Big[\\
&\quad S_{\mathrm{d}}^{\Lambda}G_{\mathrm{d}}^{\Lambda}\left(\Gamma_{\mathrm{xx}}^{\Lambda}(\Gamma_{\mathrm{d}}^{\Lambda}-\Gamma_{\mathrm{zz}}^{\Lambda})+i\Gamma_{\mathrm{DM}}^{\Lambda}(\Gamma_{\mathrm{zd}}^{\Lambda}-\Gamma_{\mathrm{dz}}^{\Lambda})\right)\\
&+S_{\mathrm{d}}^{\Lambda}G_{\mathrm{s}}^{\Lambda}\left(\Gamma_{\mathrm{xx}}^{\Lambda}(\Gamma_{\mathrm{dz}}^{\Lambda}-\Gamma_{\mathrm{zd}}^{\Lambda})-i\Gamma_{\mathrm{DM}}^{\Lambda}(\Gamma_{\mathrm{d}}^{\Lambda}-\Gamma_{\mathrm{zz}}^{\Lambda})\right)\\
&+S_{\mathrm{s}}^{\Lambda}G_{\mathrm{d}}^{\Lambda}\left(\Gamma_{\mathrm{xx}}^{\Lambda}(\Gamma_{\mathrm{zd}}^{\Lambda}-\Gamma_{\mathrm{dz}}^{\Lambda})+i\Gamma_{\mathrm{DM}}^{\Lambda}(\Gamma_{\mathrm{d}}^{\Lambda}-\Gamma_{\mathrm{zz}}^{\Lambda})\right)\\
&+S_{\mathrm{s}}^{\Lambda}G_{\mathrm{s}}^{\Lambda}\left(\Gamma_{\mathrm{xx}}^{\Lambda}(\Gamma_{\mathrm{zz}}^{\Lambda}-\Gamma_{\mathrm{d}}^{\Lambda})-i\Gamma_{\mathrm{DM}}^{\Lambda}(\Gamma_{\mathrm{zd}}^{\Lambda}-\Gamma_{\mathrm{dz}}^{\Lambda})\right)\\
&\quad\Big]_{(i_1,i_2)(i_2,i_2)}(\omega_{1'},\omega_3;\omega_1,\omega_{2'}+\omega_3-\omega_2)(\omega_{2'}+\omega_3-\omega_2,\omega_{2'};\omega_2,\omega_3)\\
&+(\omega_{2'}+\omega_3-\omega_2)(\omega_3)\Big[\\
&\quad S_{\mathrm{d}}^{\Lambda}G_{\mathrm{d}}^{\Lambda}\left((\Gamma_{\mathrm{d}}^{\Lambda}-\Gamma_{\mathrm{zz}}^{\Lambda})\Gamma_{\mathrm{xx}}^{\Lambda}+i(\Gamma_{\mathrm{zd}}^{\Lambda}-\Gamma_{\mathrm{dz}}^{\Lambda})\Gamma_{\mathrm{DM}}^{\Lambda}\right)\\
&+S_{\mathrm{d}}^{\Lambda}G_{\mathrm{s}}^{\Lambda}\left((\Gamma_{\mathrm{zd}}^{\Lambda}-\Gamma_{\mathrm{dz}}^{\Lambda})\Gamma_{\mathrm{xx}}^{\Lambda}+i(\Gamma_{\mathrm{d}}^{\Lambda}-\Gamma_{\mathrm{zz}}^{\Lambda})\Gamma_{\mathrm{DM}}^{\Lambda}\right)\\
&+S_{\mathrm{s}}^{\Lambda}G_{\mathrm{d}}^{\Lambda}\left((\Gamma_{\mathrm{dz}}^{\Lambda}-\Gamma_{\mathrm{zd}}^{\Lambda})\Gamma_{\mathrm{xx}}^{\Lambda}-i(\Gamma_{\mathrm{d}}^{\Lambda}-\Gamma_{\mathrm{zz}}^{\Lambda})\Gamma_{\mathrm{DM}}^{\Lambda}\right)\\
&+S_{\mathrm{s}}^{\Lambda}G_{\mathrm{s}}^{\Lambda}\left((\Gamma_{\mathrm{zz}}^{\Lambda}-\Gamma_{\mathrm{d}}^{\Lambda})\Gamma_{\mathrm{xx}}^{\Lambda}-i(\Gamma_{\mathrm{zd}}^{\Lambda}-\Gamma_{\mathrm{dz}}^{\Lambda})\Gamma_{\mathrm{DM}}^{\Lambda}\right)\\
&\quad\Big]_{(i_1,i_1)(i_1,i_2)}(\omega_{1'},\omega_{2'}+\omega_3-\omega_2;\omega_3,\omega_1)(\omega_3,\omega_{2'};\omega_{2'}+\omega_3-\omega_2,\omega_2)\\
&+(\omega_{2'}+\omega_3-\omega_2)(\omega_3)\Big[\\
&\quad S_{\mathrm{d}}^{\Lambda}G_{\mathrm{d}}^{\Lambda}\left((\Gamma_{\mathrm{d}}^{\Lambda}-\Gamma_{\mathrm{zz}}^{\Lambda})\Gamma_{\mathrm{xx}}^{\Lambda}+i(\Gamma_{\mathrm{zd}}^{\Lambda}-\Gamma_{\mathrm{dz}}^{\Lambda})\Gamma_{\mathrm{DM}}^{\Lambda}\right)\\
&+S_{\mathrm{d}}^{\Lambda}G_{\mathrm{s}}^{\Lambda}\left((\Gamma_{\mathrm{dz}}^{\Lambda}-\Gamma_{\mathrm{zd}}^{\Lambda})\Gamma_{\mathrm{xx}}^{\Lambda}-i(\Gamma_{\mathrm{d}}^{\Lambda}-\Gamma_{\mathrm{zz}}^{\Lambda})\Gamma_{\mathrm{DM}}^{\Lambda}\right)\\
&+S_{\mathrm{s}}^{\Lambda}G_{\mathrm{d}}^{\Lambda}\left((\Gamma_{\mathrm{zd}}^{\Lambda}-\Gamma_{\mathrm{dz}}^{\Lambda})\Gamma_{\mathrm{xx}}^{\Lambda}+i(\Gamma_{\mathrm{d}}^{\Lambda}-\Gamma_{\mathrm{zz}}^{\Lambda})\Gamma_{\mathrm{DM}}^{\Lambda}\right)\\
&+S_{\mathrm{s}}^{\Lambda}G_{\mathrm{s}}^{\Lambda}\left((\Gamma_{\mathrm{zz}}^{\Lambda}-\Gamma_{\mathrm{d}}^{\Lambda})\Gamma_{\mathrm{xx}}^{\Lambda}-i(\Gamma_{\mathrm{zd}}^{\Lambda}-\Gamma_{\mathrm{dz}}^{\Lambda})\Gamma_{\mathrm{DM}}^{\Lambda}\right)\\
&\quad\Big]_{(i_1,i_1)(i_1,i_2)}(\omega_{1'},\omega_3;\omega_{2'}+\omega_3-\omega_2,\omega_1)(\omega_{2'}+\omega_3-\omega_2;,\omega_{2'};\omega_3,\omega_2)\\
&+(\omega_{1'}+\omega_3-\omega_2)(\omega_3)\Big[\\
&\quad S_{\mathrm{d}}^{\Lambda}G_{\mathrm{d}}^{\Lambda}\left(\Gamma_{\mathrm{xx}}^{\Lambda}(\Gamma_{\mathrm{d}}^{\Lambda}+\Gamma_{\mathrm{zz}}^{\Lambda})+(\Gamma_{\mathrm{d}}^{\Lambda}+\Gamma_{\mathrm{zz}}^{\Lambda})\Gamma_{\mathrm{xx}}^{\Lambda}-i\Gamma_{\mathrm{DM}}^{\Lambda}(\Gamma_{\mathrm{zd}}^{\Lambda}+\Gamma_{\mathrm{dz}}^{\Lambda})+i(\Gamma_{\mathrm{zd}}^{\Lambda}+\Gamma_{\mathrm{dz}}^{\Lambda})\Gamma_{\mathrm{DM}}^{\Lambda}\right)\\
&+S_{\mathrm{d}}^{\Lambda}G_{\mathrm{s}}^{\Lambda}\left(\Gamma_{\mathrm{xx}}^{\Lambda}(\Gamma_{\mathrm{zd}}^{\Lambda}+\Gamma_{\mathrm{dz}}^{\Lambda})+(\Gamma_{\mathrm{zd}}^{\Lambda}+\Gamma_{\mathrm{dz}}^{\Lambda})\Gamma_{\mathrm{xx}}^{\Lambda}-i\Gamma_{\mathrm{DM}}^{\Lambda}(\Gamma_{\mathrm{d}}^{\Lambda}+\Gamma_{\mathrm{zz}}^{\Lambda})+i(\Gamma_{\mathrm{d}}^{\Lambda}+\Gamma_{\mathrm{zz}}^{\Lambda})\Gamma_{\mathrm{DM}}^{\Lambda}\right)\\
&+S_{\mathrm{s}}^{\Lambda}G_{\mathrm{d}}^{\Lambda}\left(\Gamma_{\mathrm{xx}}^{\Lambda}(\Gamma_{\mathrm{zd}}^{\Lambda}+\Gamma_{\mathrm{dz}}^{\Lambda})+(\Gamma_{\mathrm{zd}}^{\Lambda}+\Gamma_{\mathrm{dz}}^{\Lambda})\Gamma_{\mathrm{xx}}^{\Lambda}-i\Gamma_{\mathrm{DM}}^{\Lambda}(\Gamma_{\mathrm{d}}^{\Lambda}+\Gamma_{\mathrm{zz}}^{\Lambda})+i(\Gamma_{\mathrm{d}}^{\Lambda}+\Gamma_{\mathrm{zz}}^{\Lambda})\Gamma_{\mathrm{DM}}^{\Lambda}\right)\\
&+S_{\mathrm{s}}^{\Lambda}G_{\mathrm{s}}^{\Lambda}\left(\Gamma_{\mathrm{xx}}^{\Lambda}(\Gamma_{\mathrm{d}}^{\Lambda}+\Gamma_{\mathrm{zz}}^{\Lambda})+(\Gamma_{\mathrm{d}}^{\Lambda}+\Gamma_{\mathrm{zz}}^{\Lambda})\Gamma_{\mathrm{xx}}^{\Lambda}-i\Gamma_{\mathrm{DM}}^{\Lambda}(\Gamma_{\mathrm{zd}}^{\Lambda}+\Gamma_{\mathrm{dz}}^{\Lambda})+i(\Gamma_{\mathrm{zd}}^{\Lambda}+\Gamma_{\mathrm{dz}}^{\Lambda})\Gamma_{\mathrm{DM}}^{\Lambda}\right)\\
&\quad\Big]_{(i_2,i_1)(i_2,i_1)}(\omega_{2'},\omega_{1'}+\omega_3-\omega_2;\omega_3,\omega_1)(\omega_3,\omega_{1'};\omega_2,\omega_{1'}+\omega_3-\omega_2)\\
&+\Big[\omega_3\leftrightarrow\omega_{1'}+\omega_3-\omega_2\Big]\Bigg\}
\end{aligned}
\tag{B.6}
$$

$$
\begin{aligned}
\frac{\mathrm{d}}{\mathrm{d}\Lambda}\Gamma^{\Lambda}_{\mathrm{DM}i_1i_2}(\omega_{1'},\omega_{2'};\omega_1,\omega_2) = \frac{1}{2\pi}\int_{-\infty}^{\infty}\mathrm{d}\omega_3 \Big\{ & (\omega_1+\omega_2-\omega_3)(\omega_3)\Big[\\
& S^{\Lambda}_{\mathrm{d}}G^{\Lambda}_{\mathrm{d}}\left(i\Gamma^{\Lambda}_{\mathrm{xx}}(\Gamma^{\Lambda}_{\mathrm{zd}}-\Gamma^{\Lambda}_{\mathrm{dz}})-i(\Gamma^{\Lambda}_{\mathrm{zd}}-\Gamma^{\Lambda}_{\mathrm{dz}})\Gamma^{\Lambda}_{\mathrm{xx}}+\Gamma^{\Lambda}_{\mathrm{DM}}(\Gamma^{\Lambda}_{\mathrm{d}}-\Gamma^{\Lambda}_{\mathrm{zz}})+(\Gamma^{\Lambda}_{\mathrm{d}}-\Gamma^{\Lambda}_{\mathrm{zz}})\Gamma^{\Lambda}_{\mathrm{DM}}\right) \\
& +S^{\Lambda}_{\mathrm{d}}G^{\Lambda}_{\mathrm{s}}\left(i\Gamma^{\Lambda}_{\mathrm{xx}}(\Gamma^{\Lambda}_{\mathrm{d}}-\Gamma^{\Lambda}_{\mathrm{zz}})-i(\Gamma^{\Lambda}_{\mathrm{d}}-\Gamma^{\Lambda}_{\mathrm{zz}})\Gamma^{\Lambda}_{\mathrm{xx}}+\Gamma^{\Lambda}_{\mathrm{DM}}(\Gamma^{\Lambda}_{\mathrm{zd}}-\Gamma^{\Lambda}_{\mathrm{dz}})+(\Gamma^{\Lambda}_{\mathrm{zd}}-\Gamma^{\Lambda}_{\mathrm{dz}})\Gamma^{\Lambda}_{\mathrm{DM}}\right) \\
& +S^{\Lambda}_{\mathrm{s}}G^{\Lambda}_{\mathrm{d}}\left(i\Gamma^{\Lambda}_{\mathrm{xx}}(\Gamma^{\Lambda}_{\mathrm{zz}}-\Gamma^{\Lambda}_{\mathrm{d}})+i(\Gamma^{\Lambda}_{\mathrm{d}}-\Gamma^{\Lambda}_{\mathrm{zz}})\Gamma^{\Lambda}_{\mathrm{xx}}+\Gamma^{\Lambda}_{\mathrm{DM}}(\Gamma^{\Lambda}_{\mathrm{dz}}-\Gamma^{\Lambda}_{\mathrm{zd}})+(\Gamma^{\Lambda}_{\mathrm{dz}}-\Gamma^{\Lambda}_{\mathrm{zd}})\Gamma^{\Lambda}_{\mathrm{DM}}\right) \\
& +S^{\Lambda}_{\mathrm{s}}G^{\Lambda}_{\mathrm{s}}\left(i\Gamma^{\Lambda}_{\mathrm{xx}}(\Gamma^{\Lambda}_{\mathrm{dz}}-\Gamma^{\Lambda}_{\mathrm{zd}})+i(\Gamma^{\Lambda}_{\mathrm{zd}}-\Gamma^{\Lambda}_{\mathrm{dz}})\Gamma^{\Lambda}_{\mathrm{xx}}+\Gamma^{\Lambda}_{\mathrm{DM}}(\Gamma^{\Lambda}_{\mathrm{zz}}-\Gamma^{\Lambda}_{\mathrm{d}})+(\Gamma^{\Lambda}_{\mathrm{zz}}-\Gamma^{\Lambda}_{\mathrm{d}})\Gamma^{\Lambda}_{\mathrm{DM}}\right) \\
& \Big]_{(i_1,i_2)(i_1,i_2)}(\omega_{1'},\omega_{2'};\omega_3,\omega_1+\omega_2-\omega_3)(\omega_3,\omega_1+\omega_2-\omega_3;\omega_1,\omega_2) \\
& +(\omega_1+\omega_2-\omega_3)(\omega_3)\Big[\\
& S^{\Lambda}_{\mathrm{d}}G^{\Lambda}_{\mathrm{d}}\left(i\Gamma^{\Lambda}_{\mathrm{xx}}(\Gamma^{\Lambda}_{\mathrm{zd}}-\Gamma^{\Lambda}_{\mathrm{dz}})+i(\Gamma^{\Lambda}_{\mathrm{dz}}-\Gamma^{\Lambda}_{\mathrm{zd}})\Gamma^{\Lambda}_{\mathrm{xx}}+\Gamma^{\Lambda}_{\mathrm{DM}}(\Gamma^{\Lambda}_{\mathrm{d}}-\Gamma^{\Lambda}_{\mathrm{zz}})+(\Gamma^{\Lambda}_{\mathrm{d}}-\Gamma^{\Lambda}_{\mathrm{zz}})\Gamma^{\Lambda}_{\mathrm{DM}}\right) \\
& +S^{\Lambda}_{\mathrm{d}}G^{\Lambda}_{\mathrm{s}}\left(i\Gamma^{\Lambda}_{\mathrm{xx}}(\Gamma^{\Lambda}_{\mathrm{zz}}-\Gamma^{\Lambda}_{\mathrm{d}})+i(\Gamma^{\Lambda}_{\mathrm{d}}-\Gamma^{\Lambda}_{\mathrm{zz}})\Gamma^{\Lambda}_{\mathrm{xx}}+\Gamma^{\Lambda}_{\mathrm{DM}}(\Gamma^{\Lambda}_{\mathrm{dz}}-\Gamma^{\Lambda}_{\mathrm{zd}})+(\Gamma^{\Lambda}_{\mathrm{dz}}-\Gamma^{\Lambda}_{\mathrm{zd}})\Gamma^{\Lambda}_{\mathrm{DM}}\right) \\
& +S^{\Lambda}_{\mathrm{s}}G^{\Lambda}_{\mathrm{d}}\left(i\Gamma^{\Lambda}_{\mathrm{xx}}(\Gamma^{\Lambda}_{\mathrm{d}}-\Gamma^{\Lambda}_{\mathrm{zz}})+i(\Gamma^{\Lambda}_{\mathrm{zz}}-\Gamma^{\Lambda}_{\mathrm{d}})\Gamma^{\Lambda}_{\mathrm{xx}}+\Gamma^{\Lambda}_{\mathrm{DM}}(\Gamma^{\Lambda}_{\mathrm{zd}}-\Gamma^{\Lambda}_{\mathrm{dz}})+(\Gamma^{\Lambda}_{\mathrm{zd}}-\Gamma^{\Lambda}_{\mathrm{dz}})\Gamma^{\Lambda}_{\mathrm{DM}}\right) \\
& +S^{\Lambda}_{\mathrm{s}}G^{\Lambda}_{\mathrm{s}}\left(i\Gamma^{\Lambda}_{\mathrm{xx}}(\Gamma^{\Lambda}_{\mathrm{dz}}-\Gamma^{\Lambda}_{\mathrm{zd}})+i(\Gamma^{\Lambda}_{\mathrm{zd}}-\Gamma^{\Lambda}_{\mathrm{dz}})\Gamma^{\Lambda}_{\mathrm{xx}}+\Gamma^{\Lambda}_{\mathrm{DM}}(\Gamma^{\Lambda}_{\mathrm{d}}-\Gamma^{\Lambda}_{\mathrm{zz}})+(\Gamma^{\Lambda}_{\mathrm{d}}-\Gamma^{\Lambda}_{\mathrm{zz}})\Gamma^{\Lambda}_{\mathrm{DM}}\right) \\
& \Big]_{(i_1,i_2)(i_1,i_2)}(\omega_{1'},\omega_{2'};\omega_1+\omega_2-\omega_3,\omega_3)(\omega_1+\omega_2-\omega_3,\omega_3;\omega_1,\omega_2) \\
& -2\sum_j(\omega_{2'}+\omega_3-\omega_2)(\omega_3)\Big[\\
& S^{\Lambda}_{\mathrm{d}}\Big(G^{\Lambda}_{\mathrm{d}}\left(\Gamma^{\Lambda}_{\mathrm{DM}}\Gamma^{\Lambda}_{\mathrm{xx}}+\Gamma^{\Lambda}_{\mathrm{xx}}\Gamma^{\Lambda}_{\mathrm{DM}}\right)+iG^{\Lambda}_{\mathrm{s}}\left(\Gamma^{\Lambda}_{\mathrm{DM}}\Gamma^{\Lambda}_{\mathrm{DM}}-\Gamma^{\Lambda}_{\mathrm{xx}}\Gamma^{\Lambda}_{\mathrm{xx}}\right)\Big) \\
& +S^{\Lambda}_{\mathrm{s}}\Big(iG^{\Lambda}_{\mathrm{d}}\left(\Gamma^{\Lambda}_{\mathrm{xx}}\Gamma^{\Lambda}_{\mathrm{xx}}-\Gamma^{\Lambda}_{\mathrm{DM}}\Gamma^{\Lambda}_{\mathrm{DM}}\right)-G^{\Lambda}_{\mathrm{s}}\left(\Gamma^{\Lambda}_{\mathrm{DM}}\Gamma^{\Lambda}_{\mathrm{xx}}+\Gamma^{\Lambda}_{\mathrm{xx}}\Gamma^{\Lambda}_{\mathrm{DM}}\right)\Big) \\
& \Big]_{(i_1,j)(j,i_2)}(\omega_{1'},\omega_{2'}+\omega_3-\omega_2;\omega_1,\omega_3)(\omega_3,\omega_{2'};\omega_{2'}+\omega_3-\omega_2,\omega_2) \\
& -2\sum_j(\omega_{2'}+\omega_3-\omega_2)(\omega_3)\Big[\\
& S^{\Lambda}_{\mathrm{d}}\Big(G^{\Lambda}_{\mathrm{d}}\left(\Gamma^{\Lambda}_{\mathrm{DM}}\Gamma^{\Lambda}_{\mathrm{xx}}+\Gamma^{\Lambda}_{\mathrm{xx}}\Gamma^{\Lambda}_{\mathrm{DM}}\right)+iG^{\Lambda}_{\mathrm{s}}\left(\Gamma^{\Lambda}_{\mathrm{xx}}\Gamma^{\Lambda}_{\mathrm{xx}}-\Gamma^{\Lambda}_{\mathrm{DM}}\Gamma^{\Lambda}_{\mathrm{DM}}\right)\Big) \\
& +S^{\Lambda}_{\mathrm{s}}\Big(iG^{\Lambda}_{\mathrm{d}}\left(\Gamma^{\Lambda}_{\mathrm{DM}}\Gamma^{\Lambda}_{\mathrm{DM}}-\Gamma^{\Lambda}_{\mathrm{xx}}\Gamma^{\Lambda}_{\mathrm{xx}}\right)-G^{\Lambda}_{\mathrm{s}}\left(\Gamma^{\Lambda}_{\mathrm{DM}}\Gamma^{\Lambda}_{\mathrm{xx}}+\Gamma^{\Lambda}_{\mathrm{xx}}\Gamma^{\Lambda}_{\mathrm{DM}}\right)\Big) \\
& \Big]_{(i_1,j)(j,i_2)}(\omega_{1'},\omega_3;\omega_1,\omega_{2'}+\omega_3-\omega_2)(\omega_{2'}+\omega_3-\omega_2,\omega_{2'};\omega_3,\omega_2) \\
& +(\omega_{2'}+\omega_3-\omega_2)(\omega_3)\Big[\\
& S^{\Lambda}_{\mathrm{d}}G^{\Lambda}_{\mathrm{d}}\left(i\Gamma^{\Lambda}_{\mathrm{xx}}(\Gamma^{\Lambda}_{\mathrm{dz}}-\Gamma^{\Lambda}_{\mathrm{zd}})+\Gamma^{\Lambda}_{\mathrm{DM}}(\Gamma^{\Lambda}_{\mathrm{d}}-\Gamma^{\Lambda}_{\mathrm{zz}})\right) \\
& +S^{\Lambda}_{\mathrm{d}}G^{\Lambda}_{\mathrm{s}}\left(i\Gamma^{\Lambda}_{\mathrm{xx}}(\Gamma^{\Lambda}_{\mathrm{zz}}-\Gamma^{\Lambda}_{\mathrm{d}})+\Gamma^{\Lambda}_{\mathrm{DM}}(\Gamma^{\Lambda}_{\mathrm{zd}}-\Gamma^{\Lambda}_{\mathrm{dz}})\right) \\
& +S^{\Lambda}_{\mathrm{s}}G^{\Lambda}_{\mathrm{d}}\left(i\Gamma^{\Lambda}_{\mathrm{xx}}(\Gamma^{\Lambda}_{\mathrm{d}}-\Gamma^{\Lambda}_{\mathrm{zz}})+\Gamma^{\Lambda}_{\mathrm{DM}}(\Gamma^{\Lambda}_{\mathrm{dz}}-\Gamma^{\Lambda}_{\mathrm{zd}})\right) \\
& +S^{\Lambda}_{\mathrm{s}}G^{\Lambda}_{\mathrm{s}}\left(i\Gamma^{\Lambda}_{\mathrm{xx}}(\Gamma^{\Lambda}_{\mathrm{zd}}-\Gamma^{\Lambda}_{\mathrm{dz}})+\Gamma^{\Lambda}_{\mathrm{DM}}(\Gamma^{\Lambda}_{\mathrm{zz}}-\Gamma^{\Lambda}_{\mathrm{d}})\right) \\
& \Big]_{(i_1,i_2)(i_2,i_2)}(\omega_{1'},\omega_{2'}+\omega_3-\omega_2;\omega_1,\omega_3)(\omega_3,\omega_{2'};\omega_2,\omega_{2'}+\omega_3-\omega_2)
\end{aligned}
$$

$$
\begin{aligned}
&+(\omega_{2'}+\omega_3-\omega_2)(\omega_3)\Big[\\
&\quad S_{\mathrm{d}}^{\Lambda}G_{\mathrm{d}}^{\Lambda}\left(i\Gamma_{\mathrm{xx}}^{\Lambda}(\Gamma_{\mathrm{dz}}^{\Lambda}-\Gamma_{\mathrm{zd}}^{\Lambda})+\Gamma_{\mathrm{DM}}^{\Lambda}(\Gamma_{\mathrm{d}}^{\Lambda}-\Gamma_{\mathrm{zz}}^{\Lambda})\right)\\
&+S_{\mathrm{d}}^{\Lambda}G_{\mathrm{s}}^{\Lambda}\left(i\Gamma_{\mathrm{xx}}^{\Lambda}(\Gamma_{\mathrm{d}}^{\Lambda}-\Gamma_{\mathrm{zz}}^{\Lambda})+\Gamma_{\mathrm{DM}}^{\Lambda}(\Gamma_{\mathrm{dz}}^{\Lambda}-\Gamma_{\mathrm{zd}}^{\Lambda})\right)\\
&+S_{\mathrm{s}}^{\Lambda}G_{\mathrm{d}}^{\Lambda}\left(i\Gamma_{\mathrm{xx}}^{\Lambda}(\Gamma_{\mathrm{zz}}^{\Lambda}-\Gamma_{\mathrm{d}}^{\Lambda})+\Gamma_{\mathrm{DM}}^{\Lambda}(\Gamma_{\mathrm{zd}}^{\Lambda}-\Gamma_{\mathrm{dz}}^{\Lambda})\right)\\
&+S_{\mathrm{s}}^{\Lambda}G_{\mathrm{s}}^{\Lambda}\left(i\Gamma_{\mathrm{xx}}^{\Lambda}(\Gamma_{\mathrm{zd}}^{\Lambda}-\Gamma_{\mathrm{dz}}^{\Lambda})+\Gamma_{\mathrm{DM}}^{\Lambda}(\Gamma_{\mathrm{zz}}^{\Lambda}-\Gamma_{\mathrm{d}}^{\Lambda})\right)\\
&\quad\Big]_{(i_1,i_2)(i_2,i_2)}(\omega_{1'},\omega_3;\omega_1,\omega_{2'}+\omega_3-\omega_2)(\omega_{2'}+\omega_3-\omega_2,\omega_{2'};\omega_2,\omega_3)\\
&+(\omega_{2'}+\omega_3-\omega_2)(\omega_3)\Big[\\
&\quad S_{\mathrm{d}}^{\Lambda}G_{\mathrm{d}}^{\Lambda}\left(i(\Gamma_{\mathrm{dz}}^{\Lambda}-\Gamma_{\mathrm{zd}}^{\Lambda})\Gamma_{\mathrm{xx}}^{\Lambda}+(\Gamma_{\mathrm{d}}^{\Lambda}-\Gamma_{\mathrm{zz}}^{\Lambda})\Gamma_{\mathrm{DM}}^{\Lambda}\right)\\
&+S_{\mathrm{d}}^{\Lambda}G_{\mathrm{s}}^{\Lambda}\left(i(\Gamma_{\mathrm{zz}}^{\Lambda}-\Gamma_{\mathrm{d}}^{\Lambda})\Gamma_{\mathrm{xx}}^{\Lambda}+(\Gamma_{\mathrm{zd}}^{\Lambda}-\Gamma_{\mathrm{dz}}^{\Lambda})\Gamma_{\mathrm{DM}}^{\Lambda}\right)\\
&+S_{\mathrm{s}}^{\Lambda}G_{\mathrm{d}}^{\Lambda}\left(i(\Gamma_{\mathrm{d}}^{\Lambda}-\Gamma_{\mathrm{zz}}^{\Lambda})\Gamma_{\mathrm{xx}}^{\Lambda}+(\Gamma_{\mathrm{dz}}^{\Lambda}-\Gamma_{\mathrm{zd}}^{\Lambda})\Gamma_{\mathrm{DM}}^{\Lambda}\right)\\
&+S_{\mathrm{s}}^{\Lambda}G_{\mathrm{s}}^{\Lambda}\left(i(\Gamma_{\mathrm{zd}}^{\Lambda}-\Gamma_{\mathrm{dz}}^{\Lambda})\Gamma_{\mathrm{xx}}^{\Lambda}+(\Gamma_{\mathrm{zz}}^{\Lambda}-\Gamma_{\mathrm{d}}^{\Lambda})\Gamma_{\mathrm{DM}}^{\Lambda}\right)\\
&\quad\Big]_{(i_1,i_1)(i_1,i_2)}(\omega_{1'},\omega_{2'}+\omega_3-\omega_2;\omega_3,\omega_1)(\omega_3,\omega_{2'};\omega_{2'}+\omega_3-\omega_2,\omega_2)\\
&+(\omega_{2'}+\omega_3-\omega_2)(\omega_3)\Big[\\
&\quad S_{\mathrm{d}}^{\Lambda}G_{\mathrm{d}}^{\Lambda}\left(i(\Gamma_{\mathrm{dz}}^{\Lambda}-\Gamma_{\mathrm{zd}}^{\Lambda})\Gamma_{\mathrm{xx}}^{\Lambda}+(\Gamma_{\mathrm{d}}^{\Lambda}-\Gamma_{\mathrm{zz}}^{\Lambda})\Gamma_{\mathrm{DM}}^{\Lambda}\right)\\
&+S_{\mathrm{d}}^{\Lambda}G_{\mathrm{s}}^{\Lambda}\left(i(\Gamma_{\mathrm{d}}^{\Lambda}-\Gamma_{\mathrm{zz}}^{\Lambda})\Gamma_{\mathrm{xx}}^{\Lambda}+(\Gamma_{\mathrm{dz}}^{\Lambda}-\Gamma_{\mathrm{zd}}^{\Lambda})\Gamma_{\mathrm{DM}}^{\Lambda}\right)\\
&+S_{\mathrm{s}}^{\Lambda}G_{\mathrm{d}}^{\Lambda}\left(i(\Gamma_{\mathrm{zz}}^{\Lambda}-\Gamma_{\mathrm{d}}^{\Lambda})\Gamma_{\mathrm{xx}}^{\Lambda}+(\Gamma_{\mathrm{zd}}^{\Lambda}-\Gamma_{\mathrm{dz}}^{\Lambda})\Gamma_{\mathrm{DM}}^{\Lambda}\right)\\
&+S_{\mathrm{s}}^{\Lambda}G_{\mathrm{s}}^{\Lambda}\left(i(\Gamma_{\mathrm{zd}}^{\Lambda}-\Gamma_{\mathrm{dz}}^{\Lambda})\Gamma_{\mathrm{xx}}^{\Lambda}+(\Gamma_{\mathrm{zz}}^{\Lambda}-\Gamma_{\mathrm{d}}^{\Lambda})\Gamma_{\mathrm{DM}}^{\Lambda}\right)\\
&\quad\Big]_{(i_1,i_1)(i_1,i_2)}(\omega_{1'},\omega_3;\omega_{2'}+\omega_3-\omega_2,\omega_1)(\omega_{2'}+\omega_3-\omega_2;,\omega_{2'};\omega_3,\omega_2)\\
&+(\omega_{1'}+\omega_3-\omega_2)(\omega_3)\Big[\\
&\quad S_{\mathrm{d}}^{\Lambda}G_{\mathrm{d}}^{\Lambda}\left(i(\Gamma_{\mathrm{zd}}^{\Lambda}+\Gamma_{\mathrm{dz}}^{\Lambda})\Gamma_{\mathrm{xx}}^{\Lambda}-i\Gamma_{\mathrm{xx}}^{\Lambda}(\Gamma_{\mathrm{zd}}^{\Lambda}+\Gamma_{\mathrm{dz}}^{\Lambda})-(\Gamma_{\mathrm{d}}^{\Lambda}+\Gamma_{\mathrm{zz}}^{\Lambda})\Gamma_{\mathrm{DM}}^{\Lambda}-\Gamma_{\mathrm{DM}}^{\Lambda}(\Gamma_{\mathrm{d}}^{\Lambda}+\Gamma_{\mathrm{zz}}^{\Lambda})\right)\\
&+S_{\mathrm{d}}^{\Lambda}G_{\mathrm{s}}^{\Lambda}\left(i(\Gamma_{\mathrm{d}}^{\Lambda}-\Gamma_{\mathrm{zz}}^{\Lambda})\Gamma_{\mathrm{xx}}^{\Lambda}+i\Gamma_{\mathrm{xx}}^{\Lambda}(\Gamma_{\mathrm{d}}^{\Lambda}+\Gamma_{\mathrm{zz}}^{\Lambda})-(\Gamma_{\mathrm{zd}}^{\Lambda}+\Gamma_{\mathrm{dz}}^{\Lambda})\Gamma_{\mathrm{DM}}^{\Lambda}-\Gamma_{\mathrm{DM}}^{\Lambda}(\Gamma_{\mathrm{zd}}^{\Lambda}+\Gamma_{\mathrm{dz}}^{\Lambda})\right)\\
&+S_{\mathrm{s}}^{\Lambda}G_{\mathrm{d}}^{\Lambda}\left(i(\Gamma_{\mathrm{d}}^{\Lambda}+\Gamma_{\mathrm{zz}}^{\Lambda})\Gamma_{\mathrm{xx}}^{\Lambda}-i\Gamma_{\mathrm{xx}}^{\Lambda}(\Gamma_{\mathrm{d}}^{\Lambda}+\Gamma_{\mathrm{zz}}^{\Lambda})-(\Gamma_{\mathrm{zd}}^{\Lambda}+\Gamma_{\mathrm{dz}}^{\Lambda})\Gamma_{\mathrm{DM}}^{\Lambda}-\Gamma_{\mathrm{DM}}^{\Lambda}(\Gamma_{\mathrm{zd}}^{\Lambda}+\Gamma_{\mathrm{dz}}^{\Lambda})\right)\\
&+S_{\mathrm{s}}^{\Lambda}G_{\mathrm{s}}^{\Lambda}\left(i(\Gamma_{\mathrm{zd}}^{\Lambda}+\Gamma_{\mathrm{dz}}^{\Lambda})\Gamma_{\mathrm{xx}}^{\Lambda}-i\Gamma_{\mathrm{xx}}^{\Lambda}(\Gamma_{\mathrm{zd}}^{\Lambda}+\Gamma_{\mathrm{dz}}^{\Lambda})-(\Gamma_{\mathrm{d}}^{\Lambda}+\Gamma_{\mathrm{zz}}^{\Lambda})\Gamma_{\mathrm{DM}}^{\Lambda}-\Gamma_{\mathrm{DM}}^{\Lambda}(\Gamma_{\mathrm{d}}^{\Lambda}+\Gamma_{\mathrm{zz}}^{\Lambda})\right)\\
&\quad\Big]_{(i_2,i_1)(i_2,i_1)}(\omega_{2'},\omega_{1'}+\omega_3-\omega_2;\omega_3,\omega_1)(\omega_3,\omega_{1'};\omega_2,\omega_{1'}+\omega_3-\omega_2)\\
&+\Big[\omega_3\leftrightarrow\omega_{1'}+\omega_3-\omega_2\Big]\Bigg\}
\end{aligned}
\tag{B.7}
$$

These equations are significantly more complex than those of a bare Heisenberg model. For the utilised numerical solving method, this yields a computational effort that is increased by a factor of about 80.

C. Flow equations for XXZ vertices

The last set of employed FRG equations is the one for the arbitrary-S XXZ model from Chap. 5. Due to the similar vertex structures as for the Heisenberg scenario, we stick to the notations introduced in App. A. Only the factor of $M = 2S$ has to be included in comparison to a spin-$\frac{1}{2}$ model [9] and the spin channel of the two-particle vertex splits up into an in-plane and an out-of-plane component. For the pseudo-fermion lifetime, we find that

$$\begin{aligned}\frac{\mathrm{d}}{\mathrm{d}\Lambda}\gamma^{\Lambda}_{\mathrm{d}\,i_1}(\omega_1) = \frac{1}{2\pi}\sum_{\omega_2=\pm\Lambda}\Bigg\{\sum_j\left[-2M\Gamma^{\Lambda}_{\mathrm{d}\,i_1 j}(\omega_1,\omega_2;\omega_1,\omega_2)\left(\frac{1}{\omega_2+\gamma^{\Lambda}_{\mathrm{d}\,j}(\omega_2)}\right)\right] \\ + \left[\Gamma^{\Lambda}_{\mathrm{d}\,i_1 i_1}(\omega_1,\omega_2;\omega_2,\omega_1) + 2\Gamma^{\Lambda}_{\mathrm{xx}i_1 i_1}(\omega_1,\omega_2;\omega_2,\omega_1) + \Gamma^{\Lambda}_{\mathrm{zz}i_1 i_1}(\omega_1,\omega_2;\omega_2,\omega_1)\right] \\ \times\left(\frac{1}{\omega_2+\gamma^{\Lambda}_{\mathrm{d}\,i_1}(\omega_2)}\right)\Bigg\}. \end{aligned} \tag{C.1}$$

The flow equation for the density component of the two-particle vertex is given by

$$
\begin{aligned}
\frac{\mathrm{d}}{\mathrm{d}\Lambda}\Gamma^{\Lambda}_{\mathrm{d}\,i_1 i_2}(\omega_{1'},\omega_{2'};\omega_1,\omega_2) = \frac{1}{2\pi}\int_{-\infty}^{\infty}\mathrm{d}\omega_3 \Big\{ \\
& S^{\Lambda}(\omega_1+\omega_2-\omega_3)G^{\Lambda}(\omega_3)\Big[\Gamma^{\Lambda}_{\mathrm{d}}\Gamma^{\Lambda}_{\mathrm{d}} + \Gamma^{\Lambda}_{\mathrm{zz}}\Gamma^{\Lambda}_{\mathrm{zz}} + 2\Gamma^{\Lambda}_{\mathrm{xx}}\Gamma^{\Lambda}_{\mathrm{xx}} \\
& \Big]_{(i_1,i_2)(i_1,i_2)}(\omega_{1'},\omega_{2'};\omega_3,\omega_1+\omega_2-\omega_3)(\omega_3,\omega_1+\omega_2-\omega_3;\omega_1,\omega_2) \\
& + \Big[\omega_3 \leftrightarrow \omega_1+\omega_2-\omega_3\Big] \\
& -2M\sum_j S^{\Lambda}(\omega_{2'}+\omega_3-\omega_2)G^{\Lambda}(\omega_3)\Big[\Gamma^{\Lambda}_{\mathrm{d}}\Gamma^{\Lambda}_{\mathrm{d}} \\
& \Big]_{(i_1,j)(j,i_2)}(\omega_{1'},\omega_{2'}+\omega_3-\omega_2;\omega_1,\omega_3)(\omega_3,\omega_{2'};\omega_{2'}+\omega_3-\omega_2,\omega_2) \\
& - \Big[\omega_3 \leftrightarrow \omega_{2'}+\omega_3-\omega_2\Big] \\
& + S^{\Lambda}(\omega_{2'}+\omega_3-\omega_2)G^{\Lambda}(\omega_3)\Big[\Gamma^{\Lambda}_{\mathrm{d}}\left(\Gamma^{\Lambda}_{\mathrm{d}}+\Gamma^{\Lambda}_{\mathrm{zz}}+2\Gamma^{\Lambda}_{\mathrm{xx}}\right) \\
& \Big]_{(i_1,i_2)(i_2,i_2)}(\omega_{1'},\omega_{2'}+\omega_3-\omega_2;\omega_1,\omega_3)(\omega_3,\omega_{2'};\omega_2,\omega_{2'}+\omega_3-\omega_2) \\
& + \Big[\omega_3 \leftrightarrow \omega_{2'}+\omega_3-\omega_2\Big] \\
& + S^{\Lambda}(\omega_{2'}+\omega_3-\omega_2)G^{\Lambda}(\omega_3)\Big[\left(\Gamma^{\Lambda}_{\mathrm{d}}+\Gamma^{\Lambda}_{\mathrm{zz}}+2\Gamma^{\Lambda}_{\mathrm{xx}}\right)\Gamma^{\Lambda}_{\mathrm{d}} \\
& \Big]_{(i_1,i_1)(i_1,i_2)}(\omega_{1'},\omega_{2'}+\omega_3-\omega_2;\omega_3,\omega_1)(\omega_3,\omega_{2'};\omega_{2'}+\omega_3-\omega_2,\omega_2) \\
& + \Big[\omega_3 \leftrightarrow \omega_{2'}+\omega_3-\omega_2\Big] \\
& + S^{\Lambda}(\omega_{1'}+\omega_3-\omega_2)G^{\Lambda}(\omega_3)\Big[\Gamma^{\Lambda}_{\mathrm{d}}\Gamma^{\Lambda}_{\mathrm{d}} + \Gamma^{\Lambda}_{\mathrm{zz}}\Gamma^{\Lambda}_{\mathrm{zz}} + 2\Gamma^{\Lambda}_{\mathrm{xx}}\Gamma^{\Lambda}_{\mathrm{xx}} \\
& \Big]_{(i_2,i_1)(i_2,i_1)}(\omega_{2'},\omega_{1'}+\omega_3-\omega_2;\omega_3,\omega_1)(\omega_3,\omega_{1'};\omega_2,\omega_{1'}+\omega_3-\omega_2) \\
& + \Big[\omega_3 \leftrightarrow \omega_{1'}+\omega_3-\omega_2\Big]\Big\}. \qquad \text{(C.2)}
\end{aligned}
$$

The out-of-plane spin vertex can be determined from

$$
\begin{aligned}
\frac{\mathrm{d}}{\mathrm{d}\Lambda}\Gamma^{\Lambda}_{\mathrm{zz}i_1i_2}(\omega_{1'},\omega_{2'};\omega_1,\omega_2) = \frac{1}{2\pi}\int_{-\infty}^{\infty}\mathrm{d}\omega_3 \Big\{ & \\
& S^{\Lambda}(\omega_1+\omega_2-\omega_3)G^{\Lambda}(\omega_3)\Big[\Gamma^{\Lambda}_{\mathrm{zz}}\Gamma^{\Lambda}_{\mathrm{d}}+\Gamma^{\Lambda}_{\mathrm{d}}\Gamma^{\Lambda}_{\mathrm{zz}}-2\Gamma^{\Lambda}_{\mathrm{xx}}\Gamma^{\Lambda}_{\mathrm{xx}} \\
& \Big]_{(i_1,i_2)(i_1,i_2)}(\omega_{1'},\omega_{2'};\omega_3,\omega_1+\omega_2-\omega_3)(\omega_3,\omega_1+\omega_2-\omega_3;\omega_1,\omega_2) \\
& +\Big[\omega_3\leftrightarrow\omega_1+\omega_2-\omega_3\Big] \\
& -2M\sum_j S^{\Lambda}(\omega_{2'}+\omega_3-\omega_2)G^{\Lambda}(\omega_3)\Big[\Gamma^{\Lambda}_{\mathrm{zz}}\Gamma^{\Lambda}_{\mathrm{zz}} \\
& \Big]_{(i_1,j)(j,i_2)}(\omega_{1'},\omega_{2'}+\omega_3-\omega_2;\omega_1,\omega_3)(\omega_3,\omega_{2'};\omega_{2'}+\omega_3-\omega_2,\omega_2) \\
& -\Big[\omega_3\leftrightarrow\omega_{2'}+\omega_3-\omega_2\Big] \\
& +S^{\Lambda}(\omega_{2'}+\omega_3-\omega_2)G^{\Lambda}(\omega_3)\Big[\Gamma^{\Lambda}_{\mathrm{zz}}\left(\Gamma^{\Lambda}_{\mathrm{d}}+\Gamma^{\Lambda}_{\mathrm{zz}}-2\Gamma^{\Lambda}_{\mathrm{xx}}\right) \\
& \Big]_{(i_1,i_2)(i_2,i_2)}(\omega_{1'},\omega_{2'}+\omega_3-\omega_2;\omega_1,\omega_3)(\omega_3,\omega_{2'};\omega_2,\omega_{2'}+\omega_3-\omega_2) \\
& +\Big[\omega_3\leftrightarrow\omega_{2'}+\omega_3-\omega_2\Big] \\
& +S^{\Lambda}(\omega_{2'}+\omega_3-\omega_2)G^{\Lambda}(\omega_3)\Big[\left(\Gamma^{\Lambda}_{\mathrm{d}}+\Gamma^{\Lambda}_{\mathrm{zz}}-2\Gamma^{\Lambda}_{\mathrm{xx}}\right)\Gamma^{\Lambda}_{\mathrm{zz}} \\
& \Big]_{(i_1,i_1)(i_1,i_2)}(\omega_{1'},\omega_{2'}+\omega_3-\omega_2;\omega_3,\omega_1)(\omega_3,\omega_{2'};\omega_{2'}+\omega_3-\omega_2,\omega_2) \\
& +\Big[\omega_3\leftrightarrow\omega_{2'}+\omega_3-\omega_2\Big] \\
& +S^{\Lambda}(\omega_{1'}+\omega_3-\omega_2)G^{\Lambda}(\omega_3)\Big[\Gamma^{\Lambda}_{\mathrm{zz}}\Gamma^{\Lambda}_{\mathrm{d}}+\Gamma^{\Lambda}_{\mathrm{d}}\Gamma^{\Lambda}_{\mathrm{zz}}+2\Gamma^{\Lambda}_{\mathrm{xx}}\Gamma^{\Lambda}_{\mathrm{xx}} \\
& \Big]_{(i_2,i_1)(i_2,i_1)}(\omega_{2'},\omega_{1'}+\omega_3-\omega_2;\omega_3,\omega_1)(\omega_3,\omega_{1'};\omega_2,\omega_{1'}+\omega_3-\omega_2) \\
& +\Big[\omega_3\leftrightarrow\omega_{1'}+\omega_3-\omega_2\Big]\Big\}, \qquad \text{(C.3)}
\end{aligned}
$$

whereas the in-plane component has to fulfill that

$$
\begin{aligned}
\frac{\mathrm{d}}{\mathrm{d}\Lambda}\Gamma^{\Lambda}_{\mathrm{xx}i_1i_2}(\omega_{1'},\omega_{2'};\omega_1,\omega_2) = \frac{1}{2\pi}\int_{-\infty}^{\infty}\mathrm{d}\omega_3 \Bigg\{ & \\
& S^{\Lambda}(\omega_1+\omega_2-\omega_3)G^{\Lambda}(\omega_3)\Big[\Gamma^{\Lambda}_{\mathrm{xx}}(\Gamma^{\Lambda}_{\mathrm{d}}-\Gamma^{\Lambda}_{\mathrm{zz}})+(\Gamma^{\Lambda}_{\mathrm{d}}-\Gamma^{\Lambda}_{\mathrm{zz}})\Gamma^{\Lambda}_{\mathrm{xx}} \\
& \Big]_{(i_1,i_2)(i_1,i_2)}(\omega_{1'},\omega_{2'};\omega_3,\omega_1+\omega_2-\omega_3)(\omega_3,\omega_1+\omega_2-\omega_3;\omega_1,\omega_2) \\
& +\Big[\omega_3 \leftrightarrow \omega_1+\omega_2-\omega_3\Big] \\
& -2M\sum_j S^{\Lambda}(\omega_{2'}+\omega_3-\omega_2)G^{\Lambda}(\omega_3)\Big[\Gamma^{\Lambda}_{\mathrm{xx}}\Gamma^{\Lambda}_{\mathrm{xx}} \\
& \Big]_{(i_1,j)(j,i_2)}(\omega_{1'},\omega_{2'}+\omega_3-\omega_2;\omega_1,\omega_3)(\omega_3,\omega_{2'};\omega_{2'}+\omega_3-\omega_2,\omega_2) \\
& +\Big[\omega_3 \leftrightarrow \omega_{2'}+\omega_3-\omega_2\Big] \\
& +S^{\Lambda}(\omega_{2'}+\omega_3-\omega_2)G^{\Lambda}(\omega_3)\Big[\Gamma^{\Lambda}_{\mathrm{xx}}\left(\Gamma^{\Lambda}_{\mathrm{d}}-\Gamma^{\Lambda}_{\mathrm{zz}}\right) \\
& \Big]_{(i_1,i_2)(i_2,i_2)}(\omega_{1'},\omega_{2'}+\omega_3-\omega_2;\omega_1,\omega_3)(\omega_3,\omega_{2'};\omega_2,\omega_{2'}+\omega_3-\omega_2) \\
& +\Big[\omega_3 \leftrightarrow \omega_{2'}+\omega_3-\omega_2\Big] \\
& +S^{\Lambda}(\omega_{2'}+\omega_3-\omega_2)G^{\Lambda}(\omega_3)\Big[\left(\Gamma^{\Lambda}_{\mathrm{d}}-\Gamma^{\Lambda}_{\mathrm{zz}}\right)\Gamma^{\Lambda}_{\mathrm{xx}} \\
& \Big]_{(i_1,i_1)(i_1,i_2)}(\omega_{1'},\omega_{2'}+\omega_3-\omega_2;\omega_3,\omega_1)(\omega_3,\omega_{2'};\omega_{2'}+\omega_3-\omega_2,\omega_2) \\
& +\Big[\omega_3 \leftrightarrow \omega_{2'}+\omega_3-\omega_2\Big] \\
& +S^{\Lambda}(\omega_{1'}+\omega_3-\omega_2)G^{\Lambda}(\omega_3)\Big[\Gamma^{\Lambda}_{\mathrm{xx}}(\Gamma^{\Lambda}_{\mathrm{d}}+\Gamma^{\Lambda}_{\mathrm{zz}})+(\Gamma^{\Lambda}_{\mathrm{d}}+\Gamma^{\Lambda}_{\mathrm{zz}})\Gamma^{\Lambda}_{\mathrm{xx}} \\
& \Big]_{(i_2,i_1)(i_2,i_1)}(\omega_{2'},\omega_{1'}+\omega_3-\omega_2;\omega_3,\omega_1)(\omega_3,\omega_{1'};\omega_2,\omega_{1'}+\omega_3-\omega_2) \\
& +\Big[\omega_3 \leftrightarrow \omega_{1'}+\omega_3-\omega_2\Big]\Bigg\}. \qquad \text{(C.4)}
\end{aligned}
$$

In comparison to a bare Heisenberg model, the numerical effort is only marginally increased for XXZ couplings.

D. Kagome lattice and Fourier transforms

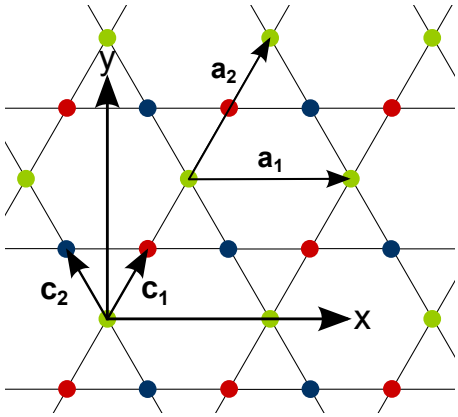

Figure D.1.: Kagome lattice as triangular Bravais lattice with three-atomic basis: The primitive lattice vectors $\boldsymbol{a}_1$ and $\boldsymbol{a}_2$ are given in the main text. Atoms of the different sublattices $\mathcal{A}$, $\mathcal{B}$, and $\mathcal{C}$ are colored green, red, and blue, respectively. They are translation invariant if considered separately.

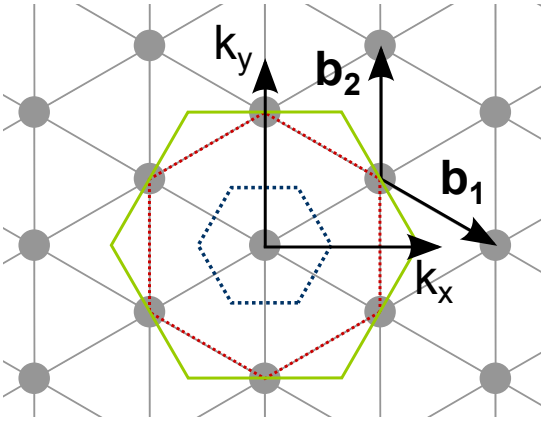

Figure D.2.: Reciprocal lattice: Due to the triangular Bravais lattice in real space, the reciprocal lattice is also triangular. Its lattice vectors $\boldsymbol{b}_1$ and $\boldsymbol{b}_2$ can be seen in Eq. (D.10). The first, second, and third Brillouin zones are indicated in dashed blue, dashed red, and solid green.

In this appendix, we want to summarise the properties of the Kagome lattice and its Fourier transformed entities such that one can compare our results to the outcomes of actual experiments.

The Kagome lattice itself is not translation invariant. It can be easiest understood as a triangular Bravais lattice with a three-atomic basis (confer Fig. D.1). We can label the three emerging sublattices $\mathcal{A}$, $\mathcal{B}$, and $\mathcal{C}$ and denote the nearest-neighbor distance by a. The primitive lattice vectors are hence given by

$$\boldsymbol{a}_1 = a \begin{pmatrix} 2 \\ 0 \end{pmatrix}, \qquad \boldsymbol{a}_2 = a \begin{pmatrix} 1 \\ \sqrt{3} \end{pmatrix}. \tag{D.1}$$

The sublattices $\mathcal{B}$ and $\mathcal{C}$ are shifted with respect to sublattice $\mathcal{A}$ by the vectors $\boldsymbol{c}_1 = a(1/2, \sqrt{3}/2)^T$ and $\boldsymbol{c}_2 = a(-1/2, \sqrt{3}/2)^T$, respectively. They are, if considered for themselves, translation invariant and can be mapped onto another with $\frac{\pi}{3}$ in-plane rotations. Therefore, every observable that depends on a single point in real space $A(\boldsymbol{r})$ is the same for all points in the Kagome lattice and $\boldsymbol{r}_i$ can be set to zero, accordingly.

We are, however, rather interested in correlation functions (like the spin susceptibility) which depend on two real-space coordinates $B(\boldsymbol{r}_i, \boldsymbol{r}_j)$. Each real-space coordinate can be written as:

$$\boldsymbol{r}_i = \boldsymbol{R}_i + \boldsymbol{b}_\alpha\,, \qquad \boldsymbol{b}_\alpha \in \{\boldsymbol{0},\, \boldsymbol{c}_1,\, \boldsymbol{c}_2\}\,, \tag{D.2a}$$

$$\boldsymbol{R}_i = k \cdot \boldsymbol{a}_1 + l \cdot \boldsymbol{a}_2\,, \qquad k, l \in \mathbb{Z}\,. \tag{D.2b}$$

We consider three-atomic unit cells (one atom each out of sublattice $\mathcal{A}$, $\mathcal{B}$, and $\mathcal{C}$) and label them by the corresponding position $\boldsymbol{R}_i$ of the atom in sublattice $\mathcal{A}$. Each lattice point is then identified by the position of its unit cell and the sublattice it is a part of. For our correlation function $B(\boldsymbol{r}_i, \boldsymbol{r}_j)$, this implies that we can store its information in a matrix that only depends on the lattice vectors $\boldsymbol{R}_i$ and $\boldsymbol{R}_j$, *e.g.*,

$$B(\boldsymbol{r}_i, \boldsymbol{r}_j) \longrightarrow \begin{pmatrix} B_{\mathcal{A},\mathcal{A}}(\boldsymbol{R}_i, \boldsymbol{R}_j) & B_{\mathcal{A},\mathcal{B}}(\boldsymbol{R}_i, \boldsymbol{R}_j) & B_{\mathcal{A},\mathcal{C}}(\boldsymbol{R}_i, \boldsymbol{R}_j) \\ B_{\mathcal{B},\mathcal{A}}(\boldsymbol{R}_i, \boldsymbol{R}_j) & B_{\mathcal{B},\mathcal{B}}(\boldsymbol{R}_i, \boldsymbol{R}_j) & B_{\mathcal{B},\mathcal{C}}(\boldsymbol{R}_i, \boldsymbol{R}_j) \\ B_{\mathcal{C},\mathcal{A}}(\boldsymbol{R}_i, \boldsymbol{R}_j) & B_{\mathcal{C},\mathcal{B}}(\boldsymbol{R}_i, \boldsymbol{R}_j) & B_{\mathcal{C},\mathcal{C}}(\boldsymbol{R}_i, \boldsymbol{R}_j) \end{pmatrix} = \bar{B}(\boldsymbol{R}_i, \boldsymbol{R}_j)\,. \tag{D.3}$$

This matrix is now defined on a translation-invariant, triangular Bravais lattice and therefore can only depend on the difference $\boldsymbol{R}_i - \boldsymbol{R}_j$. Hence, we can set one of the coordinates to zero and let the unit cell at the origin be the reference site for our convenience. Further, the mappings of the sublattices onto another by $\frac{\pi}{3}$ in-plane rotations yield the following relations, *i.e.*,

$$B_{\mathcal{A},\mathcal{A}}(\boldsymbol{R}_i) = B_{\mathcal{B},\mathcal{B}}(R_z(\boldsymbol{R}_i, -\pi/3)) = B_{\mathcal{C},\mathcal{C}}(R_z(\boldsymbol{R}_i, \pi/3))\,, \tag{D.4a}$$

$$B_{\mathcal{A},\mathcal{B}}(\boldsymbol{R}_i) = B_{\mathcal{B},\mathcal{C}}(R_z(\boldsymbol{R}_i, -\pi/3)) = B_{\mathcal{C},\mathcal{A}}(R_z(\boldsymbol{R}_i, \pi/3))\,, \tag{D.4b}$$

$$B_{\mathcal{A},\mathcal{C}}(\boldsymbol{R}_i) = B_{\mathcal{B},\mathcal{A}}(R_z(\boldsymbol{R}_i, -\pi/3)) = B_{\mathcal{C},\mathcal{B}}(R_z(\boldsymbol{R}_i, \pi/3))\,. \tag{D.4c}$$

Finally, it is worth mentioning that the DM interaction (confer Sec. 4.3) breaks the lattice's mirror symmetries with respect to the x and y axes. Only the mirror symmetry in the origin $\bar{B}(\boldsymbol{R}_i) = \bar{B}(-\boldsymbol{R}_i)$ is upheld.

All these symmetries and the translation invariance have consequences in momentum space. Let us first define the standard transform of the original function $B(\boldsymbol{r}_i, \boldsymbol{r}_j)$. It is given by

$$\tilde{B}(\boldsymbol{k}, \boldsymbol{k}') = \sum_{i,j} e^{-i\boldsymbol{k}\cdot\boldsymbol{r}_i} e^{-i\boldsymbol{k}'\cdot\boldsymbol{r}_j} B(\boldsymbol{r}_i, \boldsymbol{r}_j)\,. \tag{D.5}$$

Making use of Eq. (D.2) and the matrix representation from Eq. (D.3), and rewriting the difference coordinate $\boldsymbol{R}_i - \boldsymbol{R}_j = \boldsymbol{d}$, we can derive that

$$\tilde{B}(\boldsymbol{k}, \boldsymbol{k}') = \delta(\boldsymbol{k} + \boldsymbol{k}')\tilde{B}(\boldsymbol{k})\,, \tag{D.6a}$$

$$\begin{aligned} \tilde{B}(\boldsymbol{k}) = \sum_{\boldsymbol{d}} e^{-i\boldsymbol{k}\cdot\boldsymbol{d}} \Big\{ & B_{\mathcal{A},\mathcal{A}}(\boldsymbol{d}) + e^{i\boldsymbol{k}\cdot\boldsymbol{c}_1} B_{\mathcal{A},\mathcal{B}}(\boldsymbol{d}) + e^{i\boldsymbol{k}\cdot\boldsymbol{c}_2} B_{\mathcal{A},\mathcal{C}}(\boldsymbol{d}) \\ & + e^{-i\boldsymbol{k}\cdot\boldsymbol{c}_1} \Big[B_{\mathcal{B},\mathcal{A}}(\boldsymbol{d}) + e^{i\boldsymbol{k}\cdot\boldsymbol{c}_1} B_{\mathcal{B},\mathcal{B}}(\boldsymbol{d}) + e^{i\boldsymbol{k}\cdot\boldsymbol{c}_2} B_{\mathcal{B},\mathcal{C}}(\boldsymbol{d}) \Big] \\ & + e^{-i\boldsymbol{k}\cdot\boldsymbol{c}_2} \Big[B_{\mathcal{C},\mathcal{A}}(\boldsymbol{d}) + e^{i\boldsymbol{k}\cdot\boldsymbol{c}_1} B_{\mathcal{C},\mathcal{B}}(\boldsymbol{d}) + e^{i\boldsymbol{k}\cdot\boldsymbol{c}_2} B_{\mathcal{C},\mathcal{C}}(\boldsymbol{d}) \Big] \Big\}\,. \end{aligned} \tag{D.6b}$$

Defining the quantity

$$\tilde{B}_{\mathcal{A}}(\boldsymbol{k}\cdot) = \sum_{\boldsymbol{d}} e^{-i\boldsymbol{k}\cdot\boldsymbol{d}} \Big[B_{\mathcal{A},\mathcal{A}}(\boldsymbol{d}) + e^{i\boldsymbol{k}\cdot\boldsymbol{c}_1} B_{\mathcal{A},\mathcal{B}}(\boldsymbol{d}) + e^{i\boldsymbol{k}\cdot\boldsymbol{c}_2} B_{\mathcal{A},\mathcal{C}}(\boldsymbol{d}) \Big] = \sum_i e^{-i\boldsymbol{k}\cdot\boldsymbol{r}_i} B(\boldsymbol{0}, \boldsymbol{r}_i)\,, \tag{D.7}$$

one verifies easily verifies

$$\tilde{B}(\boldsymbol{k}) = \tilde{B}_{\mathcal{A}}(\boldsymbol{k}) + \tilde{B}_{\mathcal{A}}(R_z(\boldsymbol{k}, \pi/3)) + \tilde{B}_{\mathcal{A}}(R_z(\boldsymbol{k}, -\pi/3))\,. \tag{D.8}$$

Here, we have used Eq. (D.4) and that the scalar product $\boldsymbol{k} \cdot \boldsymbol{d}$ is invariant under simultaneous rotation of both vectors. Finally, we employ the mirror symmetry with respect to the coordinate origin in order to find

$$\begin{aligned}\tilde{B}_{\mathcal{A}}(\boldsymbol{k}) &= \sum_{x_i,y_i} e^{-i(k_x x_i + k_y y_i)} B(x_i, y_i) \\ &= B(0,0) + \sum_{x_i>0} 2\cos(k_x x_i) B(x_i, 0) + \sum_{y_i>0} 2\cos(k_y y_i) B(0, y_i) \\ &+ \sum_{x_i,y_i>0} \{2\cos(k_x x_i + k_y y_i) B(x_i, y_i) + 2\cos(k_x x_i - k_y y_i) B(-x_i, y_i)\}\,,\end{aligned} \tag{D.9}$$

where we have omitted all zeros for the first real-space coordinate in $B(\boldsymbol{0}, \boldsymbol{r_i})$ and wrote explicitly $\boldsymbol{r}_i = (x_i, y_i)$. This proves that $\tilde{B}_{\mathcal{A}}(\boldsymbol{k}) = \tilde{B}_{\mathcal{A}}(-\boldsymbol{k})$. Together with Eq. (D.8), we obtain a $\boldsymbol{k}$-space-resolved function $\tilde{B}(\boldsymbol{k})$ which has the typical six-fold rotation symmetry.

In order to derive the correct periodicities in $\boldsymbol{k}$ space, we have a look at the reciprocal lattice itself. It is also a triangular lattice and its lattice vectors are in correspondence to the real-space lattice vectors $\boldsymbol{a}_1$ and $\boldsymbol{a}_2$ given by

$$\boldsymbol{b}_1 = \frac{\pi}{a} \begin{pmatrix} 1 \\ -1/\sqrt{3} \end{pmatrix}\,, \qquad \boldsymbol{b}_2 = \frac{\pi}{a} \begin{pmatrix} 0 \\ 2/\sqrt{3} \end{pmatrix}\,. \tag{D.10}$$

However, the smallest real-space distance that occurs in our correlation functions is precisely half of the distance which is set by the primitive lattice vectors. All functions in momentum space hence have to be periodic for any combination of the doubled reciprocal lattice vectors

$$\tilde{B}(\boldsymbol{k}) = \tilde{B}(\boldsymbol{k} + n \cdot 2\boldsymbol{b}_1 + m \cdot 2\boldsymbol{b}_2)\,, \qquad \forall\ n, m \in \mathbb{Z}\,, \tag{D.11}$$

and are, due to the fact that $\tilde{B}(\boldsymbol{k}) = \tilde{B}(-\boldsymbol{k})$, symmetric around the edges of the third Brillouin zone (confer Fig. D.2).

This discussion seems a bit tedious, but in order to understand the outcomes of our calculations and recent experiments clearly, we consider it to be worth the effort.

E. Symmetry transformations for Abrikosov fermions

Here, we summarise the frequently utilised properties of local gauge transformations and global spin rotations in the language of Abrikosov fermions, see Eq. (4.2). Since we write our spin operators in a second quantisation representation of the spin's z component, the relevant terms in the following analysis are

$$S_i^x = \frac{1}{2}\left(f_{i\uparrow}^\dagger f_{i\downarrow} + f_{i\downarrow}^\dagger f_{i\uparrow}\right), \tag{E.1a}$$

$$S_i^y = \frac{i}{2}\left(f_{i\downarrow}^\dagger f_{i\uparrow} - f_{i\uparrow}^\dagger f_{i\downarrow}\right), \tag{E.1b}$$

$$S_i^z = \frac{1}{2}\left(f_{i\uparrow}^\dagger f_{i\uparrow} - f_{i\downarrow}^\dagger f_{i\downarrow}\right), \tag{E.1c}$$

$$D_i = \frac{1}{2}\left(f_{i\uparrow}^\dagger f_{i\uparrow} + f_{i\downarrow}^\dagger f_{i\downarrow}\right), \tag{E.1d}$$

$$S_i^+ = S_i^x + iS_i^y = f_{i\uparrow}^\dagger f_{i\downarrow}, \tag{E.1e}$$

$$S_i^- = S_i^x - iS_i^y = f_{i\downarrow}^\dagger f_{i\uparrow}. \tag{E.1f}$$

In the following, we determine the effect of the possible symmetry transformations on these operators.

E.1. Local gauge transformations

The Nambu space from Chap. 6 is defined in terms of the pseudo-fermion creation and annihilation operators as

$$a_i = \begin{pmatrix} f_{i\uparrow} \\ f_{i\downarrow}^\dagger \end{pmatrix}, \qquad a_i^\dagger = \begin{pmatrix} f_{i\uparrow}^\dagger \,, & f_{i\downarrow} \end{pmatrix}. \tag{E.2}$$

A local gauge transformation acts on these spinors via

$$a_i \longrightarrow W_i a_i\,, \qquad a_i^\dagger \longrightarrow a_i^\dagger W_i^\dagger\,, \tag{E.3}$$

where W_i is an arbitrary $SU(2)$ matrix which we subsequently express as

$$W_i = \begin{pmatrix} x_i & y_i \\ -y_i^* & x_i^* \end{pmatrix}, \qquad \det W_i = |x_i|^2 + |y_i|^2 = 1\,. \tag{E.4}$$

This implies that the four constituents of the operators from Eqs. (E.1) transform according to

$$f_{i\uparrow}^\dagger f_{i\uparrow} \longrightarrow |x_i|^2 f_{i\uparrow}^\dagger f_{i\uparrow} - |y_i|^2 f_{i\downarrow}^\dagger f_{i\downarrow} + x_i^* y_i f_{i\uparrow}^\dagger f_{i\downarrow}^\dagger + x_i y_i^* f_{i\downarrow} f_{i\uparrow} + |y_i|^2\,, \tag{E.5a}$$

$$f_{i\downarrow}^\dagger f_{i\downarrow} \longrightarrow |x_i|^2 f_{i\downarrow}^\dagger f_{i\downarrow} - |y_i|^2 f_{i\uparrow}^\dagger f_{i\uparrow} + x_i^* y_i f_{i\uparrow}^\dagger f_{i\downarrow}^\dagger + x_i y_i^* f_{i\downarrow} f_{i\uparrow} + |y_i|^2\,, \tag{E.5b}$$

$$f_{i\uparrow}^\dagger f_{i\downarrow} \longrightarrow f_{i\uparrow}^\dagger f_{i\downarrow}\,, \tag{E.5c}$$

$$f_{i\downarrow}^\dagger f_{i\uparrow} \longrightarrow f_{i\downarrow}^\dagger f_{i\uparrow}\,, \tag{E.5d}$$

where we employed standard anticommutation relations, the relation $|x_i|^2 + |y_i|^2 = 1$, and the fact that every squared fermionic operator equals zero. Using these relations, one can verify that all spin operators, *i.e.*, S_i^x, S_i^y, S_i^z, S_+^x, and S_-^x are trivially unaffected by a global gauge transformation. For the spin density D_i, this is formally not the case. The reason behind this is that the gauge transformations only act on the unphysical sector of the Hilbert space. Hence, only the spin density can be altered. If only physically allowed states can contribute, *e.g.*, the products $f_{i\uparrow}^\dagger f_{i\downarrow}^\dagger$ and $f_{i\downarrow} f_{i\uparrow}$ are identical to zero and $D_i \equiv \frac{1}{2}$, then also the spin density is invariant under local gauge transformations.

This shows that any type of spin Hamiltonian which, in general, can be a function of all spin and density operators on the entire lattice is unaltered by transformations as defined in Eq. (E.3). Unless spontaneous symmetry breaking occurs or unphysical states become occupied, all results obtained by an analysis of such a Hamiltonian via the Abrikosov decomposition therefore have to be independent of the locally chosen gauges.

E.2. Global spin rotations

According to the more traditional representation of spins via spinors and Pauli matrices, a spin rotation by an angle θ around the unit vector $\boldsymbol{d} = (d_x, d_y, d_z)^T$ is for spin-$\frac{1}{2}$ particles generated by the $SU(2)$ matrix

$$W = e^{-i\frac{\theta}{2}\boldsymbol{d}\cdot\boldsymbol{\sigma}} = \begin{pmatrix} \cos\frac{\theta}{2} - id_z \sin\frac{\theta}{2} & -(id_x + d_y)\sin\frac{\theta}{2} \\ -(id_x - d_y)\sin\frac{\theta}{2} & \cos\frac{\theta}{2} + id_z \sin\frac{\theta}{2} \end{pmatrix} = \begin{pmatrix} x & y \\ -y^* & x^* \end{pmatrix}, \tag{E.6}$$

where $\boldsymbol{\sigma} = (\sigma^x, \sigma^y, \sigma^z)^T$. In terms of Abrikosov fermions, this can be expressed for the regular spinors

$$b_i = \begin{pmatrix} f_{i\uparrow}^\dagger \\ f_{i\downarrow}^\dagger \end{pmatrix}, \qquad b_i^\dagger = \begin{pmatrix} f_{i\uparrow} \, , & f_{i\downarrow} \end{pmatrix} \tag{E.7}$$

in a similar way as the gauge transformations from above. Let the matrix W again be given by Eq. (E.4), but now it does not depend on a real space coordinate. Then, a global spin rotation acts on the spinors as

$$b_i \longrightarrow W b_i \,, \qquad b_i^\dagger \longrightarrow b_i^\dagger W^\dagger \,. \tag{E.8}$$

Considering the same four products as before, this transformation is characterised by

$$f_{i\uparrow}^\dagger f_{i\uparrow} \longrightarrow |x|^2 f_{i\uparrow}^\dagger f_{i\uparrow} + |y|^2 f_{i\downarrow}^\dagger f_{i\downarrow} + x^* y f_{i\downarrow}^\dagger f_{i\uparrow} + x y^* f_{i\uparrow}^\dagger f_{i\downarrow} \,, \tag{E.9a}$$

$$f_{i\downarrow}^\dagger f_{i\downarrow} \longrightarrow |x|^2 f_{i\downarrow}^\dagger f_{i\downarrow} + |y|^2 f_{i\uparrow}^\dagger f_{i\uparrow} - x^* y f_{i\downarrow}^\dagger f_{i\uparrow} - x y^* f_{i\uparrow}^\dagger f_{i\downarrow} \,, \tag{E.9b}$$

$$f_{i\uparrow}^\dagger f_{i\downarrow} \longrightarrow x^2 f_{i\uparrow}^\dagger f_{i\downarrow} - y^2 f_{i\downarrow}^\dagger f_{i\uparrow} - xy f_{i\uparrow}^\dagger f_{i\uparrow} + xy f_{i\downarrow}^\dagger f_{i\downarrow} \,, \tag{E.9c}$$

$$f_{i\downarrow}^\dagger f_{i\uparrow} \longrightarrow (x^*)^2 f_{i\downarrow}^\dagger f_{i\uparrow} - (y^*)^2 f_{i\uparrow}^\dagger f_{i\downarrow} - x^* y^* f_{i\uparrow}^\dagger f_{i\uparrow} + x^* y^* f_{i\downarrow}^\dagger f_{i\downarrow} \,. \tag{E.9d}$$

The situation is now reversed in comparison to the previous section. A global spin rotation formally only does not affect the spin density operator whereas all spin-dependent terms are changed. We span the influenced subspace by using the operators S_i^+, S_i^-, and S_i^z in the following. Under a global spin rotation they are sent to

$$\begin{pmatrix} S_i^+ \\ S_i^- \\ S_i^z \end{pmatrix} \longrightarrow \begin{pmatrix} x^2 & -y^2 & -2xy \\ -(y^*)^2 & (x^*)^2 & -2x^*y^* \\ xy^* & x^*y & \left(|x|^2 - |y|^2\right) \end{pmatrix} \begin{pmatrix} S_i^+ \\ S_i^- \\ S_i^z \end{pmatrix}, \tag{E.10}$$

where we chose a standard vector and matrix notation for convenience.

One might now believe that only Hamiltonians involving spin-density operators are invariant under global spin rotations. However, there is one symmetry-allowed term which is bilinear in spins, namely the scalar product of two spins. This should only depend on the length of the involved spins and their relative angle to each other. Therefore, a Heisenberg Hamiltonian is invariant under the transformation in Eqs. (E.10) as we shall see.

E.2.1. Heisenberg Hamiltonian

Any Heisenberg interaction is a linear combination of scalar products between two spins $\boldsymbol{S}_i$ and $\boldsymbol{S}_j$ where i and j can be arbitrary sites. Since the involved lattice sites do not have to be identical, it should also be clear why we are considering global and not local spin rotations at this point. The scalar product is given by

$$\begin{aligned} \boldsymbol{S}_i \cdot \boldsymbol{S}_j &= S_i^x S_j^x + S_i^y S_j^y + S_i^z S_j^z \\ &= \frac{1}{4}\left(S_i^+ + S_i^-\right)\left(S_j^+ + S_j^-\right) - \frac{1}{4}\left(S_i^+ - S_i^-\right)\left(S_j^+ - S_j^-\right) + S_i^z S_j^z \\ &= \frac{1}{2}\left(S_i^+ S_j^- + S_i^- S_j^+\right) + S_i^z S_j^z \end{aligned} \tag{E.11}$$

Employing Eqs. (E.10), we find that it transforms under an arbitrary global spin rotation as

$$\boldsymbol{S}_i \cdot \boldsymbol{S}_j \longrightarrow \frac{1}{2}\left(S_i^+ S_j^- + S_i^- S_j^+ + 2S_i^z S_j^z\right)\left(|x|^2 + |y|^2\right)^2 = \boldsymbol{S}_i \cdot \boldsymbol{S}_j\,. \tag{E.12}$$

This proves that any scalar product of two spins is invariant under all transformations that can be represented by Eq. (E.8). This property is hence passed onto Heisenberg Hamiltonians which are as well as spin-density-dependent Hamiltonians symmetric under global $SU(2)$ rotations of the spin system.

E.2.2. Dzyaloshinsky-Moriya interactions

The DM interaction from Chap. 4 is due to the cross product also bilinear in the considered spin operators. In our chosen basis of S^+, S^-, and S^z, it is given by

$$\boldsymbol{S}_i \times \boldsymbol{S}_j = \begin{pmatrix} \frac{1}{2i}\left[\left(S_i^+ - S_i^-\right)S_j^z - S_i^z\left(S_j^+ - S_j^-\right)\right] \\ \frac{1}{2}\left[S_i^z\left(S_j^+ + S_j^-\right) - \left(S_i^+ + S_i^-\right)S_j^z\right] \\ \frac{1}{2i}\left[S_i^- S_j^+ - S_i^+ S_j^-\right] \end{pmatrix}, \tag{E.13}$$

where the vector notation on the right-hand side represents Cartesian coordinates. According to Eqs. (E.8), this transforms under global spin rotations as

$$\boldsymbol{S}_i \times \boldsymbol{S}_j \to \begin{pmatrix} \frac{1}{2i}\left[\left(\alpha S_i^+ - \alpha^* S_i^-\right)S_j^z - S_i^z\left(\alpha S_j^+ - \alpha^* S_j^-\right) - \beta\left(S_i^- S_j^+ - S_i^+ S_j^-\right)\right] \\ \frac{1}{2}\left[S_i^z\left(\gamma S_j^+ + \gamma^* S_j^-\right) - \left(\gamma S_i^+ + \gamma^* S_i^-\right)S_j^z + \delta\left(S_i^- S_j^+ - S_i^+ S_j^-\right)\right] \\ \frac{1}{2i}\left[\left(\epsilon S_i^+ - \epsilon^* S_i^-\right)S_j^z - S_i^z\left(\epsilon S_j^+ - \epsilon^* S_j^-\right) + \zeta\left(S_i^- S_j^+ - S_i^+ S_j^-\right)\right] \end{pmatrix}. \tag{E.14}$$

The coefficients are defined as $\alpha = \left((x^*)^2 - y^2\right)$, $\beta = \left(x^* y^* + xy\right)$, $\gamma = \left((x^*)^2 + y^2\right)$, $\delta = \left(x^* y^* - xy\right)$, $\epsilon = 2x^* y$, and $\zeta = 2|x|^2 - 1$. For a global invariance of the DM term under a global spin rotation, it is hence required that

$$\alpha = \alpha^* = 1\,, \qquad \beta = 0\,, \qquad \text{for the } x \text{ component}\,, \tag{E.15a}$$

$$\gamma = \gamma^* = 1\,, \qquad \delta = 0\,, \qquad \text{for the } y \text{ component}\,, \tag{E.15b}$$

$$\epsilon = \epsilon^* = 0\,, \qquad \zeta = 1\,, \qquad \text{for the } z \text{ component}\,. \tag{E.15c}$$

These conditions can all be fulfilled simultaneously if and only if $x = \pm 1$, $y = 0$. Using Eq. (E.6), one verifies that this holds for arbitrary $\boldsymbol{d}$ if $\theta = 2\pi n$ with $n \in \mathbb{Z}$. Therefore, the cross product in Eq. (E.13) is only invariant under 2π spin rotations which also must be true by the definition of spin operators which transform under such rotations as $\boldsymbol{S} \to -\boldsymbol{S}$.

However, the vector $\boldsymbol{D}_{ij}$ selects certain components of the cross product with corresponding weights which then appear in the Hamiltonian [cf. Eq. (4.1)]. Because of that, the DM interaction can be invariant under the transformation in Eq. (E.8) for arbitrary θ if only one component of the cross product contributes. Due to the global $SU(2)$ spin-rotation invariance of the scalar product, any Hamiltonian as defined in Eq. (4.1) is then invariant under those $U(1)$ spin rotations which result from Eq. (E.8) with

$$\boldsymbol{d} = \begin{cases} (1,0,0)^T\,, & \text{if } \boldsymbol{D}_{ij} = (D_{ij},0,0)^T \;\forall\; i\,,\; j\,, \\ (0,1,0)^T\,, & \text{if } \boldsymbol{D}_{ij} = (0,D_{ij},0)^T \;\forall\; i\,,\; j\,, \\ (0,0,1)^T\,, & \text{if } \boldsymbol{D}_{ij} = (0,0,D_{ij})^T \;\forall\; i\,,\; j\,. \end{cases} \tag{E.16}$$

Thus, the model considered in Chap. 4 is invariant under global $U(1)$ spin rotations around the z axis since the Moriya selection rules require that $\boldsymbol{D}_{ij} \| \boldsymbol{e}_z$ for the kagome lattice [129].

It should be noted that also S_i^z and $S_i^x S_j^x + S_i^y S_j^y$ are invariant under these rotations ($y = 0$, $|x|^2 = 1$) which directly implies the vertex parameterisation from Eqs. (4.19) and (4.22).

Nevertheless, if the vector $\boldsymbol{D}_{ij}$ has two non-vanishing components on a single bond, only the $\mathbb{Z}_2$ invariance with respect to the spin transformation $\boldsymbol{S} \to -\boldsymbol{S}$ remains. In such a case, the FRG equations necessary for describing the system would probably involve all 16 possible spin-spin interaction channels. For our capability to present results as in the main chapters of this thesis, the remaining $U(1)$ symmetry of the Hamiltonian is vital.

Bibliography

[1] A. A. Abrikosov. "Electron scattering on magnetic impurities in metals and anomalous resistivity effects". In: *Physics Physique Fizika* 2 (1 Sept. 1965), pp. 5–20.

[2] A. A. Abrikosov and A. A. Migdal. "On the theory of the Kondo effect". In: *Journal of Low Temperature Physics* 3.5 (Nov. 1970), pp. 519–536.

[3] Ian Affleck and J. Brad Marston. "Large-n limit of the Heisenberg-Hubbard model: Implications for high-T_c superconductors". In: *Phys. Rev. B* 37 (7 Mar. 1988), pp. 3774–3777.

[4] S. Andergassen, T. Enss, and V. Meden. "Kondo physics in transport through a quantum dot with Luttinger-liquid leads". In: *Phys. Rev. B* 73.15 (Apr. 2006).

[5] S. Andergassen et al. "Functional renormalization group for Luttinger liquids with impurities". In: *Phys. Rev. B* 70.7 (Aug. 2004).

[6] P. W. Anderson. "Resonating valence bonds: A new kind of insulator?" In: *Materials Research Bulletin* 8.2 (Feb. 1973), pp. 153–160.

[7] P. W. Anderson. "The Resonating Valence Bond State in La_2CuO_4 and Superconductivity". In: *Science* 235.4793 (Mar. 1987), pp. 1196–1198.

[8] P. W. Anderson et al. "The physics behind high-temperature superconducting cuprates: the plain vanilla version of RVB". In: *J. Phys.: Condens. Matter* 16.24 (June 2004), R755–R769.

[9] M. L. Baez and J. Reuther. "Numerical treatment of spin systems with unrestricted spin length S: A functional renormalization group study". In: *Phys. Rev. B* 96 (4 July 2017), p. 045144.

[10] Leon Balents. "Spin liquids in frustrated magnets". In: *Nature* 464.7286 (Mar. 2010), pp. 199–208.

[11] Christian Balz et al. "Physical realization of a quantum spin liquid based on a complex frustration mechanism". In: *Nature Physics* 12.10 (July 2016), pp. 942–949.

[12] G. Baskaran, Z. Zou, and P. W. Anderson. "The resonating valence bond state and high-Tc superconductivity - A mean field theory". In: *Solid State Communications* 63.11 (1987), pp. 973–976.

[13] Doron Bergman et al. "Order-by-disorder and spiral spin-liquid in frustrated diamond-lattice antiferromagnets". In: *Nature Physics* 3 (May 2007), 487 EP.

[14] Jean-Sébastien Bernier, Michael J. Lawler, and Yong Baek Kim. "Quantum Order by Disorder in Frustrated Diamond Lattice Antiferromagnets". In: *Phys. Rev. Lett.* 101 (4 July 2008), p. 047201.

[15] Samuel Bieri, Claire Lhuillier, and Laura Messio. "Projective symmetry group classification of chiral spin liquids". In: *Phys. Rev. B* 93 (9 Mar. 2016), p. 094437.

[16] Raymond F. Bishop, Damian J. J. Farnell, and John B. Parkinson. "Phase transitions in the spin-half J_1-J_2 model". In: *Phys. Rev. B* 58 (10 Sept. 1998), pp. 6394–6402.

[17] J. H. de Boer and E. J. W. Verwey. "Semi-conductors with partially and with completely filled 3 d -lattice bands". In: *Proceedings of the Physical Society* 49.4S (1937), p. 59.

[18] Finn Lasse Buessen and Simon Trebst. "Competing magnetic orders and spin liquids in two- and three-dimensional kagome systems: Pseudofermion functional renormalization group perspective". In: *Phys. Rev. B* 94 (23 Dec. 2016), p. 235138.

[19] Finn Lasse Buessen et al. "Functional renormalization group approach to SU(N) Heisenberg models: Real-space renormalization group at arbitrary N". In: *Phys. Rev. B* 97 (6 Feb. 2018), p. 064415.

[20] Finn Lasse Buessen et al. "Quantum Spin Liquids in Frustrated Spin-1 Diamond Antiferromagnets". In: *Phys. Rev. Lett.* 120 (5 Jan. 2018), p. 057201.

[21] B. Canals. "From the square lattice to the checkerboard lattice: Spin-wave and large-n limit analysis". In: *Phys. Rev. B* 65 (18 Apr. 2002), p. 184408.

[22] B. Canals and C. Lacroix. "Pyrochlore Antiferromagnet: A Three-Dimensional Quantum Spin Liquid". In: *Phys. Rev. Lett.* 80 (13 Mar. 1998), pp. 2933–2936.

[23] B. Canals and C. Lacroix. "Quantum spin liquid: The Heisenberg antiferromagnet on the three-dimensional pyrochlore lattice". In: *Phys. Rev. B* 61 (2 Jan. 2000), pp. 1149–1159.

[24] Luca Capriotti and Subir Sachdev. "Low-Temperature Broken-Symmetry Phases of Spiral Antiferromagnets". In: *Phys. Rev. Lett.* 93 (25 Dec. 2004), p. 257206.

[25] Luca Capriotti and Sandro Sorella. "Spontaneous Plaquette Dimerization in the $J_1 - J_2$ Heisenberg Model". In: *Phys. Rev. Lett.* 84 (14 Apr. 2000), pp. 3173–3176.

[26] Luca Capriotti et al. "Resonating Valence Bond Wave Functions for Strongly Frustrated Spin Systems". In: *Phys. Rev. Lett.* 87 (9 Aug. 2001), p. 097201.

[27] O. Cépas et al. "Quantum phase transition induced by Dzyaloshinskii-Moriya interactions in the kagome antiferromagnet". In: *Phys. Rev. B* 78.14 (Oct. 2008).

[28] Jiří Chaloupka, George Jackeli, and Giniyat Khaliullin. "Kitaev-Heisenberg Model on a Honeycomb Lattice: Possible Exotic Phases in Iridium Oxides A_2IrO_3". In: *Phys. Rev. Lett.* 105 (2 July 2010), p. 027204.

[29] J. R. Chamorro and Tyrel M. McQueen. "Frustrated S = 1 On A Diamond Lattice". In: (). eprint: `arXiv:1701.06674`.

[30] J. R. Chamorro et al. "Frustrated spin one on a diamond lattice in $NiRh_2O_4$". In: *Phys. Rev. Materials* 2 (3 Mar. 2018), p. 034404.

[31] P. Chandra, P. Coleman, and A. I. Larkin. "Ising transition in frustrated Heisenberg models". In: *Phys. Rev. Lett.* 64 (1 Jan. 1990), pp. 88–91.

[32] P. Chandra and B. Doucot. "Possible spin-liquid state at large S for the frustrated square Heisenberg lattice". In: *Phys. Rev. B* 38 (13 Nov. 1988), pp. 9335–9338.

[33] Gang Chen. "Quantum paramagnet and frustrated quantum criticality in a spin-one diamond lattice antiferromagnet". In: *Phys. Rev. B* 96 (2 July 2017), p. 020412.

[34] Gang Chen, Leon Balents, and Andreas P. Schnyder. "Spin-Orbital Singlet and Quantum Critical Point on the Diamond Lattice: $FeSc_2\mathbf{S}_4$". In: *Phys. Rev. Lett.* 102 (9 Mar. 2009), p. 096406.

[35] Gang Chen, Andreas P. Schnyder, and Leon Balents. "Excitation spectrum and magnetic field effects in a quantum critical spin-orbital system: The case of $FeSc_2S_4$". In: *Phys. Rev. B* 80 (22 Dec. 2009), p. 224409.

[36] A. L. Chernyshev and M. E. Zhitomirsky. "Order and excitations in large-S kagomé-lattice antiferromagnets". In: *Phys. Rev. B 92, 144415 (2015)* (Aug. 26, 2015).

[37] A. L. Chernyshev and M. E. Zhitomirsky. "Quantum Selection of Order in an XXZ Antiferromagnet on a Kagome Lattice". In: *Phys. Rev. Lett.* 113.23 (Dec. 2014).

[38] Andrey Chubukov. "Order from disorder in a kagomé antiferromagnet". In: *Phys. Rev. Lett.* 69.5 (Aug. 1992), pp. 832–835.

[39] Chung-Hou Chung. "Dynamical properties of a nonequilibrium quantum dot close to a dissipative quantum phase transition". In: *Phys. Rev. B* 83.11 (Mar. 2011).

[40] Chung-Hou Chung et al. "Nonequilibrium quantum transport through a dissipative resonant level". In: *Phys. Rev. B* 87.24 (June 2013).

[41] Elbio Dagotto and Adriana Moreo. "Phase diagram of the frustrated spin-1/2 Heisenberg antiferromagnet in 2 dimensions". In: *Phys. Rev. Lett.* 63 (19 Nov. 1989), pp. 2148–2151.

[42] R. Darradi et al. "Ground state phases of the spin-1/2 $J_1 - J_2$ Heisenberg antiferromagnet on the square lattice: A high-order coupled cluster treatment". In: *Phys. Rev. B* 78 (21 Dec. 2008), p. 214415.

[43] Dirk van Delft and Peter Kes. "The discovery of superconductivity". In: *Physics Today* 63 (9 Sept. 1, 2010).

[44] Stefan Depenbrock, Ian P. McCulloch, and Ulrich Schollwöck. "Nature of the Spin-Liquid Ground State of the $S = 1/2$ Heisenberg Model on the Kagome Lattice". In: *Phys. Rev. Lett.* 109 (6 Aug. 2012), p. 067201.

[45] J.-C. Domenge et al. "Twelve sublattice ordered phase in the J_1-J_2 model on the kagomé lattice". In: *Phys. Rev. B* 72.2 (July 2005).

[46] A. V. Dotsenko and O. P. Sushkov. "Quantum phase transition in the frustrated Heisenberg antiferromagnet". In: *Phys. Rev. B* 50 (18 Nov. 1994), pp. 13821–13824.

[47] I. Dzyaloshinsky. "A thermodynamic theory of 'weak' ferromagnetism of antiferromagnetics". In: *Journal of Physics and Chemistry of Solids* 4.4 (Jan. 1958), pp. 241–255.

[48] T. Einarsson and H. J. Schulz. "Direct calculation of the spin stiffness in the J_1-J_2 Heisenberg antiferromagnet". In: *Phys. Rev. B* 51 (9 Mar. 1995), pp. 6151–6154.

[49] M. Elhajal, B. Canals, and C. Lacroix. "Symmetry breaking due to Dzyaloshinsky-Moriya interactions in the kagomé lattice". In: *Phys. Rev. B* 66.1 (July 2002).

[50] T. Enss et al. "Impurity and correlation effects on transport in one-dimensional quantum wires". In: *Phys. Rev. B* 71.15 (Apr. 2005).

[51] L. D. Faddeev and L. A. Takhtajan. "What is the spin of a spin wave?" In: *Phys. Lett. A* 85.6 (1981), pp. 375–377.

[52] Francesco Ferrari and Federico Becca. "Spectral signatures of fractionalization in the frustrated Heisenberg model on the square lattice". In: *Phys. Rev. B* 98 (10 Sept. 2018), p. 100405.

[53] R. P. Feynman. "Mathematical Formulation of the Quantum Theory of Electromagnetic Interaction". In: *Phys. Rev.* 80 (3 Nov. 1950), pp. 440–457.

[54] R. P. Feynman. "Space-Time Approach to Quantum Electrodynamics". In: *Phys. Rev.* 76 (6 Sept. 1949), pp. 769–789.

[55] R. P. Feynman. "The Theory of Positrons". In: *Phys. Rev.* 76 (6 Sept. 1949), pp. 749–759.

[56] V. Fritsch et al. "Spin and Orbital Frustration in $MnSc_2S_4$ and $FeSc_2S_4$". In: *Phys. Rev. Lett.* 92 (11 Mar. 2004), p. 116401.

[57] Shang Gao et al. "Spiral spin-liquid and the emergence of a vortex-like state in $MnSc_2S_4$". In: *Nature Physics* 13 (Oct. 2016), 157 EP.

[58] Philipp Gegenwart and Simon Trebst. "Spin-orbit physics: Kitaev matter". In: *Nature Physics* 11.6 (May 2015), pp. 444–445.

[59] Martin P. Gelfand. "Series investigations of magnetically disordered ground states in two-dimensional frustrated quantum antiferromagnets". In: *Phys. Rev. B* 42 (13 Nov. 1990), pp. 8206–8213.

[60] Shou-Shu Gong et al. "Global phase diagram of competing ordered and quantum spin-liquid phases on the kagome lattice". In: *Phys. Rev. B* 91.7 (Feb. 2015).

[61] Shou-Shu Gong et al. "Plaquette Ordered Phase and Quantum Phase Diagram in the Spin-$\frac{1}{2}$ J_1-J_2 Square Heisenberg Model". In: *Phys. Rev. Lett.* 113 (2 July 2014), p. 027201.

[62] Martin C. Gutzwiller. "Correlation of Electrons in a Narrow *s* Band". In: *Phys. Rev.* 137 (6A Mar. 1965), A1726–A1735.

[63] Martin C. Gutzwiller. "Effect of Correlation on the Ferromagnetism of Transition Metals". In: *Phys. Rev. Lett.* 10 (5 Mar. 1963), pp. 159–162.

[64] R. Haghshenas and D. N. Sheng. "$U(1)$-symmetric infinite projected entangled-pair states study of the spin-1/2 square J_1-J_2 Heisenberg model". In: *Phys. Rev. B* 97 (17 May 2018), p. 174408.

[65] F. D. M. Haldane. ""Fractional statistics" in arbitrary dimensions: A generalization of the Pauli principle". In: *Phys. Rev. Lett.* 67 (8 Aug. 1991), pp. 937–940.

[66] F. D. M. Haldane. ""Spinon gas" description of the S=1/2 Heisenberg chain with inverse-square exchange: Exact spectrum and thermodynamics". In: *Phys. Rev. Lett.* 66 (11 Mar. 1991), pp. 1529–1532.

[67] F. D. M. Haldane and M. R. Zirnbauer. "Exact calculation of the ground-state dynamical spin correlation function of a S=1/2 antiferromagnetic Heisenberg chain with free spinons". In: *Phys. Rev. Lett.* 71 (24 Dec. 1993), pp. 4055–4058.

[68] Tian-Heng Han et al. "Correlated impurities and intrinsic spin-liquid physics in the kagome material herbertsmithite". In: *Phys. Rev. B* 94.6 (Aug. 2016).

[69] Tian-Heng Han et al. "Fractionalized excitations in the spin-liquid state of a kagome-lattice antiferromagnet". In: *Nature* 492.7429 (Dec. 2012), pp. 406–410.

[70] M. B. Hastings. "Dirac structure, RVB, and Goldstone modes in the kagomé antiferromagnet". In: *Phys. Rev. B* 63 (1 Dec. 2000), p. 014413.

[71] Yin-Chen He et al. "Signatures of Dirac Cones in a DMRG Study of the Kagome Heisenberg Model". In: *Phys. Rev. X* 7 (3 July 2017), p. 031020.

[72] R. Hedden et al. "A functional renormalization group approach to zero-dimensional interacting systems". In: *J. Phys.: Condens. Matter* 16.29 (July 2004), pp. 5279–5296.

[73] J. S. Helton et al. "Spin Dynamics of the Spin-1/2 Kagome Lattice Antiferromagnet $ZnCu_3(OH)_6Cl_2$". In: *Phys. Rev. Lett.* 98 (10 Mar. 2007), p. 107204.

[74] Christopher L. Henley. "Ordering due to disorder in a frustrated vector antiferromagnet". In: *Phys. Rev. Lett.* 62 (17 Apr. 1989), pp. 2056–2059.

[75] Michael Hermele et al. "Stability of $U(1)$ spin liquids in two dimensions". In: *Phys. Rev. B* 70 (21 Dec. 2004), p. 214437.

[76] Wen-Jun Hu et al. "Direct evidence for a gapless Z_2 spin liquid by frustrating Néel antiferromagnetism". In: *Phys. Rev. B* 88 (6 Aug. 2013), p. 060402.

[77] John Hubbard. "Electron correlations in narrow energy bands". In: *Proceedings of the Royal Society of London A: Mathematical, Physical and Engineering Sciences* 276.1365 (1963), pp. 238–257.

[78] John Hubbard. "Electron correlations in narrow energy bands II. The degenerate band case". In: *Proceedings of the Royal Society of London A: Mathematical, Physical and Engineering Sciences* 277.1369 (1964), pp. 237–259.

[79] John Hubbard. "Electron correlations in narrow energy bands III. An improved solution". In: *Proceedings of the Royal Society of London A: Mathematical, Physical and Engineering Sciences* 281.1386 (1964), pp. 401–419.

[80] John Hubbard. "Electron correlations in narrow energy bands IV. The atomic representation". In: *Proceedings of the Royal Society of London A: Mathematical, Physical and Engineering Sciences* 285.1403 (1965), pp. 542–560.

[81] John Hubbard. "Electron correlations in narrow energy bands V. A perturbation expansion about the atomic limit". In: *Proceedings of the Royal Society of London A: Mathematical, Physical and Engineering Sciences* 296.1444 (1967), pp. 82–99.

[82] John Hubbard. "Electron correlations in narrow energy bands VI. The connexion with many-body perturbation theory". In: *Proceedings of the Royal Society of London A: Mathematical, Physical and Engineering Sciences* 296.1444 (1967), pp. 100–112.

[83] Yasir Iqbal, Federico Becca, and Didier Poilblanc. "Projected wave function study of $\mathbb{Z}_2$ spin liquids on the kagome lattice for the spin-1/2 quantum Heisenberg antiferromagnet". In: *Phys. Rev. B* 84.2 (July 2011).

[84] Yasir Iqbal, Federico Becca, and Didier Poilblanc. "Valence-bond crystal in the extended kagome spin-$\frac{1}{2}$ quantum Heisenberg antiferromagnet: A variational Monte Carlo approach". In: *Phys. Rev. B* 83 (10 Mar. 2011), p. 100404.

[85] Yasir Iqbal, Didier Poilblanc, and Federico Becca. "Spin-$\frac{1}{2}$ Heisenberg J_1-J_2 antiferromagnet on the kagome lattice". In: *Phys. Rev. B* 91 (2 Jan. 2015), p. 020402.

[86] Yasir Iqbal, Didier Poilblanc, and Federico Becca. "Vanishing spin gap in a competing spin-liquid phase in the kagome Heisenberg antiferromagnet". In: *Phys. Rev. B* 89 (2 Jan. 2014), p. 020407.

[87] Yasir Iqbal et al. "Functional renormalization group for three-dimensional quantum magnetism". In: *Phys. Rev. B* 94.14 (Oct. 2016).

[88] Yasir Iqbal et al. "Gapless spin-liquid phase in the kagome spin-1/2 Heisenberg antiferromagnet". In: *Phys. Rev. B* 87.6 (Feb. 2013).

[89] Yasir Iqbal et al. "Intertwined nematic orders in a frustrated ferromagnet". In: *Phys. Rev. B* 94 (22 Dec. 2016), p. 224403.

[90] Yasir Iqbal et al. "Paramagnetism in the kagome compounds $(\mathrm{Zn},\mathrm{Mg},\mathrm{Cd})\mathrm{Cu}_3(\mathrm{OH})_6\mathrm{Cl}_2$". In: *Phys. Rev. B* 92 (22 Dec. 2015), p. 220404.

[91] L. Isaev, G. Ortiz, and J. Dukelsky. "Hierarchical mean-field approach to the J_1-J_2 Heisenberg model on a square lattice". In: *Phys. Rev. B* 79 (2 Jan. 2009), p. 024409.

[92] G. Jackeli and G. Khaliullin. "Mott Insulators in the Strong Spin-Orbit Coupling Limit: From Heisenberg to a Quantum Compass and Kitaev Models". In: *Phys. Rev. Lett.* 102.1 (Jan. 2009).

[93] Harald O. Jeschke, Francesc Salvat-Pujol, and Roser Valentí. "First-principles determination of Heisenberg Hamiltonian parameters for the spin-1/2 kagomé antiferromagnet $ZnCu_3(OH)_6Cl_2$". In: *Phys. Rev. B* 88.7 (Aug. 2013).

[94] H. C. Jiang, Z. Wang, and L. Balents. "Identifying topological order by entanglement entropy". In: *Nature Physics* 8 (Nov. 2012), 902 EP.

[95] H. C. Jiang, Z. Y. Weng, and D. N. Sheng. "Density Matrix Renormalization Group Numerical Study of the Kagome Antiferromagnet". In: *Phys. Rev. Lett.* 101.11 (Sept. 2008).

[96] H. C. Jiang, H. Yao, and L. Balents. "Spin liquid ground state of the spin-$\frac{1}{2}$ square J_1-J_2 Heisenberg model". In: *Phys. Rev. B* 86 (2 July 2012), p. 024424.

[97] C. Karrasch, S. Andergassen, and V. Meden. "Supercurrent through a multilevel quantum dot close to singlet-triplet degeneracy". In: *Phys. Rev. B* 84.13 (Oct. 2011).

[98] C. Karrasch, T. Enss, and V. Meden. "Functional renormalization group approach to transport through correlated quantum dots". In: *Phys. Rev. B* 73.23 (June 2006).

[99] A. A. Katanin. "Fulfillment of Ward identities in the functional renormalization group approach". In: *Phys. Rev. B* 70.11 (Sept. 2004).

[100] B. J. Kim et al. "Novel $J_{\text{eff}} = 1/2$ Mott State Induced by Relativistic Spin-Orbit Coupling in Sr_2IrO_4". In: *Phys. Rev. Lett.* 101.7 (Aug. 2008).

[101] Alexei Kitaev. "Anyons in an exactly solved model and beyond". In: *Annals of Physics* 321.1 (Jan. 2006), pp. 2–111.

[102] John B. Kogut. "An introduction to lattice gauge theory and spin systems". In: *Rev. Mod. Phys.* 51 (4 Oct. 1979), pp. 659–713.

[103] F. Kolley et al. "Phase diagram of the J_1-J_2 Heisenberg model on the kagome lattice". In: *Phys. Rev. B* 91.10 (Mar. 2015).

[104] Gabriel Kotliar and Jialin Liu. "Superexchange mechanism and d-wave superconductivity". In: *Phys. Rev. B* 38 (7 Sept. 1988), pp. 5142–5145.

[105] M. A. Laakso et al. "Functional renormalization group study of the Anderson-Holstein model". In: *New J. Phys.* 16.2 (Feb. 2014), p. 023007.

[106] Andreas Läuchli and Claire Lhuillier. "Dynamical Correlations of the Kagome S=1/2 Heisenberg Quantum Antiferromagnet". In: (Jan. 2009). eprint: `0901.1065`.

[107] P. Lecheminant et al. “Order versus disorder in the quantum Heisenberg antiferromagnet on the kagomé lattice using exact spectra analysis”. In: *Phys. Rev. B* 56 (5 Aug. 1997), pp. 2521–2529.

[108] SungBin Lee and Leon Balents. “Theory of the ordered phase in A-site antiferromagnetic spinels”. In: *Phys. Rev. B* 78 (14 Oct. 2008), p. 144417.

[109] P. H. Y. Li et al. “Spin-1/2 Heisenberg antiferromagnet on an anisotropic kagome lattice”. In: *Phys. Rev. B* 86.21 (Dec. 2012).

[110] H. J. Liao et al. “Gapless Spin-Liquid Ground State in the $S = 1/2$ Kagome Antiferromagnet”. In: *Phys. Rev. Lett.* 118 (13 Mar. 2017), p. 137202.

[111] Yuan-Ming Lu, Ying Ran, and Patrick A. Lee. “$\mathbb{Z}_2$ spin liquids in the $S = \frac{1}{2}$ Heisenberg model on the kagome lattice: A projective symmetry-group study of Schwinger fermion mean-field states”. In: *Phys. Rev. B* 83 (22 June 2011), p. 224413.

[112] J. M. Luttinger. “A Note on the Ground State in Antiferromagnetics”. In: *Phys. Rev.* 81 (6 Mar. 1951), pp. 1015–1018.

[113] J. M. Luttinger and L. Tisza. “Theory of Dipole Interaction in Crystals”. In: *Phys. Rev.* 70 (11-12 Dec. 1946), pp. 954–964.

[114] Matthieu Mambrini et al. “Plaquette valence-bond crystal in the frustrated Heisenberg quantum antiferromagnet on the square lattice”. In: *Phys. Rev. B* 74 (14 Oct. 2006), p. 144422.

[115] J. B. Marston and I. Affleck. “Large-n limit of the Hubbard-Heisenberg model”. In: *Phys. Rev. B* 39 (16 June 1989), pp. 11538–11558.

[116] J. B. Marston and C. Zeng. “Spin-Peierls and spin-liquid phases of Kagomé quantum antiferromagnets”. In: *Journal of Applied Physics* 69.8 (1991), pp. 5962–5964.

[117] Volker Meden. *Funktionale Renormierungsgruppe*. Nov. 1, 2018. URL: `http://www.statphys.rwth-aachen.de/go/id/qygs/lidx/1`.

[118] Jia-Wei Mei et al. “Gapped spin liquid with $\mathbb{Z}_2$ topological order for the kagome Heisenberg model”. In: *Phys. Rev. B* 95 (23 June 2017), p. 235107.

[119] P. Mendels et al. “Quantum Magnetism in the Paratacamite Family: Towards an Ideal Kagomé Lattice”. In: *Phys. Rev. Lett.* 98 (7 Feb. 2007), p. 077204.

[120] L. Messio, B. Bernu, and C. Lhuillier. “Kagome Antiferromagnet: A Chiral Topological Spin Liquid?” In: *Phys. Rev. Lett.* 108.20 (May 2012).

[121] L. Messio, C. Lhuillier, and G. Misguich. “Lattice symmetries and regular magnetic orders in classical frustrated antiferromagnets”. In: *Phys. Rev. B* 83.18 (May 2011).

[122] L. Messio, C. Lhuillier, and G. Misguich. “Time reversal symmetry breaking chiral spin liquids: Projective symmetry group approach of bosonic mean-field theories”. In: *Phys. Rev. B* 87 (12 Mar. 2013), p. 125127.

[123] L. Messio et al. “Chiral Spin Liquid on a Kagome Antiferromagnet Induced by the Dzyaloshinskii-Moriya Interaction”. In: *Phys. Rev. Lett.* 118 (26 June 2017), p. 267201.

[124] Walter Metzner. “Functional Renormalization Group Computation of Interacting Fermi Systems”. In: *Progress of Theoretical Physics Supplement* 160 (2005), pp. 58–78.

[125] Walter Metzner et al. “Functional renormalization group approach to correlated fermion systems”. In: *Rev. Mod. Phys.* 84.1 (Mar. 2012), pp. 299–352.

[126] Grégoire Misguich. “Quantum Spin Liquids and Fractionalization”. In: *Introduction to Frustrated Magnetism* (Jan. 1, 2011).

[127] R. Moessner and J. T. Chalker. “Low-temperature properties of classical geometrically frustrated antiferromagnets”. In: *Phys. Rev. B* 58 (18 Nov. 1998), pp. 12049–12062.

[128] R. Moessner and J. T. Chalker. “Properties of a Classical Spin Liquid: The Heisenberg Pyrochlore Antiferromagnet”. In: *Phys. Rev. Lett.* 80 (13 Mar. 1998), pp. 2929–2932.

[129] Tôru Moriya. “Anisotropic Superexchange Interaction and Weak Ferromagnetism”. In: *Phys. Rev.* 120.1 (Oct. 1960), pp. 91–98.

[130] Tim R. Morris. “THE EXACT RENORMALIZATION GROUP AND APPROXIMATE SOLUTIONS”. In: *International Journal of Modern Physics A* 09.14 (1994), pp. 2411–2449.

[131] N. F. Mott and R. Peierls. “Discussion of the paper by de Boer and Verwey”. In: *Proceedings of the Physical Society* 49.4S (1937), p. 72.

[132] S. Mühlbauer et al. “Skyrmion Lattice in a Chiral Magnet”. In: *Science* 323.5916 (Feb. 2009), pp. 915–919.

[133] Naoto Nagaosa and Yoshinori Tokura. “Topological properties and dynamics of magnetic skyrmions”. In: *Nature Nanotechnology* 8.12 (Dec. 2013), pp. 899–911.

[134] Yoichiro Nambu. “Quasi-Particles and Gauge Invariance in the Theory of Superconductivity”. In: *Phys. Rev.* 117 (3 Feb. 1960), pp. 648–663.

[135] J. W. Negele and H. Orland. *Quantum Many-particle Systems (Advanced Books Classics)*. Perseus Books, 1998. ISBN: 0-7382-0052-2.

[136] Masaki Oshikawa and T. Senthil. “Fractionalization, Topological Order, and Quasiparticle Statistics”. In: *Phys. Rev. Lett.* 96 (6 Feb. 2006), p. 060601.

[137] K. W. Plumb et al. “Quasiparticle-continuum level repulsion in a quantum magnet”. In: *Nature Physics* 12.3 (Nov. 2015), pp. 224–229.

[138] K. W. Plumb et al. “α-RuCl 3: A spin-orbit assisted Mott insulator on a honeycomb lattice”. In: *Phys. Rev. B* 90.4 (July 2014).

[139] Didier Poilblanc and Grégoire Misguich. "Competing valence bond crystals in the kagome quantum dimer model". In: *Phys. Rev. B* 84 (21 Dec. 2011), p. 214401.

[140] Ying Ran et al. "Projected-Wave-Function Study of the Spin-1/2 Heisenberg Model on the Kagomé Lattice". In: *Phys. Rev. Lett.* 98.11 (Mar. 2007).

[141] N. Read and Subir Sachdev. "Large-N expansion for frustrated quantum antiferromagnets". In: *Phys. Rev. Lett.* 66 (13 Apr. 1991), pp. 1773–1776.

[142] J. D. Reger and A. P. Young. "Monte Carlo simulations of the spin-(1/2 Heisenberg antiferromagnet on a square lattice". In: *Phys. Rev. B* 37 (10 Apr. 1988), pp. 5978–5981.

[143] J. Reiss, D. Rohe, and W. Metzner. "Renormalized mean-field analysis of antiferromagnetism and d-wave superconductivity in the two-dimensional Hubbard model". In: *Phys. Rev. B* 75 (7 Feb. 2007), p. 075110.

[144] Johannes Reuther. "Frustrated Quantum Heisenberg Antiferromagnets: Functional Renormalization-Group Approach in Auxiliary-Fermion Representation". Dissertation. Karlsruher Institut für Technologie (KIT), 2011.

[145] Johannes Reuther and Ronny Thomale. "Cluster functional renormalization group". In: *Phys. Rev. B* 89.2 (Jan. 2014).

[146] Johannes Reuther, Ronny Thomale, and Stephan Rachel. "Spiral order in the honeycomb iridate Li_2IrO_3". In: *Phys. Rev. B* 90.10 (Sept. 2014).

[147] Johannes Reuther and Peter Wölfle. "J 1 - J 2 frustrated two-dimensional Heisenberg model: Random phase approximation and functional renormalization group". In: *Phys. Rev. B* 81.14 (Apr. 2010).

[148] Johannes Reuther et al. "Quantum phases of the planar antiferromagnetic $J_1 - J_2 - J_3$ Heisenberg model". In: *Phys. Rev. B* 83 (6 Feb. 2011), p. 064416.

[149] Marcos Rigol and Rajiv R. P. Singh. "Kagome lattice antiferromagnets and Dzyaloshinsky-Moriya interactions". In: *Phys. Rev. B* 76.18 (Nov. 2007).

[150] Dietrich Roscher et al. "Functional renormalization group approach to SU(N) Heisenberg models: Momentum-space renormalization group for the large-N limit". In: *Phys. Rev. B* 97 (6 Feb. 2018), p. 064416.

[151] Ioannis Rousochatzakis et al. "Dzyaloshinskii-Moriya anisotropy and nonmagnetic impurities in the s = 1/2 kagome system $ZnCu_3(OH)_6Cl_2$". In: *Phys. Rev. B* 79.21 (June 2009).

[152] Ioannis Rousochatzakis et al. "Quantum dimer model for the spin-1/2 kagomé $\mathbb{Z}_2$ spin liquid". In: *Phys. Rev. B* 90.10 (Sept. 2014).

[153] Subir Sachdev. "Kagomé - and triangular-lattice Heisenberg antiferromagnets: Ordering from quantum fluctuations and quantum-disordered ground states with unconfined bosonic spinons". In: *Phys. Rev. B* 45 (21 June 1992), pp. 12377–12396.

[154] Subir Sachdev and N. Read. "LARGE N EXPANSION FOR FRUSTRATED AND DOPED QUANTUM ANTIFERROMAGNETS". In: *International Journal of Modern Physics B* 05.01n02 (1991), pp. 219–249.

[155] M. Salmhofer and C. Honerkamp. "Fermionic Renormalization Group Flows: Technique and Theory". In: *Progress of Theoretical Physics* 105.1 (Jan. 2001), pp. 1–35.

[156] M. Salmhofer et al. "Renormalization Group Flows into Phases with Broken Symmetry". In: *Progress of Theoretical Physics* 112.6 (Dec. 2004), pp. 943–970.

[157] Lucile Savary and Leon Balents. "Quantum spin liquids: a review". In: *Reports on Progress in Physics* 80.1 (2017), p. 016502.

[158] Lucile Savary et al. "Impurity effects in highly frustrated diamond-lattice antiferromagnets". In: *Phys. Rev. B* 84 (6 Aug. 2011), p. 064438.

[159] H. Schmidt and P. Wölfle. "Transport through a Kondo quantum dot: Functional RG approach". In: *Annalen der Physik* 19.1-2 (Dec. 2009), pp. 60–74.

[160] H. J. Schulz and T. A. L. Ziman. "Finite-size scaling for the two-dimensional frustrated quantum Heisenberg antiferromagnet". In: *EPL (Europhys. Lett.)* 18 (Feb. 1992), p. 355.

[161] H. J. Schulz, T. A. L. Ziman, and D. Poilblanc. "Magnetic Order and Disorder in the Frustrated Quantum Heisenberg Antiferromagnet in Two Dimensions". In: *J. Phys. I France* 6.5 (Jan. 22, 1996), pp. 675–703.

[162] Tsezar F. Seman et al. "The many faces of quantum kagome materials: Interplay of further-neighbour exchange and Dzyaloshinskii-Moriya interaction". In: (Aug. 2015). eprint: 1508.01523.

[163] T. Senthil and Matthew P. A. Fisher. "Z_2 gauge theory of electron fractionalization in strongly correlated systems". In: *Phys. Rev. B* 62 (12 Sept. 2000), pp. 7850–7881.

[164] Tokuro Shimokawa and Hikaru Kawamura. "Finite-Temperature Crossover Phenomenon in the S = 1/2 Antiferromagnetic Heisenberg Model on the Kagome Lattice". In: *Journal of the Physical Society of Japan* 85.11 (Nov. 2016), p. 113702.

[165] Matthew P. Shores et al. "A Structurally Perfect S = 1/2 Kagomé Antiferromagnet". In: *Journal of the American Chemical Society* 127.39 (Oct. 2005), pp. 13462–13463.

[166] Rajiv R. P. Singh and Marcos Rigol. "Thermodynamic properties of Kagome antiferromagnets with different perturbations". In: *Journal of Physics: Conference Series* 145 (Jan. 2009), p. 012003.

[167] Rajiv R. P. Singh et al. "Dimer order with striped correlations in the J_1-J_2 Heisenberg model". In: *Phys. Rev. B* 60 (10 Sept. 1999), pp. 7278–7283.

[168] Yogesh Singh et al. "Relevance of the Heisenberg-Kitaev Model for the Honeycomb Lattice Iridates A_2IrO_3". In: *Phys. Rev. Lett.* 108.12 (Mar. 2012).

[169] J. Sirker et al. "$J1-J2$ model: First-order phase transition versus deconfinement of spinons". In: *Phys. Rev. B* 73 (18 May 2006), p. 184420.

[170] Jonas Sonnenschein and Johannes Reuther. "Topological spinon bands and vison excitations in spin-orbit coupled quantum spin liquids". In: *Phys. Rev. B* 96 (23 Dec. 2017), p. 235113.

[171] O. P. Sushkov, J. Oitmaa, and Zheng Weihong. "Critical dynamics of singlet and triplet excitations in strongly frustrated spin systems". In: *Phys. Rev. B* 66 (5 Aug. 2002), p. 054401.

[172] O. P. Sushkov, J. Oitmaa, and Zheng Weihong. "Quantum phase transitions in the two-dimensional J_1-J_2 model". In: *Phys. Rev. B* 63 (10 Feb. 2001), p. 104420.

[173] Raik Suttner et al. "Renormalization group analysis of competing quantum phases in the J_1-J_2 Heisenberg model on the kagome lattice". In: *Phys. Rev. B* 89.2 (Jan. 2014).

[174] T. Suzuki et al. "Melting of antiferromagnetic ordering in spinel oxide $CoAl_2O_4$". In: *Journal of Physics: Condensed Matter* 19.14 (2007), p. 145265.

[175] N. Tristan et al. "Geometric frustration in the cubic spinels MAl_2O_4 (M = Co, Fe, and Mn)". In: *Phys. Rev. B* 72 (17 Nov. 2005), p. 174404.

[176] Menke U. Ubbens and Patrick A. Lee. "Flux phases in the t-J model". In: *Phys. Rev. B* 46 (13 Oct. 1992), pp. 8434–8439.

[177] M. A. de Vries et al. "Scale-Free Antiferromagnetic Fluctuations in the s = 1/2 Kagome Antiferromagnet Herbertsmithite". In: *Phys. Rev. Lett.* 103.23 (Dec. 2009).

[178] Fa Wang and Ashvin Vishwanath. "Spin-liquid states on the triangular and Kagomé lattices: A projective-symmetry-group analysis of Schwinger boson states". In: *Phys. Rev. B* 74 (17 Nov. 2006), p. 174423.

[179] Jing Wang, Andreas Eberlein, and Walter Metzner. "Competing order in correlated electron systems made simple: Consistent fusion of functional renormalization and mean-field theory". In: *Phys. Rev. B* 89 (12 Mar. 2014), p. 121116.

[180] Ling Wang and Anders W. Sandvik. "Critical Level Crossings and Gapless Spin Liquid in the Square-Lattice Spin-1/2 $J_1 - J_2$ Heisenberg Antiferromagnet". In: *Phys. Rev. Lett.* 121 (10 Sept. 2018), p. 107202.

[181] X. G. Wen. "Mean-field theory of spin-liquid states with finite energy gap and topological orders". In: *Phys. Rev. B* 44 (6 Aug. 1991), pp. 2664–2672.

[182] X. G. Wen. "Quantum orders and symmetric spin liquids". In: *Phys. Rev. B* 65 (16 Apr. 2002), p. 165113.

[183] X. G. Wen. "Vacuum degeneracy of chiral spin states in compactified space". In: *Phys. Rev. B* 40 (10 Oct. 1989), pp. 7387–7390.

[184] X. G. Wen and Q. Niu. "Ground-state degeneracy of the fractional quantum Hall states in the presence of a random potential and on high-genus Riemann surfaces". In: *Phys. Rev. B* 41 (13 May 1990), pp. 9377–9396.

[185] X. G. Wen, Frank Wilczek, and A. Zee. "Chiral spin states and superconductivity". In: *Phys. Rev. B* 39 (16 June 1989), pp. 11413–11423.

[186] Christof Wetterich. "Exact evolution equation for the effective potential". In: *Phys. Lett. B* 301.1 (Feb. 1993), pp. 90–94.

[187] Edward Witten. "Quantum field theory and the Jones polynomial". In: *Comm. Math. Phys.* 121.3 (1989), pp. 351–399.

[188] Fengcheng Wu et al. "Hubbard Model Physics in Transition Metal Dichalcogenide Moiré Bands". In: *Phys. Rev. Lett.* 121 (2 July 2018), p. 026402.

[189] Youhei Yamaji et al. "First-Principles Study of the Honeycomb-Lattice Iridates Na_2IrO_3 in the Presence of Strong Spin-Orbit Interaction and Electron Correlations". In: *Phys. Rev. Lett.* 113 (10 Sept. 2014), p. 107201.

[190] S. Yan, D. A. Huse, and S. R. White. "Spin-Liquid Ground State of the $S = 1/2$ Kagome Heisenberg Antiferromagnet". In: *Science* 332.6034 (Apr. 2011), pp. 1173–1176.

[191] Shun-Li Yu et al. "Deconfinement of spinons in frustrated spin systems: Spectral perspective". In: *Phys. Rev. B* 98 (13 Oct. 2018), p. 134410.

[192] A. Zorko et al. "Dzyaloshinsky-Moriya Anisotropy in the Spin-1/2 Kagome Compound $ZnCu_3(OH)_6Cl_2$". In: *Phys. Rev. Lett.* 101.2 (July 2008).

List of publications

The Chaps. 4, 5, and 6 are based on one so far unpublished and two published collaborations with Johannes Reuther, Finn Lasse Buessen, Simon Trebst, Jonas Sonnenschein, and Yasir Iqbal. They are summarised in the following.

1. Chap. 4: Max Hering and Johannes Reuther. "Functional-renormalization-group analysis of Dzyaloshinsky-Moriya and Heisenberg spin interactions on the kagome lattice". In: *Phys. Rev. B* 95 (5 Feb. 2017), p. 054418.
   The concept was provided by Johannes Reuther. The analytical and numerical techniques and results are my original work. I also created all figures unless noted otherwise.

2. Chap. 5: Finn Lasse Buessen, Max Hering, Johannes Reuther, and Simon Trebst. "Quantum Spin Liquids in Frustrated Spin-1 Diamond Antiferromagnets". In: *Phys. Rev. Lett.* 120 (5 Jan. 2018), p. 057201.
   Simon Trebst suggested the project. All numerical results and figures in the published article are the work of Finn Lasse Buessen. Johannes Reuther contributed the expertise for implementing single-ion anisotropies in combination with level-repulsion terms. For the models considered in Chap. 5, I derived the FRG flow equations and produced additional numerical data confirming a correct implementation. The numerical results presented in Chap. 5 that are not part of the publication were performed by me.

3. Chap. 6: Max Hering, Jonas Sonnenschein, Yasir Iqbal, and Johannes Reuther. "Characterization of quantum spin liquids and their spinon band structures via functional renormalization". Online preprint: *arXiv.org:1806.05021* (13 Jun. 2018).
   Johannes Reuther inspired this study. Jonas Sonnenschein and Yasir Iqbal contributed the PSG classifications on the square and the kagome lattice, respectively. I developed the analytical and numerical methods, and obtained all presented results. The figures in the online article were created by Johannes Reuther. All additional figures are my work.

Abstract

We enhance the pseudo-fermion functional-renormalisation-group (PFFRG) method for the investigation of highly frustrated quantum spin systems in two significant ways. On one hand, we generalise the method towards off-diagonal Dzyaloshinsky-Moriya (DM) interactions and single-ion anisotropies. On the other hand, we develop a self-consistent Fock-like mean-field technique which is based on vertex functions from a PFFRG analysis and calculates effective free spinon models for the considered systems at low energies.

In Chap. 1, we introduce the fundamental mathematical concepts on which our studies rely. The so-called flow equations for the PFFRG are then derived in Chap. 3. The first part of our original work is presented in Chap. 4 where we, for the first time, extend the PFFRG scheme towards off-diagonal spin interactions and therefore confirm the quite general applicability of this method. There are two important results from our investigations of the spin-$\frac{1}{2}$ Heisenberg-DM model on the kagome lattice in this chapter. One is that a finite DM interaction enlarges magnetically ordered phases and thereby shrinks the paramagnetic phases which possibly house spin liquid states. The other important result is that the mineral *herbertsmithite* which inspired this project lies in close proximity to a quantum critical point. We obtain a phase diagram for the considered Hamiltonian and qualitatively good results in comparison to experimental data for *herbertsmithite* [68, 69].

Our collaboration with a research group from Cologne is summarised in Chap. 5. Here, we investigate two different XXZ models with tetragonally split-up second-neighbour Heisenberg interactions and single-ion anisotropies on the diamond lattice in order to study the spin-1 A-site spinel $NiRh_2O_4$. We are able to confirm the existence of a paramagnetic phase for one of the considered models. However, such a paramagnetic behaviour cannot be verified for the Hamiltonians suggested in Refs. [29] and [30].

The second main part of this thesis is contained in Chap. 6. The developed PFFRG plus mean-field method enables us to characterise the effective low-energy spinon band structure of the spin-$\frac{1}{2}$ J_1-J_2 (nearest-neighbour) Heisenberg model on the square (kagome) lattice. This is achieved by comparing self-consistently determined overall amplitudes for different mean-field ansätze which are taken from corresponding PSG classifications in Refs. [182] and [111]. Our studies imply that the square lattice model realises a $SU(2)$ spin liquid with π-fluxes through elementary plaquettes and that the spin-$\frac{1}{2}$ kagome antiferromagnet is most likely described by a $\mathbb{Z}_2$ spin liquid called $\mathbb{Z}_2[0,\pi]\alpha$.

We argue that our analysed models have current experimental relevance and that the developed techniques show plenty of possibilities for future applications. A detailed summary and discussion of all methods and results is provided in Chap. 7.

Kurzfassung

Wir verbessern die Methode der Pseudofermion funktionalen Renormierungsgruppe (PFFRG) für die Untersuchung stark frustrierter Quantenspinsysteme auf zwei signifikante Weisen. Einerseits erweitern wir die Methode auf Dzyaloshinsky-Moriya (DM) Wechselwirkungen und Einzelionenanisotropien. Andererseits entwickeln wir eine Fock-artige *mean-field* Technik, die auf Vertices von einer PFFRG Analyse beruht und effektive Spinonbandstrukturen der betrachteten Systeme berechnet.

In Kap. 1 führen wir die mathematischen Konzepte ein, auf denen unsere Studien basieren. Die Flussgleichungen der PFFRG werden in Kap. 3 hergeleitet. Der erste Teil unseres Originalwerks wird in Kap. 4 präsentiert, wo wir erstmals das PFFRG Schema auf nebendiagonale Spinwechselwirkungen erweitern und damit die sehr breite Anwendbarkeit dieser Methode bestätigen. Unsere Untersuchung des Spin-$\frac{1}{2}$ Heisenberg-DM Modells auf dem Kagomegitter zeigt, dass eine finite DM Wechselwirkung magnetisch geordnete Phasen vergrößert und somit die paramagnetischen (PM) Phasen verkleinert, welche möglicherweise Spinflüssigkeiten beherbergen. Zudem zeigen wir, dass sich das Mineral *herbertsmithite*, welches dieses Projekt inspirierte, in der Nähe zu einem quantenkritischen Punkt befindet. Wir erhalten ein Phasendiagramm des betrachteten Hamiltonians und qualitativ gute Ergebnisse im Vergleich zu den experimentellen Daten für *herbertsmithite* [68, 69].

Unsere Kollaboration mit Forschern aus Köln ist in Kap. 5 zusammengefasst. Hier untersuchen wir zwei verschieden XXZ Modelle mit tetragonal aufgespaltenen Heisenberg Wechselwirkungen und Einzelionenanisotropien auf dem Diamantgitter, um das Spinel $NiRh_2O_4$ zu studieren. Wir bestätigen die Existenz einer PM Phase in einem unserer Modelle. Allerdings verifizieren wir solch ein PM Verhalten nicht für die in den Referenzen [29] und [30] vorgeschlagenen Hamiltonians.

Der zweite Hauptteil dieser Dissertation ist in Kap. 6 enthalten. Die dort entwickelte PFFRG plus *mean-field* Methode ermöglicht es uns, die effektive Spinonenbandstruktur des Spin-$\frac{1}{2}$ J_1-J_2 (nächste-Nachbar) Heisenberg Modells auf dem Quadratgitter (Kagomegitter) zu charakterisieren. Dies wird durch einen Vergleich der Gesamtamplituden für verschiedene *mean-field* Ansätze erreicht, welche den PSG Klassifizierungen der Referenzen [182] und [111] entstammen. Unsere Studien implizieren, dass das Quadratgittermodell eine $SU(2)$ Spinflüssigkeit realisiert, während der Spin-$\frac{1}{2}$ Kagome-Antiferromagnet wahrscheinlich durch eine $\mathbb{Z}_2$ Spinflüssigkeit beschrieben wird.

Wir argumentieren, dass unsere Modelle aktuelle Relevanz besitzen und die entwickelten Techniken vielerlei Möglichkeiten für zukünftige Anwendungen bieten. Eine detaillierte Zusammenfassung und Diskussion aller Methoden und Resultate ist in Kap. 7 bereitgestellt.

Acknowledgements

I want to thank all gods in this world for that I am healthy as far as I know. I thank my parents, my siblings, and my grandparents for my life and their love. I am truly grateful for having so many friends which support me at all times and costs. This work would not have been possible without you! Of course, the same applies to those who taught me physics. Martin Henze inspired my studies with his passion for the subject and by introducing me to the quantum world. Eros Mariani gave me strength to fight my enemies one at a time. Piet Brouwer then familiarised me with the weapons I need for my current struggles and motivated me to exercise. Johannes Reuther deserves special acknowledgement because he not only shared his fascination for quantum magnets with me, but he also fed me for the last years which is always a noble gesture. Furthermore, I have to thank Maria Laura Baez, Elina Locane, Felix "FU-King" von Oppen, Björn Sbierski, Maximilian Trescher, Max Geier, Christian Fräßdorf, Jonas Sonnenschein, Dominik Kiese, Finn Lasse Buessen, Yasir Iqbal, and many more for fruitful discussions about physics. An indispensable contribution to this thesis was also provided by Jörg Behrmann and Jens Dreger who maintain the computers at the physics institute and keep the moving parts clean.

I am also incredibly glad and proud to be able to enjoy music, to have it as my spirit and my balance. In this respect, I thank Fender and Gibson guitars as well as Marshall amplifiers for the greatest sound on earth, Pitti Piatkowski for teaching me the Rock and Roll, Steve Vai for his guidance, Rush for the spirit of my radio, the entire LiveKaraoke band and crew for our legendary gigs at Wacken Open Air, Get Stoned for my satisfaction, and Mars for the empire. There are many musicians who inspired not only me but also thousands of others, who gave us strength and peace. We will never forget their thoughts and melodies. Their names are Prince, David Bowie, Leonard Cohen, George Michael, B. B. King, Chuck Berry, Malcolm Young, Lemmy Kilmister, Mike Porcaro, Pat Torpey, Vinnie Paul, Aretha Franklin, and Montserrat Caballé to mention only a few. I am glad that I could experience tremendous concerts in the past and I sincerely believe that we should all be united by our love for living our lives rather than torn apart by our history and religion. Life is precious and comprises millions of chances. Let's keep it that way!